

KATHOLIEKE UNIVERSITEIT LEUVEN
FACULTEIT TOEGEPASTE WETENSCHAPPEN
DEPARTEMENT ELECTROTECHNIEK
AFDELING ESAT
Kardinaal Mercierlaan 94 — 3001 Leuven (Heverlee)

Virtual Engineering for Design and Control of Continuously Variable Transmissions

Promotoren :
Prof. Dr. Ir. B. DE MOOR
Prof. Dr. Ir. J. VANDEWALLE

Proefschrift voorgedragen tot
het behalen van het doctoraat
in de toegepaste wetenschappen

door

Paul VANVUCHELEN

6 mei 1997



KATHOLIEKE UNIVERSITEIT LEUVEN
FACULTEIT TOEGEPASTE WETENSCHAPPEN
DEPARTEMENT ELECTROTECHNIEK
AFDELING ESAT
Kardinaal Mercierlaan 94 — 3001 Leuven (Heverlee)

Virtual Engineering for Design and Control of Continuously Variable Transmissions

Jury :
Prof. Dr. Ir. E. Aernoudt, voorzitter
Prof. Dr. Ir. B. De Moor, promotor
Prof. Dr. Ir. J. Vandewalle, promotor
Prof. Dr. Ir. J. De Schutter
Prof. Dr. Ir. R. Belmans
Prof. Dr. Ir. P.P.J. van den Bosch (TU Eindhoven, NL)
Ir. R. Buckinx (VCST-VT), toegevoegd lid

Proefschrift voorgedragen tot
het behalen van het doctoraat
in de toegepaste wetenschappen

door

Paul VANVUCHELEN

UDC : 681.51

6 mei 1997

© Copyright by Katholieke Universiteit Leuven
Zonder voorafgaandelijke toestemming van de auteur en de promotor is overnemen, copiëren, gebruiken of realiseren van deze uitgave of gedeelten ervan verboden.
Voor aanvragen tot of informatie i.v.m. het overnemen en/of gebruik en/of realisatie van gedeelten van dit werk, wendt U tot de K.U.Leuven, Faculteit Toegepaste Wetenschappen, Dept. Elektrotechniek, Onderzoeksgroep SISTA, Kardinaal Mercierlaan 94, 3001 Heverlee-Leuven, België.
Voorafgaandelijke toestemming is eveneens vereist voor het aanwenden van de in dit proefschrift vermelde (originele) methoden, schakelingen en programma's voor industrieel of commercieel nut.

D/1997/7515/09

ISBN 90-5682-074-5

Voorwoord

Aan het einde van dit doctoraat neem ik graag de gelegenheid te baat om iedereen te bedanken voor zijn of haar steun en inspiratie.

In de eerste plaats wil ik mijn promotor Professor Bart de Moor bedanken. Zijn enthousiasme en oprechte verwondering bij het bekijken van de allereerste klep-simulaties op basis van bondgraafmodellen hebben mij de kracht van fysisch modelleren doen beseffen. De lijnrechte tegenstellingen tussen 'zijn' identificatie-modellen en 'mijn' fysische modellen waren dan ook telkens weer een dankbaar onderwerp voor discussie. Uit zijn lessen en seminaries onthoud ik vooral dat de boodschapper grotendeels het effect van een boodschap bepaalt: door zijn uitstraling op het podium werd regeltechniek een feest.

Zijn betogen over de financiële aspecten van onderzoeksprojecten werkten echter even aanstekelijk als zijn lessen regeltechniek: hij toonde mij de weg in het labyrint van de overheidsfinanciering en hij stimuleerde mij bij het aanvragen van verschillende industriële projecten. Op dergelijke momenten droomden wij ook van ondernemerschap en van een eigen bedrijfje, dat de echte vragen van de industrie met de modernste ingenieurstechnieken zou aanpakken. Ongeveer een jaar geleden werd uiteindelijk de spin-off Intelligent Systems Modelling and Control N.V. opgericht, een brug tussen de universiteit en de industrie.

Als mechatronica-student van het eerste uur, op zoek naar een afstudeerwerk met praktische toepassingen, kwam ik na vele omzwervingen terecht bij mijn promotor Professor Joos Vandewalle. Uit één van zijn vele documentatie-kasten kwam een eindwerkvoorstel bij het toenmalige Volvo Car Sint-Truiden tevoorschijn. Na dit eindwerk gaf hij mij de kans om een, naar zijn zeggen, 'horizontaal' doctoraat binnen de groep SISTA aan te vatten. De meerkosten tengevolge van dit 'horizontale' karakter nam hij steeds voor zijn rekening. Van hem kreeg ik bovendien de gelegenheid om mijn horizon te verruimen via buitenlandse cursussen en lesopdrachten.

Professor Joris De Schutter bedank ik voor zijn deelname aan mijn leescomité

en voor het grondig nalezen van deze tekst. In zijn cursus over toegepaste kinematica en dynamica maakte ik kennis met toegepaste fysische modellering.

Professor Ronnie Belmans wil ik bedanken als jury-lid, maar vooral ook voor alle kennis en medewerking die ik van hem en zijn laboratorium-personeel heb mogen ontvangen, bij het bouwen van de testopstelling voor CVTs in de kelders van ESAT.

Professor Paul Van den Bosch wil ik als lid van mijn jury eveneens bedanken voor zijn interesse en voor het in mij gestelde vertrouwen tijdens de begeleiding van één van zijn Erasmus-afstudeerders.

Ingenieur Ronnie Buckinx wil ik als lid van mijn jury, maar ook als projectleider van het huidige IWT-project bedanken voor de steun, medewerking en collegialiteit die ik in al die jaren mocht ervaren. Zijn geloof in 'modelgebaseerd werken' motiveerde mij om dit onderzoeksproject uit te voeren.

Vervolgens wil ik ook een aantal medewerkers van VCST-VT in Sint-Truiden bedanken. Jaak Vandermaesen dank ik voor het in mij gestelde vertrouwen. Als manager toonde hij mij dat persoonlijk contact en communicatie het welslagen van vernieuwingen binnen R&D-afdelingen bepalen. Peter Aberson, Dirk Reniers, Gert-Jan Vogelaar, Stijn Helsen, Peter Vandemoortele en Marc Thijs dank ik voor hun medewerking bij het formuleren van problemen, het zoeken naar informatie en het beoordelen van oplossingen en voor hun hulp bij het begeleiden van mijn 17 eindwerkstudenten.

Mijn ISMC-collega Christiaan Moons dank ik in de eerste plaats voor het realiseren van de proefstand, maar ook voor zijn geduldige uiteenzettingen over hardware en zijn verwoede maar vergeefse pogingen om mij met alle software van ESAT vertrouwd te maken. Mijn ISMC-collega Peter Van Overschee dank ik voor zijn hulp bij het oplossen van numerieke problemen, voor de talrijke discussies over het verschil tussen theorie en praktijk en voor de Latex-hulp bij het tot stand komen van deze tekst. Mijn thesismaatje Wim Minten bedank ik voor de prettige samenwerking tijdens en na ons eindwerk, voor de urenlange babbels over fysisch modelleren en voor de overtuiging en vakkennis waarmee hij mij de geheimen van bondgrafen heeft bijgebracht. Nog steeds laat de bondgraaffilosofie mij toe om een fysisch proces gestructureerd en correct te modelleren. Alle overige collega's van SISTA bedank ik voor de prettige werksfeer en voor de plezierige activiteiten buitenuit.

Mijn CVT-eindwerkstudenten Wim, Joris, Peter, Jan, Gert, Frank, Koen, Jan, Geert, Rudy, Phillipe, Dirk, Patricia, Roel, Anje, Jan en Kris wil ik eveneens bedanken voor hun inzet en enthousiasme bij het ontrafelen van het CVT-kluwen.

Het IWT en VCST zou ik willen bedanken voor het in mij gestelde vertrouwen en voor de bijhorende financiële steun: dankzij twee IWT-projecten in samenwerk-

ing met VCST Sint-Truiden heb ik steeds in optimale omstandigheden kunnen werken.

Mijn vroegere wiskunde-leraar Mathieu Caenen bedank ik omdat hij mij steeds aangemoedigd heeft om de ingenieursstudies aan te vatten. Mijnheer Caenen, wiskunde is inderdaad mooi.

Mijn ouders en broer bedank ik voor het onvoorwaardelijke vertrouwen dat zij steeds in mij gehad hebben, vóór, tijdens en na mijn studies. Bedankt voor de dagelijkse trips naar Leuven tijdens de examens, bedankt voor het geduld en de aanmoedigingen in moeilijke momenten, bedankt voor alles. Ook mijn schoonouders dank ik voor hun steun.

Tenslotte bedank ik mijn echtgenote Ine, voor haar geduld, haar begrip, haar steun en haar aanmoedigingen, maar bovenal voor haar liefde voor mij en onze twee peuters Gilles en Nathalie. Zonder hen zou ik niet zijn wie ik nu ben, niet staan waar ik nu sta. Ik draag deze thesis dan ook op aan mijn gezin.

Paul Vanvuchelen
Kinrooi, Mei 1997

Abstract

This thesis focusses on the *development and application of virtual engineering techniques for design and control of Continuously Variable Transmissions.* The major contributions are the following:

1. Physical modeling techniques are used to obtain generic models of the environment, the car, the drive train, the engine, the various types of couplings, the push-belt variator and the wide variety of valve-bodies.

   The characteristic behavior of each component as well as the interactions between components are described in detail. This leads to highly non-linear, multi-variable system equations, that are useful for both simulation-based analysis and design.
   Analytical linearization is used to derive linearized equations from the physical descriptions. These equations are physically parameterized and are useful for analytical analysis and design.

2. Specific experiments have been defined and conducted, to generate model calibration data. Design-of-experiments-techniques are used to increase the reliability of the experiments and to reduce the number of experiments.

   The generic models are tuned for a wide range of applications. The following applications have been considered:

   - **Cars**: Rover Metro, Rover 216, Rover 416, X, Y, Volvo 440 and Volvo 850. Preliminary work has been done for Korean car manufacturers.
   - **Combustion engines**: Volvo engines (B18U-1800 cc, N2P20-2000 cc) and Rover engines (7 types).
   - **Coupling elements**: a wet multi-plate clutch (P811) and a torque convertor (Daikin YT220).
   - **Push-belt variators**: all important VCST variators (VT-1, VT-2, VT-3) and their application-specific variants.

- **Valve-bodies**: VCSTs hydro-mechanical controlled valve-body (VT1-H) and some of their electro-hydraulical controlled valve-bodies (VT1-E, EVT2, VTF). These valve-body models include the gear pump, the regulator and servo valves, the pulley and clutch pistons and the control system (actuators, sensors and intelligence).

3. The derived models have been used for design and optimization of the valves, the variator and the control system, for a wide variety of car-engine-coupling combinations.

   In this context, effective performance indices, based on customer's specifications and on experimental results are defined. Specific attention is paid to fuel consumption, dynamic car performance (accelerations, speed, hill-climbing), and vertical and longitudinal drive comfort.

4. Model-based controllers were designed, implemented and validated if possible.

   Model-based optimization of the actual digital control algorithms (PID and (non-linear) static feedforward) has been done extensively. To analyse and validate these controllers, a computer-controlled test-rig has been constructed.

   Advanced model-based digital control algorithms are developped also. At this moment, these algorithms are being implemented and validated on the 'upgraded' power test-rig at VCST. Implementation in cars will only be possible when the electronic control unit (ECU) is no longer a cost constraint for series production.

   All derived controllers fully exploit the derived physical models. Feedback linearization theory and linear control theory are combined to design the controllers.

5. The virtual engineering framework has been implemented in Matlab and Simulink, in the tailor-made toolbox VIRTUES (VIRTUal Engineering Software). In this toolbox, the models and the proposed controllers are implemented. Dedicated techniques for model calibration, system analysis and optimizationbased parameter design are implemented also.
   Currently, a graphical user interface and a CAD-database are being added.

Contents

Voorwoord i

Abstract v

Notation xvii

1 Introduction and Motivation 1
- 1.1 Virtual engineering for mechatronic design . . . 2
  - 1.1.1 A special attitude for mechatronics . . . 2
  - 1.1.2 Virtual engineering . . . 3
- 1.2 A glimpse on CVTs . . . 7
  - 1.2.1 Changing gears: an historical overview . . . 7
  - 1.2.2 Functional description of a CVT . . . 11
  - 1.2.3 Virtual engineering of CVTs . . . 20
- 1.3 Overview and contributions . . . 21
  - 1.3.1 Chapter by chapter overview . . . 21
  - 1.3.2 Contributions . . . 23

2 Modeling Vehicle Motion 27
- 2.1 Introduction . . . 28
- 2.2 Resistances to car motion . . . 28
  - 2.2.1 Roll resistance . . . 28
  - 2.2.2 Air drag and lift . . . 30
- 2.3 Disturbances for car motion . . . 30
  - 2.3.1 Wind dynamics . . . 31
  - 2.3.2 Road profile noise . . . 33
- 2.4 Car modeling . . . 36
  - 2.4.1 A car model to describe longitudinal and vertical motion 39
  - 2.4.2 A linearized model for comfort analysis . . . 42
  - 2.4.3 A reduced model for longitudinal motion control . . . 45
- 2.5 Modeling of industrial applications . . . 46

3 Comfort and Performance **47**
3.1 Introduction 47
3.2 Car performance and fuel economy 49
3.2.1 A benchmark test for CVT-equipped cars 49
3.2.2 Dynamic performance 50
3.2.3 Fuel economy 52
3.3 Drive comfort 54
3.3.1 The human sensitivity filters 55
3.3.2 Comfort indices 58
3.3.3 An integrated car-comfort model 59
3.4 A sample of results and conclusions 60

4 Drive Train Modeling and Control **71**
4.1 Description of the drive train 72
4.2 Drive train component models 75
4.2.1 The combustion engine 75
4.2.2 The wet multi-plate clutch 76
4.2.3 The torque converter 80
4.2.4 The gear pump 83
4.2.5 The push-belt variator 86
4.2.6 The pinion gear 87
4.2.7 The drive axle 87
4.3 Drive train modeling 88
4.3.1 A physical model of the drive train 89
4.3.2 A reduced model for clutch control 92
4.3.3 A reduced model for variator control 93
4.4 Drive train control 93
4.4.1 Drive train management via variogram control 94
4.4.2 An algorithm for control in clutch mode 98
4.4.3 An algorithm for control in variator mode 100
4.5 A sample of results and conclusions 101

5 Modeling and Control of the Push Belt Variator **107**
5.1 Introduction 107
5.2 Modeling of the push-belt variator 108
5.2.1 Geometric relations 108
5.2.2 Kinematic relations 110
5.2.3 Static flow and pressure requirements 111
5.2.4 Dynamic flow and pressure requirements 115
5.2.5 Efficiency 125
5.3 Variator control 129
5.3.1 Outer control 130

5.3.2 Inner controllers for pressure and flow steering 131

6 Valves and mechanisms for piston control 139
6.1 Introduction 139
6.2 A configuration for variator control 141
6.2.1 The variator pistons 144
6.2.2 The used transmission oil 145
6.2.3 The gear pump 146
6.3 Typical spool valves for piston control 147
6.3.1 A double stage flow valve for piston control 149
6.3.2 A flow valve with pressure feedback for piston control . . 157
6.4 Control systems 164
6.4.1 Hydro-mechanical control 164
6.4.2 Electro-hydraulic control 166

7 VIRTUES: VIRTUal Engineering Software 169
7.1 Objectives 169
7.2 VIRTUES: Virtual Engineering Software 170
7.2.1 The model descriptions of VIRTUES 171
7.2.2 The VIRTUES database 171
7.2.3 The graphical user interface of VIRTUES 172
7.3 Conclusions 177

8 A Test-Rig for Valve Body Analysis and Control 179
8.1 Introduction 179
8.2 Objectives 180
8.3 Steered inputs and measured outputs 180
8.4 Test-rig lay-out 181
8.4.1 The induction motor 183
8.4.2 The variator 183
8.4.3 The cooling unit 184
8.4.4 The data acquisition and control system 184

9 Conclusions and open problems 187
9.1 Conclusions 187
9.2 Open problems 189

A Parameter tuning using numerical optimization 191
A.1 Practical parameter tuning problems 191
A.2 Mathematical formulation 192
A.3 A practical approach 195
A.4 An illustrative example 196

Bibliography 201

Nederlandse Samenvatting 212

List of Figures

1.1 A typical virtual engineering cycle 5
1.2 The Variomatic from DAF 9
1.3 A modern belt-type Continuously Variable Transmission 16
1.4 The metal push-belt of Hub Van Doorne 17
1.5 Shifting of the CVT 18
1.6 Valve-body of an hydro-mechanically controlled transmission . . 19
1.7 Organization of the thesis 22

2.1 A simple model for roll resistance 29
2.2 Experimental roll resistance coefficients 29
2.3 The air drag coefficient and the air lift coefficient 31
2.4 Experimentally determined wind spectrum 33
2.5 Measured and modeled wind spectra 34
2.6 Experimentally determined road spectrum 35
2.7 Different car models for different purposes 36
2.8 Functional model of the car 37
2.9 Relations between fixed points on the car body 40

3.1 Experimentally determined torque-speed curves (engine B18U) . 49
3.2 Experimentally determined fuel consumption curves (engine B18U) 50
3.3 The desired car speed profile for the Urban cycle 53
3.4 The desired car speed profile for the Highway cycle 53
3.5 The desired car speed profile for the ECE-cycle 54
3.6 The human sensitivity for longitudinal comfort 57
3.7 The human sensitivity for transversal comfort 58
3.8 Influence of the control unit and control strategy for a Rover 216, engine 1.6K16MPI, VT1 variator, wet multi-plate clutch (P811) (simulation) 64
3.9 Influence of the control unit and control strategy for a Rover 216, with engine 1.6K16MPI, VT1 variator, wet multi-plate clutch (P811) (experiment) 65

3.10 Influence of the control unit and control strategy for a Rover 216, with engine 1.6K16MPI, VT1 variator, wet multi-plate clutch (P811) (experiment) 66
3.11 Variator optimization: influence of OD and FD on the consumed fuel at constant car speeds, for a Volvo 850, with engine N2-P20 and a VT1-E variator and a wet multi-plate clutch (P811) (simulation) 67
3.12 Plate clutch versus torque converter for a Rover 216, with engine 1.6K16MPI and a VT1-H variator (simulation) 68
3.13 Plate clutch versus torque converter for a Volvo 850, with engine N2-P20 and a VT1-E variator (simulation) 69

4.1 Functional model of the drive train 72
4.2 A functional model of the drive train 74
4.3 Experimental torque time constant $\tau_e(\dot{\theta}_e)$ 76
4.4 An example of a wet multi-plate clutch 77
4.5 A cross section and a longitudinal section of the wet multi-plate clutch 78
4.6 Experimentally determined clutch friction coefficient μ_{cl} for Esso EZL 799 and Lubrizol oil 78
4.7 A functional model for clutch piston displacement 80
4.8 The experimentally determined force-displacement characteristic of the VT1 clutch plate package 81
4.9 Cross section of a modern torque converter 82
4.10 Experimentally determined torque ratio $M_{tc}(s_{N,tc})$ as a function of speed ratio $s_{N,tc}$, for a Daikin YT220 torque converter 83
4.11 The experimentally determined capacity factor $S_{tc}(s_{N,tc})$ as a function of the speed ratio $s_{N,tc}$, for a Daikin YT220 torque converter 84
4.12 A modern push-belt variator 85
4.13 Functional model of a push-belt variator 86
4.14 The experimentally determined torque-speed characteristic and the optimal operating line for sport mode, for a B18U engine . . 95
4.15 The experimentally determined fuel consumption characteristic and the optimal operating line for economy mode for a B18U engine 96
4.16 An economy variogram for a B18U engine 97
4.17 A scheme for variogram control 97
4.18 Feedback linearization and model reference CVT control 99
4.19 Influence of the control unit and control strategy for a Rover 216, engine 1.6K16MPI, VT1 variator, wet multi-plate clutch (P811) (simulation) 102

4.20 Influence of the control unit and control strategy for a Rover 216, with engine 1.6K16MPI, VT1-H variator, wet multi-plate clutch (P811) (experiment) 103
4.21 Influence of the control unit and control strategy for a Rover 216, with engine 1.6K16MPI, VT1-F variator, wet multi-plate clutch (P811) (experiment) 104
4.22 Plate clutch versus torque converter for a Rover 216, with engine 1.6K16MPI and a VT1-H variator (simulation) 105

5.1 The geometry of a metal V-belt variator 109
5.2 The running radii R_s and R_p as a function of the ratio i_v 110
5.3 The oil flows Q_p and Q_s to obtain a rate of ratio change equal to $\frac{di_v}{dt} = -0.5\text{s}^{-1}$ 111
5.4 Forces on the belt and the pulleys 113
5.5 The experimentally determined force ratio $\frac{K_p}{K_s}$ as a function of the variator ratio i_v, for different primary speeds (VT1-variator), at $T_p = 40$ Nm 114
5.6 The experimentally determined force ratio $\frac{K_p}{K_s}$ as a function of the variator ratio i_v, for different primary torques (VT1-variator), at a primary speed of 2000 rpm 115
5.7 A physical model to describe shifting of the push-belt variator around Medium 117
5.8 Response of a flow steered variator 121
5.9 Response of a pressure steered variator 122
5.10 Response of a pressure-flow steered variator 123
5.11 Matlab/Simulink implementation of the experimental variator shifting model 124
5.12 A static neural network to fit the variator efficiency map 126
5.13 The predicted variator efficiency η_v as a function of the primary torque T_p, for an hydraulical (VT1-H) and an electronical (VT1-E) controlled drive train 127
5.14 Predicted relations between loss torque, variator ratio, secondary pressure and primary speed, for a primary torque of 35 Nm (simulation) 128
5.15 Two stage variator control 129
5.16 A single-piston model to design inner control algorithms 131
5.17 Two configurations to realize a flow into a piston 133
5.18 Feedback linearization and model reference piston control 135
5.19 Performance of an inner loop for pressure control, based on linear control and feedback linearization (VT1-variator, NO-configuration) 136
5.20 Performance of an inner loop for speed control, based on linear control and feedback linearization (VT1-variator, NO-configuration) 137

6.1 A configuration for variator control (pp-configuration, VT1-E) . 142
6.2 A configuration for variator control (pQ-configuration, VT1-H) . 143
6.3 A functional model of a single variator piston 144
6.4 The experimental mass density and kinematic viscosity of Esso EZL 799 146
6.5 A double stage flow valve for piston control 149
6.6 Orifices at the servo pilot and the main pilot of a double stage flow valve 150
6.7 Static characteristics of a double stage flow valve 154
6.8 Dynamic characteristics of a double stage flow valve 155
6.9 Influence of the feedback gain $w_{sv,2}$ on the dynamic characteristics of the double stage flow valve 156
6.10 A flow valve with pressure feedback for piston control 157
6.11 Orifice for a flow valve with pressure feedback 159
6.12 Static characteristics of a flow valve with pressure feedback (experiment versus simulation). 161
6.13 Dynamic characteristics of a flow valve with pressure feedback (experiment versus simulation) 162
6.14 Influence of included air on the dynamic characteristics of a flow valve with pressure feedback (simulation) 163
6.15 Components in a control scheme 164
6.16 Experimentally obtained pitot pressure parabola, for a VT1-H variator 166
6.17 Experimentally obatined servo pressure as a function of applied duty cycle, for a Bosch 3/2 PWM valve 168

7.1 Hierarchical Simulink block scheme of the drive train 174
7.2 Specific component file of a B18U combustion engine 175
7.3 Specific component file of a VT-175 variator 176

8.1 Functional description of the test rig 182
8.2 Photograph of the test-rig (ESAT-SISTA, K.U.Leuven) 183
8.3 Interface of CVT-Log program 186

A.1 A 1DOF configuration with a control law $K(s)$ to be designed . . 196
A.2 Step responses with a PI-controller: the initial design and non-inferior designs for various weights 198
A.3 The trade-off curve for the classical PI-parametrization 199
A.4 Trade-off curves for the classical parametrizations and the modern parametrization 200

List of Tables

2.1 Typical values of the parameters that determine the coefficients C_x and C_z 30
2.2 Disturbances for car motion 32
2.3 Important parameters of the car model and typical values 38

3.1 A design benchmark for a CVT-equipped passenger car 51
3.2 Dynamic performance VT1-H versus VT1-F (Rover 216, engine 1.6K16MPI) 61
3.3 CVT benchmark test (Rover 216, engine 1.6K16MPI, variator VT1-E) 63

4.1 Parameters to describe an ideal clutch 79
4.2 Friction coefficient parameters, for different types of oil (Esso EZL 799 and Lubrizol) and operating conditions 79
4.3 Additional parameters of a non-ideal clutch 80
4.4 Drive train parameters of a Volvo 480, equipped with a VT1-H transmission, Esso EZL 799 oil, 12 mm gear pump, wet multi-plate clutch, variator and pinion 89
4.5 The proposed control strategy for drive train control 98

5.1 Important CVT-parameters (VT1) 109
5.2 Parameters and typical values for the simplified variator model (around Medium) 118
5.3 Piston and load related parameters 132

6.1 Piston and load related parameters 145
6.2 Important oil characteristics 145
6.3 Pump flow parameters (12 mm gear pump) 147
6.4 Double stage flow valve parameters 153
6.5 Pressure feedback flow valve parameters 158

8.1 Measurement range, accuracy and bandwidth of the test-rig sensing equipment 181

A.1 PI-designs on the trade-off boundary 198
A.2 Four different control laws to realize closed-loop performance . . 200
A.3 Designs on the trade-off boundary, for four different control laws 200

Notation

Symbol	Property	Units
F	Force.	(N)
M	Torque.	(Nm)
N	Rotation speed.	$(\frac{rad}{s})$
p	Pressure.	$(Pa,\ bar)$
P	Instantaneous power.	(W)
Q	Volume flow.	$(\frac{m^3}{s})$
s_x	Translational slip speed.	$(\frac{m}{s})$
s_θ	Rotational slip speed.	$(\frac{rad}{s},\ rpm)$
t	Time.	(s)
T	Temperature.	$(^oF,\ ^oC)$
v	Translational speed.	$(\frac{m}{s},\ \frac{km}{h},\ mph)$
x, z	Horizontal, vertical position.	(m)
θ	Angular position.	(rad)
a	Section, orifice.	$(m^2,\ mm^2)$
A	Surface.	(m^2)
b	Translational damping.	$(\frac{N}{m/s})$
c	Torsional stiffness.	$(\frac{Nm}{rad})$
d	Torsional damping.	$(\frac{Nm}{rad/s})$
i	Transmission ratio.	$(-)$
I	Rotation inertia.	(kgm^2)
k	Translational stiffness.	$(\frac{N}{m})$

L	Distance, length.	(m)
m	Mass.	$(kg,\ g)$
r	Radius.	$(m,\ mm)$
R	Running radius.	$(m,\ mm)$
β, γ, δ	Angle.	$(rad,\ degr)$
η	Efficiency.	$(-)$
μ	Friction coefficient.	$(-)$
ρ	Mass density.	$(\frac{kg}{m^3})$
ν	Kinematic viscosity.	$(\frac{m^2}{s})$
τ	Time constant of a linear first order system.	$(s,\ ms)$
ζ	Damping ratio of a linear second order system.	$(-)$
ω_n	Natural frequency of a linear second order system.	$(\frac{rad}{s},\ Hz)$
t_d	Time delay.	$(s,\ ms)$

Symbol	Description
A, B ,C ,D	State space representation of a linear dynamic system.
M, R, K, N	Mass-damper-spring representation of a linear dynamic system.
X, U, Y	States, inputs and outputs of a state space model.
Z, W	States and inputs of a mass-damper-spring model.
σ	Variance of a Gaussian white noise signal.
$n_{\bar{m},\sigma}(t)$	Gaussian white noise signal, mean m, variance σ.
$\triangle L$	Period of harmonic space vectors.
$\triangle T$	Period of harmonic time vectors.
ω	Time-based frequency.
Ω	Space-based frequency.
ξ	Noisy part of a vector.
$P_{\xi(t)}(\omega)$	Time-based spectrum of $\xi(t)$.
$P_{\xi(x)}(\Omega)$	Space-based spectrum of $\xi(x)$.

$\bar{x}(t)$	Mean value of a time signal $x(t)$.
$\dot{x}(t)$	First derivative of time signal $x(t)$.
$\ddot{x}(t)$	Second derivative of time signal $x(t)$.
$\sqrt[\pm]{\lvert x\rvert}$	$\sqrt{\lvert x\rvert}\text{sign}(x)$.

Subscript	Related to
a	Driving axle.
air	Air around the car.
b	Back wheels.
$brake$	Brake.
c	Car body.
cl	Wet multi-plate clutch.
cp	Controlled piston.
cv	Control valve.
dl	Drive-line.
ds	Double stage flow valve.
dyn	Dynamical property.
e	Combustion engine.
f	Front wheels.
FD	Final drive reduction.
gp	Gear pump.
lk	Oil leakage.
oil	Transmission oil.
p	Primary art of the variator.
pc	Internal compensated pressure valve.
r	Road characteristics.
s	Secondary part of the variator.
sf	Safety considerations.
ss	Single stage flow valve.
$stat$	Static property.
tc	Torque converter.

up	Uncompensated pressure valve.
v	Variator.
w	Wind that acts on the car.
x	Longitudinal property.
z	Transversal property.
0	Initial condition.

Abreviation	Description
AT	Automatic Transmission.
CAD	Computer Aided Design.
CVT	Continuously Variable Transmission.
DOE	Design Of Experiments.
DOF	Degrees Of Freedom.
ECU	Electronic Control Unit.
I/O	Input/Output.
LOW	The highest transmission ratio (low).
MT	Manual Transmission.
MEDIUM	A transmission ratio of 1 (medium).
OD	The lowest transmission ratio (overdrive).
PID	Proportional-Integral-Derivative control.
PWM	Pulse Width Modulated.
VCST	Vehicle Components, Systems and Transmissions N.V. (before Volvo Car Sint-Truiden N.V.).
VIRTUES	VIRTUal Engineering Software.
cog	Center Of Gravity.
pp	Pressure-Pressure control of a CVT.
pQ	Pressure-Flow control of a CVT.

Chapter 1

Introduction and Motivation

" Mechatronics is a combination of mature technologies.
It is the clever combination of methodologies, technologies
and application knowledge that brings success,
not basic research."
Jacob Buur from Lyngby Institute for Engineering Design, Denmark
at the first Conference on Mechatronics,
Tampere, Finland, February 1994.

In this Chapter, we summarize our main contributions. In Section 1.1, we discuss different aspects of mechatronics. From this, we show that a virtual engineering framework is natural within mechatronics and that it leads to excellent tools for development of mechatronic products. In Section 1.2, we start with a short overview of the developments in changing gears. We also describe the basic properties of a Continuously Variable Transmission. Notes on the organization of this book and a Chapter by Chapter overview can be found in Section 1.3.

1.1 Virtual engineering for mechatronic design

1.1.1 A special attitude for mechatronics

Mechatronics has become a catch-word, and the fast penetration of this word in Europe and in the USA has indicated a growing awareness of the competitive potential of combining mechanics, electronics and computer sciences.

Although a generally accepted definition of mechatronic products does not exist, one can get an idea of the elements of such a definition by enumerating some typical mechatronic products such as a video recorder, a CD-player, a Xerox copier, a printer, a robot, a CNC-machine or an electronically controlled car. In [Buu 92], Buur gives the following definition of mechatronics:

> *Mechatronics is a technology which combines mechanics with electronics and information technology to form both functional interaction and spatial integration in components, modules, products and systems.*

It points out two important aspects of mechatronics:

- The functional interaction which must occur between different technologies.
- The spatial integration of subsystems in a single physical unit.

This implies that an acceptable mechatronic design integrates and fully exploits components and modules from different technologies. To implement mechatronics in practice, different needs must be fulfilled:

- The need for competitive strategies

  The mechatronics business is a field of fast and constant changes: shifts in technologies, in markets, in buyer's attitudes and in competition. A mechatronics company will only survive if it is constantly on the watch for new developments and if its organization is geared for frequent upheavals in marketing, research and manufacturing.

  Fast product development is one of the key factors to increase manoeuvrability and speed of reaction in the fast moving competitive environment. Of course, the development projects can not be shortened ad libitum. There is a relation between the development time and the achievable innovative change in the product.

- The need for interdisciplinarity

  It is in the nature of mechatronics that design requires wide, interdisciplinary knowledge of several areas of technology, e.g. mechanics, hydraulics, pneumatics, electronics and software. Within a project team, this knowledge may be achieved in two ways. One is to educate all designers with a general knowledge, the other is to put together specialists and to encourage communication and cooperation within the team.

  Without interdisciplinary knowledge, it may be possible to suggest a mechatronic product concept, but it is certainly not possible to realize it or to create a full range of alternative concepts and to evaluate those in a total context in order to choose the best. Interdisciplinary education and intensive communication and cooperation are required both.

- The need for design methodology and tools

  The field of mechatronics design is very young and there is hardly any support from design research for the central task of creating a mechatronic product.

  A key point in mechatronics design methodology research is to develop tools which support the designer in allocating technologies to the functions of the product (=dividing the product into modules), and that allow the designer to translate the functions of the modules into objective specifications.

  A second point is to establish product models in a common 'language', that can deal with mixed concepts. The product models can be used for evaluation of alternatives in a total context. The product models address all important technological issues and application specific knowledge.

  A third point is to develop tools that link dedicated experimental results to the product models, in order to tune the models towards reality.

From this, one might conclude that mechatronics needs indeed a special attitude: it is not simply a question of pooling the design skills of mechanical, electronics and software engineers.

1.1.2 Virtual engineering

The interest in mechatronics arises from the awareness of its competitive potentials. Speed and reliability in product development are important factors when dealing with the constant changes in technology, markets, buyer's attitudes and competitors. When doing product development, two approaches are possible:

- A classical prototyping approach

  A physical prototype of the product is the key element in this approach. In many cases, an earlier version of the product or a competitor's product is used as a starting point. Based on experiments with the prototype, the designers use prior knowledge and experience to iterate towards a new product.

  In this approach, effort and time are mainly used for:

  - Construction and adaptation of the prototype
  - Preparation and execution of experiments
  - Conditioning and maintenance of the prototype
  - Analysis of the obtained data and product iteration

- A model-based approach

  A mathematical model of the product is the key element in this approach. In many cases, a model of an existing product is used as a starting point. Based on simulations with the product model, the designers use dedicated tools to iterate towards a new product.

  In this approach, effort and time are mainly used for:

  - Modeling, calibration and implementation of the model
  - Simulation
  - Product optimization

In the proposed virtual engineering framework, we tried to combine the best of both worlds:

> *Based on physical knowledge and on dedicated experiments, an accurate mathematical description with physical parameters (the model) is constructed. In this way, the real system (the prototype) might be replaced by the virtual system (the mathematical model). Simulations are used instead of real-life experiments, to analyze and to optimize the system. User-specific knowledge is combined with powerful optimization tools to ensure fast iteration.*

In practice, a virtual engineering cycle goes through the following stages (see figure 1.1):

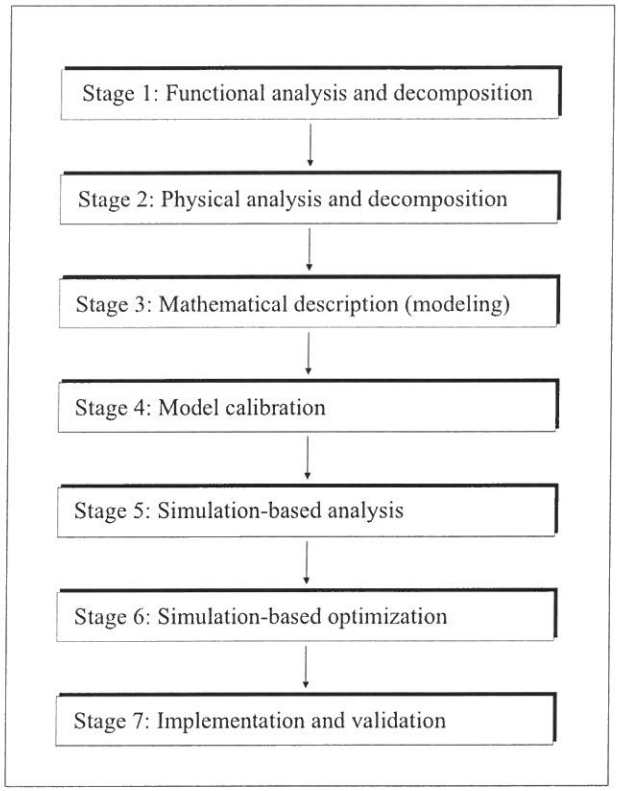

Figure 1.1 *A typical virtual engineering cycle*

1. Functional analysis and decomposition of the product

   In this stage, the operation of the product is analyzed in detail. The product is decomposed into different functional modules. The functionality of each module is implemented by combining different components.

2. Physical analysis and inventarization of each module

   The physical operation of each module is analyzed in detail. For each module, a preliminary list of important physical phenomena and components is created, based on data sheets, technical drawings and experimental results. The physical inputs and outputs of each module are defined also.

3. Mathematical description of the product and its modules

   First, a mathematical description of the product is derived. Basically, the interactions between the different functional modules are described. To

avoid causality problems afterwards, the inputs and outputs as determined in stage 2 must be carefully examined.

Next, a detailed mathematical description of the physical operation of each module is derived. The characteristic equations that describe each phenomenon or component can be found in the literature. The parameter values are determined from technical drawings, data sheets and experimental results. Each module is described by a set of mathematical equations with physical inputs, outputs and parameters.

4. Calibration of the product model

   For each module, preliminary simulations are compared with experimental results. If the simulations are accurate enough, no further calibration is required. If not, additional experiments are done, to complete the list of important phenomena (in the case of a structural error) or to adapt one or more physical parameters (in the case of a parametric error). This is repeated for each module. Once the descriptions of all modules are calibrated, they are integrated into the product model. The product model is now ready for analysis and design.

5. Simulation-based analysis of the product and its modules

   Extensive simulation is used to compute static and dynamic characteristics of each module and of the product itself. Sensitivity analysis and tolerance analysis are done also.

6. Simulation-based optimization of the product and its modules

   Optimization tools are used to iterate on the physical parameters of the modules, to meet user-defined performance specifications. If a set of specifications is given, trade-off surfaces for a given module or for the complete product can be computed. These trade-off surfaces represent the limits-of-performance of the considered module or product.

7. Validation

   The optimized product is constructed and experiments are used to validate the followed approach.

Following this procedure, a wide variety of industrial engineering problems can be solved:

- Analysis and sizing of physical systems (see [BE 91], [WAB 91]).
- Tolerance optimization of physical systems (see [Roel 91], [BS], [Styb 91]).

- Tuning of analog or digital controllers (e.g. [LC 90], [WN 93], [MFMV 91]).

To compare alternative concepts, the approach must be repeated for each concept. Comparison of the trade-off surfaces allows evaluation in a total context, since these surfaces take into account all user-defined performance specifications (see [BB 91], [FP 85], [Grace 89], [Toiv 84], [YA 90], [ZA 73]).

Although not mentioned as specific stages in the cycle, one should notice that the implementation of all physical equations and the development and implementation of application-specific analysis and optimization tools are time-consuming activities that require specific skills, techniques and algorithms (see [FMc 68], [GM 89], [PM 76], [Sim 96], [PMS 84], [ST 90]).

The effort spent on virtual engineering depends on the knowledge that is present in the design team. In practice, an optimal mix of application knowledge and mathematical concepts is required. A so-called 'virtual engineer' definitely needs the following skills:

- Knowledge of the application: product, used technologies, specifications, problems, possible experiments.
- Knowledge of physical modeling concepts and techniques.
- Knowledge of simulation and optimization concepts and techniques.
- Ability to program in dedicated packages like Matlab [Mlab] or Xmath [Xmath 96].

Since the application presented in this book is not widely spread, the next section starts with an historical background. It also explains the basic properties of the application and motivates the use of virtual engineering.

1.2 A glimpse on CVTs

1.2.1 Changing gears: an historical overview

Every car has a transmission. It is the collection of gears, clutches and other devices that connects the engine to the final drive. The modern automatic transmission is so transparent that the driver needs to pay little attention to this very complex piece of machinery. Yet it was not always the case (see [Got 91] for a complete overview).

In the early days, the lack of an acceptably "user friendly" transmission was a major factor in limiting sales and use of the motor car. The development of an easy-to-use transmission was the keystone to make mobility possible for everybody.

While the basic configuration of the engine was decided upon long before 1930, transmission design continued to evolve. The operation and configuration of most automatic transmissions are based on the following four major components which had been developed during a period of some fifteen years (1945-1960):

- The torque converter is a three-element unit consisting of impeller, turbine and stator. The stator is connected to the output shaft and serves to redirect the fluid flow from the driven turbine to the driving impeller for torque multiplication. When torque multiplication is not required, the stator free-wheels with the turbine and the torque converter acts as a fluid coupling (for details, see e.g. [Hur 94]).

- The friction clutch in automatic transmissions is mostly used to engage different elements of the gear train. Only in applications with restricted power, it replaces the torque converter (for details, see e.g. [Bak 92]).

- The planetary gear train is used to accelerate a vehicle with the performance requirements of today's automobiles. The engagement element (torque converter or multi-plate clutch) needs to be augmented by an automatically operated ratio-changing mechanism (usually a gear box) to yield acceptable performance.

- Control units effect the automatic operation of the gear box insuring smooth execution of shifts at appropriate vehicle speeds and loads. All transmissions developed prior to 1975 used hydraulics for both actuation and control. After 1975, many units incorporated some degree of electronic control and used hydraulics for control as well as actuation. The Chrysler A-604, introduced in 1978, was the first electronically controlled transmission in the world using hydraulics exclusively for actuation.

From the '60s through the '70s, the big manufacturers settled on a fairly standard design. Innovations and developments focused largely on cost reduction and shift quality. Only private industry spent time and effort for the development of alternative types of transmissions. In 1955, the Dutch car company DAF began production of a variable cone pulley transmission known as the Variomatic (see figure 1.2). This transmission is the predecessor of modern belt-type Continuously Variable Transmissions.

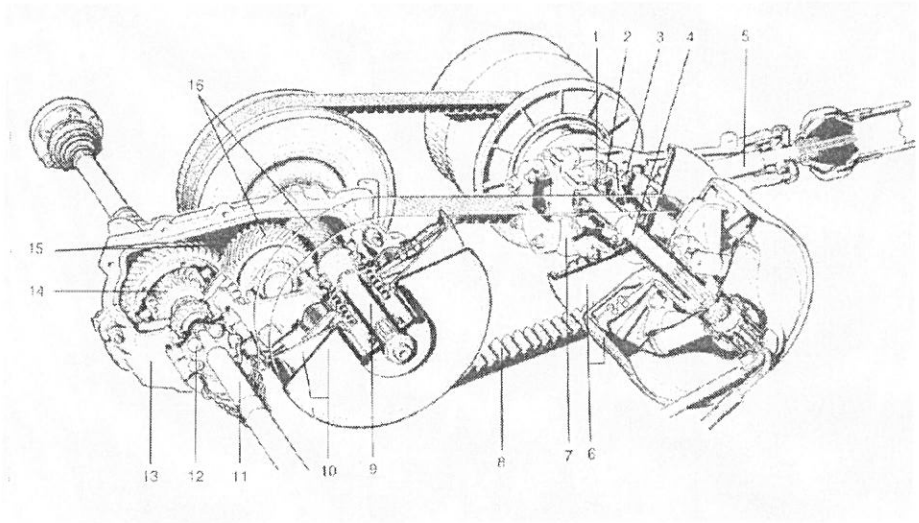

Figure 1.2 *The Variomatic from DAF, one of the fore-runners of the modern belt-type Continuously Variable Transmission. Pinion (3), driving shaft (5), primary pulleys (6), rubber V-belt (8), secondary shaft (9), secondary pulleys (10), driven shaft (11) and final drive reduction (16) can be observed (Source: [MS92]).*

In the '70s, the industry was faced with pressures for increased fuel economy and cleaner air. Transmissions, the basic design of which appeared to be stagnated since the early '60s, became an object of intensive research and development. Three-speed automatics shared the market with four- and five-speed automatics, while CVT transmissions were being developed for use in the '90s. Hydraulics were demoted from control and actuation functions to purely actuation, controlled by electronics.

Specific attention was paid to the contribution from the transmission to overall vehicle fuel consumption. In practice, this contribution is twofold:

- Presence of inherent losses

  The transmission has inherent power and thus fuel consuming features. Some of these losses are due to inefficiencies such as slip in the torque converter or friction in bearings, while other losses are those from parasitic energy consumers such as pumps required for the operation of the transmission.

- Limited ratio range

  The gear ratio affects the speed at which the engine runs. In general, lower engine speeds for the same output power result in higher engine efficiency. The greater the ratio range of the transmission, the greater the potential for reduced engine speeds.

To take this into account, lock-up torque converters were developed to reduce the torque converter losses, intelligent control units were designed to reduce the pump pressures and the ratio range of most transmissions was increased.

> *In the '70s, the role of the transmission changed from that of a slave to the demands made upon the engine, to an integral part of the engine control strategy.*
>
> *Although the current generation of classical automatic transmissions is refined and reconfigured, the industry and the government are well aware that more significant changes are required. CVTs and electronic controls hold promise of even greater fuel economy.*

The advantages of Continuously Variable Transmissions fall into three categories:

- Improved drive-ability and passenger comfort due to the lack of shifting and the corresponding uneven vehicle acceleration.
- Improved vehicle performance and fuel economy, because a CVT allows an engine to run at his most effective point with respect to torque production, power production or fuel consumption, virtually independent of vehicle speed (see [Sun 88], [NSS 90] and [Gie 89]).
- Minimum manufacturing cost for a drive train which will maximize fleet average fuel economy. A CVT is cost-effective due to its ability to optimize the fuel economy of a range of vehicles using the same transmission.

Today, some very novel and unique variable transmission configurations are being evaluated (see figure 1.3). Although the Variomatic, equipped with a rubber belt, has specific advantages over a metal belt (no need for lubrication and a higher coefficient of friction (0.4 opposed to 0.1) which reduces axial forces and thus pump pressures), the restricted durability and the high inherent power losses made it disappear. Advantages of the metal belt over the rubber belt are the power capacity and efficiency, the compactness and the fact that the entire unit runs in lubricant, thus protecting it while ensuring predictable operating conditions.

The most successful metal belt, developed by Huub Van Doorne, is a segmented belt with no connection between the segments, thereby transmitting power by compression (see figure 1.4, for details see [MS 92] and [Roo 91]). In 1987, it was put into production for passenger cars. It was equipped with hydraulic controls for both the wet multi-plate clutch and the variator. Based on this transmission, various manufacturers developed alternative CVTs with hydraulic controls (VT1H (VCST), CTX (Ford),).

The first electronic controls appeared with Subaru's ECVT, which was equipped with an electro-magnetic powder clutch controlled by a micro-processor. Shifting was still performed by hydraulic actuation and controls. In '95, Honda presented the Multimatic, a full electronically controlled CVT that uses hydraulics only for actuation.

Since engine and drive train controls evolve (see e.g. [COYVBJF 84], [DH 95], [FM 92], [GS 95], [LRWK 93], [NSS 90], [Spijk 94]), the potential benefits of the CVT increase when compared to conventional fixed ratio, stepped transmissions. Electronic engine controls will allow variable engine emissions, fuel consumption and output characteristics such as those afforded by variable valve timing and air/fuel ratio control. Engine and transmission controls will become integrated, such that the engine and transmission are treated as a single prime mover system. When this occurs, only a CVT can provide the precise, independent coupling of engine speed and torque output with drive wheel requirements which allow an optimized combination of performance, fuel consumption and emissions.

1.2.2 Functional description of a CVT

Although most material is valid for other CVTs, it is important to notice that the following description is based on the VT-1 transmission developed at VCST-VT in Sint-Truiden (see [Rov 92]).

Basics of CVT operation

The transmission uses a fixed length steel drive belt and two adjustable V-shaped pulleys to transmit the drive power and to vary the gear ratio.

The primary pulley, driven by the engine, is connected by the belt to the secondary pulley which drives the wheels. Both pulleys have one fixed half, and one mobile half which is splined to its shaft and attached to a hydraulic chamber, which controls its position.

The gear ratio is varied by moving the mobile half of the primary pulley towards or away from its fixed half, which increases or reduces the radius that the belt

is forced to follow around the pulley (see figure 1.5).
When the primary pulley mobile half is moved away from its fixed half, the drive belt is allowed to sit 'into' the pulley, providing a small belt diameter on the primary pulley. The secondary halves will be positioned at this stage, forcing the belt to follow a large diameter. This combination will provide a high gear ratio, suitable for pulling away from rest, i.e. high engine speed/low vehicle speed.
To provide a lower gear ratio, suitable for higher speed driving and cruising, i.e. low engine speed/high vehicle speed, the primary pulley mobile half is forced towards its fixed partner, which makes the belt follow a larger diameter on the primary pulley. Because the belt is of fixed length and will not stretch, this movement results in it being pulled into the secondary pulley, forcing its mobile half away from its fixed half, and providing a lower gear ratio.

The transmission control unit automatically and continuously adjusts the position of the primary pulley mobile half, to ensure the most suitable gear ratio is supplied for the prevailing driving conditions. It's this continuous adjustment which provides the smooth step-less change in gear ratio.

Driving a CVT equipped car

Driving a vehicle equipped with a CVT will initially feel strange to those used to a more conventional automatic gear box. Although the vehicle speed and rate of acceleration is as usual, controlled by movement of the throttle pedal, there is no fixed connection between the engine speed and the vehicle speed.

The selector lever has five available positions:

- Park (P) locks the transmission and must only be engaged when the vehicle is stationary with the hand brake applied.
- Reverse (R) provides reverse drive in a high gear ratio and is the only position where the transmission does not vary the gear ratio.
- In Neutral (N), no power is transmitted to the front wheels. It should be used when the vehicle is stationary with the engine running.
- Drive (D) is used for normal driving and provides forward power to the front wheels. When accelerating in D, an immediate increase in engine speed will precede a more gradual increase in vehicle speed. The gear ratio will be automatically and continuously varied in a smooth and step-less manner, always providing a ratio that matches the driving condition.
- Low (L) is also used to drive forward. The gear ratio will again be varied, although ratio up-changes will be delayed until a higher vehicle speed is

achieved. Increased engine braking is also offered in L, making it suitable for towing, hilly or sporty driving conditions.

Maximum vehicle speed can be obtained in D and in L. The vehicle will creep forward when the brakes are released while the engine is idling and either D or L is selected. Creep in the reverse direction will occur when R is selected.

Transmission components

The transmission is composed of a number of components which can be classified into three main sections. The first group consists of all elements which provide mechanical torque flow through the transmission. The elements in the second group are associated with the actuation and control unit, and enable the transmission to transmit torque, control the clutches and vary the gear ratio, to correspond with load conditions and the drivers requirement. The third group consists of components which connect the transmission to other vehicle subsystems.

- Group 1: elements which provide mechanical torque flow through the transmission.
  - Input shaft and epicyclic gear train
    Engine torque enters the transmission via a torsional damper which is bolted to the engine flywheel and splined to the input shaft. The input shaft transmits power to the planet gears. The epicyclic gear train enables the transmission to deliver driving torque to the drive shafts in two directions.
  - Forward and reverse clutches
    Both multi-plate clutches are composed of three double-sided friction plates, each sandwiched by a steel plate. They are designed to provide a smooth take up of drive, and also allow the vehicle to be held stationary while a drive gear is engaged.
  - Torque converter
    A torque converter with lock-up facilities might be added in cases where severe comfort specifications and high initial accelerations are required simultaneously.
  - Pulleys and steel belt
    Two V-shaped pulleys and a steel belt are used to transmit torque and are the heart of the transmission. Each pulley consists of one fixed half and one axially slidable half, both have 11° sloping sides.

The two movable sheaves are each connected to a hydraulic chamber which is used to control its position. These are diagonally opposed to each other in order to reduce misalignment of the belt as the gear ratio changes. Ball splines on each pulley prevent the mobile halves from rotating independently to their fixed partners.

A 24mm wide push-type steel drive belt is used to transfer torque between the two pulleys. It's assembled from more than 300 randomly selected stainless steel segments which vary in thickness to reduce belt operating noise. The flanks of each segment are tapered to match the pulley cone angle. A dimple and hollow feature helps keeping each segment engaged with its two neighboring segments. The belt is further aligned and guided by two bands, each of which is composed of ten steel straps (see figure 1.4).

The belt is tightly gripped by the halves of both pulleys. As driving torque is delivered to the primary pulley, the segments are forced against one another, creating a continuous strut which transmits force to the secondary pulley in compression, rather than in tension. The speed at which the secondary pulley revolves is determined by the gear ratio, i.e. the combined position of the drive belt on the pulleys.

- Pinion gear

  The pinion gear provides a two step reduction between the secondary pulley and the crown wheel. The reduction must be large enough to provide good vehicle performance.

- Differential unit

  Torque delivered to the crown wheel is distributed to the drive shafts via a conventional gear differential.

- Group 2: elements associated with the actuation and control unit.

  - Oil pump

    The oil pump is an external gear pump, driven at engine speed. Pressurized fluid is supplied by the pump, to the hydraulic unit, and is used for actuation of the transmission as well as for lubrication purposes.

  - Valve body and control unit

    Basically, the valve body (see figure 1.6) is used to regulate the pulley positions (gear ratio) and the clutch engagement. It does this using spool valves which respond to a variety of inputs.

    Basically, there are five inputs to the control unit: drive mode, engine speed, primary pulley speed, transmission ratio and throttle position.

These inputs are used by the control unit to regulate four output pressures: secondary pressure, primary pressure and forward and reverse clutch pressure.

Although actuation will always be performed hydraulically, three types of control are possible:

* Hydro-mechanical control: the valve-body and the control unit are integrated in a single component. The control inputs are generated by mechanical (kick-down cable, sensing shoe on the primary pulley, selector lever) and hydraulic (pitot systems) assemblies and are directly fed to the valve-body. This type of control is said to be analog, since no sampling is involved.
* Electro-mechanical control: the valve-body is additionally equipped with electro-mechanical actuators (stepper motors or linear motors) that steer the position of the spool valves. The control unit is an ECU (electronic control unit, consisting of a processor and I/O facilities). All previously defined control inputs are measured by dedicated sensors. Pressure sensors generate additional control inputs and allow to construct inner and outer control loops (master-slave). This type of control is said to be digital, since sampling is done by the ECU.
* Electro-hydraulic control: the valve body is additionally equipped with electro-hydraulic actuators (PWM valves) that steer one of the forces on the spool valves. The control unit is again an ECU. All previously defined control inputs are measured by dedicated sensors. Pressure sensors generate additional control inputs and allow to construct inner and outer control loops (master-slave). This type of control is also digital.

The secondary valve is used to control the secondary piston, while the primary valve is used to control the primary piston. The clutch valve controls the engagement of the clutch.

- Group 3: connections to other vehicle subsystems.
  - Selector mechanism to change between P, R, N, D and L-position.
  - Oil cooling facilities to restrict the oil temperature ($< 120\ ^oC$).

Additional aspects of the CVT will be addressed in detail in specific chapters of this book.

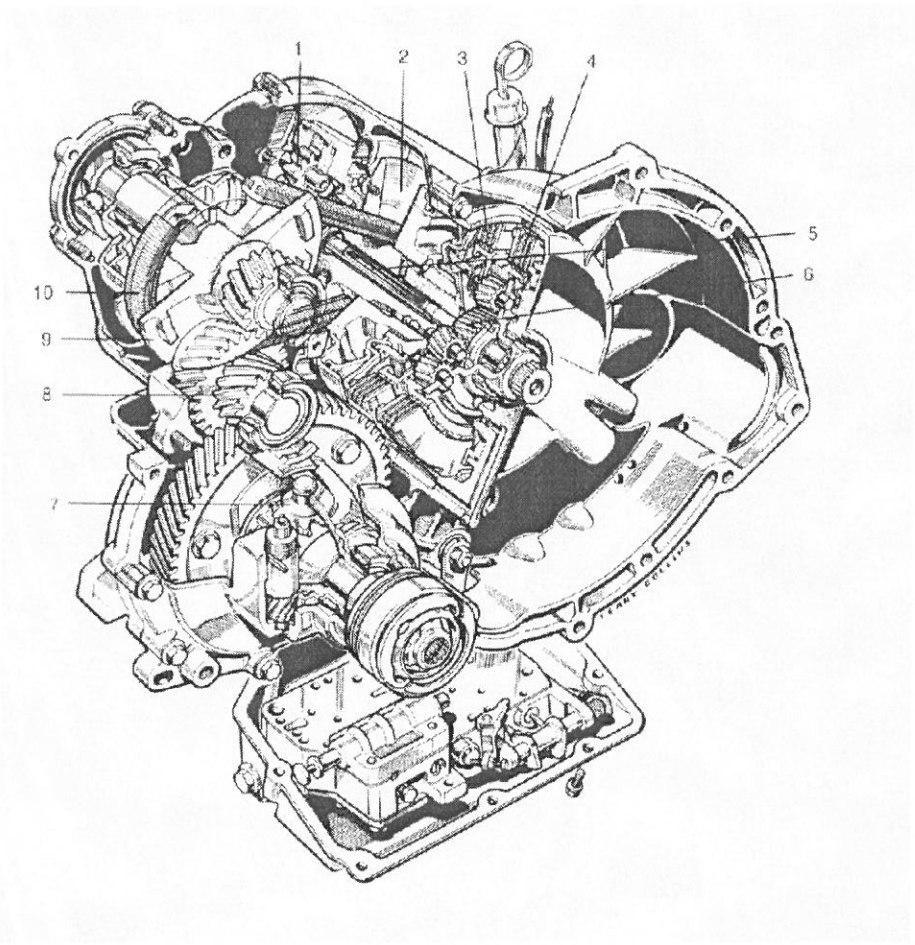

Figure 1.3 *A modern belt-type Continuously Variable Transmission. Different components can be observed: oil pump (1), primary pulleys (2), forward clutch (3), backward clutch (4), pump shaft (5), planetary set (6), differential gears (7), final drive reduction (8), secondary pulleys (9) and metal push-belt (10) (Source: [MS 92]).*

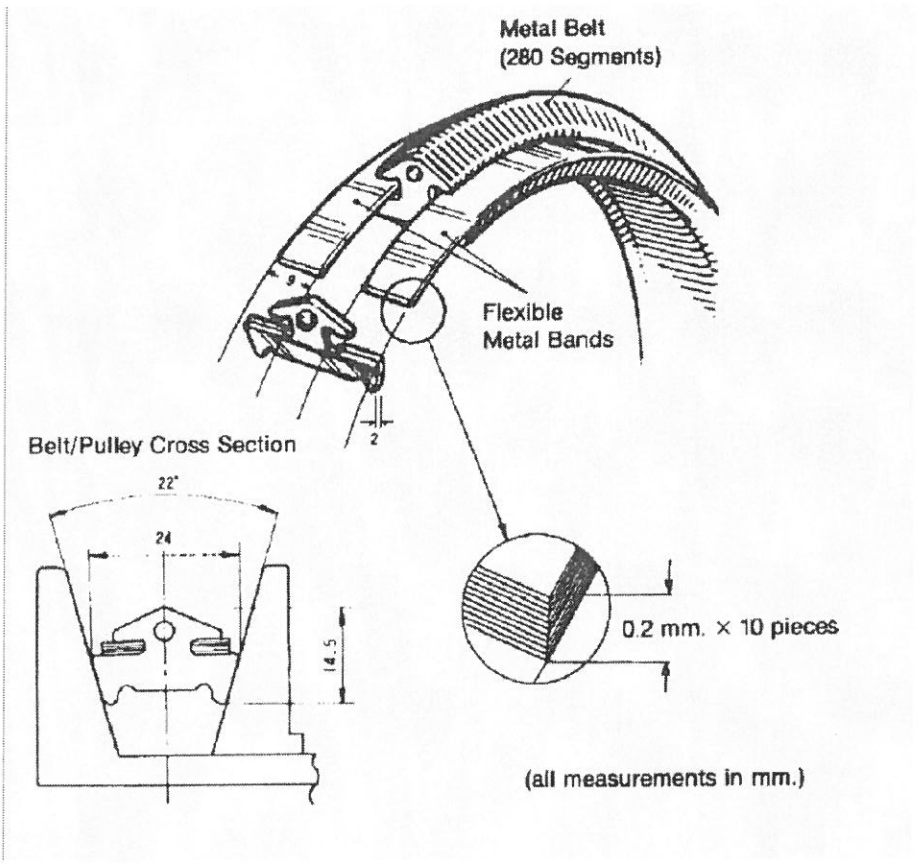

Figure 1.4 *The metal push-belt of Hub Van Doorne. This belt is used in almost all today's push-belt variator (Source: [MS 92]).*

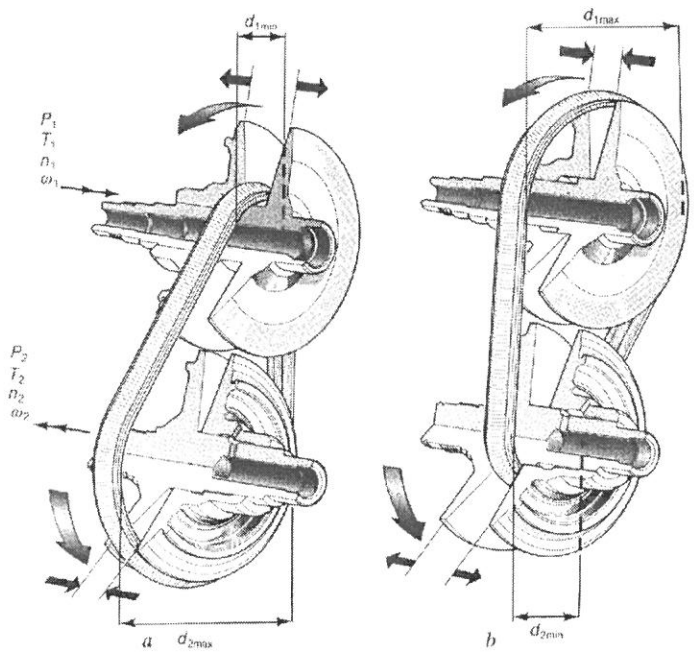

Figure 1.5 *Shifting of the CVT: pulley and belt positions corresponding to maximal ratio (LOW) (a) and a minimal ratio (OD) (b).*

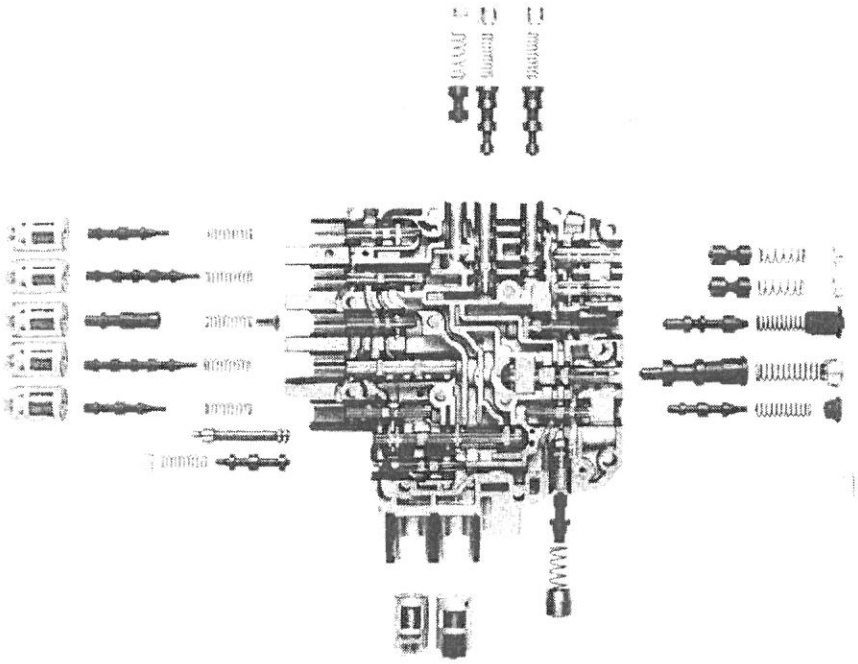

Figure 1.6 *Valve-body of an hydro-mechanically controlled transmission (Source: [MS 92]).*

1.2.3 Virtual engineering of CVTs

In the beginning of the '90s, the increased specifications with respect to performance, comfort and fuel economy forced the CVT designers to look for alternatives: couplings, valves and control mechanisms needed to be (re)designed, electronic control strategies had to be investigated and transmission control became the key element in drive train management.

This change from an hydraulic to a mechatronic system, required fundamental insights in the physical operation of the system. Furthermore, with the introduction of electronic control, additional experience and skills, apart from hydraulic engineering were required to make these new products.

Managers as well as engineers were aware that the classical prototyping approach was no longer a time- and cost effective way to compare alternatives and to generate high quality products. An urgent need for physical models and computer-aided analysis and design techniques was expressed.

In effect, the virtual engineering approach advocates the efficient evaluation of a large number of candidate designs under an effective control of the designer. It makes extensive use of computation and physical models.

The five key areas where further innovation and development is required for more effective, extensive and successful application of the approach are summarized here (see [Ng 93]):

- Effective parameterizations are required, to ensure that the true system lies in the model set.
- Effective performance indices are required and must be derived from clients specifications.
- Efficient analysis and design methods are required, to allow the evaluation of multiple alternatives and to reduce development times (see [Pha 89], [PMS 84],[BB 91]).
- Human-computer interface facilities are required, to allow the designer to control the process and to present the information in a clear and attractive way (see [FWKT 89], [PSWN 85],[Roel 91]).
- Database facilities are required, to allow the user to work with models of various complexity, with experimental results and with engineering design data.

1.3 Overview and contributions

1.3.1 Chapter by chapter overview

When confronted with a sizeable amount of research material and results, there are different ways of organizing it:

- A first possible organization is to present the theory behind modeling, optimization and control. The advantage of this organization is that theorems, definitions and proofs can be presented as research results. In this case, the application (the CVT) serves as a showcase, that fits in a general mathematical frame. The disadvantage however is that the reader might think he found the ultimate solution to all his engineering problems, because no application-oriented knowledge seems to be required.
- In the second application-oriented organization the reader is slowly introduced to the application and has the time to assimilate it. The advantage of this organization is that the reader understands all aspects of the application and of the virtual engineering approach, and that he sees the consequences of the approach with respect to required time, effort and skills. The disadvantage however is that no neat mathematical proofs can be given. However, we think the advantage of increased understanding of both the application and the approach is a good reason to select the second organization

The Chapters of this thesis are organized as follows (see figure 1.7):

- Chapter 1: Introduction and motivation

  contains an introduction and motivation for mechatronic product design. It is shown that a virtual engineering approach is required to obtain quality products in a cost and time effective way. Next, the origin and the operation of the Continuously Variable Transmission are described, and its potentials with respect to performance, comfort and fuel economy are shown. Finally, the important issues for development of a virtual engineering framework are discussed.
- Chapter 2: A system's approach to vehicle motion

  starts with a description of the physical interactions between the car and the environment. Experimental results from different car manufacturers are compared. Next, a physical car model for longitudinal and transversal motion is derived (9 DOF). For analysis of comfort, this model is linearized

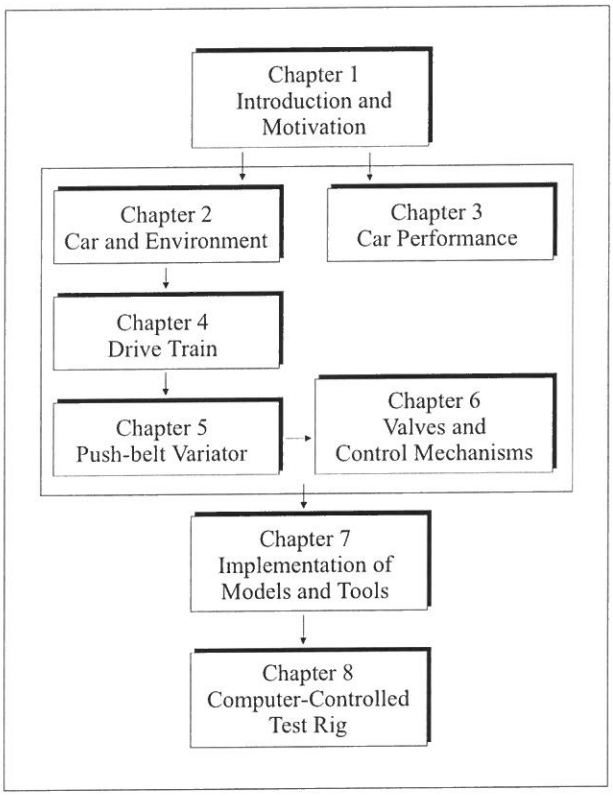

Figure 1.7 *Organization of the thesis.*

using singular perturbation techniques. For longitudinal motion control, the car model is only reduced (1 DOF), but not linearized.

- Chapter 3: Performance, fuel economy and comfort

  treats the different specifications that are imposed on today's cars. Based on specifications from various car manufacturers, a CVT challenge is defined. Special attention is given to acceleration, efficiency and comfort.

- Chapter 4: Drive train modeling and control

  treats the physical interactions between the drive train components. Based on idealized components, a model of the drive train is constructed. Reduced models for coupling mode and variator mode are derived for control purposes. Based on these models, a drive train control algorithm based on feedback linearization is obtained.

- Chapter 5: Modeling and control of the push-belt variator

  starts with the derivation of a reduced variator model, to compare the two basic control alternatives (pressure-pressure versus pressure-flow control). Next, the non-ideal characteristics of the variator are considered. Geometrical and kinematic properties and flow and pressure requirements are combined to analyze how hydraulics and mechanics interact, and to model the non-ideal variator. The efficiency of the variator is discussed also, and is used to point out the advantages of electronic control for drive train management. Finally, we present two strategies to realize shifting while avoiding belt slip, and we derive the required outer and inner controllers.

- Chapter 6: Hydraulic valves and mechanisms for piston control

  treats the modeling, analysis and optimization of typical hydraulic valves and mechanisms that are used in CVT control. First, two typical valves are discussed in detail: a double-stage flow valve and a pressure valve with hydraulic feedback. Next, the different control mechanisms for hydraulic piston control are treated: hydro-mechanical control, electro-mechanical control and electro-hydraulic control.

- Chapter 7: Implementation of models and techniques

  treats the implementation of all developed models and techniques. First, the philosophy behind the software is explained, next the software itself is discussed in detail.

- Chapter 8: A test rig for CVT valve bodies

  treats the computer-controlled test-rig for analysis and validation of valve-bodies and control mechanisms. First, the philosophy behind the test-rig is explained, next the used hardware and software are discussed in detail.

1.3.2 Contributions

Since this book is the result of an intensive cooperation between the author and at least 25 other people, either engineers from VCST or colleagues and graduate students from different faculties and universities, it is important to point out that this thesis is a result of joint research. Although initiated in the author's master's thesis (see [VD *et al* 96]), most of the work has been done within two research projects, sponsored by the IWT and VCST:

- IWT-project 92/064, *A development system for electronically controlled Continuously Variable Transmissions.* Leuven/Sint-Truiden, 1992-1994.

- IWT-project 95/0117, *Feasibility analysis and implementation of a framework for design and control of Continuously Variable Transmissions.* Leuven/Sint-Truiden, 1995-1997.

Within this context, the author had the opportunity to guide 17 master students. This work resulted in 12 master's theses (referred to as [VD *et al* 96]). Multiple details that are omitted in this book are carefully derived and explained in the theses.

Other experiments and results on modeling, design and control are described in detail in [MVD 93], [VDM 93], [VDRV 93], [VMD 94], [EVV 95], [VMMD 95], [MVMD 95], [MMVD 95], [MV 96], [Van 96a], [Van 96b], [Van 96c], [Van 96d], [Van 96e], [VVo 96a], [VVo 96b], [VVo 96c], [VVo 96d], [Van 97], [VV 96a], [VV 96b], [VV 96c], [VV 96d] and [VVM 96].

The contributions to design and control of CVTs are the following[1]:

1. Physical modeling techniques are used to obtain generic models of the environment, the car, the drive train, the engine, the various types of couplings, the push-belt variator and the wide variety of valve-bodies (see [MVD 93], [VDRV 93], [MMVD 95], [VMMD 95], [MV 96], [VD *et al* 96]).

   The characteristic behavior of each component as well as the interactions between components are described in detail. This leads to highly non-linear, multi-variable system equations, that are useful for both simulation-based analysis and design.
   Based on singular perturbation techniques, linearized equations are derived from the physical descriptions. These equations are physically parameterized and are useful for analytical analysis and design.

   The bond graph technique was very useful when dealing with specific modeling problems (stick-slip, causality, input and output assignment (see [VD *et al* 96])).

2. Specific experiments have been defined and conducted, to generate model calibration data (see [Van 96c], [Van 96d], [Van 96e], [VV 96a], [VV 96b], [VV 96c], [VV 96d] and [VVM 96]). Design-of-experiments-techniques are used to increase the reliability of the experiments and to reduce the number of experiments.

   The generic models are tuned for a wide range of applications. The applications that have been considered are (see [Van 96a]):

[1] The major contributions of this thesis are situated at the level of the coordination of the research project and its researchers, the organization of the sizeable amount of information and results in a single book and the development of a general engineering approach towards model-based design and control of CVTs.

- **Cars**: Rover Metro, Rover 216, Rover 416, X, Y, Volvo 440 and Volvo 850. Preliminary work has been done for Korean car manufacturers.
- **Combustion engines**: Volvo engines (B18U-1800 cc, N2-P20-2000 cc) and Rover engines (7 types).
- **Coupling elements**: a wet multi-plate clutch (P811) and a torque convertor (Daikin YT220).
- **Push-belt variators**: all important VCST variators (VT-175, VT-200, VT-3) and their application-specific variants.
- **Valve-bodies**: VCSTs hydro-mechanical controlled valve-body (VT1-H) and some of their electro-hydraulical controlled valve-bodies (VT1-E, EVT2, VTF). Valve-body models include the gear pump, the regulator and servo valves, the pulley and clutch pistons and the control system (actuators, sensors and intelligence).

3. The derived models have been used for design and optimization of the valves, the variator and the control system, for a wide variety of car-engine-coupling combinations (see [VVo 96a], [VVo 96b], [VVo 96c], [VVo 96d], [VD *et al* 96] for examples).

   In this context, effective performance indices, based on customer's specifications and on experimental results are defined. Specific attention is paid to fuel consumption, dynamic car performance (accelerations, speed, hill-climbing), and vertical and longitudinal drive comfort (see [Van 96b]).

4. Model-based controllers were designed, implemented and validated (if possible).

   Model-based optimization of the actual digital control algorithms (PID and (non-linear) static feedforward) has been done extensively (VT1E, EVT2, VT1F).
   To analyse and validate these controllers, a computer-controlled test-rig has been constructed (see [VMD 94], [MVMD 95], [VD *et al* 96]). Some results on fuzzy control of the valve-body for EVT2 were obtained also, (see [EVV 95]), to analyse the advantages and disadvantages of fuzzy control over gain-scheduled PID-control.

   Advanced model-based digital control algorithms are developped also. At this moment, these algorithms are being implemented and validated on the 'upgraded' power test-rig at VCST. Implementation in cars will only be possible when the electronic control unit (ECU) is no longer a cost constraint for series production.

   All derived controllers fully exploit the derived physical models. Feedback linearization theory and linear control theory are combined to design the controllers.

5. The virtual engineering framework has been implemented in Matlab and Simulink, in a tailor-made toolbox VIRTUES (VIRTUal Engineering Software) (see [Van 96a]). In this toolbox, the models and the proposed controllers are implemented. Dedicated techniques for model calibration, system analysis and optimization-based parameter design are implemented also.
   Currently, a graphical user interface and a CAD-database are being added (see [Van 97]).

It should be noticed that the project has been executed in cooperation with an industrial partner. For reasons of confidentiality, not all results are shown explicitly. For the same reason, parameters and simulation results are sometimes scaled or omitted. However, this book contains all information, required to explain the developped approach[2].

[2]This constraint may be unacceptable for the pure scientist, whose scientific beliefs may be shocked by such a non-disclosure agreement and who may argue that the essential requirements of scientific research - namely full experimental details to guarantee complete reproducibility by independent third parties - are not respected. This scientist may contact the author or VCST for additional information.

Chapter 2

Modeling Vehicle Motion

In this Chapter, we analyze the car and its physical interaction with the environment in detail. In Section 2.2, we describe the major resistances for car motion. First, the roll resistance of a car is discussed. Experimental results show that the roll characteristics mainly depend on car speed, and little on car design. Next, we analyze the effect of the surrounding air. At high car speeds, the air resistance becomes important for longitudinal motion. Lift effects due to air drag are of less importance. Wind tunnel experiments show that the distance between the car bottom and the road and the frontal surface of the car are key elements to reduce the effect of air drag and air lift. In Section 2.3, we model the stochastic disturbances that act on the car. Based on measured wind spectra, the wind dynamics are modeled by a simple linear system. To model the noise in the road profile, we use available road spectra. At constant car speeds, we proof that road profile noise may be produced by an integrator, driven by Gaussian white noise. In Section 2.4, we finally model the car. Since CVT-equipped cars are shifting continuously, both transversal and longitudinal accelerations are important for comfort and must be included in a single model. For comfort evaluation, we linearize this model using singular perturbations. For longitudinal motion control, the original model is physically reduced, but not linearized. These generic models (known equations, parameters depend on the application) are tuned (fully or partially) for 7 different industrial applications (Rover, Volvo, MG, Renault, Daewoo, Daihatsu and Hyundai).

2.1 Introduction

When dealing with car modeling (and system modeling in general), a wide variety of methods is described in the literature. The selected method mainly depends on the properties of the system under consideration and on the objectives and preferences of the modeller.

Although parameter estimation techniques are succesfully applied in car and drive train modelling (see [Lju 87], [SM 93], [MD 93]), we prefer to use physical modeling techniques to model the car and its interactions (see [Mit 84], [KL 93], [Fun 95], [Granda 90], [Granda 91], [Rau 92]).

This allows us to create generic models, with physical parameters that depend on the application. The model parameters can be obtained from car manufacturer's data-sheets and from rather familiar experiments that every car manufacturer is willing and able to do.

In a context of tuning transmission characteristics towards car and engine characteristics, it is advantageous that only data-sheets and a few experiments are required to tune the car model for a new application.

2.2 Resistances to car motion

Driving a car at a constant speed requires energy. Although part of this energy is consumed by the drive train components (friction in bearings, pump losses, slip in a coupling, transmission losses), most of the energy is required to overcome roll resistance, air resistance and gravity forces.

2.2.1 Roll resistance

Roll resistance is caused by the dissimilarity in tire deformation (see [Mit 84], [KL 93], [Dub 90] and the references therein), as shown in figure 2.1. At a constant longitudinal car speed v_c and a wheel rotation speed N, the relation between the roll resistance force F_x and the vertical force F_z is given by:

$$F_x = -f_r F_z \tag{2.1}$$

The force F_x is assumed to apply as a force on the wheel, delivering a negative torque $F_x r$ to the wheels. The roll resistance coefficient f_r mainly depends

on the tire characteristics. It remains constant at low car speeds, but changes drastically when car speed increases. Curves from the literature (see [KL 93]) and own experimental results are shown in figure 2.2.

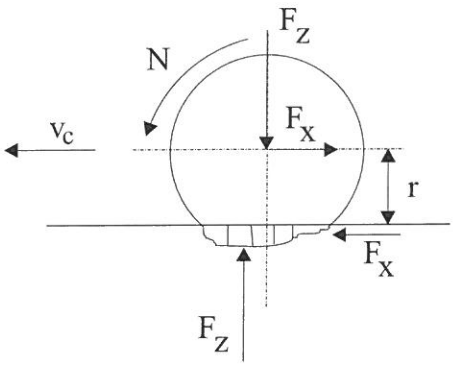

Figure 2.1 *Roll resistance: forces on a non-driven wheel, at a constant car speed v_c and a wheel rotation speed N.*

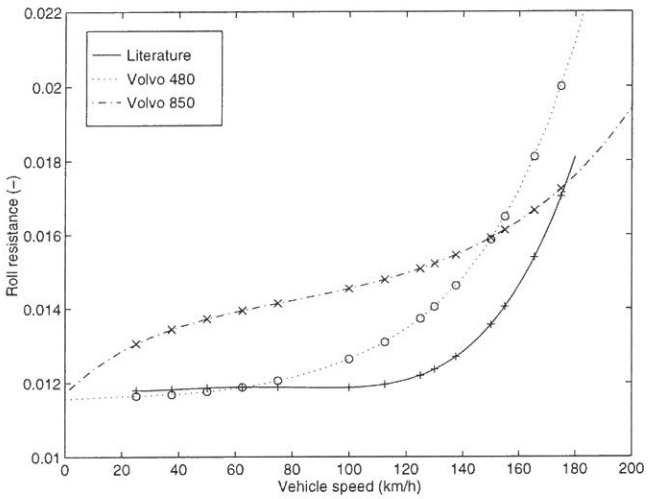

Figure 2.2 *Experimental roll resistance coefficients f_r, as a function of car speed v_c, for different cars (Source: VCST).*

2.2.2 Air drag and lift

In practice, especially at higher car speeds, air resistance forces become even more important than roll resistance forces (see [Mit 84], [KL 93]). At a constant car speed v_c and a wind speed v_w (assume the same reference direction), the horizontal and vertical forces due to car motion and air flow are given by:

$$W_x = \frac{f_x A_c \rho_{air}}{2}(v_c + v_w)^2 = C_x(v_c + v_w)^2 \tag{2.2}$$

$$W_z = \frac{f_z A_c \rho_{air}}{2}(v_c + v_w)^2 = C_z(v_c + v_w)^2 \tag{2.3}$$

These forces are assumed to apply on the center of gravity of the car. The air drag coefficient f_x and the lift coefficient f_z depend on the free height e_c between the road and the car bottom (see figure 2.3 for some characteristics from [KL 93]). Experiments in wind tunnels are required to obtain these characteristics. Typical values of all the parameters that effect air resistance forces are given in table 2.1.

Parameters	Meaning	Value	Units
f_x	Air drag coefficient	0.35	-
f_z	Air lift coefficient	0.5	-
A_c	Frontal surface of the car	1.9	m^2
ρ_{air}	Density of air	1.23	kg/m^3

Table 2.1 *Typical values of the parameters that determine the coefficients C_x and C_z (car speed v_c in km/h).*

2.3 Disturbances for car motion

Longitudinal and transversal accelerations of a car body are the result of the interplay between the driver (via throttle and brake pedal), the road (via the road profile, obstacles and slopes) and the environment (wind, tunnels). Some of these accelerations are explicitly desired by the driver, while others are considered to be disturbing. The influence of the steering wheel is neglected, since only motions in the XZ-plane are considered in this thesis. Table 2.2 shows the different disturbances for car motion.

In the next subsections, the road noise and the wind dynamics (which are stochastic disturbances) will be described in detail. Experimental data from

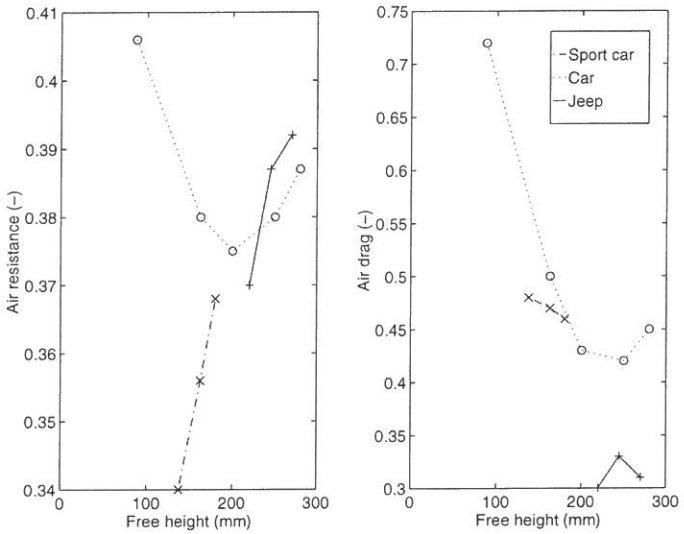

Figure 2.3 *The air drag coefficient f_x and the air lift coefficient f_z as a function of the free height e_c between the road and the car bottom, for three types of cars. A low drag and high lift coefficient guarantee highest dynamic performance (Source: [KL 93]).*

the literature (see [Dub 90], [Mit 84], [DDVDB 91]) will be used to model these disturbances by white noise driven linear dynamic systems.

2.3.1 Wind dynamics

The frequency contents of the wind can be determined experimentally (see [DDVDB 91], [Dub 90]). Figure 2.4 shows the spectrum of the wind, for nominal wind speeds and for extreme wind speeds[1].

It can be seen from this figure that there are high frequency components present, probably due to turbulence in the air. The gap between the high frequency contents (over 10 cycles/hour) and the low frequency contents (below 0.1 cycles/hour) is quite wide. The amplitude of the high frequency contents depends on the mean wind speed $\bar{v}_w$. For car applications, only the high frequency contents are important. In that case, the wind can be modeled approximately by:

[1] Due to the stochastic character of the wind, both in time and in place, reproduction of these characteristics is hard and time-consuming. Therefore, we used available experimental data.

Source		Applies on	Type of disturbance
Car			
	Drive train	Car	Deterministic
	Unbalance	Car, suspension	Deterministic
Road			
	Obstacles	Suspension	Deterministic
	Wave profile	Suspension	Deterministic
	Noise	Suspension	Stochastic
Environment			
	Wind dynamics	Car	Stochastic
	Tunnels	Car	Deterministic

Table 2.2 *Disturbances for car motion.*

$$v_w = \bar{v}_w + \xi_w(t) \tag{2.4}$$

with the noisy part of the wind $\xi_w(t)$ generated by a linear dynamic system, driven by a Gaussian white noise signal $n_w(t) = n_{0,\bar{v}_w}(t)$:

$$\dot{\mathrm{X}}_w = \mathrm{A}_w\mathrm{X}_w + \mathrm{B}_w n_w \tag{2.5}$$
$$\xi_w = \mathrm{C}_w\mathrm{X}_w + \mathrm{D}_w n_w \tag{2.6}$$

The matrices A_w, B_w, C_w and D_w can easily be computed from the experimental results, using a continuous-time frequency domain identification technique (see [VDM 96]). Figure 2.5 compares the modeled and the measured spectra of the wind.

$$\mathrm{A}_w = \begin{pmatrix} -0.6729 & -0.051 & -0.0021 \\ 1 & 0 & 0 \\ 0 & 1 & 0 \end{pmatrix}$$

$$\mathrm{B}_w = \begin{pmatrix} 1 \\ 0 \\ 0 \end{pmatrix}$$

$$\mathrm{C}_w = \begin{pmatrix} 2.0219 & 0.1894 & 0.0032 \end{pmatrix}$$

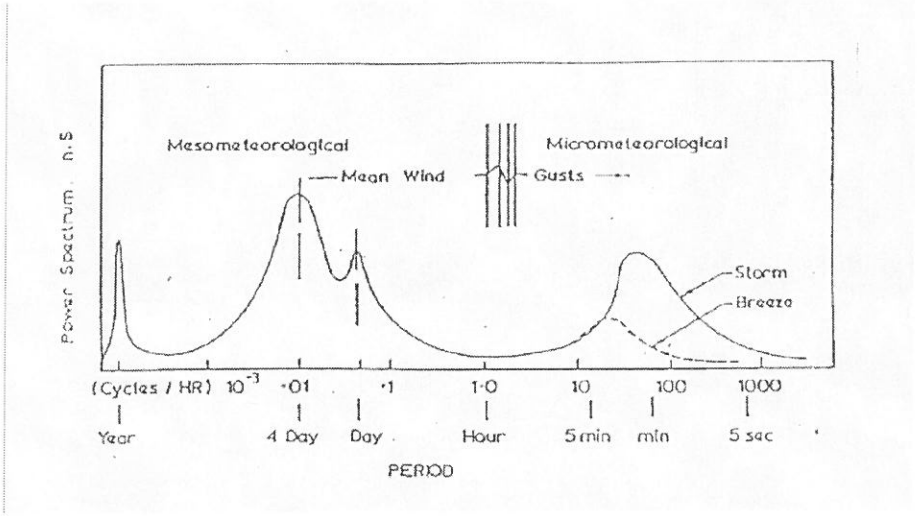

Figure 2.4 *Experimentally determined spectrum of the wind (Source: [DDVDB 91]).*

$$D_w = 0.0402$$

2.3.2 Road profile noise

For different types of road materials, the spectrum of the road profile $\xi_r(x)$ can be determined experimentally[2] (see [Dub 90], [Mit 84]).

Define the spatial frequency Ω as:

$$\Omega = \frac{2\pi}{\triangle L} \text{ (rad/m)} \tag{2.7}$$

with $\triangle L$ being the road period. From figure 2.6, it follows that for the frequency range $10^{-3} \leq \Omega \leq 1$ (rad/cm), the road spectrum $P_{\xi_r(x)}(\Omega)$ can be described by:

[2]Due to the stochastic character of the road, reproduction of these characteristics is hard and time-consuming. Therefore, we used available experimental data.

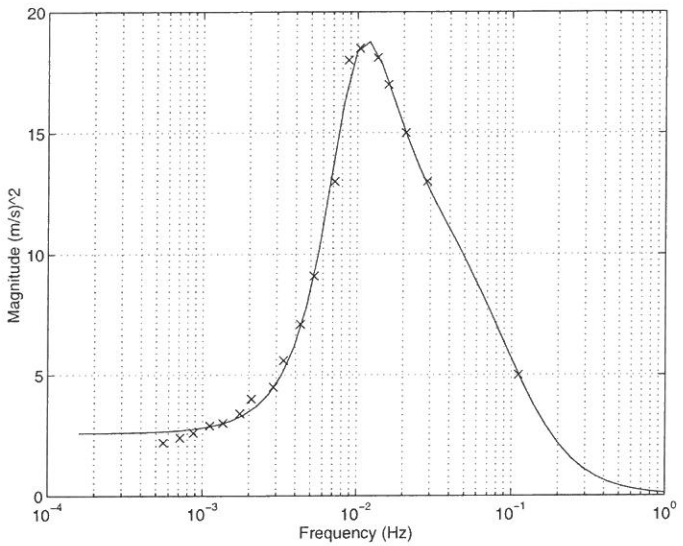

Figure 2.5 *Measured and modeled wind spectra.*

$$P_{\xi_r(x)}(\Omega) = P_0 \left(\frac{\Omega_0^2}{\Omega^2} \right) \tag{2.8}$$

In order to describe the road noise as a time sequence rather than as spatial sequence, the space-based spectrum needs to be used to compute the corresponding time-based spectrum. The relation between the spatial frequency $\Omega = \frac{2\pi}{\triangle L}$ (rad/m) and the time frequency $\omega = \frac{2\pi}{\triangle T}$ (rad/s) is found from the definition of car speed:

$$v_c = \frac{dx}{dt} = \frac{\triangle L}{\triangle T} \tag{2.9}$$

At a constant car speed v_c, it holds that:

$$\omega = v_c \Omega$$

From Parceval's theorem, it follows that:

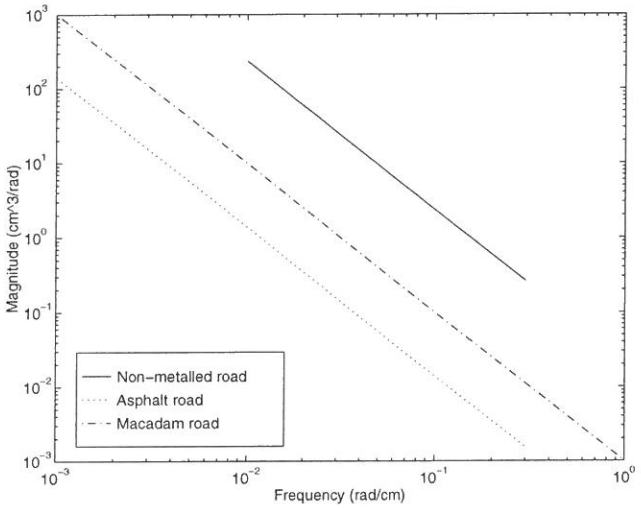

Figure 2.6 *Experimentally determined road spectrum* $P_{\xi_r(x)}(\Omega)$ *(Source: [Dub 90]).*

$$P_{\xi_r(t)}(\omega) = P_{\xi_r(x)}(\Omega)\frac{d\Omega}{d\omega}$$

The spectrum $P_{\xi_r(t)}(\omega)$ is then easily computed as:

$$P_{\xi_r(t)}(\omega) = P_0\frac{\Omega_0^2}{\omega^2}v_c \tag{2.10}$$

This corresponds to the spectrum of the output signal of a single integrator, driven by Gaussian white noise $n_r(t)$ (zero mean, $\sigma_r^2 = P_0\Omega_0^2 v_c$).

In state space representation, this corresponds to:

$$\dot{\mathrm{X}}_r = \mathrm{A}_r\mathrm{X}_r + \mathrm{B}_r n_r \tag{2.11}$$
$$\xi_r = \mathrm{C}_r\mathrm{X}_r + \mathrm{D}_r n_r \tag{2.12}$$

with

$$A_r = 0,\ B_r = 1,\ C_r = 1,\ D_r = 0$$

In practice, the disturbance $\xi_{r,f}(t)$ at the front wheels is also applied at the back wheels, but with a time delay $t_d = \frac{L_b+L_f}{v_c}$ (proportional to the wheel distance $L_b + L_f$). This implies that:

$$\xi_{r,b}(t) = \xi_{r,f}(t - t_d) \tag{2.13}$$

2.4 Car modeling

Since CVT-equipped cars are shifting continuously, both transversal and longitudinal accelerations are important for comfort (see [Ket 91]) and must be computed using one integrated car model. For comfort evaluation, this model is linearized around an operating point. For longitudinal motion control, the car model is physically reduced, but not linearized. An overview is given in figure 2.7.

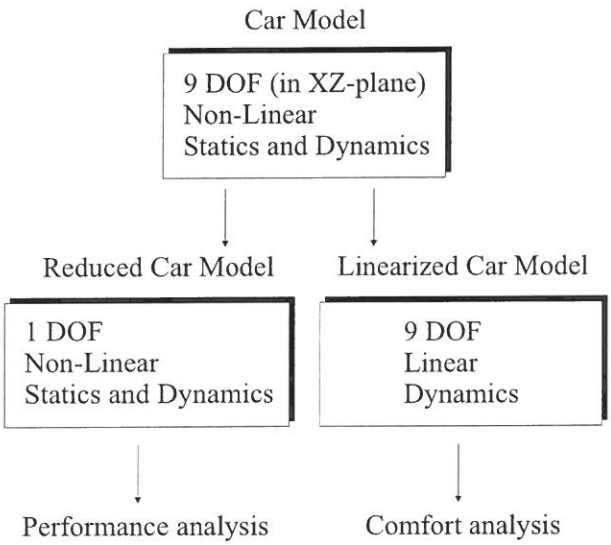

Figure 2.7 *Different car models for different purposes.*

Figure 2.8 shows the functional car model under consideration. The front wheels as well as the back wheels are reduced to equivalent single wheels, to reduce the

model complexity. Transversal (Z) and longitudinal (X) translation and rotation in the XZ-plane are considered only. Translations of the car body, the front wheel drive and suspension and the back wheel drive and suspension are considered. Rotations of the car body, the front and the back wheels are considered also[3]. The considered system has 9 degrees of freedom (9 DOF).

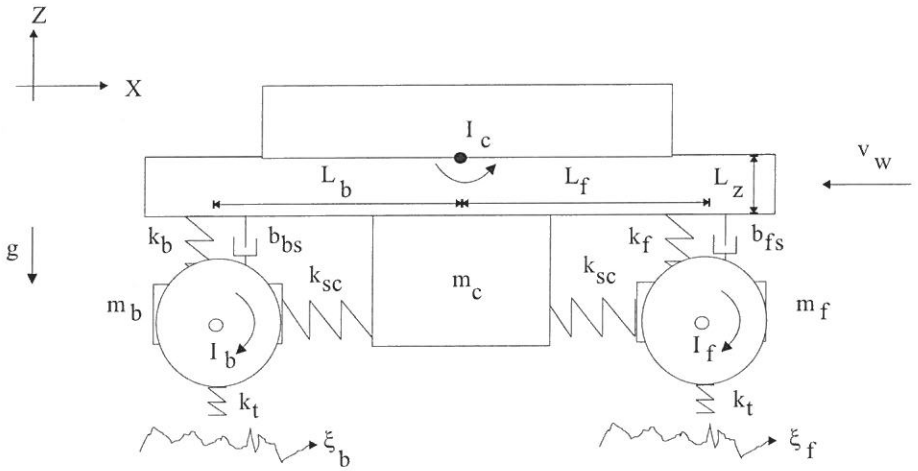

Figure 2.8 *Functional model of the car. Only motion in the XZ-plane is considered.*

Before deriving the equations that describe the car movement, an overview of all important phenomena is given (for details, see [KL 93], [Mit 84], [Granda 90]). All important parameters and their typical values are listed in table 2.3.

- The car body is modeled as a mass for translation and as an inertia for rotation.
- The stiffness and viscous damping of each suspension is modeled.
- The wheels and axles are modeled as masses for translation and as inertias for rotation. The stiffness of the tires is assumed to be linear. The damping for wheel slip is assumed to be proportional to the relative slip at each wheel. By assuming this, the complex tyre-road interaction can be described easily (see [KL 93], [Pac 76]).
- The horizontal stiffness of the connection between the wheels and the car

[3]The X-axis is assumed to remain parallel to the mean road slope. Only car body rotations relative to this slope are considered.

body is taken into account. In practice, this connection is almost infinitely stiff.

- The driving torque M_{fw} is applied at the front wheels (all CVT equipped cars use front wheel drive).

- The air resistance (air resistance W_x, air drag W_z, and assume a wind speed $v_w = \bar{v}_w + \xi_w$), the roll resistance and the road slope (assume a slope angle θ_r) generate load forces. The road noise ξ_r is taken into account also.

	Meaning	Value	Units
m_b	Mass of back wheels and axle	50	kg
m_f	Mass of front wheels and axle	70	kg
m_c	Mass of car body and passengers	1450	kg
I_b	Inertia of back wheels and axle	1.6	kgm^2
I_f	Inertia of front wheels and axle	1.6	kgm^2
I_c	Inertia of car body with passengers	1500	kgm^2
k_b	Stiffness of back suspension	27000	N/m
k_f	Stiffness of front suspension	30000	N/m
k_t	Stiffness of tires	250000	N/m
k_{sc}	Hor. stiffness of wheel-to-body connection	800000	N/m
b_{bs}	Viscous damping of back suspension	2820	Ns/m
b_{fs}	Viscous damping of front suspension	3230	Ns/m
L_b	Hor. distance between back suspension and cog	1.3	m
L_f	Hor. distance between front suspension and cog	1.1	m
L_z	Vert. distance between suspension connection and cog	0.1	m
r	Dynamic radius of the wheels	0.3	m
C_x	Roll coefficient	0.5	Ns^2/m^2
C_z	Lift coefficient	0.5	Ns^2/m^2
b_{bw}	Slip coefficient at back wheels	128000	N
b_{fw}	Slip coefficient at front wheels	128000	N
g	Nominal gravity constant on earth	9.81	m/s^2
f_r	Nominal roll resistance	0.012	-

Table 2.3 *Important parameters of the car model and typical values.*

2.4.1 A car model to describe longitudinal and vertical motion

From the torque and force balances of the car body, the following equations can be obtained:

$$\begin{aligned} I_c\ddot{\theta}_c &= M_{fw} + k_{sc}(x_f - x_2)c_3 - k_{sc}(x_1 - x_b)c_1 + k_f(z_f - z_2)c_4 + \\ &\quad b_{fs}(\dot{z}_f - \dot{z}_2)c_4 - k_b(z_b - z_1)c_2 - b_{bs}(\dot{z}_b - \dot{z}_1)c_2 \qquad (2.14) \\ m_c\ddot{x}_c &= k_{sc}(x_f - x_2) - k_{sc}(x_1 - x_b) - W_x - m_c g\sin\theta_r \qquad (2.15) \\ m_c\ddot{z}_c &= k_b(z_b - z_1) + b_{bs}(\dot{z}_b - \dot{z}_1) + k_f(z_f - z_2) \\ &\quad + b_{fs}(\dot{z}_f - \dot{z}_2) - m_c g\cos\theta_r + W_z \qquad (2.16) \end{aligned}$$

Expressions for the coefficients (c_1, c_2, c_3, c_4) and for the coordinates (x_1, z_1) and (x_2, z_2) are computed further in this section. From the torque balance on the back wheels and axle, and the force balances of the back wheels and suspension, the following equations are obtained:

$$\begin{aligned} I_b\ddot{\theta}_b &= -F_{bw}r - k_t(\xi_b - z_b)f_r r \qquad (2.17) \\ m_b\ddot{x}_b &= F_{bw} + k_{sc}(x_1 - x_b) - m_b g\sin\theta_r \qquad (2.18) \\ m_b\ddot{z}_b &= k_t(\xi_b - z_b) - k_b(z_b - z_1) - b_{bs}(\dot{z}_b - \dot{z}_1) - m_b g\cos\theta_r \qquad (2.19) \end{aligned}$$

From the torque balance on the front wheels and axle, and the force balances of the front wheels and suspension, the following equations are obtained:

$$\begin{aligned} I_f\ddot{\theta}_f &= -F_{fw}r - k_t(\xi_f - z_f)f_r r + M_{fw} \qquad (2.20) \\ m_f\ddot{x}_f &= F_{fw} - k_{sc}(x_f - x_2) - m_f g\sin\theta_r \qquad (2.21) \\ m_f\ddot{z}_f &= k_t(\xi_f - z_f) - k_f(z_f - z_2) - b_{fs}(\dot{z}_f - \dot{z}_2) - m_f g\cos\theta_r \qquad (2.22) \end{aligned}$$

The tire-road interaction at the front and the back wheels is modeled by a damping for wheel slip. To describe this effect more accurate, complex models are available in the literature (see [Pac 76], [KL 93]). In this book, damping is assumed to be proportional to the relative slip at each wheel:

$$F_{bw} = b_{bw}\frac{r\dot{\theta}_b - \dot{x}_b}{\dot{x}_b} \qquad (2.23)$$

$$F_{fw} = b_{fw}\frac{r\dot{\theta}_f - \dot{x}_f}{\dot{x}_f} \tag{2.24}$$

The wind forces W_x and W_z are given by:

$$W_x = C_x(\dot{x}_c + v_w)^2 \tag{2.25}$$
$$W_z = C_z(\dot{x}_c + v_w)^2 \tag{2.26}$$

The absolute coordinates (x_1, z_1) and (x_2, z_2), corresponding to fixed points on the car body (i.e. the points where the suspension forces apply) are related to the car body coordinates (x_c, z_c, θ_c) by geometrical relations (see figure 2.9). The coefficients (c_1, c_2, c_3, c_4) can easily be obtained.

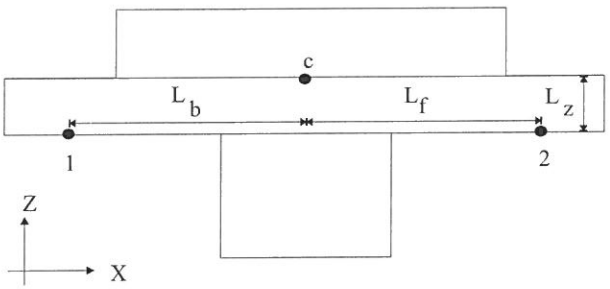

Figure 2.9 *Relations between fixed points on the car body.*

The absolute coordinates (x_1, z_1) and (x_2, z_2), corresponding to fixed points on the car body, are given by:

$$\begin{aligned} x_1 &= x_c - L_1\cos(\alpha_1 + \theta_c) \\ z_1 &= z_c - L_1\sin(\alpha_1 + \theta_c) \\ x_2 &= x_c + L_2\cos(\alpha_2 - \theta_c) \\ z_2 &= z_c - L_2\sin(\alpha_2 - \theta_c) \end{aligned}$$

with L_1, L_2, α_1 and α_2 given by:

$$L_1 = \sqrt{L_z^2 + L_b^2}$$

$$
\begin{aligned}
L_2 &= \sqrt{L_z^2 + L_f^2} \\
\alpha_1 &= \arctan \frac{L_z}{L_b} \\
\alpha_2 &= \arctan \frac{L_z}{L_f}
\end{aligned}
$$

The finite differences, required for model linearization, can easily be computed:

$$
\begin{aligned}
dx_1 &= dx_c + (L_z \cos\theta_c + L_b \sin\theta_c) d\theta_c \\
dz_1 &= dz_c + (L_z \sin\theta_c - L_b \cos\theta_c) d\theta_c \\
dx_2 &= dx_c + (L_z \cos\theta_c - L_f \sin\theta_c) d\theta_c \\
dz_2 &= dz_c + (L_z \sin\theta_c + L_f \cos\theta_c) d\theta_c
\end{aligned}
$$

The coefficients c_1, c_2, c_3 and c_4 are obtained from geometry also:

$$
\begin{aligned}
c_1 &= L_z \cos\theta_c + L_b \sin\theta_c \\
c_2 &= -L_z \sin\theta_c + L_b \cos\theta_c \\
c_3 &= L_z \cos\theta_c - L_f \sin\theta_c \\
c_4 &= L_z \sin\theta_c + L_f \cos\theta_c
\end{aligned}
$$

For $\theta_c \approx 0$, the finite difference equations reduce to:

$$
\begin{aligned}
dx_1 &= dx_c + L_z d\theta_c && (2.27) \\
dz_1 &= dz_c - L_b d\theta_c && (2.28) \\
dx_2 &= dx_c + L_z d\theta_c && (2.29) \\
dz_2 &= dz_c + L_f d\theta_c && (2.30)
\end{aligned}
$$

and the coefficients are given by:

$$
\begin{aligned}
c_1 &= L_z && (2.31) \\
c_2 &= L_b && (2.32) \\
c_3 &= L_z && (2.33) \\
c_4 &= L_f && (2.34)
\end{aligned}
$$

2.4.2 A linearized model for comfort analysis

To analyze the influence of deterministic inputs (basically changes in the applied torque M_{fw}) on transversal and longitudinal comfort, the full non-linear model is used to perform time-domain simulations. However, to analyze the influence of stochastic disturbances (road profile and wind dynamics) on transversal and longitudinal comfort, a linearized model is required to generate the frequency response characteristics (see [Mit 84], [KL 93]).

At a nominal longitudinal car speed v_c and a mean wind speed $\bar{v}_w$, linearization around an operating point Y_0 of the earlier derived non-linear equations and recombination of the terms finally results in the following description:

$$\mathrm{M}_c\ddot{\mathrm{Y}} + \mathrm{R}_c\dot{\mathrm{Y}} + \mathrm{K}_c\mathrm{Y} = \mathrm{N}_c\mathrm{W} \tag{2.35}$$

with the vector Y and the input vector W defined as:

$$\mathrm{Y} = \begin{pmatrix} \triangle\theta_c & \triangle x_c & \triangle z_c & \triangle\theta_b & \triangle x_b & \triangle z_b & \triangle\theta_f & \triangle x_f & \triangle z_f \end{pmatrix}'$$

$$\mathrm{W} = \begin{pmatrix} \xi_b & \xi_f & \xi_w & \triangle\theta_r & \triangle M_{fw} \end{pmatrix}'$$

The operating point Y_0 is computed from the nominal working conditions and the non-linear model, and is given by:

$$\mathrm{Y}_0 = \begin{pmatrix} \theta_{c,0} & x_{c,0} & z_{c,0} & \theta_{b,0} & x_{b,0} & z_{b,0} & \theta_{f,0} & x_{f,0} & z_{f,0} \end{pmatrix}'$$

The matrices M_c, R_c, K_c and N_c are given on the next page:

$$\mathrm{M}_c = \begin{pmatrix} I_c & 0 & 0 & 0 & 0 & 0 & 0 & 0 & 0 \\ 0 & m_c & 0 & 0 & 0 & 0 & 0 & 0 & 0 \\ 0 & 0 & m_c & 0 & 0 & 0 & 0 & 0 & 0 \\ 0 & 0 & 0 & I_b & 0 & 0 & 0 & 0 & 0 \\ 0 & 0 & 0 & 0 & m_b & 0 & 0 & 0 & 0 \\ 0 & 0 & 0 & 0 & 0 & m_b & 0 & 0 & 0 \\ 0 & 0 & 0 & 0 & 0 & 0 & I_f & 0 & 0 \\ 0 & 0 & 0 & 0 & 0 & 0 & 0 & m_f & 0 \\ 0 & 0 & 0 & 0 & 0 & 0 & 0 & 0 & m_f \end{pmatrix}$$

$$
\mathrm{R}_c = \begin{pmatrix}
b_{bs}L_b^2 + b_{fs}L_f^2 & 0 & -b_{bs}L_b + b_{fs}L_f & 0 & 0 \\
0 & 2C_x(v_c + \bar{v}_w) & 0 & 0 & 0 \\
-b_{bs}L_b + b_{fs}L_f & -2C_z(v_c + \bar{v}_w) & b_{bs} + b_{fs} & 0 & 0 \\
0 & 0 & 0 & \frac{r^2 b_{bw}}{v_c} & -\frac{r b_{bw}}{v_c} \\
0 & 0 & 0 & -\frac{r b_{bw}}{v_c} & \frac{b_{bw}}{v_c} \\
b_{bs}L_b & 0 & -b_{bs} & 0 & 0 \\
0 & 0 & 0 & 0 & 0 \\
0 & 0 & 0 & 0 & 0 \\
-b_{fs}L_f & 0 & -b_{fs} & 0 & 0
\end{pmatrix} \cdots
$$

$$
\cdots \begin{pmatrix}
b_{bs}L_b & 0 & 0 & -b_{fs}L_f \\
0 & 0 & 0 & 0 \\
-b_{bs} & 0 & 0 & -b_{fs} \\
0 & 0 & 0 & 0 \\
0 & 0 & 0 & 0 \\
b_{bs} & 0 & 0 & 0 \\
0 & \frac{r^2 b_{fw}}{v_c} & -\frac{r b_{fw}}{v_c} & 0 \\
0 & -\frac{r b_{fw}}{v_c} & \frac{b_{fw}}{v_c} & 0 \\
0 & 0 & 0 & b_{fs}
\end{pmatrix}
$$

$$
\mathrm{K}_c = \begin{pmatrix}
k_b L_b^2 + k_f L_f^2 + 2k_{sc} L_z^2 & 2k_{sc}L_z & -k_b L_b + k_f L_f & 0 & -k_{sc}L_z \\
2k_{sc}L_z & 2k_{sc} & 0 & 0 & -k_{sc} \\
k_f L_f - k_b L_b & 0 & k_b + k_f & 0 & 0 \\
0 & 0 & 0 & 0 & 0 \\
-k_{sc}L_z & -k_{sc} & 0 & 0 & k_{sc} \\
k_b L_b & 0 & -k_b & 0 & 0 \\
0 & 0 & 0 & 0 & 0 \\
-k_{sc}L_z & -k_{sc} & 0 & 0 & 0 \\
-k_f L_f & 0 & -k_f & 0 & 0
\end{pmatrix} \cdots
$$

$$
\cdots \begin{pmatrix}
k_b L_b & 0 & -k_{sc}L_z & -k_f L_f \\
0 & 0 & -k_{sc} & 0 \\
-k_b & 0 & 0 & -k_f \\
-k_t f_r r & 0 & 0 & 0 \\
0 & 0 & 0 & 0 \\
k_b + k_t & 0 & 0 & 0 \\
0 & 0 & 0 & -k_t f_r r \\
0 & 0 & k_{sc} & 0 \\
0 & 0 & 0 & k_f + k_t
\end{pmatrix}
$$

$$\mathrm{N}_c = \begin{pmatrix} 0 & 0 & 0 & 0 & 1 \\ 0 & 0 & -2C_x(v_c + \bar{v}_w) & -m_c g & 0 \\ 0 & 0 & 2C_z(v_c + \bar{v}_w) & 0 & 0 \\ -k_t f_r r & 0 & 0 & 0 & 0 \\ 0 & 0 & 0 & -m_b g & 0 \\ k_t & 0 & 0 & 0 & 0 \\ 0 & -k_t f_r r & 0 & 0 & 1 \\ 0 & 0 & 0 & -m_f g & 0 \\ 0 & k_t & 0 & 0 & 0 \end{pmatrix}$$

To analyze the vertical and longitudinal comfort of the car, accelerations, being states of the model, need to be computed. This is easily done by taking the time derivative of the matrix differential equation 2.35. Define the state vector X_c as:

$$\mathrm{X}_c = \begin{pmatrix} \dot{\mathrm{Y}} \\ \ddot{\mathrm{Y}} \end{pmatrix}$$

and the input vector U_c as:

$$\mathrm{U}_c = \dot{\mathrm{W}}$$

The state space representation of the system is now given by:

$$\dot{\mathrm{X}}_c = \mathrm{A}_c\mathrm{X}_c + \mathrm{B}_c\mathrm{U}_c \tag{2.36}$$

with the matrices A_c and B_c given by:

$$\mathrm{A}_c = \begin{pmatrix} 0 & I \\ -\mathrm{M}_c^{-1}\mathrm{K}_c & -\mathrm{M}_c^{-1}\mathrm{R}_c \end{pmatrix}$$

$$\mathrm{B}_c = \begin{pmatrix} 0 \\ \mathrm{M}_c^{-1}\mathrm{N}_c \end{pmatrix}$$

Note that the time derivatives of the road profiles $\xi_{r,b}(t)$ and $\xi_{r,f}(t)$ become time shifted white noise sequences.

2.4.3 A reduced model for longitudinal motion control

For drive train control, the earlier derived non-linear 9 DOF model is far too complex. For longitudinal motion control, only longitudinal motion of the car needs to be described (see [NSS 90], [Spijk 94], [GS 95], [LRWK 93]).

Assume a stiff connection between the wheels and the car body ($\ddot{x}_c = \ddot{x}_b = \ddot{x}_f$) and no transversal motion ($\ddot{z}_c = \ddot{z}_b = \ddot{z}_f = 0$). Define the total mass $m_{tot} = m_c + m_b + m_f$. By summing the force equations 2.15, 2.18, 2.21, and 2.16, 2.19, 2.22, the following equations are obtained:

$$m_{tot}\ddot{x}_c = F_{bw} + F_{fw} - W_x - m_{tot}g\sin\theta_r \quad (2.37)$$

$$0 = k_t(\xi_b - z_b) + k_t(\xi_f - z_f) + W_z - m_{tot}g\cos\theta_r \quad (2.38)$$

After summing equations 2.17 and 2.20, and assuming equal wheel speeds ($\dot{\theta}_b = \dot{\theta}_f$), it follows that:

$$(I_c + I_b)\ddot{\theta}_f = -(F_{bw} + F_{fw})r - k_t(\xi_b - z_b)f_r r - k_t(\xi_f - z_f)f_r r + M_{fw} \quad (2.39)$$

Assuming no wheel slip ($r\dot{\theta}_f = \dot{x}_f$), the equations 2.37, 2.38 and 2.39 can be combined in a single equation (1 DOF):

$$I_{tot}\ddot{\theta}_f = M_{fw} - r(W_x - f_r W_z) - m_{tot}gr(\sin\theta_r + f_r\cos\theta_r) \quad (2.40)$$

with I_{tot} the total inertia for rotation $I_{tot} = I_b + I_f + m_{tot}r^2$. If no wind is assumed ($W_x = C_x\dot{x}_c^2, W_z = C_z\dot{z}_c^2$), the final equation becomes:

$$I_{tot}\ddot{\theta}_f = M_{fw} - R_{tot}\dot{\theta}_f^2 - T_{ext} \quad (2.41)$$

with:

$$T_{ext} = m_{tot}gr(\sin\theta_r + f_r\cos\theta_r) \quad (2.42)$$

$$R_{tot} = r^3(C_x - f_r C_z) \quad (2.43)$$

2.5 Modeling of industrial applications

Based on manufacturer's data, the parameters given in table 2.3 are determined for a wide range of applications (Rover Metro, Rover 216, Rover 416, MGF, Renault Clio, MGF, Volvo 480, Volvo 850). Although sizes, masses and tyres change over the different applications, all simulations in this book are done with the parameters of table 2.3 for confidentiality reasons.

In Chapter 4, these models will be used for simulation of car motion and for longitudinal motion control. Notice that only vibrations below 25 Hz can be studied with this model. For higher frequencies, the deformation of the coach-work comes into play and a finite element model is required (see [KL 93], [Mit 84]).

Chapter 3

Comfort and Performance

In this Chapter, we treat the different specifications that are imposed on today's passenger cars. In Section 3.2, the specifications for performance and fuel economy are discussed. Based on specifications of various car manufacturers (Rover, Volvo and Chrysler) and on our experiences, a CVT benchmark test is defined. Next, it is shown how all defined indices can be computed from simulation results. In Section 3.3, we discuss a possible approach to deal with car comfort. Since comfort is related to accelerations, caused by stochastic or deterministic disturbances, it is intuitively right to use acceleration signals for comfort evaluation. From experimental results of human's sensitivity for longitudinal and transversal accelerations, two human sensitivity models are constructed. Section 3.4 shows a sample of results and conclusions.

3.1 Introduction

Performance, fuel economy and comfort of a CVT-equipped car depend on the characteristics of the following components (see [COYVBJF 84], [FM 92], [Gie 89], [Ket 91], [Rek 90], [Roo 91] and [Spijk 94]):

- The combustion engine

  For CVT equipped cars, integrated engine-transmission control allows to optimize to either performance, fuel economy or comfort. In practice, an acceptable trade-off is chosen. Two engine characteristics are of major importance (see [CA 94], [Hey 88]):

  - The *torque-speed characteristic* $T_e(N_e, \alpha_{th})$ relates the delivered static engine torque T_e to the engine rotation speed N_e and the throttle position α_{th} (see figure 3.1)
  - The *fuel consumption characteristic* $\Phi_e(T_e, N_e)$ relates the consumed fuel Φ_e to the delivered engine torque T_e and the engine rotation speed N_e (see figure 3.2).

- The coupling device

  Two possible alternatives will be discussed:

  - The *wet multi-plate clutch* has small inherent power losses, but requires an accurate control system to avoid comfort losses at engagement and at low speeds (see [Bak 92], [Gie 89], [Hur 94]).
  - The *torque converter* has larger inherent power losses due to permanent slip, but provides drive-away acceleration by torque multiplication at engagement and comfort due to inherent viscous damping. If a lock-up facility is added, the power losses are reduced significantly (see [Hur 94]).

- The variator and pinion gear

  In practice, the following parameters (exact definitions are given in Chapter 4) determine the performance of the variator and pinion:

  - The maximum (LOW) and minimum (OD, overdrive) ratio of the variator.
  - The gear ratio (FD) of the pinion.
  - The maximal torque that can be transmitted.
  - The push-belt properties (see [Roo 91]).

  The inherent power losses in the variator, due to friction between components, depend on the point of operation (see [Dev 93], [MLB 94], [Rek 90] and [Sun 88]) and are strongly related to the quality of the drive train control unit.

- The drive train control unit

  The power consumed by the oil pump and the power losses in the variator (fuel economy), the shifting quality (comfort) and the shifting speed (performance) are all determined by the quality of the drive train control unit (see [Gie 89], [Dev 93], [MLB 94], [NSS 90]).

- The car characteristics $(C_x, C_z, m_{tot}, I_{tot}), r, f_r(v_c))$ also determine comfort, performance and fuel consumption. Customers accept that fuel consumption is exchanged for performance and comfort, when car size increases.
- The environmental conditions (wind and road) are important also.

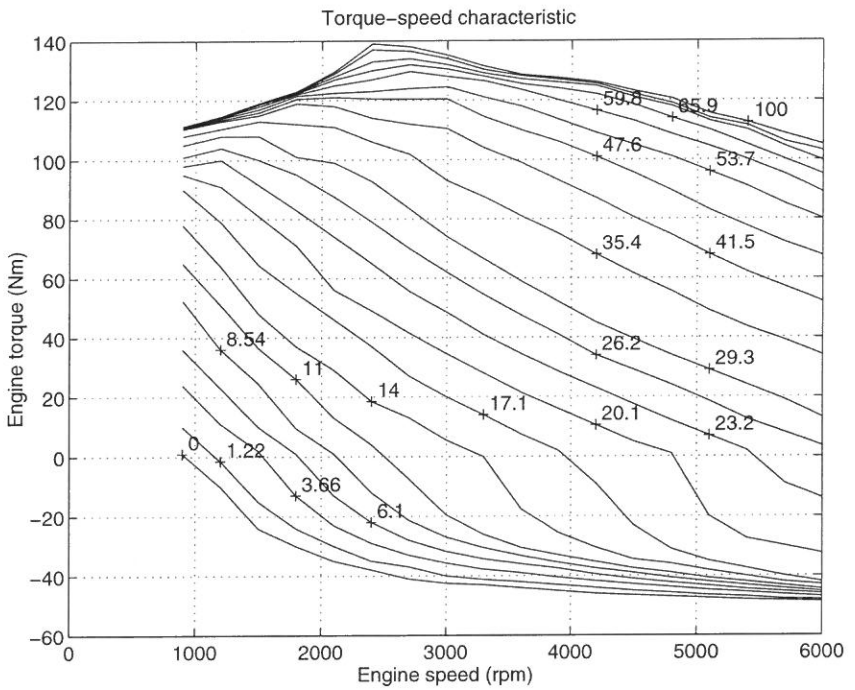

Figure 3.1 *Experimentally determined torque-speed curves (engine B18U). Lines of constant throttle position (%) are shown (Source: VCST).*

3.2 Car performance and fuel economy

3.2.1 A benchmark test for CVT-equipped cars

Comfort and fuel economy of a car are strongly related to the considered application (engine-transmission-car combination). However, since the specifications

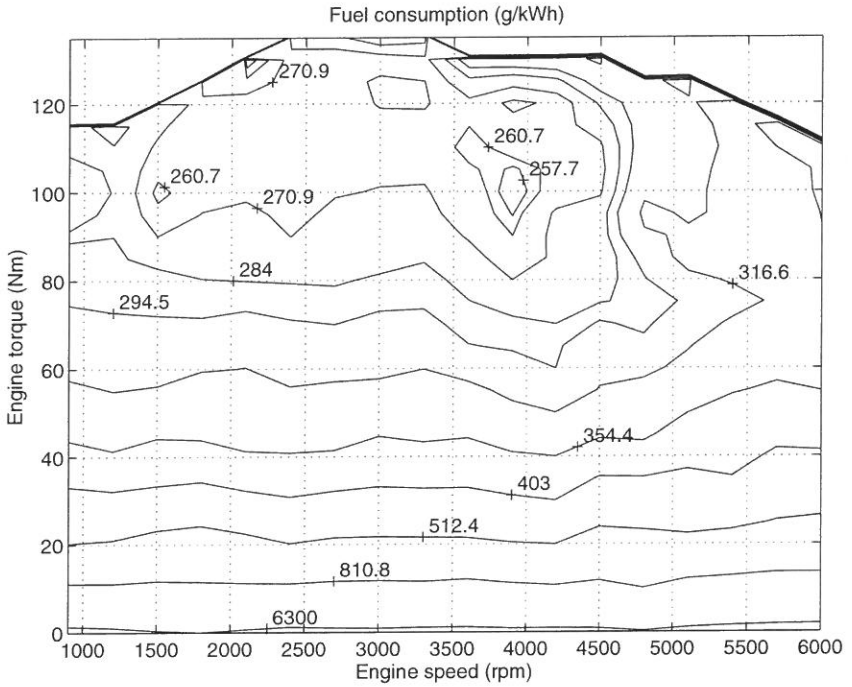

Figure 3.2 *Experimentally determined fuel consumption curves (engine B18U). Lines of constant specific fuel consumption are shown (g/kWh) (Source: VCST).*

of different manufacturers (Rover, Volvo, Chrysler) for CVT-equipped cars exhibited similarity, we organized the indices in a single benchmark test for CVT-equipped passenger cars. Within VCST, this benchmark test is now used to tune transmissions towards applications ([Van 96b]).

Table 3.1 shows the benchmark test. Nineteen different indices are included. Typical values for a specific application are added also. Once the car, the drive train and the control unit are modelled, these indices are easily computed from time-domain simulations.

3.2.2 Dynamic performance

Dynamic performance of a car is expressed by times, distances and accelerations. Four different tests (simulation or test-ride) must be conducted to obtain values

Index	Description	Objective	Units
$G_{kd,1}$	5 sec. distance at kick-down from rest	45	m
$G_{kd,2}$	Delay (0-1 km/h) at kick-down from rest	0.15	s
$G_{kd,3}$	Peak acc. at kick-down from rest	5.4	m/s^2
$G_{kd,4}$	Time to peak acc. at kick-down from rest	0.8	s
$G_{kd,5}$	0-60 mph time at kick-down from rest	8.7	s
$G_{kd,6}$	Attainable car speed (top speed)	210	km/h
$G_{kd,7}$	Max. allowed sec. speed at top speed	12000	rpm
G_{im}	40-60 mph time at kick-down from 40 mph	5.0	s
$G_{sl,1}$	Initial acceleration on a 12 % slope	0.6	m/s^2
$G_{sl,2}$	Attainable speed on a 12 % slope	85	km/h
G_{no}	Peak acc., no throttle, no brake from 60 mph	-0.3	m/s^2
$G_{fs,1}$	Consumed fuel at 40 mph	5.7	ltr/100 km
$G_{fs,2}$	Consumed fuel at 50 mph	6.3	ltr/100 km
$G_{fs,3}$	Consumed fuel at 60 mph	7.1	ltr/100 km
$G_{fs,4}$	Consumed fuel at 70 mph	8.1	ltr/100 km
$G_{fs,5}$	Consumed fuel at 80 mph	10.1	ltr/100 km
$G_{fc,1}$	Consumed fuel Urban cycle	9.5	ltr/100 km
$G_{fc,2}$	Consumed fuel Highway cycle	6.5	ltr/100 km
$G_{fc,3}$	Consumed fuel ECE cycle	11.5	ltr/100 km

Table 3.1 *A design benchmark for a CVT-equipped passenger car (Volvo 850, engine N2-P20, variator VT1-E). Speeds are given in miles per hour (mph, 1 mile = 1609,23 m).*

for all indices related to car performance:

- Kick-down starting from rest (indices $G_{kd,i}$)

  Before $t = 0$, full throttle and full brake are applied. The selector lever is in D-position. The engine is controlled at stall speed. At $t = 0$, the brake is released. The indices can be computed from car position, car speed, secondary speed and car acceleration.

- Kick-down starting from 40 MPH (index G_{im})

  Before $t = 0$, the car speed is constant and equal to 40 MPH. At $t = 0$, full throttle is applied. The index can be computed from car speed.

- Performance on a 12 % slope (indices $G_{sl,i}$)

  At $t = 0$, the road slope is 12 % and full throttle is applied. The initial acceleration and the final car speed are observed.

- Peak acceleration at no throttle, no brake, from 60 MPH (index G_{no})

  Before $t = 0$, the car speed is constant and equal to 60 MPH. At $t = 0$, the throttle is released. Shifting and engine braking will start. The index can be computed from car acceleration.

3.2.3 Fuel economy

Fuel economy is expressed by the consumed fuel per unit distance, in this case liters fuel per 100 kilometer (ltr/100 km). Basically, two types of tests (simulation or test-ride) are required to obtain values for all related indices:

- Five tests at constant car speed (indices $G_{fs,i}$)

  The car speed is held constant at the prescribed value. By combining the fuel consumption characteristic of the engine with the stationary values of the delivered engine torque and engine rotation speed, the corresponding index can be computed.

- Three tests while driving well-defined cycles (indices $G_{fc,i}$)

  A controller (the driver) forces the car to follow a prescribed speed profile (a cycle). By combining the fuel consumption characteristic of the engine with the values of the delivered engine torque and engine rotation speed, the corresponding index can be computed.

  Three different cycles are generally accepted in the automotive world. Detailed descriptions of these cycles (subcycles, handling instructions, prescribed car mass, allowed tracking error) are found in [Eur 91].

  - The Urban cycle is a good mix of city traffic and highway traffic (see figure 3.3).
  - The Highway cycle is used for highway traffic (see figure 3.4).
  - The ECE-cycle is used for city traffic (see figure 3.5).

The drive train model derived in Chapter 4 allows simulation of all required signals, under static and dynamic conditions, and is used for computation of performance and fuel economy indices.

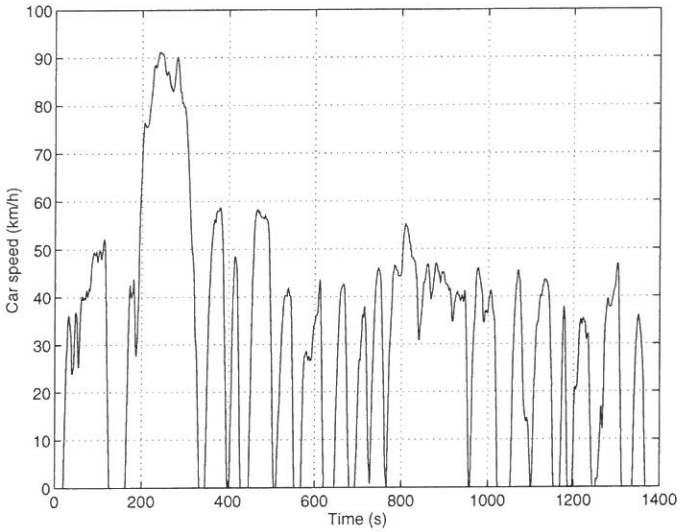

Figure 3.3 *The desired car speed profile for the Urban cycle (Source: VCST).*

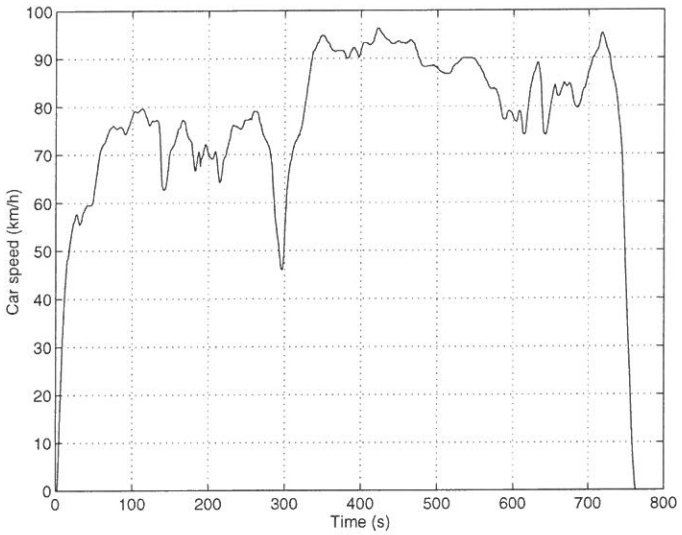

Figure 3.4 *The desired car speed profile for the Highway cycle (Source: VCST).*

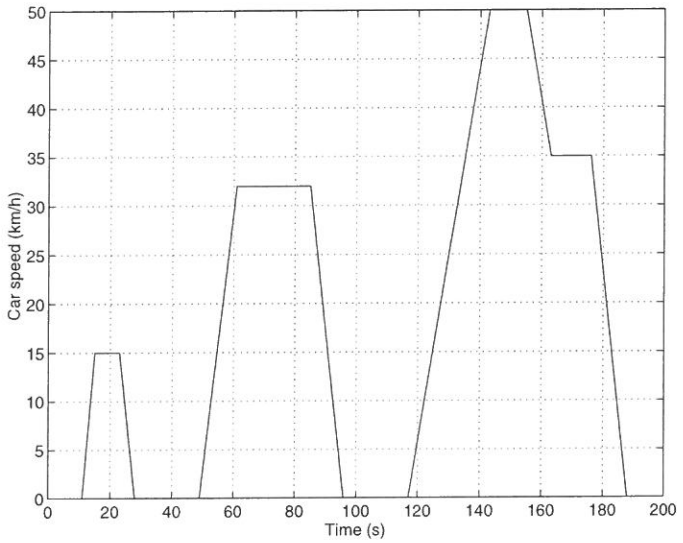

Figure 3.5 *The desired car speed profile for the ECE-cycle (Source: [Eur 91]).*

3.3 Drive comfort

Comfort is related to accelerations, caused by disturbances. The way the driver senses the accelerations determines the level of comfort in a car. In practice, two types of disturbances are distinguished:

- Stochastic disturbances: the road profile and the wind dynamics.
- Deterministic disturbances, e.g. step-alike changes in drive torque at kick down, braking or power shifting, and permanent drive torque oscillations due to drive axle compliance or CVT control.

Since comfort is related to accelerations, caused by stochastic or deterministic disturbances, acceleration signals are used for comfort evaluation. Much effort (see [ISO 86] and [VDI 87]) has been done to characterize the subjective human reactions on these accelerations. Five important factors are indicated:

- The direction of acceleration (transversal (z) versus longitudinal (x)).

- The point where the disturbance comes in (car body, suspension).
- The frequency contents of the acceleration (humans are most sensitive to accelerations within the frequency range from 1 to 80 Hz).
- The time that the disturbance works.
- The occurrence and height of peak accelerations.

From experimental data[1] of human sensitivity for harmonic longitudinal and transversal accelerations, two linear dynamic filters are constructed. These filters describe human sensitivity and are used to filter the computed or measured acceleration signals. The filtered accelerations are used to compute the comfort indices.

3.3.1 The human sensitivity filters

In the literature (see [ISO 86], [VDI 87], [Ket 91], [Mit 84], [KL 93]), most experimental results on human sensitivity are based on periodic excitations and are stated in terms of rms-values, so computation in the frequency domain is preferred. Longitudinal and transversal comfort appreciation is described by human sensitivity filters $H_{a_x}(\omega)$ and $H_{a_z}(\omega)$. The rms-values of the filtered acceleration signals $\underline{a}_x$ and $\underline{a}_z$ are computed from:

$$\underline{a}^2_{x,rms} = \int_0^\infty P_{a_x}(\omega) H^2_{a_x}(\omega) d\omega \tag{3.1}$$

$$\underline{a}^2_{z,rms} = \int_0^\infty P_{a_z}(\omega) H^2_{a_z}(\omega) d\omega \tag{3.2}$$

with $P_{a_x}(\omega)$ and $P_{a_z}(\omega)$ the spectra of the accelerations a_x and a_z. In the time domain, these human sensitivity filters take acceleration as an input, and compute the filtered accelerations.

Longitudinal sensitivity filter

A description of this filter is obtained from [ISO 86]. In the frequency range of interest (1 to 80 Hz), the filter amplitude $H_{a_x}(\omega)$ as a function of the frequency ω (rad/s) is specified as:

[1] The experimental data, found in [ISO 86] and [VDI 87], are used to construct the human sensitivity models.

$$2\pi \leq \omega \leq 4\pi \quad : \quad H_{a_x}(\omega) = 1 \tag{3.3}$$

$$4\pi \leq \omega \leq 160\pi \quad : \quad H_{a_x}(\omega) = \frac{4\pi}{\omega} \tag{3.4}$$

The non-linear filter $H_{a_x}(\omega)$ can easily be approximated by a linear filter (see figure 3.6) using a continuous-time frequency identification technique (see [VDM 96]). The filter is driven by a_x. The filtered acceleration is denoted as $\underline{a}_x$, and the state space equations of the approximating linear filter are given by:

$$\dot{\mathrm{X}}_{fx} = \mathrm{A}_{fx}\mathrm{X}_{fx} + \mathrm{B}_{fx}a_x \tag{3.5}$$

$$\underline{a}_x = \mathrm{C}_{fx}\mathrm{X}_{fx} \tag{3.6}$$

with

$$\mathrm{A}_{fx} = \begin{pmatrix} -14.30 & -111.884 \\ 1 & 0 \end{pmatrix}$$

$$\mathrm{B}_{fx} = \begin{pmatrix} 1 \\ 0 \end{pmatrix}$$

$$\mathrm{C}_{fx} = \begin{pmatrix} 12.3425 & 79.7614 \end{pmatrix}$$

Transversal sensitivity filter

A similar approach is used to describe a filter for transversal comfort evaluation. The description of the filter is also obtained from [ISO 86]. In the frequency range of 1 to 80 Hz, the filter amplitude $H_{a_z}(\omega)$ as a function of the frequency ω (rad/s) is specified as:

$$2\pi \leq \omega \leq 8\pi \quad : \quad H_{a_z}(\omega) = 0.5\sqrt{\frac{\omega}{2\pi}} \tag{3.7}$$

$$8\pi \leq \omega \leq 16\pi \quad : \quad H_{a_z}(\omega) = 1 \tag{3.8}$$

$$16\pi \leq \omega \leq 160\pi \quad : \quad H_{a_z}(\omega) = \frac{16\pi}{\omega} \tag{3.9}$$

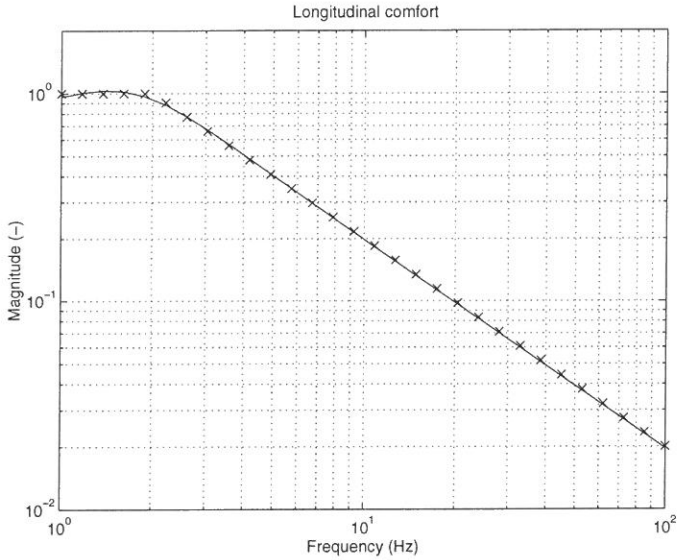

Figure 3.6 *The human sensitivity filter for longitudinal comfort (x) and its linear approximation (solid).*

This non-linear filter can easily be approximated by a linear filter (see figure 3.7) using a continuous-time frequency domain identification technique ([VDM 96]). The filter is driven by a_z. The filtered acceleration is denoted as $\underline{a}_z$ and the state space equations of the approximating linear filter are given by:

$$\dot{\mathrm{X}}_{fz} = \mathrm{A}_{cz}\mathrm{X}_{fz} + \mathrm{B}_{cz}a_z \tag{3.10}$$

$$\underline{a}_z = \mathrm{C}_{cz}\mathrm{X}_{fz} \tag{3.11}$$

with

$$\mathrm{A}_{fz} = \begin{pmatrix} -52.73 & -1240.5 \\ 1 & 0 \end{pmatrix}$$

$$\mathrm{B}_{fz} = \begin{pmatrix} 1 \\ 0 \end{pmatrix}$$

$$\mathrm{C}_{fz} = \begin{pmatrix} 52.5907 & 571.167 \end{pmatrix}$$

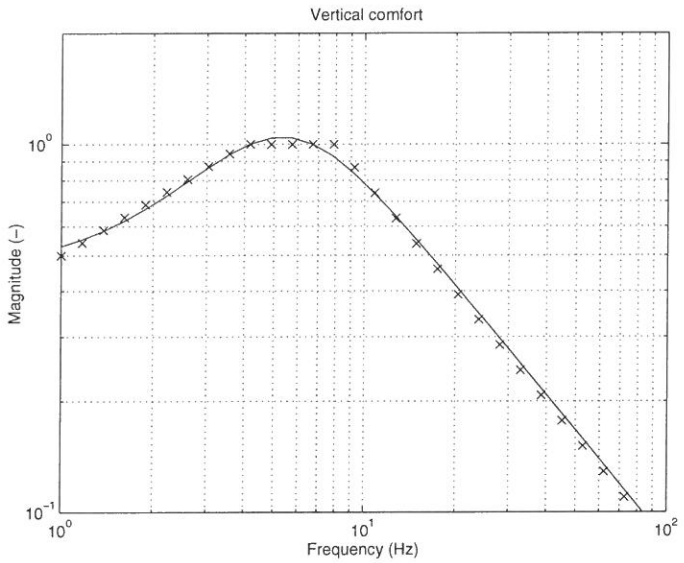

Figure 3.7 *The human sensitivity filter for transversal comfort (x) and its linear approximation (solid).*

3.3.2 Comfort indices

Although most results in the literature are stated in terms of rms-values of the filtered accelerations, practice has shown that peak values in the unfiltered acceleration signals are of similar importance, especially when evaluating the influence of step-wise throttle changes (kick-down (full throttle), tip-in (small positive throttle step at 20 km/h), tip-out (small negative throttle step at 20 km/h)) and braking actions (see [VCST 95]).

Therefore, four comfort measures are defined:

$$G_{x,rms} = 28\, \underline{a}_{x,rms} \tag{3.12}$$

$$G_{x,max} = \max_{t_1<t<t_2} \underline{a}_x(t) \tag{3.13}$$

$$G_{z,rms} = 20\, \underline{a}_{z,rms} \tag{3.14}$$

$$G_{z,max} = \max_{t_1<t<t_2} \underline{a}_z(t) \tag{3.15}$$

where t_1 and t_2 are well-defined times for each peak value test (see [VCST 95]).

From the definitions, it follows that smaller index-values correspond to higher comfort levels.

3.3.3 An integrated car-comfort model

The linearized car model derived in Chapter 2, can be combined with the human sensitivity filters, to construct an integrated car-comfort model[2].

The longitudinal comfort in a car is determined by the longitudinal acceleration a_x at the car's center of gravity (cog), while the vertical comfort at a position λ in the car is determined by the vertical acceleration a_z at that point. Both accelerations are linear combinations of the model states (see equation 2.36):

$$a_x = \ddot{x}_c \tag{3.16}$$
$$a_z = \ddot{z}_c + \lambda\ddot{\theta}_c \tag{3.17}$$

With the car's state vector denoted by X_c and the acceleration vector $\mathrm{V} = (a_x, a_z)'$, equations 3.16 and 3.17 can be combined as:

$$\mathrm{V} = \mathrm{C}_c\mathrm{X}_c \tag{3.18}$$

with the output vector C_c equal to:

$$\mathrm{C}_c = \begin{pmatrix} 0 & 0 & 0 & 0 & 0 & 0 & 0 & 0 & 0 & 0 & 1 & 0 & 0 & 0 & 0 & 0 & 0 & 0 \\ 0 & 0 & 0 & 0 & 0 & 0 & 0 & 0 & 0 & \lambda & 0 & 1 & 0 & 0 & 0 & 0 & 0 & 0 \end{pmatrix}$$

The system matrices A_{cf}, B_{cf} and C_{cf} of the combined system (car and human sensitivity filters) are given by:

$$\mathrm{A}_{cf} = \begin{pmatrix} \mathrm{A}_c & 0 \\ \mathrm{B}_f\mathrm{C}_c & \mathrm{A}_f \end{pmatrix}$$

$$\mathrm{B}_{cf} = \begin{pmatrix} \mathrm{B}_c \\ 0 \end{pmatrix}$$

[2]Note that the filters can also be combined with the non-linear model (in Matlab/Simulink, it can be done via block diagrams). In that case, the accelerations and the filtered accelerations are obtained by numerical integration

$$C_{cf} = \begin{pmatrix} 0 & C_f \end{pmatrix}$$

with the matrices A_f, B_f and C_f given by:

$$A_f = \begin{pmatrix} A_{fx} & 0 \\ 0 & A_{fz} \end{pmatrix}$$

$$B_f = \begin{pmatrix} B_{fx} & 0 \\ 0 & B_{fz} \end{pmatrix}$$

$$C_f = \begin{pmatrix} C_{fx} & 0 \\ 0 & C_{fz} \end{pmatrix}$$

This model uses the car inputs U_c to compute the filtered acceleration vector $(\underline{a}_x, \underline{a}_z)'$, required for comfort analysis. This model can be used for different purposes:

- To analyze the influence of drive torque variations, braking actions and wind dynamics on longitudinal comfort.
- To analyze the influence of drive train control on longitudinal comfort.
- To analyze the influence of road profile noise and drive torque variations on transversal comfort.
- For suspension analysis and optimization.

3.4 A sample of results and conclusions

This Section contains a sample of results that have been obtained when doing practical computations and experiments.

- Kick-down test: VT1-H versus VT1-E (simulation)

  Figure 3.8 shows the influence of the control unit and control strategy on car motion for a Rover 216, with engine 1.6K16MPI, equipped with

a VT1 variator and a wet multi-plate clutch (P811). When applying hydraulic control (VT1-H), the realized variogram is fixed and determined by the hydro-mechanical control hardware (see Chapters 5 and 6). When applying electronic control (VT1-E), the realized variogram depends on the user's specifications (economy, sport, mixed) and is determined by a look-up table in the control software (see Chapters 5 and 6). By adapting the look-up table, the performance of a car with an electronically controlled variator can be changed easily. In this simulation, an economy variogram was used, which resulted in minimal fuel consumption, high comfort (smooth acceleration, minimal two-stage engagement (see Chapter 4)) and moderate dynamic performance (compared to the potentials of a sport variogram).

- VT1-H versus VT1-F (experiments)

  Figures 3.9 and 3.10 and table 3.2 show the influence of the control unit and control strategy on car motion for a Rover 216, with engine 1.6K16MPI, equipped with a VT1 variator and a wet multi-plate clutch (P811). When applying hydraulic control (VT1-H), the realized variogram is fixed and determined by the hydro-mechanical control hardware (see Chapters 5 and 6). When applying electronic control (VT1-F), the realized variogram depends on the user's specifications (economy, sport, mixed) and is determined by a look-up table in the control software (see Chapters 5 and 6). In these experiments, a mixed variogram was used, to obtain a good trade-off in fuel consumption, comfort (smooth acceleration, minimal two-stage engagement (see Chapter 4)) and dynamic performance. With respect to comfort and dynamic performance, it follows from the acceleration and speed profiles that the electronically controlled CVT performs better than the hydraulically controlled CVT.

Throttle (%)	Car speed (km/h)	VT1-H (s)	VT1-F (s)
10	20	6.76	5.77
25	50	10.1	8.93
50	50	4.79	5.26
100	100	10.21	9.64

Table 3.2 *Dynamic performance VT1-H versus VT1-F (Rover 216, engine 1.6K16MPI). For different throttle positions, the time to reach a reference car speed was measured.*

- Variator optimization: influence of OD and FD (simulation)

  Figure 3.11 shows the influence of the variator geometry (minimal variator ratio OVERDRIVE (OD) and final drive reduction (FD), see Chapter 4) on

the consumed fuel at constant car speeds (indices $G_{fs,i}$), for a Volvo 850, with engine N2-P20, equipped with a VT1-E variator and a wet multi-plate clutch (P811). Reduced fuel consumption can be obtained by minimizing overdrive (OD) and the final drive reduction (FD). In practice, OD will be minimized, since FD must be maximized to guarantee good dynamic performance (see figure 3.12, for indices $G_{kd,1}$, $G_{kd,3}$ and $G_{kd,5}$).

- Plate clutch versus torque converter (simulation)

  Figures 3.12 and 3.13 show the influence of the coupling device (plate clutch P811 versus torque converter Daikin YT 220) on dynamic car performance. The torque converter shows higher dynamic performance (due to torque multiplication) and increased comfort (limited two-stage engagement).

- Benchmark test: plate clutch versus torque converter (simulation)

  Table 3.3 shows the simulation results of a partial CVT-benchmark test for a Rover 216, with engine 1.6K16MPI, equipped with a VT1-E variator and a wet multi-plate clutch (P811) or a torque converter (Daikin YT220). These simulations were done to analyze the influence of the coupling device on the car performance and to quantify the expected potentials of a torque converter. The test shows that the torque converter is advantageous with respect to dynamic car performance (due to torque multiplication, see Chapter 4) and that fuel consumption at constant car speeds is not affected if a converter lock-up facility is present (as we assumed here).

Index	Plate clutch	Torque converter	Units
$G_{kd,1}$	36	39	m
$G_{kd,2}$	0.12	0.05	s
$G_{kd,3}$	3.4	4.2	m/s^2
$G_{kd,4}$	0.67	0.5	s
$G_{kd,5}$	11.6	11.4	s
$G_{kd,6}$	185	185	km/h
$G_{kd,7}$	10100	10100	rpm
G_{im}	6	6	s
$G_{fs,1}$	5.92	5.92	ltr/100 km
$G_{fs,2}$	6.80	6.80	ltr/100 km
$G_{fs,3}$	7.25	7.25	ltr/100 km
$G_{fs,4}$	8.24	8.24	ltr/100 km
$G_{fs,5}$	9.18	9.18	ltr/100 km

Table 3.3 *CVT benchmark test (Rover 216, engine 1.6K16MPI, variator VT1-E): wet multi-plate clutch (P811) versus torque converter (Daikin YT220).*

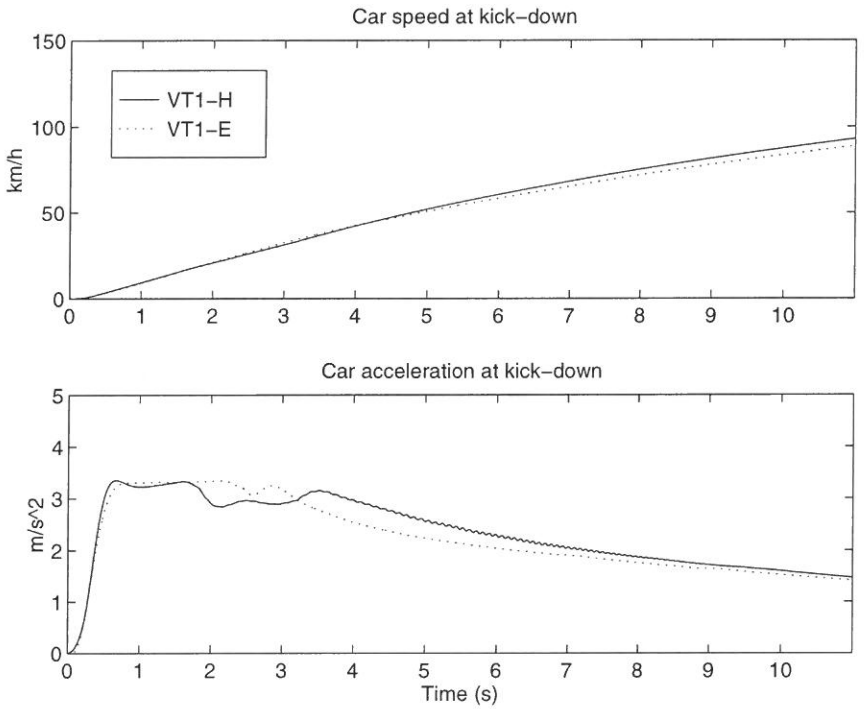

Figure 3.8 *Car acceleration and speed at kick-down from rest: influence of the control unit and control strategy on car motion for a Rover 216, with engine 1.6K16MPI, equipped with a VT1 variator and a wet multi-plate clutch (P811) (simulation).*

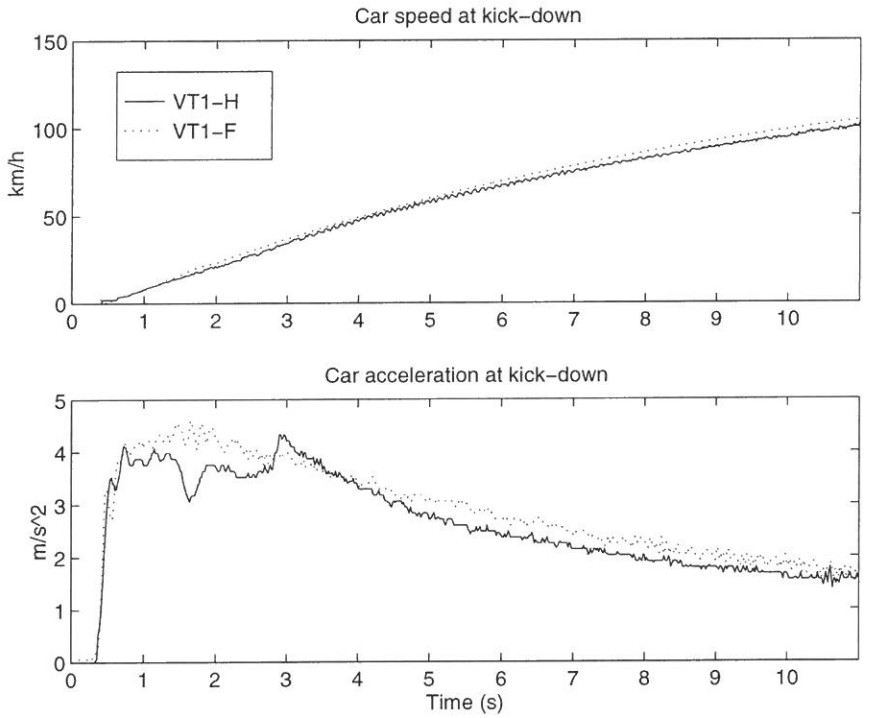

Figure 3.9 *Car acceleration and speed at kick-down from rest: influence of the control unit and control strategy on car motion for a Rover 216, with engine 1.6K16MPI, equipped with a VT1 variator and a wet multi-plate clutch (P811) (experiment).*

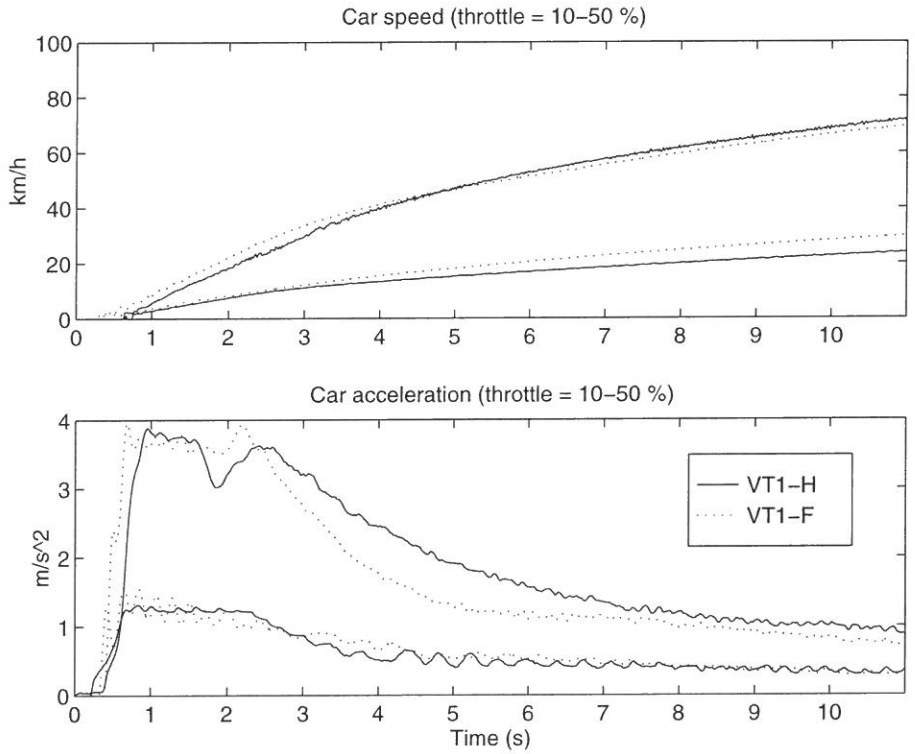

Figure 3.10 *Car acceleration and speed at intermediate throttle positions: influence of the control unit and control strategy on car motion for a Rover 216, with engine 1.6K16MPI, equipped with a VT1 variator and a wet multi-plate clutch (P811) (experiment).*

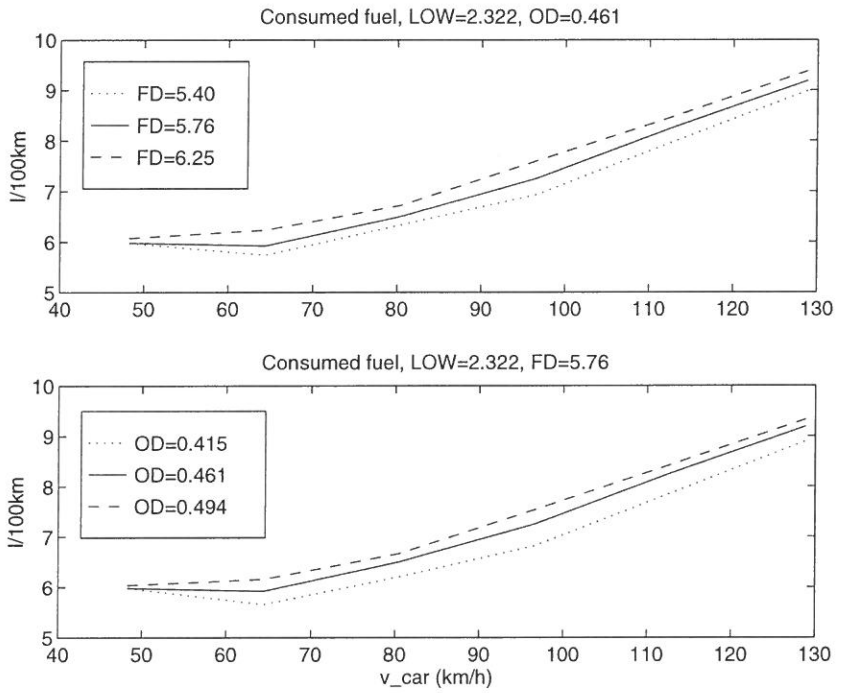

Figure 3.11 *Influence of the variator geometry (minimal variator ratio OVERDRIVE (OD) and final drive reduction (FD)) on the consumed fuel at constant car speeds (indices $G_{fs,i}$), for a Volvo 850, with engine N2-P20, equipped with a VT1-E variator and a wet multi-plate clutch (P811) (simulation).*

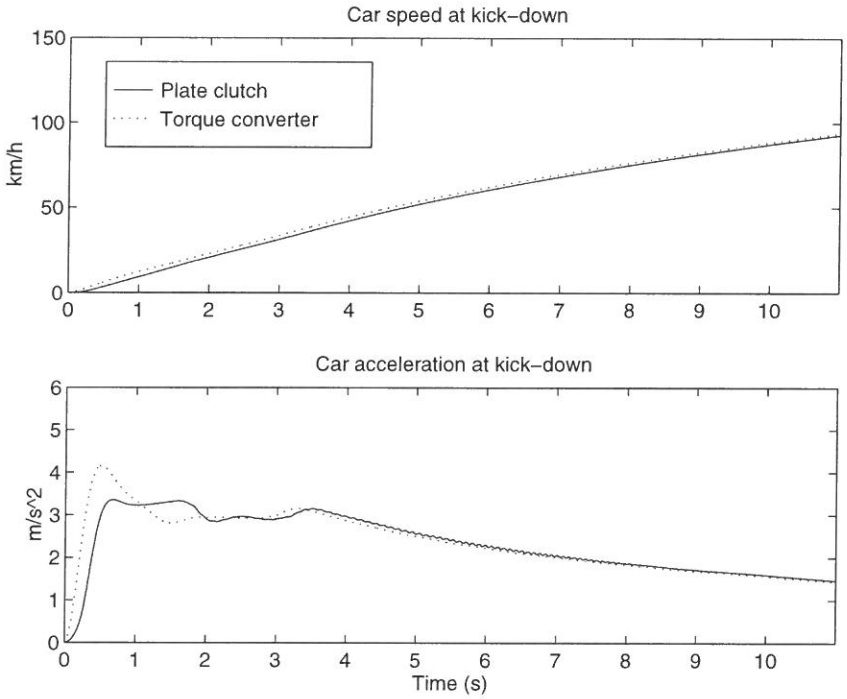

Figure 3.12 *Acceleration and speed at kickdown from rest: influence of the coupling device (plate clutch P811 versus torque converter Daikin YT 220) on dynamic car performance, for a Rover 216, with engine 1.6K16MPI, equipped with a VT1-H variator (simulation).*

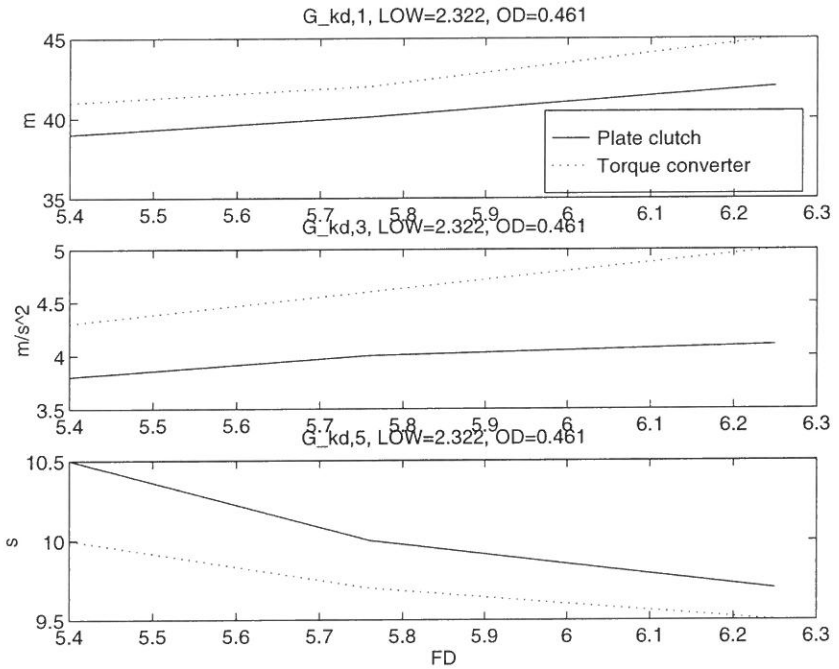

Figure 3.13 *Influence of the coupling device (plate clutch P811 versus torque converter Daikin YT 220) and the final drive reduction (FD) on dynamic car performance, for a Volvo 850, with engine N2-P20 and a VT1-E variator (simulation).*

Chapter 4

Drive Train Modeling and Control

In this Chapter, we analyze and describe a drive train with a Continuously Variable Transmission. In Section 4.2, the operation and the characteristics of all important drive train components are analyzed in detail. In order to estimate performance, fuel economy and comfort accurately, all relevant static and dynamic characteristics of the drive train and its components are considered. First, the combustion engine is treated. In the ideal case, the static characteristics are sufficient to describe the combustion engine accurately. In practice, experimental results on a B18U engine show that the delivered engine torque is delayed, inversely proportional to engine speed. Next, the wet multi-plate clutch is discussed. In the ideal case, the maximum torque that can be transmitted is only determined by the pressure in the clutch piston. Dynamic experiments with a P811 wet multi-plate clutch indicate that this torque depends on both the clutch pressure and the piston position. As an alternative for a wet multi-plate clutch, a torque converter is discussed. Two experimental characteristics are used to describe the Daikin YT220 torque converter. Afterwards, the variator is discussed. In the ideal case, it is a power transformer with a variable ratio i_v and a constant torque efficiency η_v. Experiments on a VT1-transmission indicate that efficiency varies with the operating point, and that the rate of ratio change is limited by oil flow requirements. These practical issues will be discussed in detail in Chapter 5. Finally, the gear pump, the pinion gear and the drive axle are described. In Section 4.3, the component equations derived in Section 4.1 are combined with the torque balances of the different inertias, to obtain a generic nonlinear physical model of the drive train. Physically reduced control models

for clutch mode (the variator ratio remains constant (LOW)) and variator mode (the clutch is locked, no clutch slip occurs) are derived also. In Section 4.4, we introduce the concept of variogram control and we use it for optimal drive train management. Finally, we use the idea of output feedback linearization to design optimal controllers for clutch mode and variator mode. Section 4.5 shows a sample of results and conclusions.

4.1 Description of the drive train

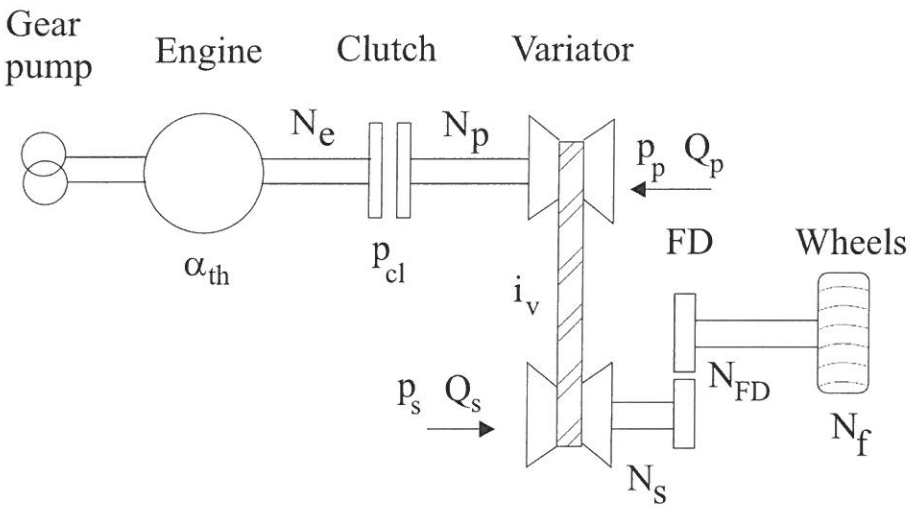

Figure 4.1 *Functional model of the drive train. The characteristics of the drive train depend on the coupling element, the metal push-belt variator, the pinion gear, the drive axle, the gear pump and the car and tire characteristics. The driver varies the throttle position α_{th} and the brake torque T_{brake}. The control unit of the transmission generates the control inputs required for drive train management. The control inputs are the variator ratio i_v and the clutch pressure p_{cl}.*

Although parameter estimation techniques are succesfully applied in car and drive train modelling (see [Lju 87], [SM 93], [MD 93]), we use physical models to describe the drive train components and their interactions (see [Mit 84], [KL 93], [Fun 95], [Granda 90], [Granda 91], [Rau 92]).

This allows us to create generic models, with physical parameters that depend on the application. The model parameters are obtained from data-sheets and dedicated experiments. In a context of tuning transmission characteristics to-

wards car and engine characteristics, it is advantageous that only data-sheets and a few experiments are required to tune the generic drive train for a new application.

Within the frequency range of interest (below 5 Hz), a lumped parameter approach is sufficient (see [Spijk 94], [GS 95], [NSS 90], [IUK 95]) to describe the drive train shown in figure 4.1). Therefore, the drive train has been considered as a system of discrete physical components that are interacting with each other:

- The combustion engine delivers the necessary power. Only the driver is allowed to change the throttle position α_{th} (i.e. ignition control is not considered).
- The wet multi-plate clutch transmits power from the engine to the variator, and is required for starting from rest. The pressure p_{cl} in the clutch piston is determined by the transmission control unit.
- The torque converter serves as an alternative for the wet multi-plate clutch. In a control context, its flexibility is rather low, because it has no control input. Only geometrical changes can be used to adapt the characteristics.
- The gear pump, driven by the engine, provides the hydraulic actuation unit with oil.
- The pinion gear, also referred to as the final drive reduction, is a gear-box that transmits power from the variator to the drive axle.
- The drive axle brings the power to the front wheels.
- The load torque is determined by the car and tire characteristics (R_{tot}), by environmental conditions (T_{ext}) and by the brake torque T_{brake}, that is applied by the driver.

Before deriving the equations of the drive train, a functional model of the drive train is discussed (see figure 4.2). Although the model is derived for a drive train with a wet multi-plate clutch, it can easily be adapted for a drive train with a torque converter. The following phenomena are taken into account:

- The engine is described as a nonlinear torque source, modulated by the engine speed and the throttle position. Internal friction is taken into account implicitly, in the static torque characteristic. The pump torque, required to drive the gear pump, mainly depends on pump pressure and pump speed.

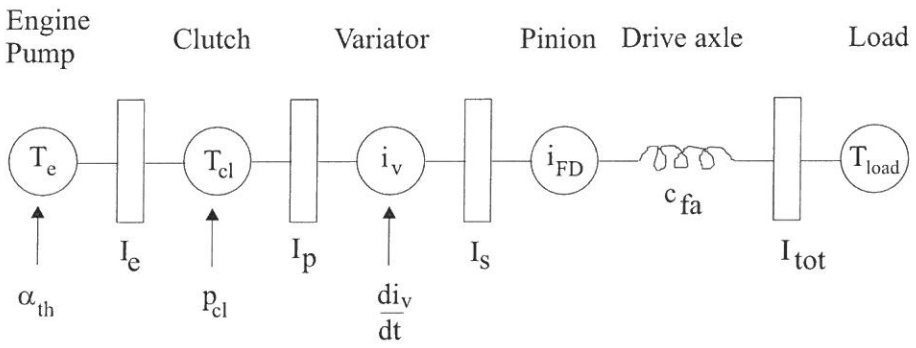

Figure 4.2 *A functional model of the drive train.*

- The flywheel inertia, the pump inertia, half of the clutch inertia and the inertia of the torsion damper are combined in a single rotational inertia, that rotates at engine speed.
- The clutch is described as a nonlinear friction element, modulated by the clutch pressure and the clutch slip.
- Half of the clutch inertia, the inertia of the primary axle and the inertia of the primary pulley are combined in a single rotational inertia, that rotates at primary speed.
- The variator is described as a variable transformer with a fixed torque efficiency (to take into account friction losses in the belt-pulley system and in all bearings. In practice, the torque efficiency is not constant, but strongly determined by the operating point of the variator (see Chapter 5)).
- The inertia of the secondary pulley, the inertia of the secondary axle and half of the pinion gears inertia is combined in a single rotational inertia, that rotates at secondary speed.
- The pinion gear-box is described as a fixed transformer with no torque losses.
- The drive axle is modeled as a linear torsional spring. The damping of the axle material is neglected.
- The total car inertia, reduced to the wheels, half of the pinion gear inertia and the drive shaft inertia are combined in a single rotational inertia I_{tot}, that rotates at wheel speed.

- The total load torque is reduced to the wheels and contains roll and air resistances, load due to road slope and brake torque.

In the following sections, the static and/or dynamic characteristics of all drive train components are discussed. Next, the system's torque balances and the drive train component characteristics are combined, to derive a generic (static and dynamic) drive train model. Inertia effects are modelled by discrete inertances, related to the different independent rotation speeds in the drive train (engine speed, primary speed, secondary speed, wheel speed). Internal friction (e.g. in bearings) is taken into account implicitly (e.g. in the engine characteristic) or explicitly via experimental component efficiency maps (e.g. torque efficiency of the variator).

4.2 Drive train component models

4.2.1 The combustion engine

The delivered static engine torque $T_e(\dot{\theta}_e, \alpha_{th})$ depends on the engine rotation speed $\dot{\theta}_e$ and the throttle position α_{th}, while the consumed fuel $\Phi_e(T_e, \dot{\theta}_e)$ depends on the delivered engine torque T_e and the engine rotation speed $\dot{\theta}_e$ (see [CA 94], [Hey 88]):

$$T_e = T_e(\dot{\theta}_e, \alpha_{th}) \tag{4.1}$$

$$\Phi_e = \Phi_e(T_e, \dot{\theta}_e) \tag{4.2}$$

In the ideal case, these static characteristics are sufficient to describe the engine. However, in practice, when evaluating clutch engagement, the torque time constant needs to be taken into account. An experimental curve from the literature and experiments on a B18U engine (see figure 4.3) show that the torque time constant $\tau_e(\dot{\theta}_e)$ strongly depends on the engine speed $\dot{\theta}_e$ (see [DH 95], [VCST 92]).

This is taken into account by embedding the static engine model in the following non-linear state-space system:

$$\dot{x_T} = \frac{1}{\tau_e} x_T + \frac{1}{\tau_e} T_e(\dot{\theta}_e, \alpha_t) \tag{4.3}$$

$$T_{e,dyn} = x_T \tag{4.4}$$

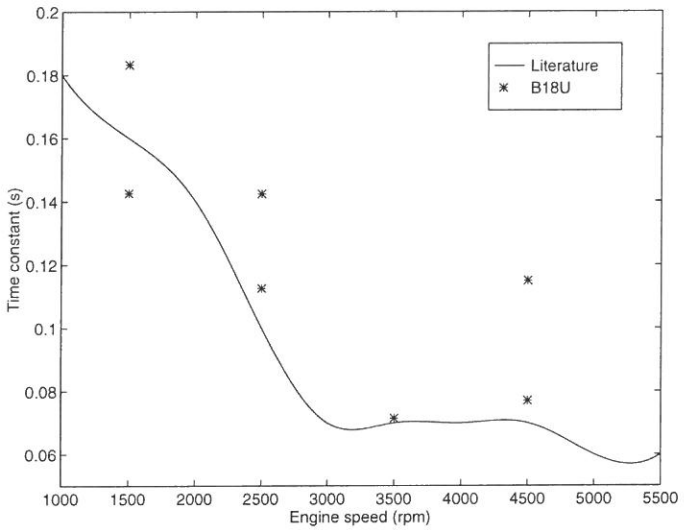

Figure 4.3 *Experimental torque time constant $\tau_e(\dot{\theta}_e)$ as a function of engine speed $\dot{\theta}_e$ (literature (see [DH 95]) and B18U (see [VCST 92])). Deviations of 40 ms were measured, due to changes in temperature, internal friction and instantaneous torque.*

The dynamic torque $T_{e,dyn}$ represents the instantaneously delivered torque and is used to compute instantaneous fuel consumption. This approximation of reality is sufficiently accurate for most operating conditions.

The engine and flywheel inertia are included in the engine inertia I_e, that rotates at engine speed.

4.2.2 The wet multi-plate clutch

The wet multi-plate clutch exists of axially slidable friction plates that are connected either to the engine shaft or to the primary shaft by a cottering (see figures 4.4 and 4.5). A piping in the primary shaft brings oil in the clutch piston. The clutch can transmit torque as soon as the plates make contact. By varying the pressure p_{cl} in the clutch piston, the distance between the plates and the torque to be transmitted is varied. The oil is also used for lubrication and cooling of the clutch plates, via small grooves in the plate surfaces (see [BW 91], [Bak 92]). A linear spring ensures that the clutch opens when zero pressure is applied.

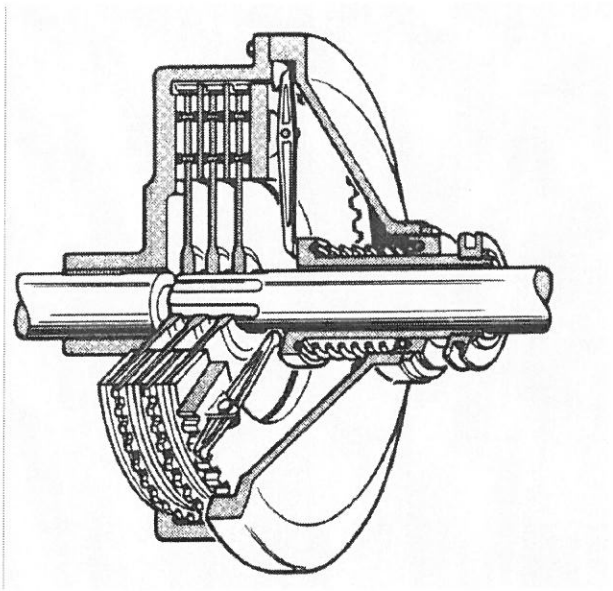

Figure 4.4 *An example of a wet multi-plate clutch. The clutch exists of axially slidable friction plates which are connected either to the engine shaft or to the primary shaft by a cottering. A piping in the primary shaft brings oil in the clutch piston. The clutch can transmit torque as soon as the plates make contact (Source: [Hur 94]).*

The clutch is described as a modulated friction element. If the clutch plates are infinitely stiff (with respect to compression) and never loose contact, the clutch is considered to be ideal. For an ideal clutch, the maximal torque T_{max} that can be transmitted is determined by the applied clutch pressure p_{cl} and equal to:

$$T_{max} = n_{cl}\mu_{cl}A_{cl}R_{cl}\eta_{cl}(p_{cl} - p_{cl,0}) \tag{4.5}$$

Table 4.1 explains the meaning of the parameters. The friction coefficient μ_{cl} is determined by the absolute clutch slip $s_{N,cl} = \dot{\theta}_e - \dot{\theta}_p$ (the difference between the engine speed and the primary speed), by the oil temperature T_{oil} and by the used oil and plate material. Experiments with different oil types (Esso EZL 799 and Lubrizol, see [Van 96c]) show that the friction coefficient can be described by the following equation:

$$\mu_{cl} = (\mu_{dyn} - \mu_{stat})\text{tgh}(\nu_{cl}s_{N,cl}) + \mu_{stat}\text{sign}(s_{N,cl}) \tag{4.6}$$

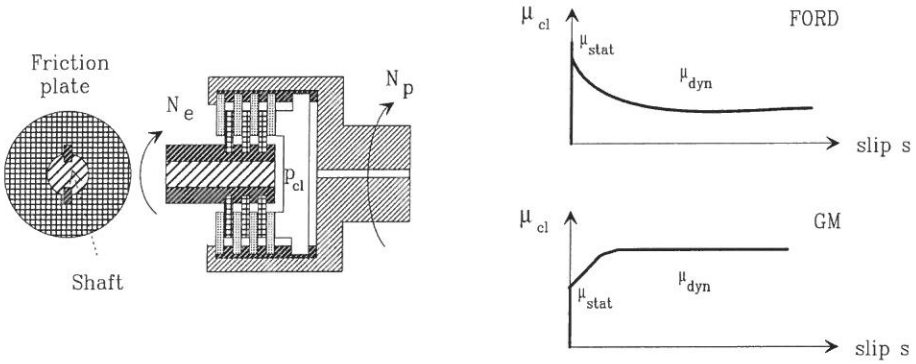

Figure 4.5 *A cross section and a longitudinal section of the wet multi-plate clutch. For reasons of clarity, only the engine shaft and a connected friction plate are shown in the cross section. For the same reasons, the spring is not shown in the longitudinal section. To guarantee smooth lock and un-lock transitions, the friction coefficient μ_{cl} must be well-designed. It seems that no optimal curve exists, since Ford asks for $\mu_{dyn} \leq \mu_{stat}$, while General Motors asks for $\mu_{dyn} \geq \mu_{stat}$ (Source: [MS 92]).*

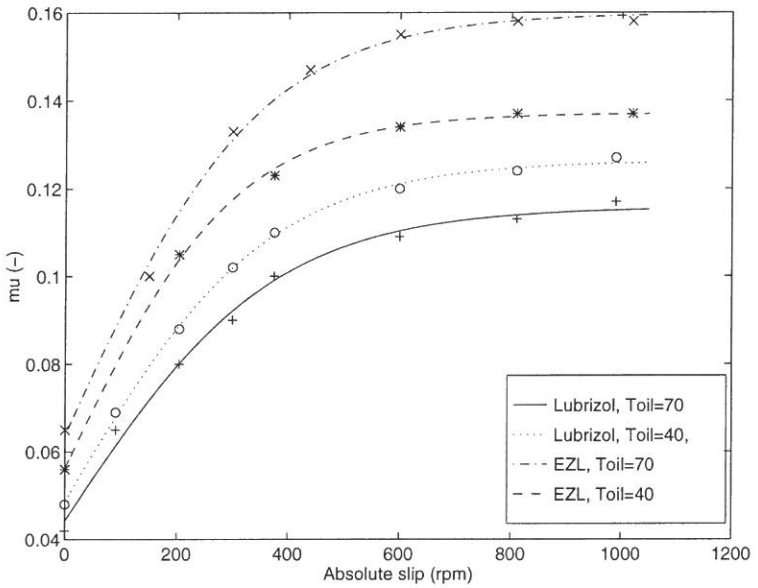

Figure 4.6 *Experimentally determined clutch friction coefficient μ_{cl} as a function of absolute clutch slip, for Esso EZL 799 and Lubrizol oil, at different temperatures (Source: [Van 96c]).*

Parameter	Meaning
$p_{cl,0}$	Minimal clutch pressure required for plate contact
A_{cl}	Pressure surface of the clutch piston
R_{cl}	Mean friction radius of a plate
n_{cl}	Number of active friction surface pairs
η_{cl}	Pressure efficiency (2.5 % loss per surface pair (see [Bak 92]))

Table 4.1 *Parameters to describe an ideal clutch.*

Parameter	EZL, 40°	EZL, 70°	Lubrizol, 40°	Lubrizol, 70°
μ_{stat}	0.0563	0.0638	0.0486	0.0443
μ_{dyn}	0.1371	0.1598	0.1263	0.1157
ν_{cl}	0.0033	0.0029	0.0028	0.0027

Table 4.2 *Friction coefficient parameters, for different types of oil (Esso EZL 799 and Lubrizol) and operating conditions ($T_{oil} = 40^o$ and $T_{oil} = 70^o$). EZL has positive temperature gradients, while Lubrizol has negative gradients.*

The parameters μ_{stat}, μ_{dyn} and ν_{cl} are found by solving a non linear least squares problem with the Matlab optimization toolbox (see [Mlab]). Table 4.2 shows the parameters of the two types of oil at different temperatures.

Until here, it is assumed that the clutch plates never loose contact. In practice, due to an additional clutch spring (to open the clutch at rest) and due to the finite stiffness of the clutch plate package, the clutch opens if insufficient clutch pressure is applied ($p_{cl} < p_{cl,0}$). Since the plate distance is not observed by the control unit, controlled timing of clutch engagement is difficult.

From figure 4.7, the force equation of the slidable part of the clutch is obtained, to compute the displacement x_{cl} of the clutch piston:

$$m_{cl}\ddot{x}_{cl} + b_{cl}\dot{x}_{cl} + (k_{pl}(x_{cl}) + k_{cl})x_{cl} = (p_{cl} - p_{cl,0})A_{cl} \tag{4.7}$$

The meaning of the parameters is explained in table 4.3. Note that $x_{cl} \geq 0$ implies plate contact, while $x_{cl} < 0$ implies lost contact. The force-position characteristic $F_{pl} = k_{pl}(x_{cl})x_{cl}$ of the VT1 clutch package has been determined experimentally (see [Van 96d] and figure 4.8). The other parameters are obtained

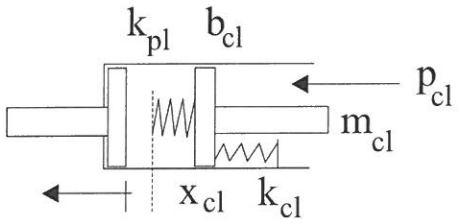

Figure 4.7 *A functional model for clutch piston displacement. The non-contact spring represents the stiffness of the clutch plate package. The make-contact situation is the reference position for the displacement x_{cl} of the clutch piston. For $x_{cl} \geq 0$, the clutch plates are in contact and compressed. For $x_{cl} < 0$, the clutch plates loose contact and no torque is transmitted.*

Parameter	Meaning
m_{cl}	Mass of the slidable clutch part
b_{cl}	Viscous damping between piston and housing
k_{cl}	Stiffness of the additional clutch spring

Table 4.3 *Additional parameters of a non-ideal clutch.*

from technical drawings and clutch engagement experiments and are included in table 4.4.

If this effect is taken into account, the instantaneous maximal torque that is transmitted equals:

$$T_{max} = n_{cl}\mu_{cl}R_{cl}\eta_{cl}k_{pl}(x_{cl})x_{cl} \tag{4.8}$$

with x_{cl} computed from the force equation.

The clutch inertia is equally distributed to the engine rotation inertia I_e and to the primary rotation inertia I_p.

4.2.3 The torque converter

A torque converter (see figure 4.9) exists of an impeller, a turbine and a stator, mounted in the same housing. In most conditions, the driving member (impeller) rotates faster than the driven member (turbine). At start-up, large differences exist between the kinetic energy of the fluid in the driving and driven members.

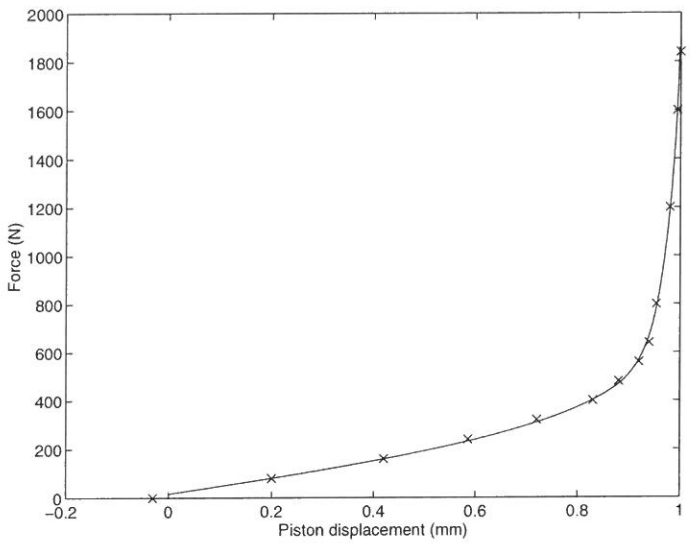

Figure 4.8 *The experimentally determined force-displacement characteristic of the VT1 clutch plate package relates the force $k_{pl}(x_{cl})x_{cl}$ to the clutch piston displacement x_{cl}. The test has been repeated 10 times, to check for hysteresis. No significant hysteresis has been detected (Source: [Van 96d])*

This difference is given as an input to the turbine. The fluid exits the impeller due to centrifugal forces, enters the turbine near its outer circumference and forces liquid from the turbine into the impeller near the inner circumference. The circulation continues as long as there is a difference in speed between the impeller and the turbine. The stator consists of a set of vanes, fixed in the housing, that redirect fluid flow from the turbine back against the impeller. This helps to turn the impeller (the engine) which in turn pushes the turbine, effectively multiplying the engine torque (see [Hur 94], [Got 91]).

Define the speed ratio $s_{N,tc}$ as $s_{N,tc} = \frac{\dot{\theta}_p}{\dot{\theta}_e}$. In practice, two static characteristics are sufficient to describe the torque converter (see [Hur 94]). Experimental data of a Daikin YT220 torque converter are taken from [Hel 94].

- The torque ratio $M_{tc}(s_{N,tc})$ is determined by the speed ratio (see figure 4.10). It relates the delivered output torque $T_{tc,out}$ to the applied input torque $T_{tc,in}$:

$$T_{tc,out} = T_{tc,in} M_{tc}(s_{N,tc}) \tag{4.9}$$

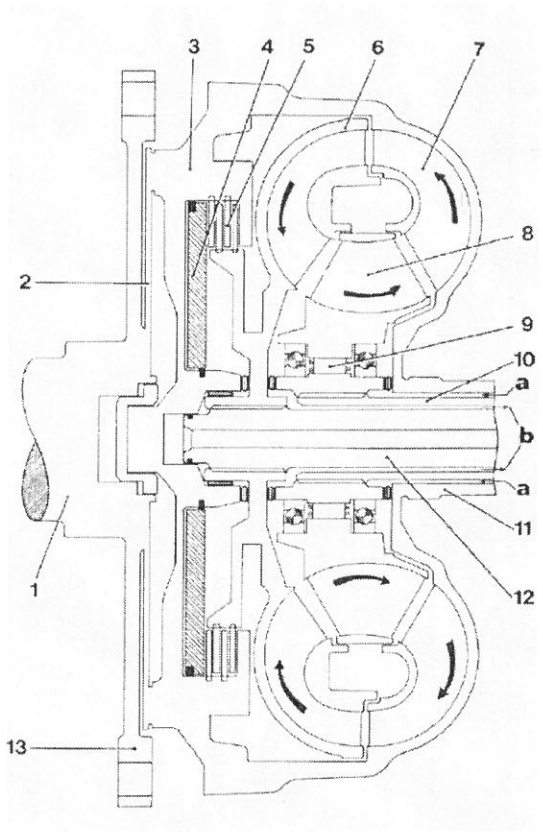

Figure 4.9 *Cross section of a modern torque converter. Different components can be observed: driving shaft (1), lock-up clutch (5), turbine (6), pump (7), stator (8) and driven shaft (10,12) (Source: [Got 91]).*

- The capacity factor $S_{tc}(s_{N,tc})$ is also determined by the speed ratio (see figure 4.11). It relates the applied input torque $T_{tc,in}$ to the engine rotation speed $\dot{\theta}_e$:

$$T_{tc,in} = \dot{\theta}_e^2 S_{tc}(s_{N,tc}) \tag{4.10}$$

Except for the lockup facility, this type of coupling has no true control input and the characteristics can only be changed by changing the geometry.

As for the multi-plate clutch, the inertia of the torque converter is distributed to the engine inertia I_e and the primary inertia I_p.

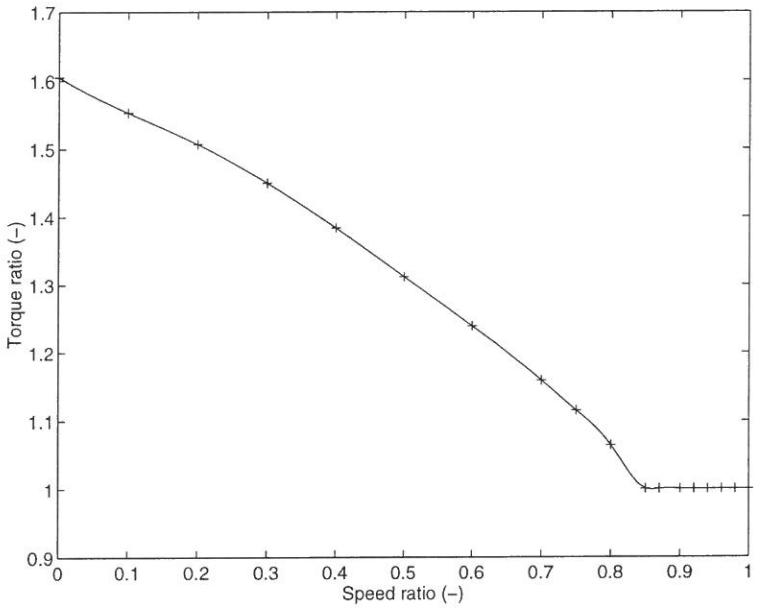

Figure 4.10 *Experimentally determined torque ratio $M_{tc}(s_{N,tc})$ as a function of speed ratio $s_{N,tc}$, for a Daikin YT220 torque converter. Only at low slip ratios, the effect of torque multiplication is present (maximal 1.6 at zero slip ratio). Due to the torque multiplication effect, high initial car acceleration is guaranteed (Source: [Hel 94]).*

4.2.4 The gear pump

In a CVT, the gear pump is driven by the combustion engine. The load torque T_{gp} of the pump is proportional to pump speed and pump pressure difference (see [Mer 67]). Experiments on a 12 mm pump show the presence of an additional static friction torque (see [Van 96e]). Therefore, the gear pump is modelled as:

$$T_{gp} = K_{T,N}\dot{\theta}_e + K_{T,p}p_{gp} + K_{T,0} \tag{4.11}$$

Linear total least squares are used to compute the coefficients $K_{T,N}$, $K_{T,p}$ and $K_{T,0}$ from experimental data of a 12 mm gear pump (see [VHV 91], [Van 96e]). The estimated parameters are included in table 4.4

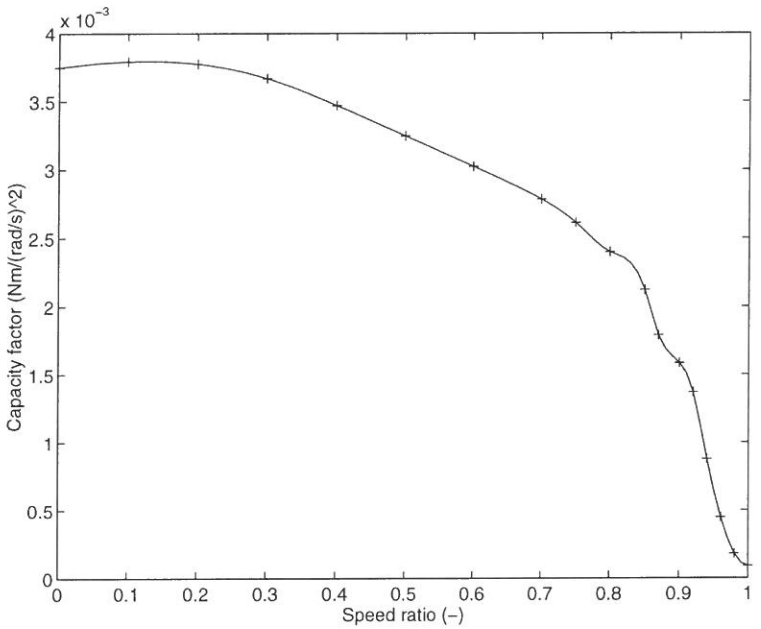

Figure 4.11 *The experimentally determined capacity factor $S_{tc}(s_{N,tc})$ as a function of the speed ratio $s_{N,tc}$, for a Daikin YT220 torque converter. At higher slip ratios, the capacity factor reduces drastically, which guarantees small slip speeds (and thus low inherent power losses) when no lockup facility is available (Source: [Hel 94]).*

The pump inertia is included in the engine inertia I_e, while the internal friction is included in the pump coefficient $K_{T,N}$.

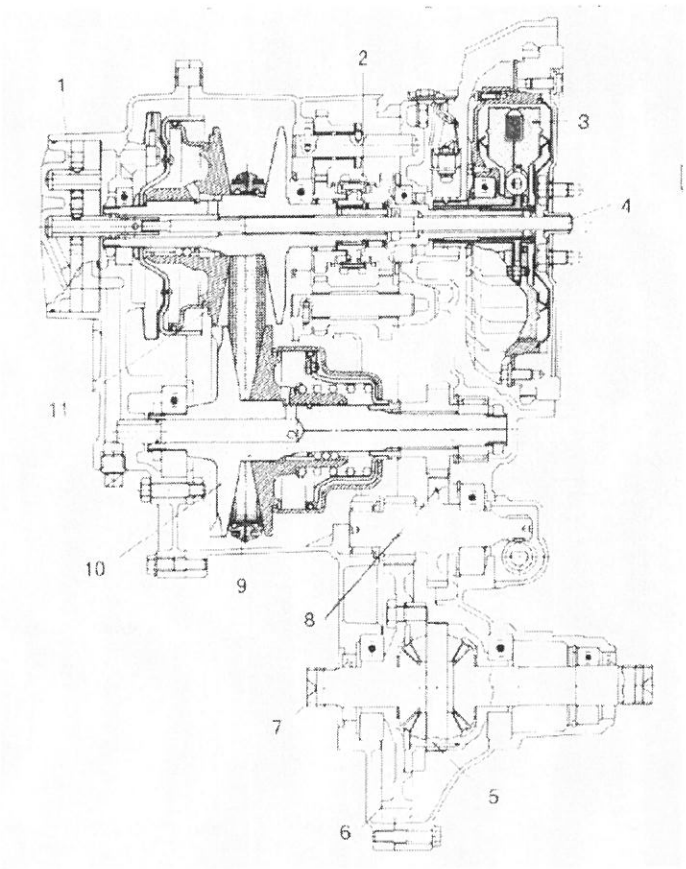

Figure 4.12 *A modern push-belt variator. Different components can be observed: oil pump (1), forward-backward selector (2), powder clutch (3), engine shaft (4), differential gears (5), final drive reduction (6,8), driven shaft (7), push-belt (9), secondary pulleys (10) and primary pulleys (11) (Source: [MS 92]).*

4.2.5 The push-belt variator

The push-belt variator (see figure 4.12) is the heart of the CVT. The circumferential force of the driving torque T_p at the primary pulley is transmitted by a flexible medium (a steel V-belt) to the secondary pulley. The metal belt exists of strings and links. To obtain flexibility, the links can rotate relatively to each other. Force is transmitted from one link to another, through the line contact of neighbouring links. Strings are used to connect the links and to avoid nodding of the belt. Compactness, efficiency, a longer life time and the possibility to transmit higher torques are the major advantages over the classical rubber-belt variator.

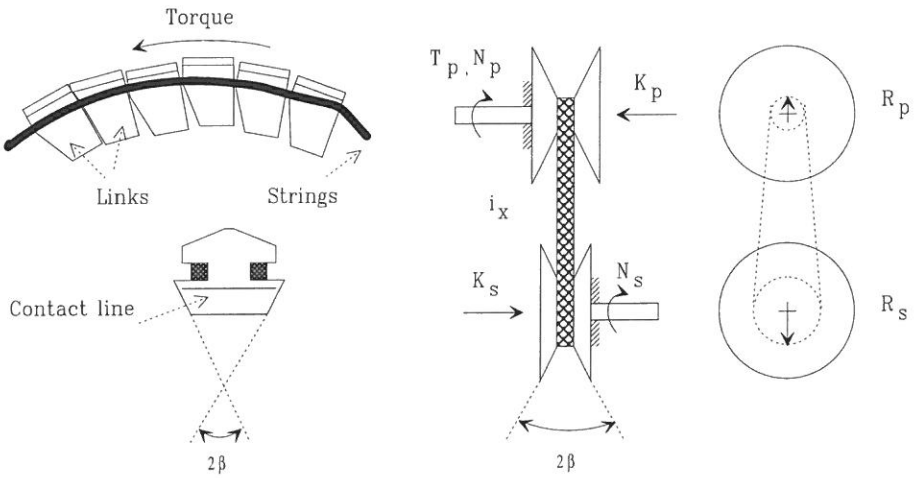

Figure 4.13 *To transmit power, a push-belt variator uses a belt that exists of metal links and metal strings. Power is transmitted by pushing, through the line contact of neighboring links. The variator ratio $i_v = R_s/R_p$ can be changed by the axial forces K_p and/or K_s.*

The ratio between the secondary running radius R_s and the primary running radius R_p is equal to the variator ratio i_v. This ratio is adjusted by axial shifting of the movable half of one of both conical pulley sheaves. Reducing the primary axial force K_p has the same effect as increasing the secondary axial force K_s, and vice versa (see 4.13).

The variator is modeled as a modulated transformer with a variable transformation ratio i_v. The ratio i_v varies between a minimal ratio (OD) and a maximal ratio (LOW), which depend on the geometry of the variator and the belt. A constant torque efficiency η_v might be assumed when electronic control is applied

(see [Gie 89], [Spijk 94], [Dev 93], [Rek 90], [SVR 92]). It holds that:

$$T_s = \eta_v i_v T_p \tag{4.12}$$
$$\dot{\theta}_p = i_v \dot{\theta}_s \tag{4.13}$$

with T_p being the applied primary torque and T_s the torque that is delivered to the secondary side. Experiments on a VT1-transmission indicate that efficiency varies with the operating point and that the rate of ratio change is limited by oil flow requirements. These practical issues will be discussed in detail in Chapter 5.

The inertia of the primary axle and the inertia of the primary pulley are included in the rotational inertia I_p, that rotates at primary speed, while the inertia of the secondary pulley, the inertia of the secondary axle and half of the pinion gears inertia are combined in a single rotational inertia I_s, that rotates at secondary speed. All friction losses (bearings, belt-pulley contact, string-link contact) are taken into account by the torque efficiency η_v.

4.2.6 The pinion gear

The pinion gear, also referred to as the final drive reduction, is a gear-box with a fixed ratio, mounted between the secondary side of the CVT and the drive axle. It is described as a transformer with a fixed ratio i_{FD}:

$$T_{FD,out} = i_{FD} T_{FD,in} \tag{4.14}$$
$$\dot{\theta}_s = i_{FD} \dot{\theta}_{FD} \tag{4.15}$$

with $T_{FD,in}$ the input torque of the gear-box, $T_{FD,out}$ the output torque of the gear-box and $\dot{\theta}_{FD}$ the output speed of the gear-box. The inertia of the gears is distributed to the secondary inertia I_s and the car inertia I_{tot}.

4.2.7 The drive axle

The compliance of the drive axle is modeled by a linear torsion spring with a stiffness c_{fa}. The drive torque M_{fw} applied at the front wheel is computed from:

$$M_{fw} = c_{fa}(\theta_{FD} - \theta_f) \tag{4.16}$$

The inertia of the shaft is added to the car inertia I_{tot}. Material damping is neglected.

4.3 Drive train modeling

As discussed in the previous section, the following phenomena have been taken into account:

- The engine is described as a nonlinear torque source, modulated by the engine speed and the throttle position.
- The flywheel inertia, the pump inertia, half of the clutch inertia and the inertia of the torsion damper are combined in a single rotational inertia I_e, that rotates at engine speed.
- The clutch is described as a nonlinear friction element, modulated by the clutch pressure and the clutch slip.
- Half of the clutch inertia, the inertia of the primary axle and the inertia of the primary pulley are combined in a single rotational inertia I_p, that rotates at primary speed.
- The variator is described as a variable transformer with a fixed torque efficiency.
- The inertia of the secondary pulley, the inertia of the secondary axle and half of the pinion gears inertia is combined in a single rotational inertia I_s, that rotates at secondary speed.
- The pinion gear-box is described as a fixed transformer with no torque losses.
- The drive axle is modeled as a linear torsional spring.
- The total car inertia, reduced to the wheels, half of the pinion gear inertia and the drive axle inertia are combined in a single rotational inertia I_{tot}, that rotates at wheel speed.
- The total load torque is reduced to the wheels and contains roll and air resistances, load due to road slope and brake torque.

An overview and typical parameter values for Volvo 480, equipped with a VT1H transmission (oil, pump, clutch, variator and pinion), are given in table 4.4.

	Meaning	Value	Units
c_{fa}	Torsion stiffness of driving axle	50000	Nm/rad
I_e	Inertia of engine and flywheel	0.1584	kgm^2
I_p	Inertia of primary system	0.0355	kgm^2
I_s	Inertia of secondary system	0.0186	kgm^2
μ_{stat}	Static friction coefficient	0.0638	-
μ_{dyn}	Dynamic friction coefficient	0.1598	-
ν_{cl}	Clutch slip coefficient	0.0029	s/rad
η_v	Torque efficiency of the variator	0.95	-
i_{FD}	Final drive reduction	5.76	-
$K_{T,N}$	Speed coefficient of gear pump	2.356e-3	s/rad
$K_{T,p}$	Pressure coefficient of gear pump	0.141e5	1/Pa
$K_{T,0}$	Offset torque of gear pump	0.350	Nm
η_{cl}	Torque efficiency of clutch	0.85	-
n_{cl}	Number of surface pairs	6	-
R_{cl}	Effective radius of the clutch	0.074	m
A_{cl}	Effective surface of the clutch	4.488e-3	m^2
$p_{cl,0}$	Offset pressure of the clutch	2e4	Pa
m_{cl}	Mass of the slidable clutch part	1	kg
b_{cl}	Viscous damping between piston and housing	1125	Ns/m
k_{cl}	Stiffness of the additional clutch spring	90000	N/m
LOW	Variator ratio in low	2.47	-
OD	Variator ratio in overdrive	0.445	-

Table 4.4 *Drive train parameters of a Volvo 480, equipped with a VT1-H transmission (Esso EZL 799 oil (T_{oil} = 70°), 12 mm gear pump, wet multi-plate clutch, variator and pinion).*

4.3.1 A physical model of the drive train

Writing the torque balances of the four inertias (see figure ??) leads to the following equations:

$$I_e\ddot{\theta}_e = T_{e,dyn} - T_{gp} - T_{cl} \quad (4.17)$$

$$I_p\ddot{\theta}_p = T_{cl} - T_p \quad (4.18)$$

$$I_s\ddot{\theta}_s = T_s - T_{FD,in} \quad (4.19)$$

$$I_{tot}\ddot{\theta}_f = T_{FD,out} - R_{tot}\dot{\theta}_f^2 - T_{ext} - T_{brake} \quad (4.20)$$

T_{brake} is the braking torque, applied by the driver and T_{cl} is the torque that is effectively transmitted through the clutch[1]. Combining the component equations 4.1 till 4.16 with the torque balances leads to a set of coupled algebraic and differential equations, which implies that elimination of variables is required to prevent simulation problems. Define the front wheel axle deformation ϵ_{fa} as the relative deformation over the torsional spring:

$$\epsilon_{fa} = \theta_{FD} - \theta_f \tag{4.21}$$

By taking the time derivative of the speed equation 4.13 of the variator, it follows that:

$$\ddot{\theta}_s = \frac{\ddot{\theta}_p}{i_v} - \frac{\dot{\theta}_p}{i_v^2}\frac{di_v}{dt} \tag{4.22}$$

Combining this equation with the torque equation 4.12 of the variator and the torque balances 4.18 and 4.19 of the primary and secondary inertias finally gives:

$$(I_p + \frac{I_s}{\eta_v i_v^2})\ddot{\theta}_p = T_{cl} - \frac{c_{fa}\epsilon_{fa}}{\eta_v i_{FD} i_v} + \frac{\dot{\theta}_p I_s}{\eta_v i_v^3}\frac{di_v}{dt} \tag{4.23}$$

$$T_s = \frac{I_s}{i_v}\ddot{\theta}_p - \frac{I_s\dot{\theta}_p}{i_v^2}\frac{di_v}{dt} + \frac{c_{fa}}{i_{FD}}\epsilon_{fa} \tag{4.24}$$

By combining the drive axle equation 4.16 with the torque balances 4.18 and 4.20 of the secondary inertia and the car inertia, the following equation is obtained:

$$\ddot{\epsilon}_{fa} = \frac{T_s}{i_{FD} I_s} - c_{fa}(\frac{1}{I_s i_{FD}^2} + \frac{1}{I_{tot}})\epsilon_{fa} + \frac{R_{tot}}{I_{tot}}(\frac{\dot{\theta}_p}{i_v i_{FD}} - \dot{\epsilon}_{fa})^2 + \frac{T_{ext} + T_{brake}}{I_{tot}}$$

[1]To compute the torque T_{cl}, two clutch operation modes must be considered (stick and slip). When the clutch is unlocked (slip), T_{cl} equals T_{max} which is computed from the earlier derived clutch equations. When the clutch is locked (stick), T_{cl} is computed as the minimum of the maximal clutch torque T_{max} and the lockup torque T_{lockup} (the torque that is required to keep the engine speed and the primary speed equal). For more details, we refer to [Sim 96] and [GM 89].

Elimination of the secondary torque T_s gives:

$$\begin{aligned} I_{p,eq}\ddot{\epsilon}_{fa} &= \frac{T_{cl}}{i_v i_{FD}} - c_{fa}\left(\frac{1}{\eta_v i_v^2 i_{FD}^2} + \frac{I_{p,eq}}{I_{tot}}\right)\epsilon_{fa} - \left(\frac{I_p \dot{\theta}_p}{i_{FD} i_v^2}\right)\frac{di_v}{dt} \\ &\quad + \frac{I_{p.eq} R_{tot}}{I_{tot}}\left(\frac{\dot{\theta}_p}{i_v i_{FD}} - \dot{\epsilon}_{fa}\right)^2 + \frac{I_{p,eq}}{I_{tot}}(T_{ext} + T_{brake}) \end{aligned}$$

with the equivalent primary inertia $I_{p,eq}$ given by:

$$I_{p,eq} = I_p + \frac{I_s}{\eta_v i_v^2}$$

The non linear differential equations that describe the drive train are summarized below:

$$I_e \ddot{\theta}_e = T_{e,dyn} - T_{gp} - T_{cl} \tag{4.25}$$

$$I_{p,eq}\ddot{\theta}_p = T_{cl} - \frac{c_{fa}\epsilon_{fa}}{\eta_v i_{FD} i_v} + \frac{\dot{\theta}_p I_s}{\eta_v i_v^3}\frac{di_v}{dt} \tag{4.26}$$

$$\begin{aligned} I_{p,eq}\ddot{\epsilon}_{fa} &= \frac{T_{cl}}{i_v i_{FD}} - c_{fa}\left(\frac{1}{\eta_v i_v^2 i_{FD}^2} + \frac{I_{p,eq}}{I_{tot}}\right)\epsilon_{fa} - \left(\frac{I_p \dot{\theta}_p}{i_{FD} i_v^2}\right)\frac{di_v}{dt} \\ &\quad + \frac{I_{p,eq}}{I_{tot}}\left(R_{tot}\left(\frac{\dot{\theta}_p}{i_v i_{FD}} - \dot{\epsilon}_{fa}\right)^2 + T_{ext} + T_{brake}\right) \end{aligned} \tag{4.27}$$

The clutch pressure p_{cl} (that determines the clutch torque T_{cl}) and the rate of ratio change $\frac{di_v}{dt}$ of the variator are considered as control inputs and are elements of the control input vector $\mathrm{U} = (u_1, u_2)'$.

The slope and brake torques and the throttle position (that partially determines the delivered engine torque) act as disturbances and are elements of the disturbance vector $\mathrm{W} = (w_1, w_2)'$:

$$\begin{aligned} u_1 &= p_{cl} \\ u_2 &= \frac{di_v}{dt} \\ w_1 &= T_{ext} + T_{brake} \\ w_2 &= \alpha_{th} \end{aligned}$$

The state vector X_{dt} of the drive train is given by:

$$X_{dt} = \begin{pmatrix} \dot{\theta}_e & \dot{\theta}_p & \epsilon_{fa} & \dot{\epsilon}_{fa} & i_v \end{pmatrix}'$$

The engine torque $T_{e,dyn}$, the gear pump torque T_{gp} and the transmitted clutch torque T_{cl} are non linear functions of the system states. When a torque converter is used instead of a wet multi-plate clutch, the following adaptations are required:

- In the engine equation, T_{cl} must be replaced with $T_{tc,in}$.
- In the equivalent primary equation, T_{cl} must be replaced with $T_{tc,out}$.
- The characteristics of the torque converter (torque ratio and capacity factor) must be used to compute $T_{tc,in}$ and $T_{tc,out}$.
- Only u_2 remains as a control input.

The generic drive train model described by equations 4.25, 4.26 and 4.27 is implemented in Matlab/Simulink and tuned for a wide variety of applications, to compute fuel economy, dynamic performance and comfort for the various customers and potential customers of VCST. Actually, 9 engines, 2 coupling devices, 6 variators, 10 cars, 2 gear pump and 2 transmission oils are included in the VIRTUES database (see [Van 96a]).

To develop advanced model-based control strategies, reduced control models for clutch mode and variator mode are derived in the next subsections.

4.3.2 A reduced model for clutch control

In clutch mode, it is assumed that the variator is not shifting (i_v remains LOW). Assuming that the drive axle is infinitely stiff, the model reduces to:

$$I_e \ddot{\theta}_e = T_{e,dyn} - T_{gp} - T_{cl} \tag{4.28}$$

$$I_{p,eqr} \ddot{\theta}_p = T_{cl} - \frac{R_{tot}}{\eta_v i_v^3 i_{FD}^3} \dot{\theta}_p^2 - \frac{T_{ext} + T_{brake}}{\eta_v i_v i_{FD}} \tag{4.29}$$

with

$$I_{p,eqr} = I_p + \frac{I_s}{\eta_v i_v^2} + \frac{I_{tot}}{\eta_v i_v^2 i_{FD}^2}$$

In Section 4.4, this model is used to derive an advanced model-based clutch controller.

4.3.3 A reduced model for variator control

In variator mode, it is assumed that the clutch is locked (no clutch slip). Assuming that the drive axle is infinitely stiff, the model reduces to:

$$\begin{aligned} I_{e,eqr}\ddot{\theta}_e &= T_{e,dyn} - T_{gp} + \frac{I_s i_{FD}^2 + I_{tot}}{\eta_v i_v^3 i_{FD}^3}\frac{di_v}{dt}\dot{\theta}_e \\ &\quad - \frac{R_{tot}}{\eta_v i_v^3 i_{FD}^3}\dot{\theta}_e^2 - \frac{T_{ext} + T_{brake}}{\eta_v i_v i_{FD}} \end{aligned} \tag{4.30}$$

with

$$I_{e,eqr} = I_e + I_p + \frac{I_s i_{FD}^2 + I_{tot}}{\eta_v i_v^2 i_{FD}^2}$$

In Section 4.4, this model is used to derive an advanced model-based variator controller.

4.4 Drive train control

In the literature, a wide variety of control concepts for CVTs is proposed (see [Spijk 94], [COYVBJF 84], [FM 92], [GS 95], [LRWK 93]). Although advantageous from multiple points of view, the proposed strategies also have some disadvantages for transmission suppliers:

- The strategies can only be implemented using digital control techniques and require a huge amount of computations. For being effective, sampling frequencies of at least 250 Hz are required. This requires dedicated ECUs, sensors and actuators, too expensive for series production.
- The drive torque needs to be measured (vulnerable) or estimated.
- An ideal hydraulic actuation unit is assumed (no interactions with the drive train, decoupled steering outputs).

In this thesis, the concept of variogram control is introduced. It is rather easy to implement (either hydraulically or digitally) and needs no expensive ECU nor drive torque information when implemented in a digital way. In practice, only speed and pressure measurements are required.

4.4.1 Drive train management via variogram control

From the engine characteristics, optimal engine rotation speeds with respect to power production or fuel consumption can be derived for each throttle position α_{th}:

$\dot{\theta}_{e,P}(\alpha_{th})$: optimal engine speed w.r.t. power production
$\dot{\theta}_{e,\Phi}(\alpha_{th})$: optimal engine speed w.r.t. fuel consumption

These optimal speeds form optimal operating lines for the engine (see [NSS 90]). Notice that only a CVT is able to track these operating lines, since continuous shifting capabilities are required to do so (see figures 4.14 and 4.15).

In theory, these engine speeds can be realized independent from vehicle speed. In practice, smoothing is required to meet comfort specifications. In the variogram, the desired engine speed is shown as a function of vehicle speed and throttle position. An economy variogram for a B18U engine is shown in figure 4.16. For a given application (engine-variator-car and specifications), the variogram is treated as a control parameter that must be tuned. Once the optimal variogram is designed, it is the task of the drive train control unit to realize variogram tracking.

For a drive train with an electronically controlled CVT, the proposed control configuration for variogram tracking is shown in figure 4.17. Table 4.5 summarizes the proposed strategy. In theory, the feedback controllers are formed by simple linear controllers, followed by linearizing controllers obtained from feedback linearization. In practice, gain scheduled PI-controllers are implemented due to cost constraints. At this moment, advanced feedback linearization controllers are being implemented on the power test rig at VCST.

In clutch mode, the clutch is controlled, to realize the desired shifting traject, while the variator remains in LOW. Throttle dependent stall speeds (engine speed control at zero car speed) and smooth acceleration/deceleration at low vehicle speeds are the major goals. In variator mode, the variator is controlled to realize variogram tracking. Reduced fuel consumption and increased dynamic performance are the major goals.

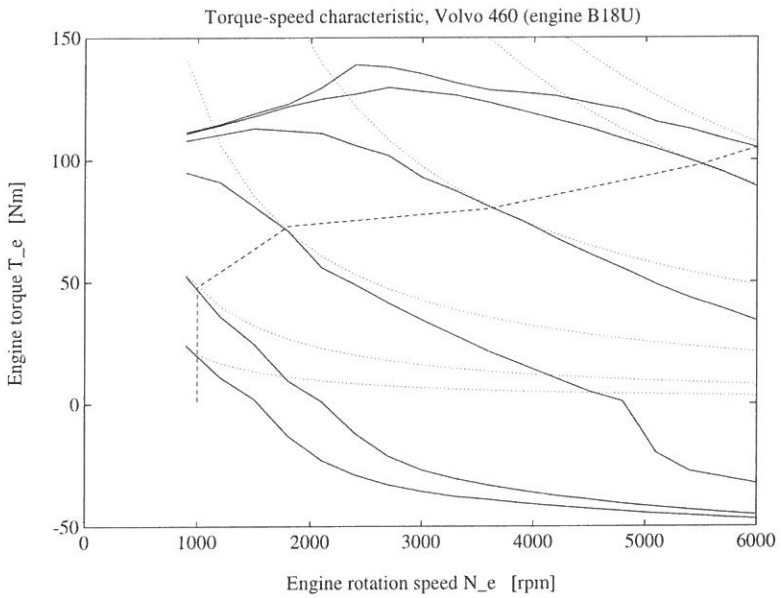

Figure 4.14 *The experimentally determined torque-speed characteristic* $T_e(\theta_e, \alpha_{th})$ *(solid, different throttle positions) and the optimal operating line for sport mode, i.e. maximal power production, for a B18U engine (dashed). Lines of constant power production are shown also (dotted). In sport mode, high engine speeds are required to increase dynamic performance. (Source: VCST)*

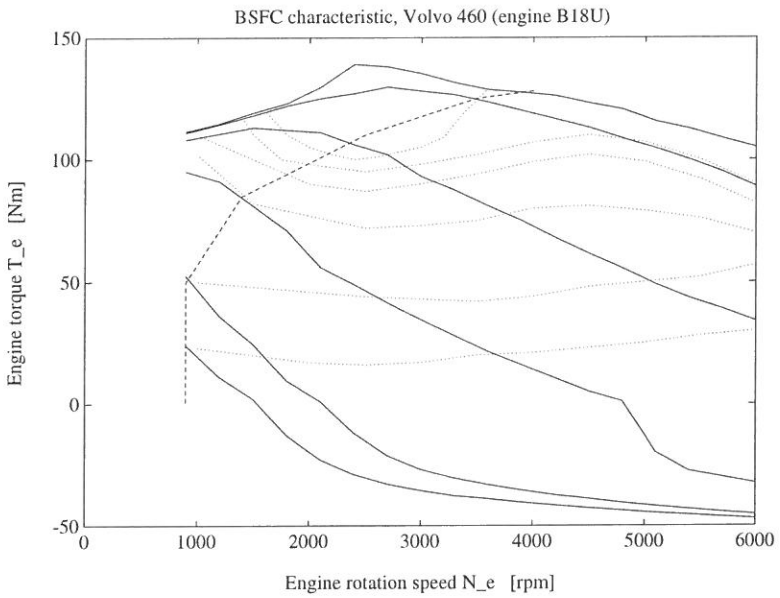

Figure 4.15 *The experimentally determined fuel consumption characteristic $\Phi_e(T_e, \dot{\theta}_e)$ (dotted, lines of constant specific fuel consumption) and the optimal operating line for economy mode, i.e. minimal fuel consumption, for a B18U engine (dashed). Lines of constant throttle position are shown also (solid). In economy mode, low engine speeds are required to decrease fuel consumption (Source: VCST).*

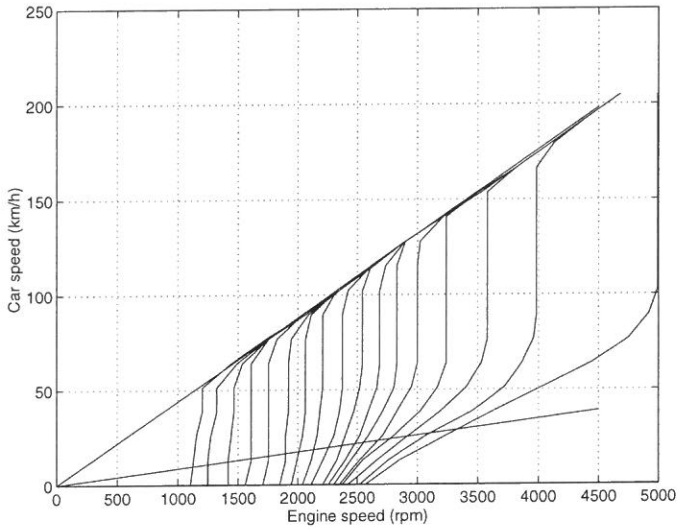

Figure 4.16 *An economy variogram for a B18U engine. The straight lines from the origin represent LOW (lowest line) and OD (highest line) and form the boundaries of the CVT's operation region. The other lines show how the desired engine speed varies with car speed, for different throttle positions. Smoothing near LOW and OD is required for drive comfort. Two-stage engagement is minimized due to throttle dependent stall speeds (Source: VCST).*

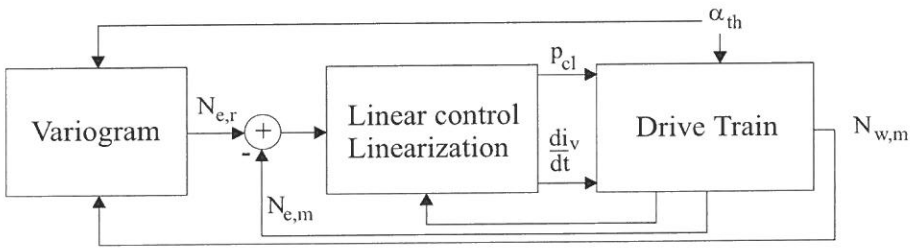

Figure 4.17 *Variogram control: the reference engine rotation speed $N_{e,r}$ is obtained from the measured wheel speed $N_{w,m}$, the measured throttle position α_{th} and the variogram. This reference speed is compared with the measured engine rotation speed $N_{e,m}$. Linear controllers, followed by output feedback linearization controllers can be used to compute the clutch control signal p_{cl} and the variator control signal i_v.*

Mode	Computation of p_{cl}	Computation of i_v
Clutch mode $\frac{\dot{\theta}_{p,m}}{\dot{\theta}_{f,m}} >$ LOW	From $\dot{\theta}_{e,r} - \dot{\theta}_{e,m}$ Linear control and feedback linearization	Keep $i =$ LOW
Variator mode $\frac{\dot{\theta}_{p,m}}{\dot{\theta}_{f,m}} <$ LOW	Sufficiently high to lock	From $\dot{\theta}_{e,r} - \dot{\theta}_{e,m}$ Linear control and feedback linearization

Table 4.5 *The proposed control strategy for drive train control. The subscripts m and r refer to measured and reference values.*

4.4.2 An algorithm for control in clutch mode

In clutch mode, the variator remains in LOW, while the clutch pressure p_{cl} is varied to control the engine speed $\dot{\theta}_e$ as required by the reference variogram. The control model for clutch mode looks like:

$$I_e \ddot{\theta}_e = T_{e,dyn} - T_{gp} - T_{cl} \tag{4.31}$$

$$I_{p,eqr} \ddot{\theta}_p = T_{cl} - \frac{R_{tot}}{\eta_v i_v^3 i_{FD}^3} \dot{\theta}_p^2 - \frac{T_{ext} + T_{brake}}{\eta_v i_v i_{FD}} \tag{4.32}$$

with

$$I_{p,eqr} = I_p + \frac{I_s}{\eta_v i_v^2} + \frac{I_{tot}}{\eta_v i_v^2 i_{FD}^2}$$

This model is used to design a clutch controller. Equation 4.5 relates the clutch torque T_cl to the clutch pressure p_{cl}. By applying output feedback linearization (see [SL 91]), the control signal $u_1 = p_{cl}$ can finally be computed as:

$$u_1 = p_{cl} = p_{cl,0} + \frac{-I_e v_1 + T_{e,dyn} - T_{gp}}{n_{cl}\mu_{cl}A_{cl}R_{cl}\eta cl}$$

with v_1 being the signal from a linear controller, designed for the linearized system given by:

$$\begin{aligned} \dot{x} &= v_1 \\ y &= x \end{aligned}$$

By applying feedback linearization, the system reduces to a simple integrator, with input $\ddot{\theta}_e$ and state $\dot{\theta}_e$.

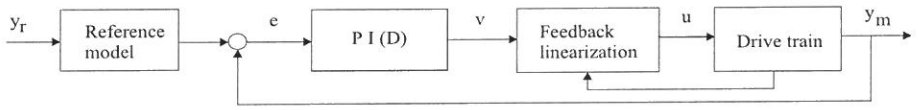

Figure 4.18 Feedback linearization and model reference CVT control: the reference engine speed $y_r = \dot{\theta}_{e,r}$ is applied to the closed loop reference model. The output of the reference model is compared with the measured engine speed $y_m = \dot{\theta}_{e,m}$ and fed to a PI-controller (in practice, there is a PI-controller for clutch mode and one for variator mode). The output v of the PI-controller(s) ($v = v_1$ for clutch mode, $v = v_2$ for variator mode) is applied to the feedback linearization block, to obtain the drive train control signal u ($u = u_1 = p_{cl}$ for clutch mode and $u = u_2 = \frac{di_v}{dt}$ for variator mode).

Although a wide variety of techniques is available to design the linear controller, we propose a model-reference controller for simplicity. The required engine speed, obtained from the variogram, is fed into a second order reference model (characterized by ζ_1 and ω_{n1}). This (internal) reference speed is compared to the measured engine speed and fed into a PI-controller. The parameters ζ_1, ω_{n1} and the PI-controller parameters are obtained from the specifications and the linear dynamics (see [Ack 93], [AW 84], [Jus 92], [Orl 94], [Per 92], [ZA 93] and [ZN 42] for model-based tuning methods for this type of controllers).

An advantage of the proposed approach is the simplicity of the controller (see figure 4.18). A disadvantage is the requirement for clutch slip measurement, to estimate μ_{cl}. The clutch slip is estimated from the difference between the measured engine speed and the measured primary speed. The engine torque $T_{e,dyn}$ and the pump torque T_{gp} are estimated from the engine and pump characteristics, since $\dot{\theta}_e$, α_{th} and p_{gp} are easily measured.

4.4.3 An algorithm for control in variator mode

In variator mode, the clutch is locked (no clutch slip). The control model for variator mode looks like:

$$I_{e,eqr}\ddot{\theta}_e = T_{e,dyn} - T_{gp} + \frac{I_s i_{FD}^2 + I_{tot}}{\eta_v i_v^3 i_{FD}^3}\frac{di_v}{dt}\dot{\theta}_e - \frac{R_{tot}}{\eta_v i_v^3 i_{FD}^3}\dot{\theta}_e^2 - \frac{T_{ext} + T_{brake}}{\eta_v i_v i_{FD}}$$

with

$$I_{e,eqr} = I_e + I_p + \frac{I_s i_{FD}^2 + I_{tot}}{\eta_v 1_v^2 i_{FD}^2}$$

This model is used to design a variator controller. By applying output feedback linearization, the control signal $u_2 = \frac{di_v}{dt}$ can now be computed as:

$$u_2 = \frac{di_v}{dt} = \frac{I_{e,eqr} v_2 + \frac{R_{tot}\dot{\theta}_e^2}{\eta_v i_v^3 i_{FD}^3} + \frac{T_{ext}+T_{brake}}{\eta_v i_v^3 i_{FD}^3} - T_{e,dyn} + T_{gp}}{\frac{I_{tot}+I_s i_{FD}^2}{\eta_v i_v^3 i_{FD}^2}\dot{\theta}_e}$$

with v_2 being the signal from the linear controller, designed for the linearized system given by:

$$\begin{aligned} \dot{x} &= v_2 \\ y &= x \end{aligned}$$

In practice, a model-reference controller is used. The required engine speed, obtained from the variogram, is fed into a second order reference model (characterized by ζ_2 and ω_{n2}). This (internal) reference speed is compared to the measured engine speed and fed into a PI-controller.

All terms in the linearization equation can be estimated from measurements and system characteristics. To estimate the torque T_{ext}, the road slope is measured and a nominal car mass m_t is assumed. The brake torque T_{brake} is easily measured on the experimental power test rig or estimated from the measured brake pedal position and the static brake characteristics. An important advantage of this controller is the absence of vulnerable torque measurements[2].

[2]Robust performance is said to become critical when dealing with output feedback linearization. In fact, the error dynamics need to be analyzed carefully ([SL 91]). This issue will be investigated in the near future, when the proposed controllers will be implemented and validated on the power test rig of VCST and in several demo cars.

4.5 A sample of results and conclusions

This Section contains a sample of results and conclusions that were obtained when doing practical computations and experiments.

- Kick-down test: VT1-H versus VT1-E (simulation)

  Figure 4.19 shows the influence of the control unit and control strategy on car motion for a Rover 216, with engine 1.6K16MPI, equipped with a VT1 variator and a wet multi-plate clutch (P811). When applying hydraulic control (VT1-H), the realized variogram is fixed and determined by the hydro-mechanical control hardware (see Chapters 5 and 6). Two stage-engagement (piece-wise linear shifting trajectory that follows LOW for a while) is important and limits drive comfort. When applying electronic control (VT1-E), the realized variogram depends on the user's specifications (economy, sport, mixed) and is determined by a look-up table in the control software (see Chapters 5 and 6). By adapting the look-up table, the performance of a car with an electronically controlled CVT can be changed easily. In this simulation, an economy variogram was used, which resulted in minimal fuel consumption, high comfort (smooth acceleration, minimal two-stage engagement) and moderate dynamic performance (compared to the potentials of a sport variogram).

- VT1-H versus VT1-F (experiments)

  Figures 4.20 and 4.21 show the influence of the control unit and control strategy on car motion for a Rover 216, with engine 1.6K16MPI, equipped with a VT1 variator and a wet multi-plate clutch (P811). When applying hydraulic control (VT1-H), the realized variogram is fixed and determined by the hydro-mechanical control hardware (see Chapters 5 and 6). Two stage-engagement (piece-wise linear shifting trajectories that follow LOW for a while) is important and limits drive comfort. When applying electronic control (VT1-F), the realized variogram depends on the user's specifications (economy, sport, mixed) and is determined by a look-up table in the control software (see Chapters 5 and 6). In these experiments, a mixed variogram was used, to obtain a good trade-off in fuel consumption, comfort (smooth acceleration, minimal two-stage engagement) and dynamic performance.

- Plate clutch versus torque converter (simulation)

  Figure 4.22 shows the influence of the coupling device (plate clutch P811 versus torque converter Daikin YT 220) on dynamic car performance. The torque converter shows higher dynamic performance (due to torque multiplication) and increased comfort (limited two-stage engagement).

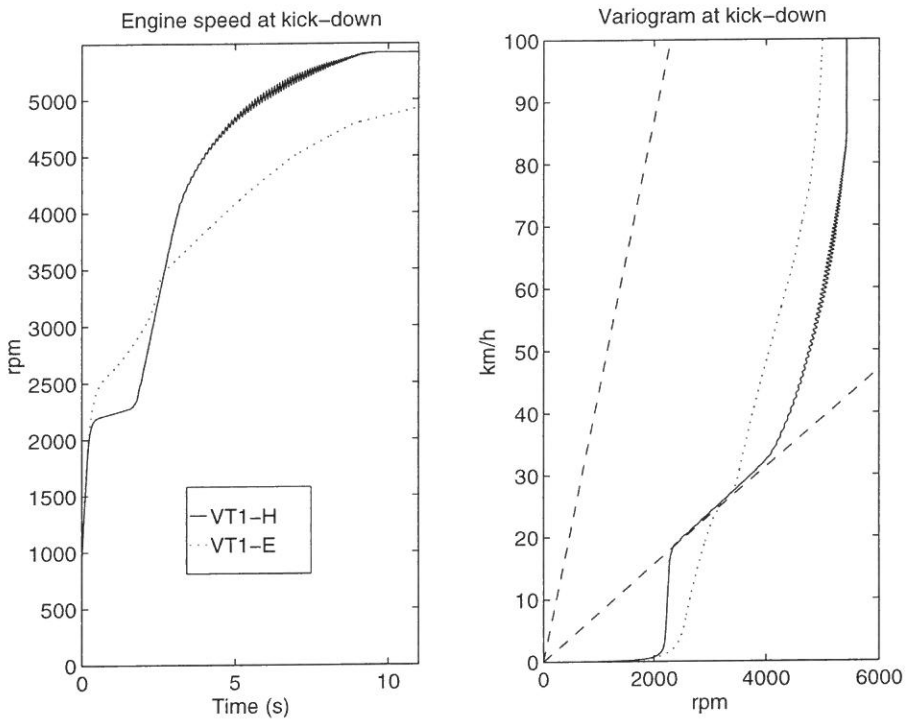

Figure 4.19 *Engine speed and realized variogram at kick-down from rest: influence of the control unit and control strategy on car motion for a Rover 216, with engine 1.6K16MPI, equipped with a VT1 variator and a wet multi-plate clutch (P811) (simulation). The oscillations in engine speed are introduced by the simulator and are absent in practical situations. By reducing the time-step for integration, these oscillations can be made arbitrarely small, at the cost of simulation time.*

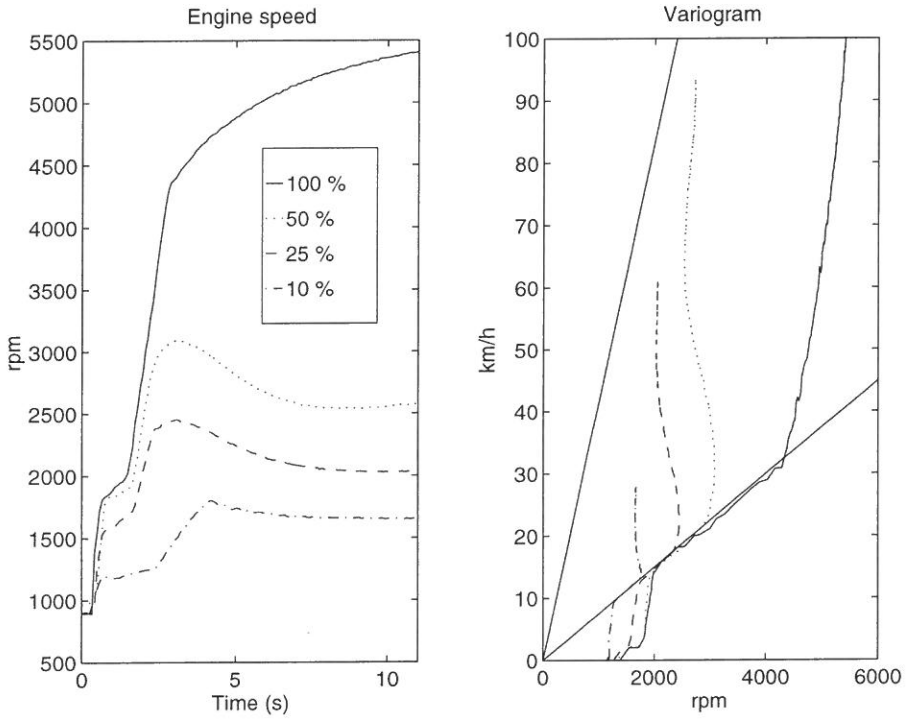

Figure 4.20 *Engine speeds and the realized variogram for different throttle positions: influence of the control unit and control strategy on car motion for a Rover 216, with engine 1.6K16MPI, equipped with a VT1-H variator and a wet multi-plate clutch (P811) (experiment).*

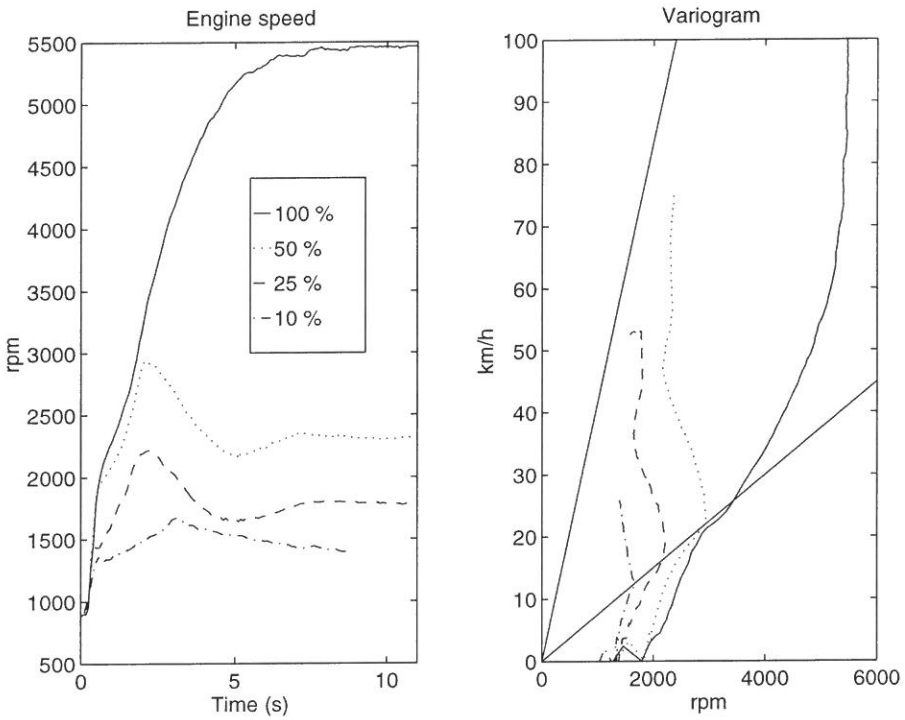

Figure 4.21 *Engine speeds and the realized variogram for different throttle positions: influence of the control unit and control strategy on car motion for a Rover 216, with engine 1.6K16MPI, equipped with a VT1-F variator and a wet multi-plate clutch (P811) (experiment).*

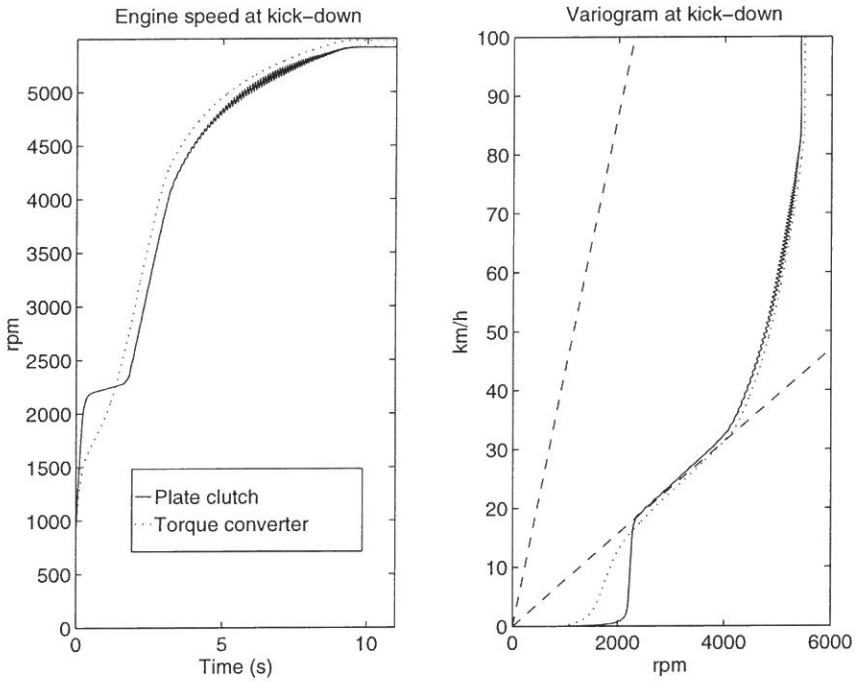

Figure 4.22 *Engine speed and the realized variogram at kickdown from rest: influence of the coupling device (plate clutch P811 versus torque converter Daikin YT 220) on dynamic car performance, for a Rover 216, with engine 1.6K16MPI, equipped with a VT1-H variator (simulation). The oscillations in engine speed are introduced by the simulator and are absent in practical situations. By reducing the time-step for integration, these oscillations can be made arbitrarely small, at the cost of simulation time.*

Chapter 5

Modeling and Control of the Push Belt Variator

In this Chapter, we describe the operation of the metal V-belt variator and derive different variator control strategies. In Section 5.1, the characteristics of the variator are discussed. First, geometrical and kinematic relations, as well as static flow and pressure requirements are derived. Next, we derive different dynamic models to describe variator shifting. A simple physical model is used to illustrate the fundamental variator control problem, while an experimental model is derived for control design. Finally, the torque efficiency of the variator is discussed. Experimental results for VCST's VT1 transmission show the advantages of electronic control for drive train management. In Section 5.2, we present two different control strategies that realize shifting while avoiding belt slip. First, we present a strategy that uses pressure steering on both pulleys (pp). Next, we treat a strategy that uses pressure steering on the secondary pulley and flow steering on the primary pulley (pQ). Finally, we present model-based control algorithms to realize pressure and flow steering in practice.

5.1 Introduction

To transmit power, the metal V-belt variator uses a belt of metal links and metal strings (see figure 4.15). Power is transmitted by pushing, through the line contact of neighboring links. In steady state, the ratio between the secondary running radius R_s and the primary running radius R_p is equal to the variator ratio i_v. This ratio is adjusted by axial positioning of the movable halves of the

conical pulley sheaves.

5.2 Modeling of the push-belt variator

In Chapter 4, drive train models for analysis and control were derived, based on idealized variator characteristics:

- The rate of ratio change $\frac{di_v}{dt}$ was treated as a control input. In practice, flows and/or pressures are steered to the primary and secondary pistons. The complex interplay between hydraulical and mechanical variator components determines the effectively realized rate of ratio change.
- The torque efficiency η_v was assumed constant. In practice, the torque efficiency of the variator strongly depends on the operating conditions.

In order to derive useful control models, different relations must be taken into account:

- The relation between the variator ratio i_v and the variator geometry.
- The kinematic relations between axial speeds and the rate of ratio change.
- The static and dynamic oil flow requirements to realize variator shifting.
- The static and dynamic pressure requirements to prevent belt slip and to realize variator shifting.
- The torque efficiency of the variator.

5.2.1 Geometric relations

The basic relations between the variator ratio i_v, the running radii R_s and R_p, the angle δ_v and the variator geometry (belt length L_{pb} and center distance a) are obtained from figure 5.1:

$$R_s = i_v R_p \tag{5.1}$$

$$L_{pb} = (\pi - 2\delta_v)R_p + (\pi + 2\delta_v)R_s + 2a\cos\delta_v \tag{5.2}$$

$$a\sin\delta_v = R_s - R_p \tag{5.3}$$

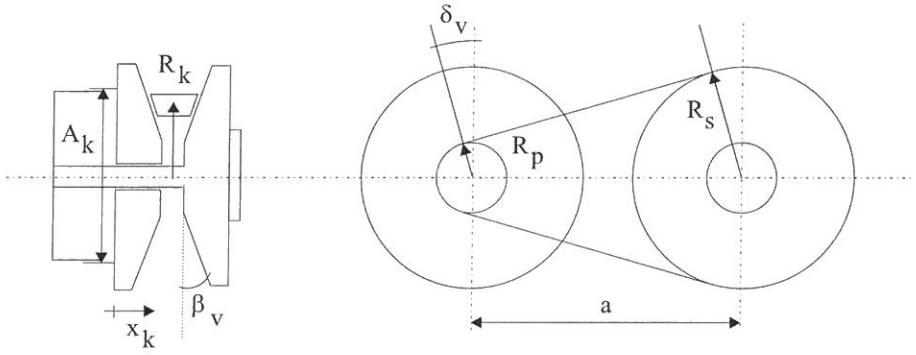

Figure 5.1 *The geometry of a metal V-belt variator.*

Equations 5.1, 5.2 and 5.3 form a set of three nonlinear equations with four unknowns (R_p, R_s , i_v and δ_v). After manipulation, the following equations are obtained:

$$\frac{L_{pb}(1-i_v)}{2a} = (1-i_v)\cos\delta_v + ((\delta_v - \frac{\pi}{2}) - i_v(\delta_v + \frac{\pi}{2}))\sin\delta_v \quad (5.4)$$

$$L_{pb} - 2a\cos\delta_v = ((\pi - 2\delta_v) + i_v(\pi + 2\delta_v))R_p \quad (5.5)$$

$$R_s = i_v R_p \quad (5.6)$$

From equation 5.4, δ_v is computed as a function of i_v. The running radii R_s and R_p for a given ratio i_v are then computed from the equations 5.5 and 5.6 (see figure 5.2). The most important CVT-parameters and typical values are listed in table 5.1.

Parameter	Meaning	Value	Units
LOW	Highest variator ratio	2.47	-
OD	Lowest variator ratio	0.445	-
L_{pb}	Belt length	0.6535	m
a	Center distance	0.155	m
β_v	Pulley angle	11	^{o}
μ_{pb}	Coulomb friction coefficient between belt and pulleys	0.09	-

Table 5.1 *Important CVT-parameters (VT1).*

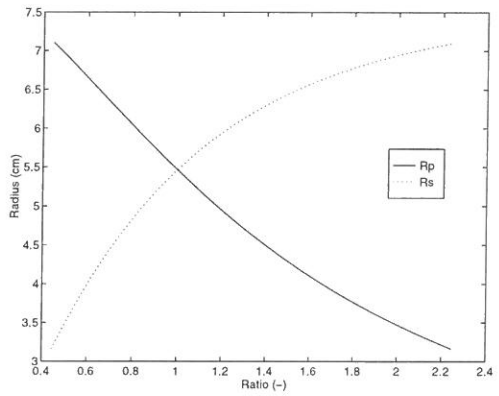

Figure 5.2 *The running radii R_s and R_p as a function of the ratio i_v. R_p increases when R_s decreases and vice versa.*

5.2.2 Kinematic relations

The axial pulley sheave velocity $\dot{x}_k$ (k=s,p) and the change of the corresponding running radius $\dot{R}_k$ are kinematically related (see figure 5.1):

$$\dot{x}_s = 2\tan\beta_v \dot{R}_s \tag{5.7}$$
$$\dot{x}_p = 2\tan\beta_v \dot{R}_p \tag{5.8}$$

with β_v being the angle of the pulleys. By taking the time derivative of the geometric relations 5.4, 5.5 and 5.6, and combining them with the kinematic relations 5.7 and 5.8, it follows that:

$$((\frac{\pi}{2} - \delta_v) + i_v(\frac{\pi}{2} + \delta_v))\dot{R}_p = -(\frac{\pi}{2} + \delta_v)R_p\frac{di_v}{dt} \tag{5.9}$$
$$((\frac{\pi}{2} - \delta_v) + i_v(\frac{\pi}{2} + \delta_v))\dot{R}_s = (\frac{\pi}{2} - \delta_v)R_p\frac{di_v}{dt} \tag{5.10}$$

These equations implicitly define the functions $g_p(i_v)$ and $g_s(i_v)$ that relate the rate of change of the running radii to the rate of ratio change:

$$\dot{R}_p = g_p(i_v)\frac{di_v}{dt} \tag{5.11}$$
$$\dot{R}_s = g_s(i_v)\frac{di_v}{dt} \tag{5.12}$$

5.2.3 Static flow and pressure requirements

Static flow requirements

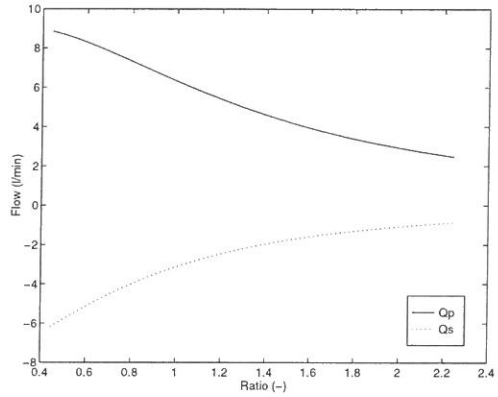

Figure 5.3 *The oil flows Q_p and Q_s to obtain a rate of ratio change equal to $\frac{di_v}{dt} = -0.5s^{-1}$.*

In the ideal static case, the required oil flow Q into an hydraulic piston is proportional to the axial pulley sheave velocity $\dot{x}$ and to the piston area A. For the primary and secondary piston (see also figure 5.3), it follows from equations 5.7, 5.8, 5.11 and 5.12 that:

$$Q_p = A_p \dot{x}_p = 2A_p \tan\beta_v g_p(i_v) \frac{di_v}{dt} \tag{5.13}$$

$$Q_s = A_s \dot{x}_s = 2A_s \tan\beta_v g_s(i_v) \frac{di_v}{dt} \tag{5.14}$$

However, these relations are only valid if:

- The piston deformation is negligible.
- The oil is incompressible.
- The oil leakage is negligible.

In practice, leakage and compressibility must be taken into account, especially when implementing piston pressure control loops (see further in this chapter).

Static pressure requirements

Pressure requirements originate from two different considerations:

- Avoidance of belt slip on both pulleys

  Belt slip destroys the pulley surfaces, reduces the life time of the belt and leads to unacceptable drive performance. Slip can be avoided by applying sufficiently high axial forces K_p and K_s (thus piston pressures) to the pulleys: in this context, the absolute values of the piston pressures p_s and p_p are important.

- Control of the variator ratio

  The pulley positions (and the corresponding variator ratio i_v) are determined by the applied piston pressures, the rotational speeds of the pulleys and the transmitted torque. Increasing K_s (via p_s) has the same effect as decreasing K_p (via p_p), and vice versa: to control the variator ratio, the ratio of the pressures p_s and p_p is important.

Pressure requirements to avoid belt slip

The required clamping forces to avoid slip are calculated from the contact forces between the belt and the sheaves. Therefore, a model of the forces that act on the pulleys and on the belt is derived (see figure 5.4).

For pulley k ($k = p, s$), the equilibrium equations are:

$$K_k = A_k p_k = \cos\beta_v R_k \int_{\psi=0}^{\gamma_k} q_k(\psi) d\psi \tag{5.15}$$

$$T_k = 2R_k^2 \int_{\psi=0}^{\gamma_k} w_k(\psi) d\psi \tag{5.16}$$

$$w_k(\psi) = \mu_{pb} q_k(\psi), \quad 0 \leq \psi \leq \gamma_k \tag{5.17}$$

The normal force $q_k(\psi)$ per unit length and the circumferential force $w_k(\psi)$ per unit length vary with the position ψ on the pulley. The Coulomb friction coefficient μ_{pb} at the pulley-belt contact is assumed to be constant ($\mu_{pb} = 0.09$). From the pulley force equations 5.15, 5.16 and 5.17, it follows that:

$$K_k \geq \frac{\cos\beta_v T_k}{2\mu_{pb} R_k} \tag{5.18}$$

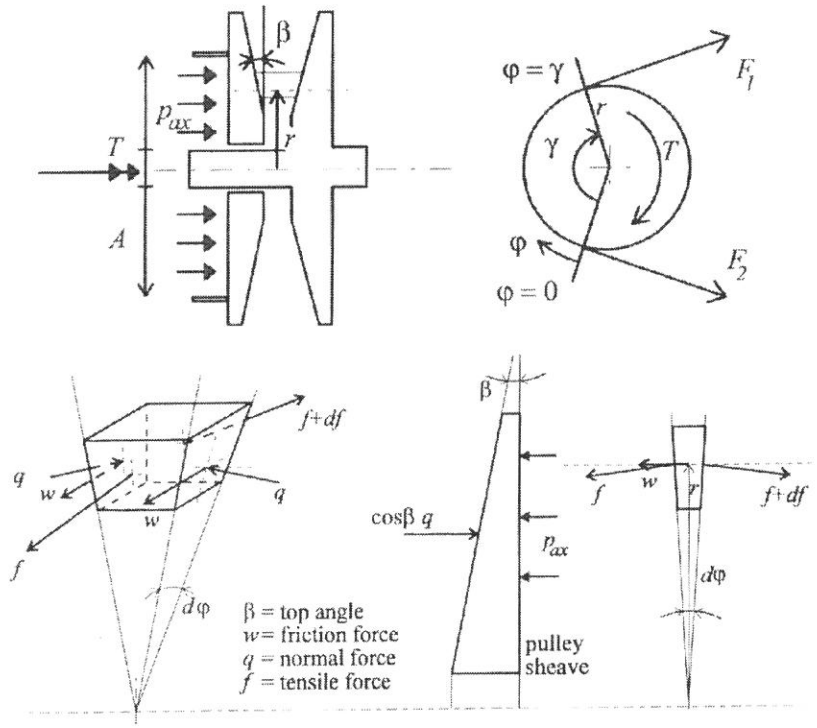

Figure 5.4 *Forces acting on the pulleys and on the belt (up). Forces acting on a cut part of the belt (down).*

is required to avoid slip on pulley k. In practice, a safety factor of 1.3 is introduced. The minimal, required pressures $p_{p,min}$ and $p_{s,min}$ in the primary and secondary piston are:

$$p_{p,min} = \frac{1.3 \cos \beta_v T_p}{2\mu_{pb} A_p R_p} \tag{5.19}$$

$$p_{s,min} = \frac{1.3 \cos \beta_v T_s}{2\mu_{pb} A_s R_s} \tag{5.20}$$

Note that p_k is the total pressure in the piston. At high piston rotation speeds, the velocity pressure due to centrifugal effects becomes important (see [VV 96a]).

Pressure requirements for variator shifting

To compute the relations between the applied pressures p_s and p_p and the variator ratio i_v for different operating conditions (primary speed $\dot{\theta}_p$ and transmitted primary torque T_p), a model of all tension and compression forces in the belt is required. In the literature, various models are described (see [MLB 94], [SVR 92], [Dev 93], [Rek 90], [MV 96], [Luy 88]). Although all authors use a nonlinear static finite element model, there is a large discrepancy in results, because the assumptions made on the friction phenomena and on the friction parameters differ strongly.

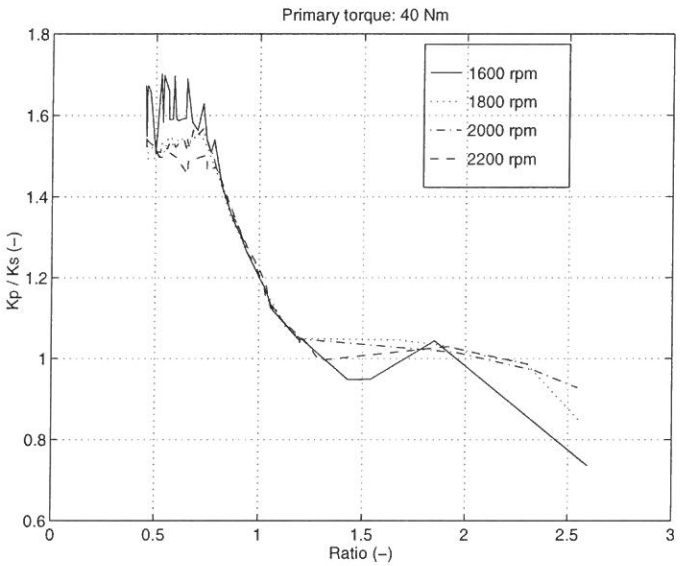

Figure 5.5 *The experimentally determined force ratio $\frac{K_p}{K_s}$ as a function of the variator ratio i_v, for different primary speeds (VT1-variator), at $T_p = 40$ Nm. Observe that $\frac{K_p}{K_s}$ strongly depends on i_v: $\frac{K_p}{K_s}$ decreases from 1.7 to 1, between OD and Medium ($i_v = 1$). From Medium to LOW, $\frac{K_p}{K_s}$ decreases rather slowly, with a minimum of 0.8-0.9 in LOW). Note that $\frac{K_p}{K_s}$ is almost independent of the primary speed.*

For that reason, and since we are mainly interested in deriving a simple model for control, an experimental approach has been taken. From static experiments on a VT1-variator (see [VVM 96]), the relation between the force ratio $\frac{K_p}{K_s}$, the variator ratio i_v, the primary torque T_p, the primary speed $\dot{\theta}_p$ and the secondary pressure p_s is obtained (see figures 5.5 and 5.6). A static neural network (4

inputs, 1 output, 1 hidden layer with 20 neurons, 1 output layer, basis function $\tanh(\sum_i w_{i,j}x_i + \alpha_j)$, 120 model parameters (weights and off-sets), 1688 data points for training, 850 data points for validation) is trained (see [VVM 96]) and fits the highly nonlinear static force ratio map very accurately (± 0.05, except at overdrive ($i_v = 0.445$), where large experimental deviations are observed). Further in this chapter, this static mapping is used to design a variator controller when doing ratio control using pressure steering.

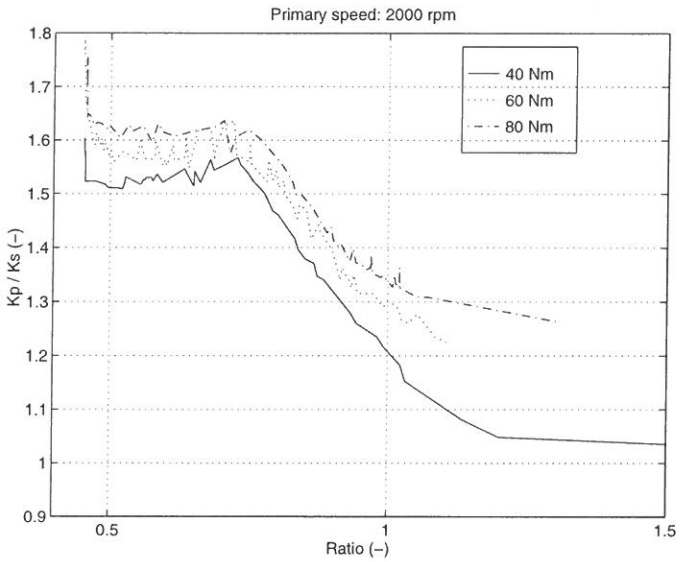

Figure 5.6 *The experimentally determined force ratio $\frac{K_p}{K_s}$ as a function of the variator ratio i_v, for different primary torques (VT1-variator), at a primary speed of 2000 rpm. Observe that $\frac{K_p}{K_s}$ strongly depends on i_v: $\frac{K_p}{K_s}$ decreases from 1.7 to 1, between OD and Medium ($i_v = 1$). From Medium to LOW, $\frac{K_p}{K_s}$ decreases rather slowly, with a minimum of 0.8-0.9 in LOW). Note that $\frac{K_p}{K_s}$ shifts up proportional to primary torque.*

5.2.4 Dynamic flow and pressure requirements

In the previous subsection, the static flow and pressure requirements for a metal V-belt variator are derived. In this subsection, the dynamics of a metal V-belt will be modelled. Two models are derived:

- A linear physical model, only valid around Medium ($i_v = 1$), that computes the rate of ratio change from the axial forces K_p and K_s only. Although only valid around Medium, it illustrates clearly the fundamental CVT-control curse of making a choice between pressure steering and flow steering to realize shifting.

- To describe the shifting dynamics over the whole CVT working range, the experimental model described in [IUK 95] is implemented[1]. This model relates the rate of ratio change $\frac{di_v}{dt}$ to the applied axial forces K_s and K_s, to the primary speed $\dot{\theta}_p$ and to the primary torque T_p.

Simple models for variator shifting

The variator ratio i_v is determined by the combined positions x_s and x_p of the movable halves of the secondary and primary pulleys and can be changed by the axial forces K_p and K_s. Reducing K_p has the same effect as increasing K_s, and vice versa. Near Medium, it holds that (this follows from equations 5.7, 5.8, 5.9 and 5.10):

$$\dot{x}_s = -\dot{x}_p \tag{5.21}$$

$$\dot{R}_s = -\dot{R}_p \tag{5.22}$$

A simple physical system that exhibits a similar property, is shown in figure 5.7. The following phenomena are taken into account:

- The movable halves of the pulleys are modeled as masses for translation. The rotation of the pulleys is neglected.

- The push-belt is modeled as a linear spring-damper system, that is kinematically connected to the pulley masses. The equivalent belt stiffness k_{pb} and damping b_{pb} transform to on axial stiffness $k_{pbx} = \frac{k_{pb}}{4\tan^2\beta_v}$ and an axial damping $b_{pbx} = \frac{b_{pb}}{4\tan^2\beta_v}$. Friction at the pulley surfaces is not considered.

- The friction between the pistons and the housing is assumed to be viscous.

- The secondary spring, required to guarantee i_v = LOW when starting the car, is modeled as a linear spring.

[1] Currently, we are configuring a test rig at VCST, to conduct the described experiments with a VT1-variator. The first results are expected within a few months (June 1997).

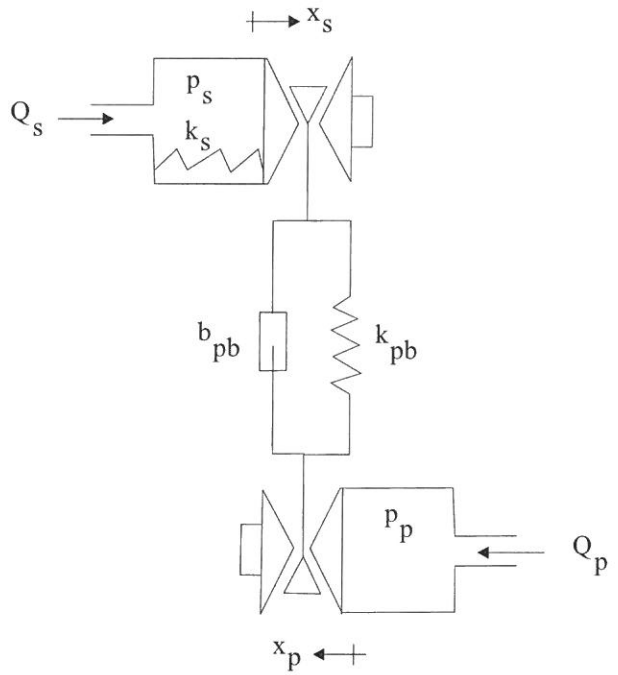

Figure 5.7 *A physical model to describe shifting of the push-belt variator around Medium.*

- The piston volumes and the oil compressibility are modeled by hydraulic capacities.
- The leakage flows in the pistons are assumed to be laminar.

Although this is definitely an oversimplification of reality, it is sufficient for qualitative evaluation purposes. An overview and typical values of all parameters are given in table 5.2

The force and flow balances of the primary and secondary pistons lead to the following equations:

$$\begin{aligned} m_s\ddot{x}_s &= -k_s x_s - b_s\dot{x}_s - k_{pbx}(x_s + x_p) - b_{pbx}(\dot{x}_s + \dot{x}_p) \\ &\quad +F_{s,0} - F_{b,0} + p_s A_s \qquad (5.23) \\ m_p\ddot{x}_p &= -b_p\dot{x}_p - k_{pbx}(x_s + x_p) - b_{pbx}(\dot{x}_s + \dot{x}_p) - F_{b,0} + p_p A_p \qquad (5.24) \end{aligned}$$

$$\frac{V_s}{B_{oil}}\dot{p}_s = Q_s - A_s\dot{x}_s - K_{lk,s}p_s \tag{5.25}$$

$$\frac{V_p}{B_{oil}}\dot{p}_p = Q_p - A_p\dot{x}_p - K_{lk,p}p_p \tag{5.26}$$

	Meaning	Value	Units
m_s	Mass of movable half of secondary pulley	2.1	kg
m_p	Mass of movable half of primary pulley	2	kg
k_s	Stiffness of secondary spring	30820	N/m
b_s	Viscous friction between sec. piston and housing	1000	Ns/m
b_p	Viscous friction between prim. piston and housing	1000	Ns/m
A_s	Effective surface of secondary piston	99e-4	m^2
A_p	Effective surface of primary piston	198e-4	m^2
k_{pb}	Longitudinal stiffness of push-belt	1.5e8	N/m
b_{pb}	Longitudinal damping of push-belt	3e4	Ns/m
$K_{lk,s}$	Laminar leakage coefficient the secondary piston	2.42e-12	m^5/Ns
$K_{lk,p}$	Laminar leakage coefficient of the primary piston	1.12e-14	m^5/Ns
B_{oil}	Bulk modulus of oil	4e8	Pa
V_s	Mean volume of the secondary piston	8.5e-5	m^3
V_p	Mean volume of the primary piston	1.7e-4	m^3
$F_{s,0}$	Pre-load of the secondary spring	1420	N
$F_{b,0}$	Pre-load of the push-belt	19790	N

Table 5.2 *Parameters and typical values for the simplified variator model (around Medium).*

Depending on the model's objectives, three different state-space descriptions can be derived:

- The description of a flow steered variator (QQ)

  In this case, the piston flows Q_s and Q_p are used as control inputs for the variator. The mechanical and the hydraulical dynamics must be taken into account.

- The description of a pressure steered variator (pp)

  In this case, the piston pressures p_s and p_p are used as control inputs for the variator. Only the mechanical dynamics must be considered.

- The description of a pressure-flow steered variator (pQ)

  In this case, pressure steering is applied to the secondary pulley while flow steering is applied to the primary pulley, so the piston pressure p_s and the

piston flow Q_p are used as control inputs for the variator. The mechanical dynamics and the dynamics of the primary piston must be taken into account.

Description of a flow steered variator (QQ)

Define the state vector X_{QQ} and the input vector U_{QQ} as:

$$\mathrm{X}_{QQ} = \begin{pmatrix} x_s & \dot{x}_s & x_p & \dot{x}_p & p_s & p_p \end{pmatrix}'$$

$$\mathrm{U}_{QQ} = \begin{pmatrix} Q_s & Q_p \end{pmatrix}'$$

The state space matrices A_{QQ} and B_{QQ} become:

$$\mathrm{A}_{QQ} = \begin{pmatrix} 0 & 1 & 0 & 0 & 0 & 0 \\ -\frac{k_s+k_{pbx}}{m_s} & -\frac{b_s+b_{pbx}}{m_s} & -\frac{k_{pbx}}{m_s} & -\frac{b_{pbx}}{m_s} & \frac{A_s}{m_s} & 0 \\ 0 & 0 & 0 & 1 & 0 & 0 \\ -\frac{k_{pbx}}{m_p} & -\frac{b_{pbx}}{m_p} & -\frac{k_{pbx}}{m_p} & -\frac{b_p+b_{pbx}}{m_p} & 0 & \frac{A_p}{m_p} \\ 0 & -\frac{A_s B_{oil}}{V_s} & 0 & 0 & -\frac{K_{lk,s} B_{oil}}{V_s} & 0 \\ 0 & 0 & 0 & -\frac{A_p B_{oil}}{V_p} & 0 & -\frac{K_{lk,p} B_{oil}}{V_p} \end{pmatrix}$$

$$\mathrm{B}_{QQ} = \begin{pmatrix} 0 & 0 \\ 0 & 0 \\ 0 & 0 \\ 0 & 0 \\ \frac{B_{oil}}{V_s} & 0 \\ 0 & \frac{B_{oil}}{V_p} \end{pmatrix}$$

In Chapter 6, this model is combined with the valve models, to evaluate candidate piston controllers, since it describes both the hydraulical and the mechanical dynamics. The dynamic response of a flow-steered variator is shown in figure 5.8.

Description of a pressure steered variator (pp)

Define the state vector X_{pp} and the input vector U_{pp} as:

$$\mathrm{X}_{pp} = \begin{pmatrix} x_s & \dot{x}_s & x_p & \dot{x}_p \end{pmatrix}'$$

$$U_{pp} = \begin{pmatrix} p_s & p_p \end{pmatrix}'$$

The state space matrices A_{pp} and B_{pp} become:

$$A_{pp} = \begin{pmatrix} 0 & 1 & 0 & 0 \\ -\frac{k_s+k_{pbx}}{m_s} & -\frac{b_s+b_{pbx}}{m_s} & -\frac{k_{pbx}}{m_s} & -\frac{b_{pbx}}{m_s} \\ 0 & 0 & 0 & 1 \\ -\frac{k_{pbx}}{m_p} & -\frac{b_{pbx}}{m_p} & -\frac{k_{pbx}}{m_p} & -\frac{b_p+b_{pbx}}{m_p} \end{pmatrix}$$

$$B_{pp} = \begin{pmatrix} 0 & 0 \\ \frac{A_s}{m_s} & 0 \\ 0 & 0 \\ 0 & \frac{A_p}{m_p} \end{pmatrix}$$

This model shows the consequences of using pressure steering for variator control (see figure 5.9).

Description of a pressure-flow controlled variator

The state vector X_{pQ} and the input vector U_{pQ} are defined as:

$$X_{pQ} = \begin{pmatrix} x_s & \dot{x}_s & x_p & \dot{x}_p & p_p \end{pmatrix}'$$

$$U_{pQ} = \begin{pmatrix} p_s & Q_p \end{pmatrix}'$$

The state space matrices A_{pQ} and B_{pQ} become:

$$A_{pQ} = \begin{pmatrix} 0 & 1 & 0 & 0 & 0 \\ -\frac{k_s+k_{pbx}}{m_s} & -\frac{b_s+b_{pbx}}{m_s} & -\frac{k_{pbx}}{m_s} & -\frac{b_{pbx}}{m_s} & 0 \\ 0 & 0 & 0 & 1 & 0 \\ -\frac{k_{pbx}}{m_p} & -\frac{b_{pbx}}{m_p} & -\frac{k_{pbx}}{m_p} & -\frac{b_p+b_{pbx}}{m_p} & \frac{A_p}{m_p} \\ 0 & 0 & 0 & -\frac{A_p B_{oil}}{V_p} & -\frac{K_{lk,p} B_{oil}}{V_p} \end{pmatrix}$$

$$\mathrm{B}_{pQ} = \begin{pmatrix} 0 & 0 \\ \frac{A_s}{m_s} & 0 \\ 0 & 0 \\ 0 & 0 \\ 0 & 0 \\ 0 & \frac{B_{oil}}{V_p} \end{pmatrix}$$

This model shows the consequences of using pressure-flow steering for variator control (see figure 5.10).

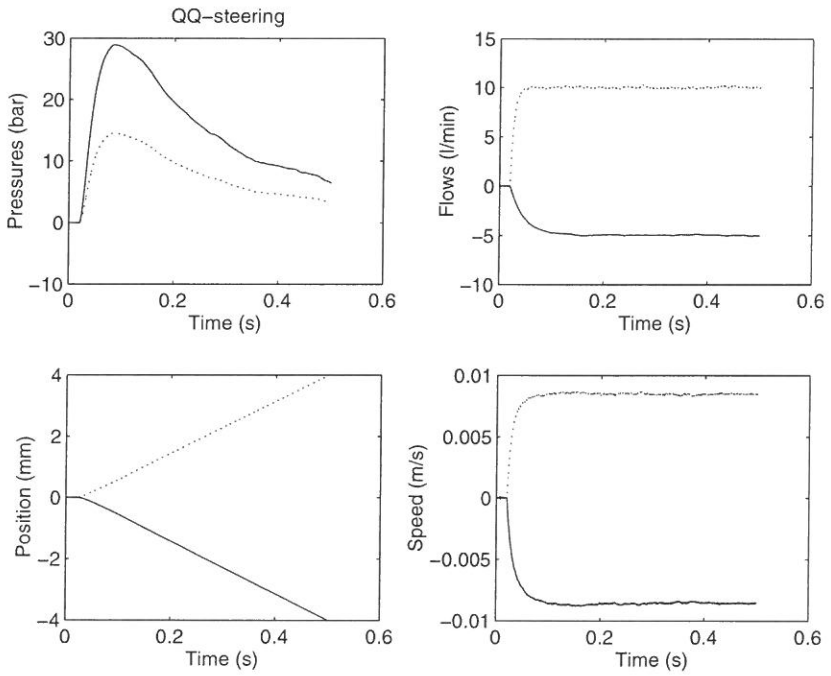

Figure 5.8 *Response of a flow steered variator (secondary signals (solid), primary signals (dotted)). Initially, a flow of 10 l/min is injected in the primary piston, next, a flow of 5 l/min is drained from the secondary piston (note that the piston surfaces A_s and A_p differ 50 %). Observe that the piston speeds are proportional to the injected/drained flows and that the pressures are changing in such a way that the pressure ratio remains almost constant ($\frac{p_s}{p_p} \approx \frac{A_p}{A_s}$).*

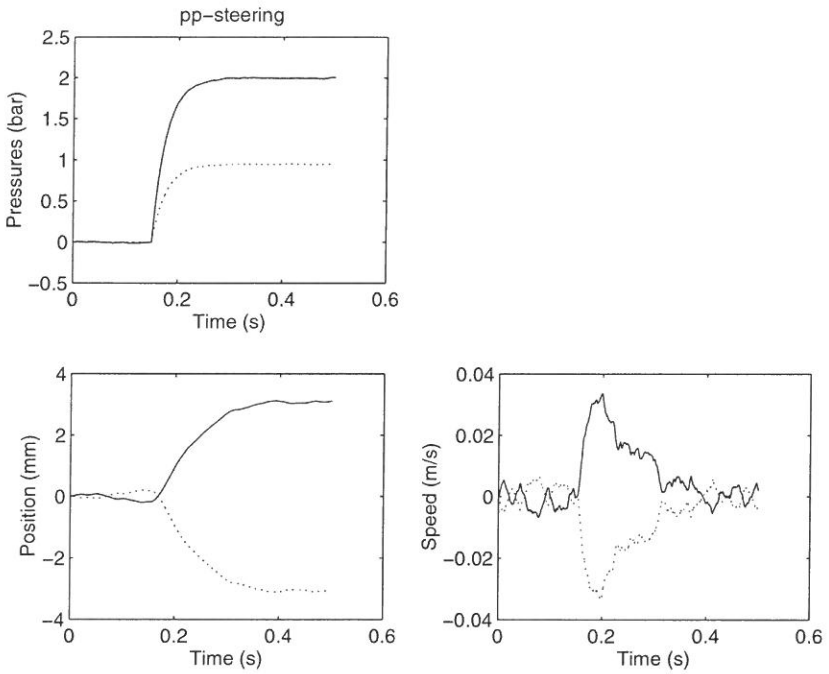

Figure 5.9 *Response of a pressure steered variator (secondary signals (solid), primary signals (dotted)). The secondary and primary pressure are increased simultaneously, with 2 and 0.95 bar respectively (which implies a pressure residu of 1-0.95=0.05 bar). Observe that this very small residu leads to high speeds and significant changes in position (which results in shifting). From this simple result, one can already conclude that accurate control of the variator ratio will be very hard, due to the high sensitivity for pressure residues. This is mainly caused by the extremely high stiffness of the metal V-belt.*

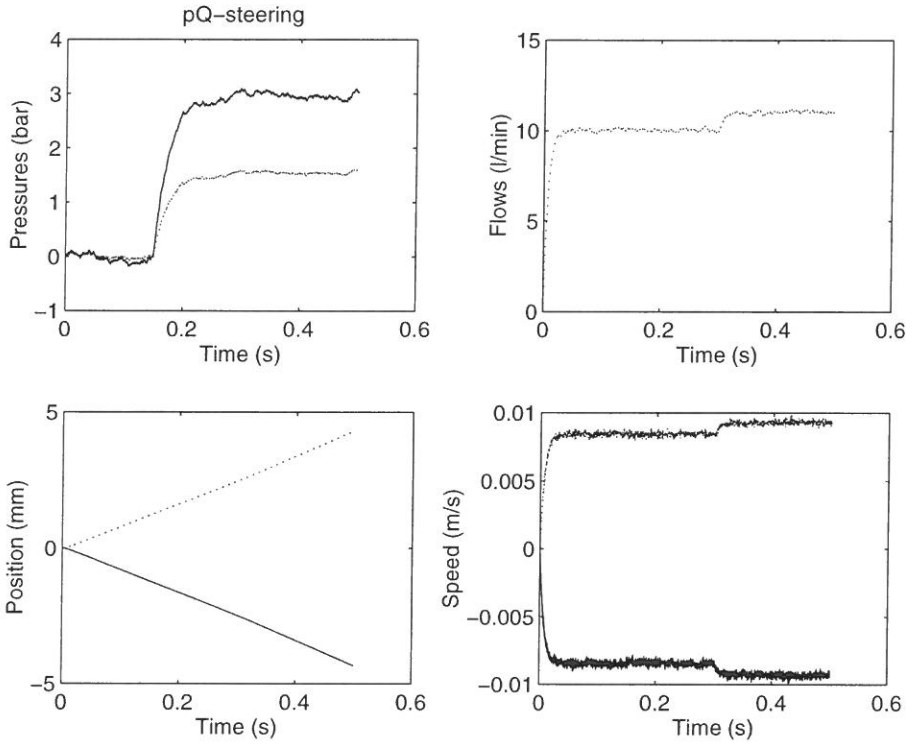

Figure 5.10 *Response of a pressure-flow steered variator (secondary signals (solid), primary signals (dotted). After 0.1 s, the pulleys are moving at constant speed. Then, the secondary pressure is increased with 3 bar, while the primary flow is kept constant. Observe that the primary pressure follows the secondary pressure automatically, without influence on the piston speed. Next, the primary flow is increased, while keeping the secondary pressure constant. The piston speeds change proportional to the primary flow, without influence on the primary pressure. From this simple result, we can conclude that accurate variator control will be rather easy, due to the physical decoupling in the system (p_p only follows p_s, while x_p and x_s only follow Q_p).*

An experimental model for variator shifting

In [IUK 95], a simple experimental model for variator shifting is presented. From dynamic experiments, the following relation has been obtained:

$$\frac{di_v}{dt} = f_v(i_v)\dot{\theta}_p \triangle p_p \tag{5.27}$$

The rate of ratio change is proportional to the primary rotation speed $\dot{\theta}_p$ and to the primary pressure residu $\triangle p_p$. The proportionality factor $f_v(i_v)$ increases piece-wise linear with the ratio i_v, with a nod at Medium. The primary pressure residu $\triangle p_p$ is the difference between the applied primary pressure p_p and the primary pressure required to remain at the actual variator ratio. This required primary pressure can be obtained from the experimentally obtained static force ratio characteristic $\frac{K_p}{K_s}$. Note that $\frac{K_p}{K_s} \approx \frac{p_p A_p}{p_s A_s}$ (only exact if no centrifugal effects take place, i.e. at very low piston rotation speeds). Observe that the influence of the transmitted torque comes in via the static $\frac{K_p}{K_s}$ characteristic.

This model describes the shifting dynamics over the whole CVT working range. Initially, due to the lack of a dedicated test rig, the experimental model described in [IUK 95] has been adopted and implemented in VIRTUES (see figure 5.11). Actually, we are configuring a dedicated test rig at VCST, to conduct the described experiments with VCST's VT1-variator. The first results are expected within a few months (June 1997).

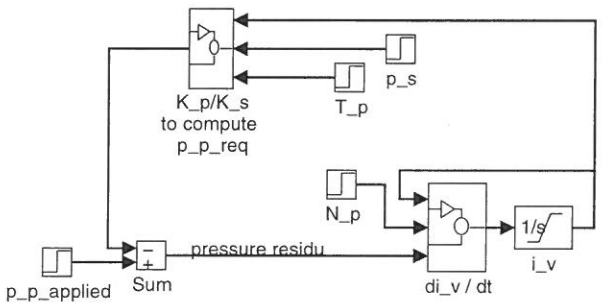

Figure 5.11 *Matlab/Simulink implementation of the experimental variator shifting model described in [IUK 95].*

5.2.5 Efficiency

In Chapter 4, it was assumed that the variator efficiency η_v was constant for all operating conditions. From experiments on a VT1-variator (see [VV 96b], [Dev 93] and [Rek 90]), it is observed that η_v is mainly determined by three variables (see figures 5.13 and 5.14):

- The variator ratio i_v.
- The primary rotation speed $\dot{\theta}_p$.
- The applied piston pressures p_s and p_p.

The applied pressures strongly depend on the transmitted torque, on the control mechanism and on the control strategy.

- If an hydro-mechanical control mechanism is used (e.g. VT1-H), both pressures far exceed the minimum required pressure to avoid slip (given by equations 5.19 and 5.20), since low control flexibility is allowed (e.g. no compensation of pressure for torque). In that case, the variator efficiency is strongly determined by the transmitted torque.
- If electronical control is used (electro-mechanical control or hydro-electrical control (e.g. VT1-E)), the controller is able to compensate for lower torques, to ensure that at least one of the pressures equals the minimum required pressure. In that case, the variator efficiency is only little affected by the transmitted torque.

In the literature, various models to compute efficiency are described (see [MLB 94], [SVR 92], [Dev 93], [Rek 90]). Although all authors use a nonlinear static finite element model, there is a large discrepancy in results, because the assumptions made on the friction phenomena and on the friction parameters differ strongly.

In this thesis, experimental data from a VT1-variator are used to describe efficiency. The static nonlinear function $\eta_v(\dot{\theta}_p, T_p, i_v, p_s)$ relates the variator efficiency η_v to the primary rotation speed $\dot{\theta}_p$, to the primary torque T_p, to the variator ratio i_v and to the secondary pressure p_s. A static neural network (4 inputs, 1 output, 1 hidden layer with 20 neurons, 1 output layer, basis function $\tanh(\sum_i w_{i,j}x_i + \alpha_j)$, 120 parameters (weights and off-sets), 1688 data points for training, 850 data points for validation) is trained (see [VV 96b]) and models the highly nonlinear static efficiency map very accurately (average absolute error of 0.3 Nm on the estimated loss torque, see figure 5.12).

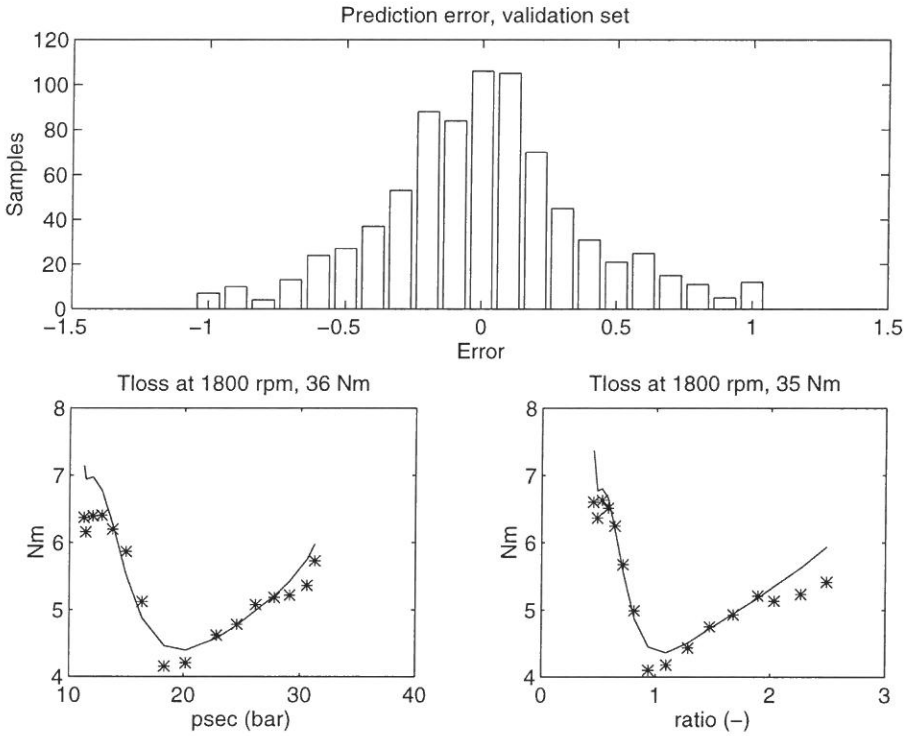

Figure 5.12 *A static neural network to fit the variator efficiency map: from the histogram of the prediction error, it follows that the neural network models the highly nonlinear static efficiency map very accurately (average absolute error of 0.3 Nm on the estimated loss torque). Comparison of experimental data (*) and model predictions (solid) shows that trends are modeled quite well.*

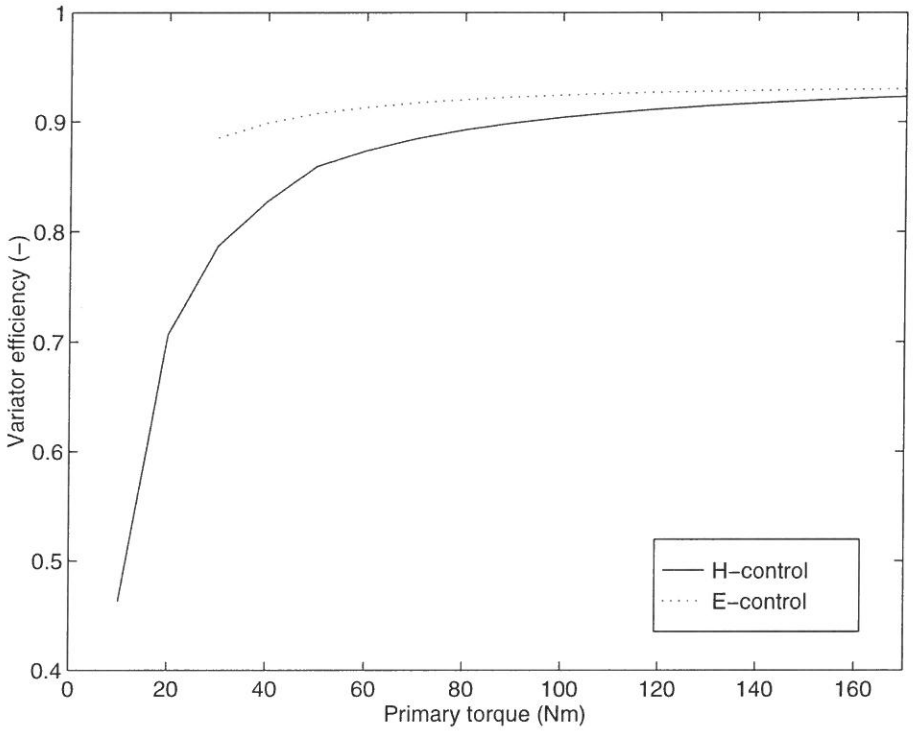

Figure 5.13 *The predicted variator efficiency η_v as a function of the primary torque T_p, for an hydraulical (VT1-H) and an electronical (VT1-E) controlled drive train (i_v = LOW, $\dot{\theta}_p$ = 2400 rpm). For H-control, the efficiency reduces drastically at lower torques, since the hydro-mechanical control unit is tuned for maximal torque (140 Nm) only. At lower torques, the safety factor farly exceeds 1.3, which results in lowered efficiencies. In E-control, the influence of the primary torque on the efficiency is limited (3-4 %), since compensation for the transmitted primary torque is included in the controller (simulation).*

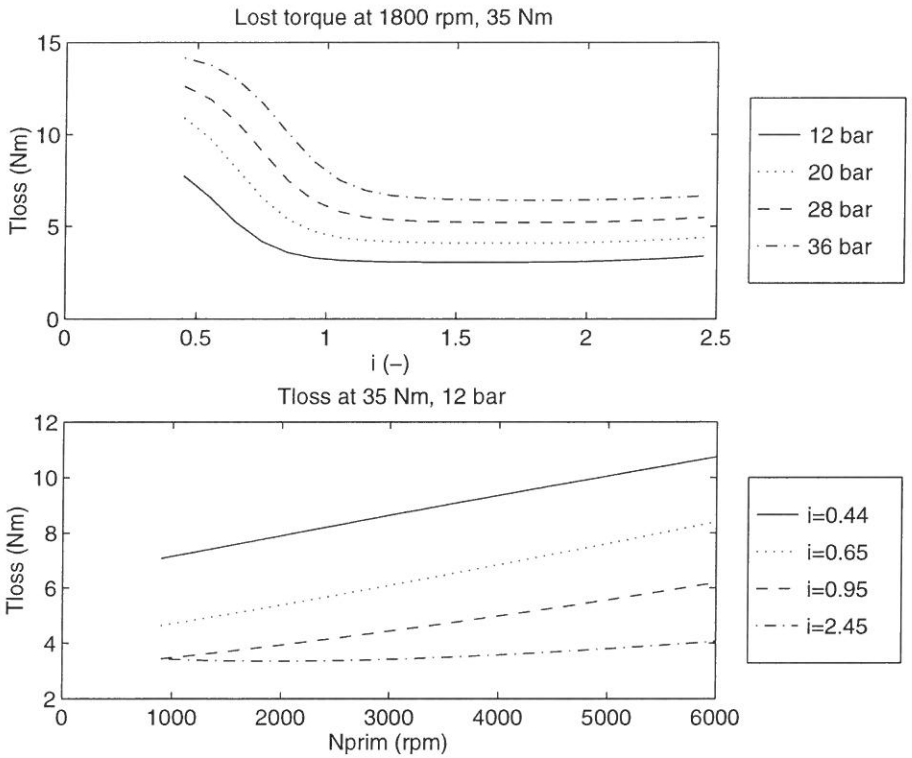

Figure 5.14 *Predicted relations between loss torque, variator ratio, secondary pressure and primary speed, for a primary torque of 35 Nm (simulation). The loss torque increases linear with secondary pressure and primary speed. From Overdrive to Medium, the loss torque decreases. From Medium to Low, the loss torque remains almost constant.*

5.3 Variator control

In this section, we discuss strategies for variator control. For variator control, the desired rate of ratio change $\frac{di_v}{dt}$, as computed by the drive train controller (see Chapter 4), and the requirement of slip avoidance under all circumstances, are the 'set points' for the variator controller. Depending on the chosen control configuration (pressure steering (pp) or pressure-flow steering (pQ)), different control strategies are required.

In practice, two-stage control (master-slave control) is required (see figure 5.15):

- An outer control algorithm (master) transforms the 'set points' into reference pressures (pp) or into a reference pressure and a reference flow (pQ)[2].
- Two inner controllers (slaves) realize the desired reference pressures and/or flow by controlling different spool valves. To increase dynamic performance, these inner controllers take into account the hydraulic characteristics of the spool valves and the pistons.

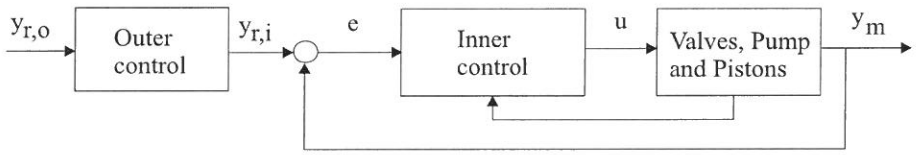

Figure 5.15 *Two stage variator control: the outer reference signals* $y_{r,o} = (\frac{di_v}{dt}, \text{no slip})$ *are transformed into inner reference signals* $y_{r,i}$ ($y_{r,i} = (p_{s,r}, p_{p,r})$ *for pressure steering and* $y_{r,i} = (p_{s,r}, \dot{x}_{p,r})$ *for pressure-flow steering). The inner controller uses the error signals to compute the control signal* $u = (u_s, u_p)$ *of the secondary and primary valve.*

First, the outer control algorithms for two control configurations are derived, next, inner controllers for pressure steering and flow steering are designed.

Note that in the hydraulic controlled variator (P811, VT1-H), the primary flow and the secondary pressure are controlled hydro-mechanically. The clamping force at the primary side is delivered either by applying a primary pressure (by injecting flow) or by the contact force between the primary pulley and the housing, due to the applied secondary pressure. In LOW, shifting starts as soon as the primary pressure beats the secondary pressure (and thus becomes higher than

[2] In pp-control, servo loops on the primary pressure and the secondary pressure are assumed. In pQ-control, servo loops on the secondary pulley pressure and the primary pulley flow are assumed.

the required clamping pressure, controlled by the secondary pressure). Therefore, from a control point of view, the hydraulic controlled variator is an example of a pQ configuration.

5.3.1 Outer control

An outer control algorithm for pressure steering (pp)

In this case, pressure steering on both pulleys is applied. The experimental model of [IUK 95] (see equation 5.27) and the experimental force ratio characteristic $\frac{K_p}{K_s}$ of [VVM 96] are used to transform the desired rate of ratio change into desired primary and secondary pressures:

The desired rate of ratio change $\frac{di_v}{dt}$ is obtained from the drive train controller. First, the primary pressure residu (assuming $p_s = p_{s,min}$) and the secondary pressure residu (assuming $p_p = p_{p,min}$) are computed from the experimental models of $\frac{di_v}{dt}$ and $\frac{K_p}{K_s}$. The pressure with a positive residu will be used to realize shifting, the other pressure will be used to avoid slip. Next, the reference for the slip avoiding pressure is computed from equation 5.19 or 5.20, while the reference pressure for shifting is increased with the required (positive) pressure residu.

To compute the pressures $p_{p,min}$ and $p_{p,max}$, the estimated actual torques T_s and T_p (from the estimated engine torque $T_e(\dot{\theta}_{e,m}, \alpha_{th,m})$ and the estimated variator ratio $i_{v,m} = \frac{\dot{\theta}_{p,m}}{\dot{\theta}_{s,m}}$) are combined with the geometrical variator relations 5.4, 5.5 and 5.6.

An outer control algorithm for pressure-flow steering (pQ)

In this case, pressure steering is applied on the secondary pulley, while flow steering is applied on the primary pulley. From the linear variator model for a pQ-configuration (see subsection 5.2.4), it follows that a strong physical decoupling between piston pressures and piston speeds (flows) exists. Therefore, we use two decoupled controllers, one for shifting (by primary flow steering) and one to avoid belt slip (by secondary pressure steering).

The reference secondary pressure is computed as:

$$p_{s,r} = \frac{1.3 \cos \beta_v T_s}{2 \mu_{pb} A_s R_s} \tag{5.28}$$

while the reference primary flow (or speed) is computed as:

$$Q_{p,r} = A_p \dot{x}_p = 2A_p \tan\beta_v g_p(i_v) \frac{di_v}{dt} \tag{5.29}$$

The desired rate of ratio change $\frac{di_v}{dt}$ is obtained from the drive train controller. The estimated actual torque T_s is computed from the estimated engine torque $T_e(\dot{\theta}_{e,m}, \alpha_{th,m})$ and the estimated variator ratio $i_{v,m} = \frac{\dot{\theta}_{p,m}}{\dot{\theta}_{s,m}}$.

5.3.2 Inner controllers for pressure and flow steering

The inner controllers take care that the reference pressures and/or flow, computed by the outer controller, are realized. The characteristics of the pistons and the spool valves must be taken into account (see Chapter 6 for spool valve characteristics).

In general, the inner controllers for pressure and flow steering operate as follows:

- An inner controller for pressure steering uses the reference pressure, the actual piston pressure and the actual piston speed to compute the control output.
- An inner controller for flow steering uses the reference flow (or speed), the actual piston speed and the actual piston pressure to compute the control output.

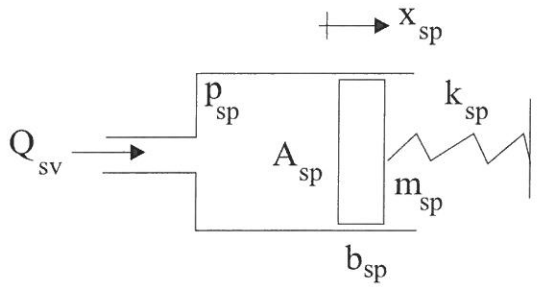

Figure 5.16 *A single-piston model that is used to design inner control algorithms.*

For inner control design, a single-piston model (see figure 5.7) is assumed to

be valid[3]. Writing down the force balance and the flow balance leads to the following equations:

$$m_{sp}\ddot{x}_{sp} = -b_{sp}\dot{x}_{sp} - k_{sp}x_{sp} + p_{sp}A_{sp} \tag{5.30}$$

$$\frac{V_{sp}}{B_{oil}}\dot{p}_{sp} = Q_{sv} - A_{sp}\dot{x}_{sp} - K_{lk}p_{sp} \tag{5.31}$$

Parameter	Meaning	Value	Units
m_{sp}	Mass of piston	2	kg
b_{sp}	Viscous friction coefficient	1000	Ns/m
k_{sp}	Stiffness of piston spring	31000	N/m
A_{sp}	Section of piston	198e-4	m^2
V_{sp}	Volume of the piston	1.8e-4	m^3
K_{lk}	Linearized leakage coefficient of piston	4e-12	$m^3/s/Pa$
B_{oil}	Bulk modulus of oil-air mixture	4e8	Pa

Table 5.3 *Piston and load related parameters.*

The parameters and typical values are listed in table 5.3. The leakage flow Q_{lk} is linearized ($Q_{lk} = K_{lk}p_{sp}$) , and thus proportional to piston pressure (see [Mer 67], [Vie 80], [Wat 89]). The flow that is directed by the spool valve into the piston is represented by Q_{sv}. In practice, two configurations are used to realize Q_{sv} (see figure 5.17):

- Normally closed configurations (NC)

  The spool valve opens only when a flow Q_{sv} into or out of the piston is required. The flow through the spool valve (in this case equal to Q_{sv}) depends on the valve section $a_{sv}(x_{sv})$, on the transmission oil (via ρ_{oil}), on the valve control signal u_{sv} (that determines the valve position x_{sv}) and on the spool valve's pressure drop $p_{sp} - p_o$, with p_o being the supply pressure (flow into piston) or the relief pressure (flow out of piston) (see [Mer 67], [Dra 81], [JE 91a], [Vie 80], [Wat 89] and [Vog 89]. More details are given in Chapter 6):

$$Q_{sv} = C_d a_{sv}(x_{sv}(u_{sv})) \sqrt[\pm]{\frac{2}{\rho_{oil}}|p_{sp} - p_o|} \tag{5.32}$$

[3]In fact, this holds only for pQ-steering. For pp-steering, the multivariable control model derived in subsection 5.2.4 should be used.

- Normally open configurations (NO)

  The spool valve is used to divide the supplied flow Q_{supply} into a piston flow Q_{sv} and a relief flow Q_{rf}. In this case, the flow into the piston is given by:

$$Q_{sv} = Q_{supply} - C_d a_{sv}(x_{sv}(u_{sv})) \sqrt[\pm]{\frac{2}{\rho_{oil}}|p_{sp} - p_o|} \tag{5.33}$$

  with p_o being the relief pressure.

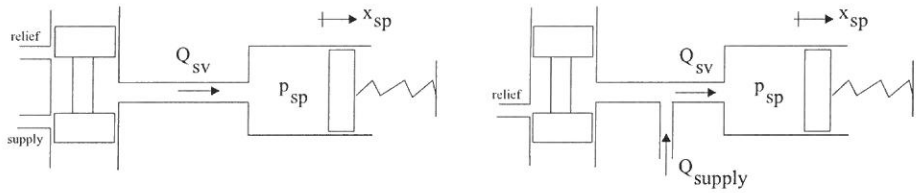

NC-configuration NO-configuration

Figure 5.17 *Two configurations to realize a flow into a piston: a normally closed configuration (l) and a normally open configuration (r).*

For control design, the following relation is used:

$$Q_{sv} = Q_{supply} + f_{sv}(u_{sv})\sqrt{|p_{sp} - p_o|} \tag{5.34}$$

For NC configurations, $Q_{supply} = 0$. The spool valve function $f_{sv}(u_{sv})$ is known from a valve model, while the supplied flow Q_{supply} is computed from a gear pump model (see Chapter 6).

An inner controller for pressure steering

In this case, the piston speed is assumed to be known (controlled at the other side of the CVT) and the force equation can be neglected. The control model for pressure steering looks like:

$$\frac{V_{sp}}{B_{oil}}\dot{p}_{sp} = Q_{sv} - A_{sp}\dot{x}_{sp} - K_{lk,sp}p_{sp} \tag{5.35}$$

with

$$Q_{sv} = Q_{supply} + f_{sv}(u_{sv})\sqrt{|p_{sp} - p_o|} \tag{5.36}$$

By applying feedback linearization (see [SL 91] for the theory, see [HW 94] for another industrial application), the control signal u_{sv} can be computed as:

$$u_{sv} = f_{sv}^{-1}\left(\frac{\frac{V_{sp}}{B_{oil}}v_{sv} + A_{sp}\dot{x}_{sp} + K_{lk,sp}p_{sp} - Q_{supply}}{\sqrt{|p_{sp} - p_o|}}\right)$$

with v_{sv} being the signal from a linear controller, designed for the linearized system given by:

$$\begin{aligned} \dot{x} &= v_{sv} \\ y &= x \end{aligned}$$

In practice, compensations for pressure error, for leakage flow, for velocity flow, for the spool valve's pressure drop and for variations in the supplied flow (for NO configuration only) are taken into account. The piston speed $\dot{x}_{sp,m}$ can be estimated from the estimated rate of ratio change (compute $i_{v,m} = \frac{\dot{\theta}_{p,m}}{\dot{\theta}_{s,m}}$ and differentiate), while the piston pressure and the pressure(s) p_o are measured. The coefficients $K_{lk,sp}$ and A_{sp} are known from piston modeling, while V_{sp} can be computed from the estimated piston speed. The oil bulk modulus B_{oil} is only known within a certain range, but can be estimated from the measured rotational speed and the measured piston pressure (see [Mer 67], [JZY 94] and [JE 91b]). The uncertainty on the oil bulk modulus B_{oil} is taken into account by experimental adaptation of the gain of the linear controller. The signal flow diagram is shown in figure 5.18.

An inner controller for flow steering

In this case, the force equation and the flow equation are both important to design the controller. It is assumed that the inertia forces are negligible ($m_{sp}\ddot{x}_{sp} \approx 0$) (see [Spijk 94]). Taking the time derivative of the force equation 5.31 and substitution of the flow equation 5.30 finally leads to the following control model:

$$b_{sp}\ddot{x}_{sp} + (k_{sp} + \frac{A_{sp}^2 B_{oil}}{V_{sp}})\dot{x}_{sp} = \frac{A_{sp}B_{oil}}{V_{sp}}Q_{sv} - \frac{K_{lk,sp}A_{sp}B_{oil}}{V_{sp}}p_{sp}$$

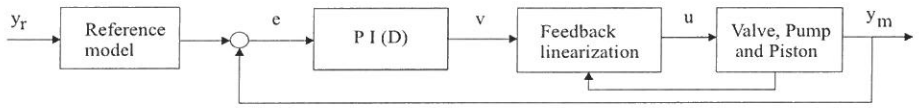

Figure 5.18 Feedback linearization and model reference piston control: the reference piston pressure $y_r = p_{sp,r}$ is applied to the closed loop reference model. The output of the reference model is compared with the measured pressure $y_m = p_{sp,m}$ and fed to a PI-controller. The output v of the PI-controller(s) is applied to the feedback linearization block, to obtain the valve control signal $u = u_{sv}$.

For flow steering, a reference flow Q_r or an equivalent reference speed $\dot{x}_r = \frac{Q_{sp}}{A_{sp}}$ must be realized. By applying feedback linearization, the control signal u_{sv} can be computed:

$$u_{sv} = f_{sv}^{-1}\left(\frac{\frac{V_{sp}b_{sp}}{A_{sp}B_{oil}}v_{sv} + (\frac{k_{sp}V_{sp}}{A_{sp}B_{oil}} + A_{sp})\dot{x}_{sp} + K_{lk,sp}p_{sp} - Q_{supply}}{\sqrt{|p_{sp} - p_o|}}\right)$$

with v_{sv} being the signal from a linear controller, designed for the linearized system given by:

$$\dot{x} = v_{sv} \tag{5.37}$$

$$y = x \tag{5.38}$$

In practice, compensations for the speed error, for the leakage flow, for the velocity flow, for the spool valve's pressure drop and for variations in the supplied flow (NO configuration) are taken into account. As before, the piston speed $\dot{x}_{sp}$ can be estimated, while the piston pressure and the pressure(s) p_o are measured. The coefficients $K_{lk,sp}$ and A_{sp} are known, while V_{sp} can be computed from the measured piston speed. The oil bulk modulus B_{oil} is only known within a certain range, but can be estimated. The mechanical spring constant k_{sp} is negligible, compared to the equivalent hydraulic spring (with equivalent spring constant $k_{eq} = \frac{A_{sp}^2 B_{oil}}{V_p}$) and must not be known exactly for good control performance. The uncertainty on the mechanical friction b_{sp} and on the oil bulk modulus B_{oil} is taken into account by experimental adaptation of the gain of the linear controller.

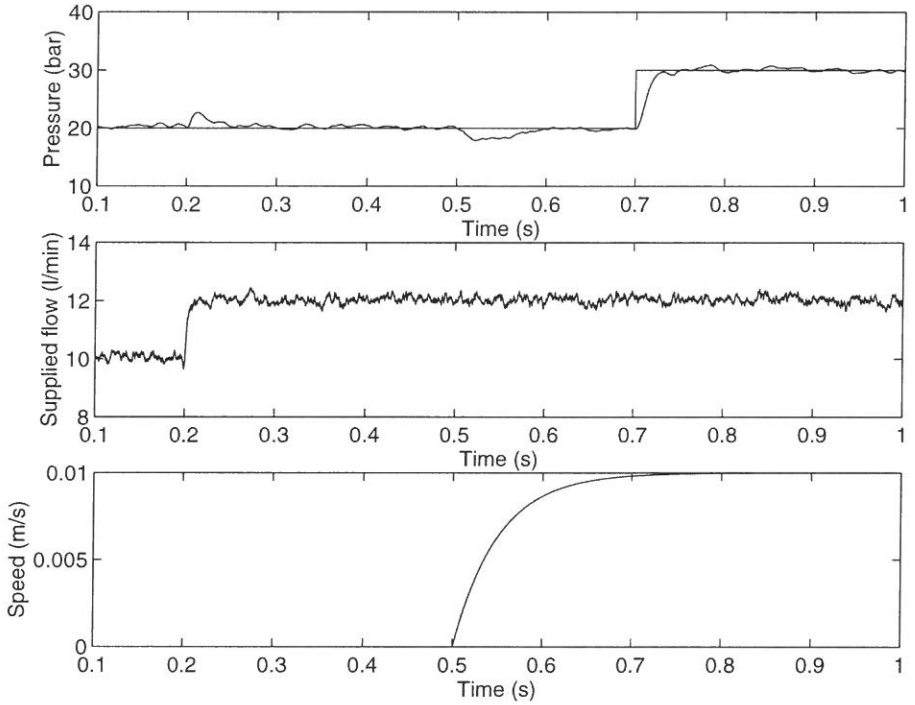

Figure 5.19 *Performance of an inner loop for pressure control, based on linear control and feedback linearization (VT1-variator, NO-configuration). Initially, the piston position and the pump speed are (almost) constant and the pressure is controlled to be 20 bar. Then, the supplied flow increases with 2 l/min. The pressure controller minimizes the influence of this disturbance. Next, the piston is unlocked and the piston position is varied in a controlled way. Since the piston volume enlarges, the pressure initially decreases, but the pressure controller compensates rapidly. Finally, the reference pressure increases with 10 bar. The pressure controller reacts well, and ensures a settling time of 30-40 ms. From this result, one can conclude that both the proposed secondary valve design and the proposed control strategy are acceptable.*

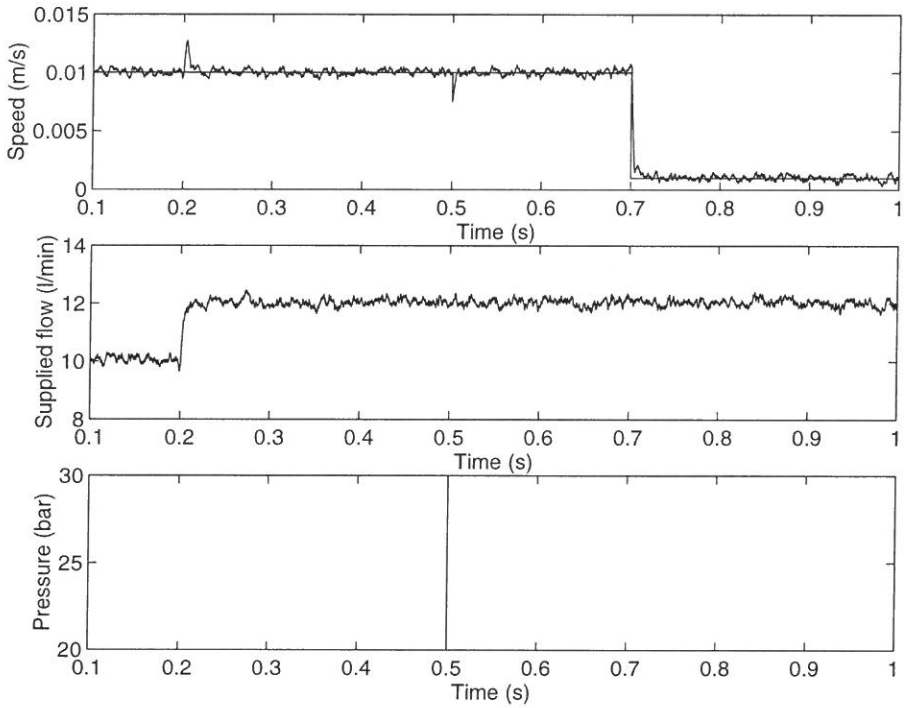

Figure 5.20 *Performance of an inner loop for speed control, based on linear control and feedback linearization (VT1-variator, NO-configuration). Initially, the piston pressure and the pump speed are almost constant and the speed is controlled to be 0.01 m/s. Then, the pump speed (and the corresponding supplied flow) increases with 2 l/min. The speed controller minimizes the influence of this disturbance. Next, the piston pressure is increased with 10 bar. Since the piston leakage will increase, the speed initially decreases, but the speed controller compensates rapidly. Finally, the reference speed decreases to almost zero. The speed controller reacts well, and ensures a settling time of 30 ms. From this result, one can conclude that both the proposed primary valve design and the proposed control strategy are acceptable.*

Chapter 6

Valves and mechanisms for piston control

In this Chapter, we analyze the operation and performance of the different components in servo systems for variator control. In Section 6.2, we describe the different components of a variator control configuration. In Section 6.3, we analyze two typical spool valves for steering and control of CVTs: a double-stage flow valve and a pressure valve with internal feedback. For each component, a non-linear and a linearized physical model are constructed. The model parameters are computed from technical drawings, material characteristics and dedicated experiments on a VT1-E transmission (see Chapter 8 for a description of the test rig). In Section 6.4, two different control mechanisms for piston control are discussed: in hydro-mechanical control, pitot assemblies, cams, bars and links are used for sensing, control and actuation, while in electro-hydraulic control, pulse width modulated solenoid valves or linear electro-mechanical actuators are combined with sensors and an ECU.

6.1 Introduction

When designing control mechanisms for variator control, different aspects are taken into account:

- Compactness
  In automotive applications, spatial integration of different drive train components is required. Therefore, the size of the CVT must be restricted.

Furthermore, in order to realize high shifting speeds under high load conditions, the actuation unit must be able to deliver relatively high power. Since hydraulic systems have a high power to size ratio, they are superior in this respect (see [Mer 67], [Bac 93]).

- Stiffness

  The mechanical stiffness of the variator increased drastically after replacing the rubber belt by a metal V-belt. To obtain good closed-loop performance, the stiffness of the actuation unit needs to be high as well. Hydraulic systems are promising, because they have higher stiffness than other drive devices, due to low leakage. This results in a high closed-loop bandwidth, a high accuracy and a high speed of response. Furthermore, since pressure to inertia ratios are large in hydraulic systems, they have a high acceleration capability.

- Control intelligence and flexibility

  From Chapters 2 to 5, it follows that functional integration is required for adequate CVT-control, since the control system of a CVT has to perform multiple tasks simultaneously (realize variogram tracking, avoid slip, limp-home facility), by controlling multiple variables (engine speeds, pressures, flows). Furthermore, to meet the wide variety of customer wishes with a standard transmission and a tunable control system, flexibility to change the control parameters is required. In this context, electro-hydraulical control systems (VT-E) hold more promises than hydro-mechanical control systems (VT-H).

- Ease of design

  To reduce cost and time needed for valve-body design, simple design procedures are advantageous. However, for hydraulic systems, basic design procedures are lacking and difficult to obtain, because of the complexity of hydraulic system analysis. For example, in contrast to Ohm's law for electrical resistors, there is no simple law that describes hydraulic resistance of passages to flow. This factor limits the degree of sophistication of hydraulic systems.

- Cost

  Replacing hydro-mechanical control systems by electro-hydraulical systems has two cost effects:

  - By reducing the number of expensive hydraulical components and mechanical operations, the cost reduces.

  - By adding sensors, an ECU and electronical actuators, the cost increases. Restrictions on these additional costs are reflected in limitations on price (and performance) of the used electronical equipment.

- Life time

  Compared to other technologies, hydraulic components are superior with respect to lubrication and cooling, since the servo oil takes also care for lubrication and carries away the heat. This increases the life time of mechanical parts (see [Mer 67]).

  However, detoriation and contamination of the oil is important and may lead to hydraulic control failures. Oppositely, hydraulic actuators may be operated under continuous, reversing and stalled conditions without damage.

From this, one may conclude that electro-hydraulical control systems hold the future for variator control. Actually, most transmission manufacturers are doing research on electro-hydraulical control systems (e.g. Multimatic (Honda), ECVT (Subaru), VT1-E and VT1-F (VCST)).

6.2 A configuration for variator control

A variator control configuration contains various elements (see figures 6.2 and 6.1):

- The primary and secondary pistons: both pressures and speeds must be controlled.
- The valve-body contains on-off valves and spool valves with specific functions. In practice, these valves realize different functions:
  - Control of piston speeds and/or piston pressures.
  - Generation of auxiliary pressures or flows (e.g. a constant supply pressure when using PWM solenoid valves).
  - At electronic system breakdown, a limp home opportunity is realized by combining on/off valves and spool valves.
- Transmission oil is used for actuation and lubrication.
- An engine driven gear pump provides oil under pressure to the hydraulic actuation unit.

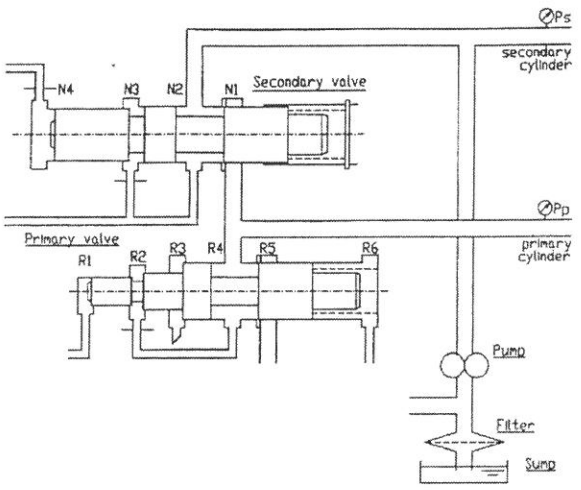

Figure 6.1 *A configuration for variator control (pp-configuration, VT1-E, Source: VCST). The primary valve and the secondary valve are both NO-valves with internal pressure feedback. The valve pressures are proportional to the servo pressures (applied at N4 and R1), that are applied using PWM solenoid valves. The valves are used in a serial configuration. The pump flow goes either to the secondary piston or to the primary circuit. The primary flow goes to the primary piston or is drained to the clutches and for lubrication. Slip at each pulley is avoided by installing a sufficiently high piston pressure, while adequate shifting is done by control of the pressure residu. In this electro-hydraulical control system, variogram tracking and slip avoidance are implemented with the aid of sensors, an ECU, solenoid valves and spool valves. The ECU allows quick changes of the desired variogram and the control parameters, and is able to adapt pressure levels to transmitted torque.*

- Different sensing and actuation devices are used. Their characteristics mainly depend on the used controller mechanism.

The pistons, the transmission oil and the gear pump are standard devices that are described in this Section. In Section 6.3, different spool valves and control mechanisms for piston control are described.

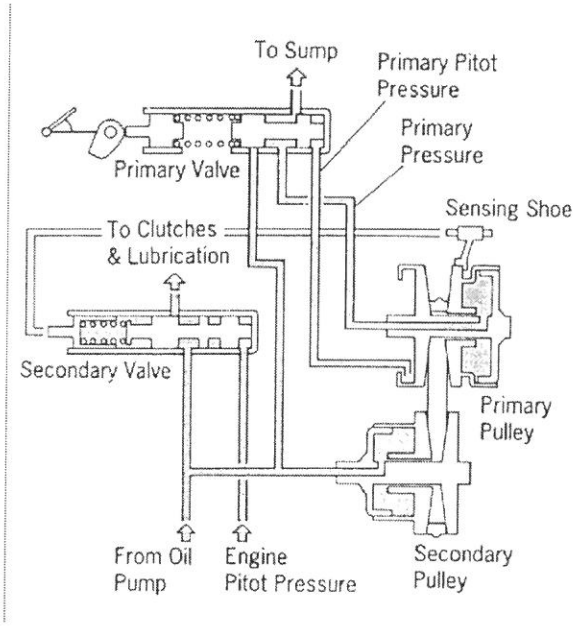

Figure 6.2 *A configuration for variator control (pQ-configuration, VT1-H, Source: VCST). The secondary valve is a NO-valve with internal pressure feedback. The resulting secondary pressure depends the engine speed (via the engine pitot pressure and the pump flow) and on the actual variatoor ratio (via the sensing shoe) and is determined by the force equilibrium of the valve (see Section 6.3). The drain flow of the secondary valve is used in the clutches and for lubrication. The secondary valve is used to avoid slip on both pulleys. The primary valve is a NC-valve that delivers flow to the primary piston, to control shifting speed. The shifting characteristics of the variator depend on the force equilibrium of the valve and are determined by the primary speed (via primary pitot pressure) and the throttle position (via the cam and the plunjer). When the throttle position increases, the variator shifts untill a corresponding (higher) primary pressure is reached, and vice versa. In this hydro-mechanical control system, variogram tracking (realization of a throttle dependent engine speed (=primary speed when clutch is locked)) and slip avoidance are implemented without electronics.*

6.2.1 The variator pistons

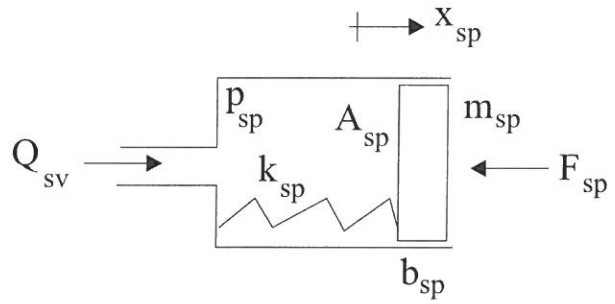

Figure 6.3 *A functional model of a single variator piston.*

A functional model of a single piston is shown in figure 6.3. For each piston, the following effects are taken into account:

- The movable half of each pulley is described as a mass for translation.
- The friction between the housing and the piston is assumed viscous only. In practice, stick-slip effects might occur, due to the Coulomb friction between housing and sealing (see [VD *et al* 96]).
- A piston spring and an additional variable load force F_{sp} are used to emulate load forces. The mechanical interaction with the other piston, via the metal V-belt, is not considered here.
- Leakage flows to the environment are assumed to be turbulent.
- The hydraulic capacitor depends on the piston volume and the oil compressibility. Here, the mean piston volume is used, since volumetric changes are small, due to the small pulley angle ($\beta_v = 11^o$).

Writing down the force balance and the flow balance leads to the following equations (note: $\sqrt[\pm]{\frac{2}{\rho_{oil}}|p_{sp}|} = \sqrt{\frac{2}{\rho_{oil}}|p_{sp}|}\ \mathrm{sign}(p_{sp})$, see also in Notations):

$$m_{sp}\ddot{x}_{sp} = -b_{sp}\dot{x}_{sp} - k_{sp}x_{sp} - F_{sp} + p_{sp}A_{sp} \tag{6.1}$$

$$\frac{V_{sp}}{B_{oil}}\dot{p}_{sp} = Q_{sv} - A_{sp}\dot{x}_{sp} - C_d a_{lk} \sqrt[\pm]{\frac{2}{\rho_{oil}}|p_{sp}|} \tag{6.2}$$

Table 6.1 gives an overview and typical values of the important parameters.

Parameter	Meaning	Value	Units
m_{sp}	Mass of piston	2	kg
b_{sp}	Viscous friction coefficient	1000	Ns/m
k_{sp}	Stiffness of piston's spring	31000	N/m
A_{sp}	Section of piston	198e-4	m^2
V_{sp}	Volume of the piston	1.8e-4	m^3
a_{lk}	Leakage orifice of piston	5e-7	m^2
B_{oil}	Bulk modulus of oil-air mixture	4e8	Pa

Table 6.1 *Piston and load related parameters.*

6.2.2 The used transmission oil

Esso EZL 799 oil is used as transmission oil. The following effects are taken into account:

- Influence of the oil temperature on the mass density ρ_{oil}.
- Influence of the oil temperature on the kinematic viscosity ν_{oil}.
- Influence of included air on the effective compressibility B_{eff}.

Table 6.2 gives an overview and typical values of important parameters.

Parameter	Meaning	Value	Units
T_{oil}	Temperature of oil	-20 - 120	°C
ρ_{oil}	Mass density of oil	850	kg/ m^3
ν_{oil}	Kinematic viscosity of oil	0.6e-4	m^2/s
X_{air}	Volume fraction of enclosed air	0 - 10	%
B_{eff}	Effective compressibility	4e6-4e8	Pa

Table 6.2 *Important oil characteristics.*

Experimental data (see [VV 96d]) are used to model the temperature dependency (see figure 6.4). From linear total least squares (see [VHV 91]), the following model to compute the mass density and the absolute viscosity of the oil is obtained:

$$\rho_{oil} = 907.5 - 1.964 T_{oil} \tag{6.3}$$

$$\ln(\nu_{oil}) = -9.2086 - 0.027 T_{oil} \tag{6.4}$$

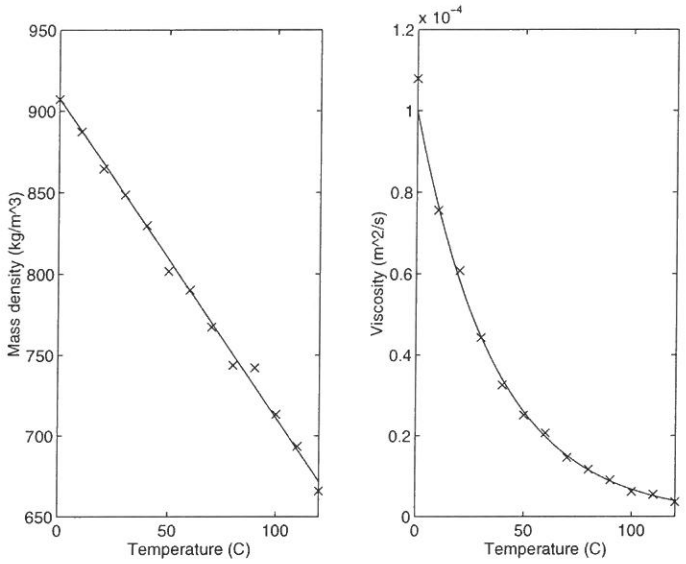

Figure 6.4 *The experimental mass density and kinematic viscosity of Esso EZL 799 oil, as a function of the oil temperature* T_{oil}.

To analyze the influence of enclosed air (volume fraction $X_{air} = \frac{V_{air}}{V_{total}}$) on the effective compressibility, we adopted the following equations from [Mer 67]:

$$\frac{1}{B_{eff}} = \frac{1}{B_{oil}} + \frac{X_{air}}{B_{air}} \tag{6.5}$$

$$B_{air} = p_{air} \tag{6.6}$$

If air is included, B_{oil} must be replaced by B_{eff} when writing down the physical models.

6.2.3 The gear pump

An engine driven gear pump provides oil under pressure to the valve body and pistons. A linear model is used to describe the mean flow Q_{gp} as a function of the engine speed $\dot{\theta}_e$, the pump pressure p_{gp} and the oil temperature T_{oil}:

$$Q_{gp} = K_{Q,N}\dot{\theta}_e - K_{Q,p}p_{gp} - K_{p,T}T_{oil} \tag{6.7}$$

For a 12 mm pump, the parameters obtained from experimental data (see [Van 96e]) are shown in table 6.3.

Parameter	Meaning	Value	Units
$K_{Q,N}$	Speed coefficient	1.2819e-6	m^3/rad
$K_{Q,p}$	Pressure coefficient	3.8127e-12	m^3/sPa
$K_{Q,T}$	Temperature coefficient	1.1541e-7	$m^3/s/°C$

Table 6.3 *Pump flow parameters (12 mm gear pump).*

6.3 Typical spool valves for piston control

In this Section, different valves for piston control are analyzed. The actuation signal of a spool valve is denoted as u_{sv} and can be a force, a pressure or a velocity. Before discussing specific spool valves, the major effects that take place in spool valves are summarized here:

- Pilots are modeled as masses for translation.
- Friction between housing and pilots is assumed to be viscous. The friction coefficient is computed as (see [Mer 67])

$$b_{sv} = \frac{\pi D_{sv} L_{svf} \rho_{oil} \nu_{oil}}{dD_{sv}}$$

  with D_{sv} being the pilot diameter, L_{svf} being the length on which the friction is working and dD_{sv} the radial clearance between the pilot and its housing.
- Springs are modeled as stiffnesses for translation.
- Pressures on surfaces deliver forces on the pilots.
- Static and dynamic flow forces on pilots become important when fluid flows into valve chambers and trough valve orifices (see [Mer 67] and [Wat 89]). The total flow force increases with the pressure difference $p_{sp} - p_o$ over the valve, with the valve section a_{sv}, with the valve section gradient w_{sv} and with the pilot speed $\dot{x}_{sv}$. The total flow force tries to close the orifice, and is computed from:

$$F_f = 2C_d C_v |p_{sp} - p_o| a_{sv} \cos\theta_{sv} + L_{sv} C_d w_{sv} \sqrt[\pm]{2\rho_{oil}|p_{sp} - p_o|}\dot{x}_{sv}$$

In the next subsections, a description and typical values of the parameters are given.

- Flow through orifices can be laminar or turbulent. Depending on the type of flow (determined by the Reynolds number), different equations are used to compute the flow. The volumetric flow Q through a round orifice with section $a_r = \frac{\pi D_r^2}{4}$ under a pressure difference $\triangle p$ is equal to:

$$\begin{aligned} Q_{laminar} &= \frac{\pi \delta^2 D_r^3}{2\rho_{oil}\nu_{oil}} \triangle p \\ Q_{turbulent} &= C_d a_r \sqrt[\pm]{\frac{2}{\rho_{oil}} |\triangle p|} \end{aligned}$$

  The quantity δ depends on geometry and is called the laminar flow coefficient (see [Mer 67]). For a sharp-edged round orifice, $\delta = 0.2$. The discharge coefficient is assumed to be constant for turbulent flows ($C_d = 0.61$). In practice, δ and C_d are uncertain model parameters that will be determined from experimental data.

- The servo signal u_{sv} might be a pressure, a force or a speed. It is treated as an input in the force and/or flow equations.

In practice, multiple spool valves are combined in one valve-body and oil is supplied by a single gear pump. The hydraulic interactions between the valves strongly depend on the connection of the valves (series, parallel or hybrid) and on the used valve configurations (NO or NC). Although not explicitly treated here, these interactions are considered in detail in [VD *et al* 96].

In the next subsections, two typical spool valves are analyzed. For these valves, the following models are derived:

- A non linear physical model

  The physical equations are derived from force and flow balances, and are highly non-linear. This model is used to compute static characteristics and to design and validate candidate inner controllers.

- A linear physically parametrized model

  The linearized dynamics are obtained from singular perturbation and are used to compute the dynamic characteristics of the valves.

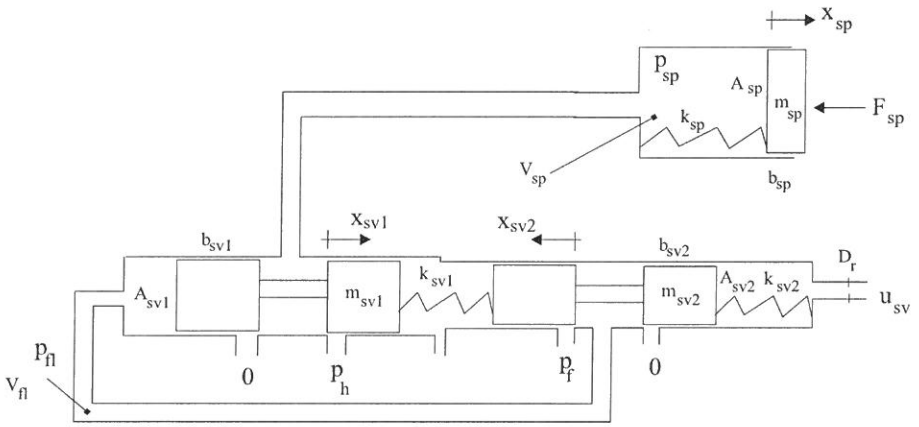

Figure 6.5 *A double stage flow valve for piston control. The servo pressure is applied to the servo pilot m_{sv2}. Via a spring, the servo force is applied to the main pilot m_{sv1}. The position of the major pilot is proportional to the applied servo pressure. The hydraulic feedback line realizes position feedback; it increases the bandwidth of the valve and reduces position errors.*

6.3.1 A double stage flow valve for piston control

A functional model of a double stage flow valve is shown in figure 6.5. This valve can be used in different ways.

- The actuating signal u_{sv} might be a servo pressure or a servo force.
- The valve is only used in NC-configurations (NC). Like all NC-configurations, it avoids permanent flow losses.

Here, a model for a pressure actuated valve is derived. In this case, the input signal u_{sv} represents the servo pressure p_{sv} Before deriving the physical equations, the important valve parameters and typical values are indicated in table 6.4:

The mechanical equations are obtained from the force balances of the valve pilots and the piston[1]. The hydraulic equations are obtained from the flow balances of the piston volume and the volume of the feedback line:

[1]If a restriction with diameter D_r is placed in the line between the servo volume and the servo pressure supply, the servo pressure source becomes flow restricted. In that case, the mechanical damping b_{sv} must be augmented with an hydraulical damping b_h. Assuming laminar servo flows, b_h can be computed from the flow balance of the servo volume as $b_h = \frac{2\rho_{oil}\nu_{oil}A_{sv}^2}{\pi\delta^2 D_r^3}$.

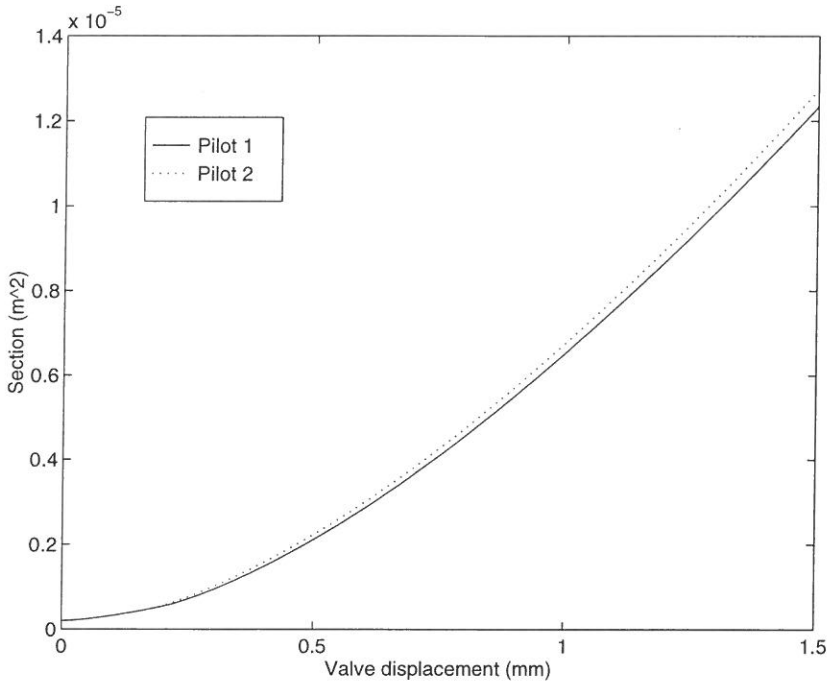

Figure 6.6 *Orifices at the servo pilot and the main pilot (the orifices are the same for positive and negative displacements, since symetrical valves are considered), computed from technical drawings.*

$$m_{sv1}\ddot{x}_{sv1} = p_{fl}A_{sv1} - F_{sv1,0} - k_{sv1}(x_{sv1} + x_{sv2}) - b_{sv1}\dot{x}_{sv1} \tag{6.8}$$

$$m_{sv2}\ddot{x}_{sv2} = u_{sv}A_{sv2} - F_{sv1,0} - k_{sv1}(x_{sv1} + x_{sv2}) - b_{sv2}\dot{x}_{sv2} + F_{sv2,0} - k_{sv2}x_{sv2} \tag{6.9}$$

$$m_{sp}\ddot{x}_{sp} = p_{sp}A_{sp} - b_{sp}\dot{x}_{sp} - k_{sp}x_{sp} - F_{sp} \tag{6.10}$$

$$\frac{V_{sp}}{B_{oil}}\dot{p}_{sp} = C_d a_{sv1,h} \sqrt[\pm]{\frac{2}{\rho_{oil}}|p_h - p_{sp}|} - C_d a_{sv1,l} \sqrt[\pm]{\frac{2}{\rho_{oil}}|p_{sp}|} - C_d a_{lk} \sqrt[\pm]{\frac{2}{\rho_{oil}}|p_{sp}|} - A_{sp}\dot{x}_{sp} \tag{6.11}$$

$$\frac{V_{fl}}{B_{oil}}\dot{p}_{fl} = C_d a_{sv2,h} \sqrt[\pm]{\frac{2}{\rho_{oil}}|p_f - p_{fl}|} - C_d a_{sv2,l} \sqrt[\pm]{\frac{2}{\rho_{oil}}|p_{fl}|} - A_{sv1}\dot{x}_{sv1} \tag{6.12}$$

By applying analytical linearization, the linearized equations are derived. After taking Laplace transforms, the following equations are obtained:

$$\begin{aligned}
(m_{sv1}s^2 + b_{sv1}s + k_{sv1})\triangle X_{sv1}(s) &= A_{sv1}\triangle P_{fl} - k_{sv1}\triangle X_{sv2}(s) \\
(m_{sv2}s^2 + b_{sv2}s + k_{sv1} + k_{sv2})\triangle X_{sv2}(s) &= A_{sv2}\triangle U_{sv}(s) - k_{sv1}\triangle X_{sv1}(s) \\
(m_{sp}s^2 + b_{sp}s + k_{sp})\triangle X_{sp}(s) &= A_{sp}\triangle P_{sp}(s) - \triangle F_{sp}(s) \\
(\frac{V_{sp}}{B_{oil}}s + K_{lk})\triangle P_{sp}(s) &= K_{x1}\triangle X_{sv1}(s) - A_{sp}s\triangle X_{sp}(s) \\
\frac{V_{fl}}{B_{oil}}s\triangle P_{fl}(s) &= K_{x2}\triangle X_{sv2}(s) - A_{sv1}s\triangle X_{sv1}(s)
\end{aligned}$$

with the valve coefficients given by:

$$\begin{aligned}
K_{x1} &= C_d w_{sv1,h} \sqrt[\pm]{\frac{2}{\rho_{oil}}|p_h - p_{sp}|} - C_d w_{sv1,l} \sqrt[\pm]{\frac{2}{\rho_{oil}}|p_{sp}|} \\
K_{x2} &= C_d w_{sv2,h} \sqrt[\pm]{\frac{2}{\rho_{oil}}|p_f - p_{fl}|} - C_d w_{sv2,l} \sqrt[\pm]{\frac{2}{\rho_{oil}}|p_{fl}|} \\
K_{lk} &= \frac{C_d a_{lk}}{\sqrt[\pm]{2\rho_{oil}|p_{sp}|}}
\end{aligned}$$

Linearization is done at $(x_{sv1} = 0, x_{sv2} = 0, \dot{x}_{sv1} = 0, \dot{x}_{sv2} = 0, p_{sp}, p_{fl})$ and the pressure coefficients become zero; this implies that the influence of the dynamics of the inlet pressures p_h and p_f is negligible.

Define the state vector X_{ds} and the input vector U_{ds} as:

$$\mathrm{X}_{ds} = \begin{pmatrix} \triangle x_{sv1} & \triangle \dot{x}_{sv1} & \triangle x_{sv2} & \triangle \dot{x}_{sv2} & \triangle x_{sp} & \triangle \dot{x}_{sp} & \triangle p_{sp} & \triangle p_{fl} \end{pmatrix}'$$

$$\mathrm{U}_{ds} = \begin{pmatrix} \triangle u_{sv} & \triangle F_{sp} \end{pmatrix}'$$

The linearized system is described by:

$$\dot{\mathrm{X}}_{ds} = \mathrm{A}_{ds}\mathrm{X}_{ds} + \mathrm{B}_{ds}\mathrm{U}_{ds} \tag{6.13}$$

$$\mathrm{Y}_{ds} = \mathrm{X}_{ds} \tag{6.14}$$

with:

$$A_{ds} = \begin{pmatrix} 0 & 1 & 0 & 0 & 0 & 0 & 0 & 0 \\ -\frac{k_{sv1}}{m_{sv1}} & -\frac{b_{sv1}}{m_{sv1}} & -\frac{k_{sv1}}{m_{sv1}} & 0 & 0 & 0 & 0 & \frac{A_{sv1}}{m_{sv1}} \\ 0 & 0 & 0 & 1 & 0 & 0 & 0 & 0 \\ -\frac{k_{sv1}}{m_{sv2}} & 0 & -\frac{k_{sv1}+k_{sv2}}{m_{sv2}} & -\frac{b_{sv2}}{m_{sv2}} & 0 & 0 & 0 & 0 \\ 0 & 0 & 0 & 0 & 0 & 1 & 0 & 0 \\ 0 & 0 & 0 & 0 & -\frac{k_{sp}}{m_{sp}} & -\frac{b_{sp}}{m_{sp}} & \frac{A_{sp}}{m_{sp}} & 0 \\ \frac{K_{x1}B_{oil}}{V_{sp}} & 0 & 0 & 0 & 0 & -\frac{A_{sp}B_{oil}}{V_{sp}} & 0 & 0 \\ 0 & -\frac{A_{sv1}B_{oil}}{V_{fl}} & \frac{K_{x2}B_{oil}}{V_{fl}} & 0 & 0 & 0 & 0 & 0 \end{pmatrix}$$

$$B_{ds} = \begin{pmatrix} 0 & 0 \\ 0 & 0 \\ 0 & 0 \\ \frac{A_{sv2}}{m_{sv2}} & 0 \\ 0 & 0 \\ 0 & -\frac{1}{m_{sp}} \\ 0 & 0 \\ 0 & 0 \end{pmatrix}$$

In practice, this valve is for piston speed control (flow steering). The hydraulic feedback increases bandwidth and stabilizes the position of pilot 1 (see figures 6.7, 6.8 and 6.9).

Parameter	Meaning	Value	Units
m_{sv1}	Mass of pilot 1	0.012	kg
m_{sv2}	Mass of pilot 2	0.009	kg
b_{sv1}	Total damping on pilot 1	30	Ns/m
b_{sv2}	Total damping on pilot 2	30	Ns/m
k_{sv1}	Stiffness of spring 1	14000	N/m
k_{sv2}	Stiffness of spring 2	2000	N/m
$F_{sv1,0}$	Pre-load of spring 1	28	N
$F_{sv2,0}$	Pre-load of spring 2	8.5	N
A_{sv1}	Section of pilot 1	112e-6	m^2
A_{sv2}	Section of pilot 2	78e-6	m^2
C_d	Discharge coefficient	0.61	-
D_{sv1}	Diameter of pilot 1	0.012	m
D_{sv2}	Diameter of pilot 2	0.010	m
V_{fl}	Volume of feedback line	6e-4	m^3
V_{sp}	Volume of piston	8e-6	m^3
$a_{sv1,h}(x_{sv1})$	Orifice at pilot 1, to p_h	see figure 6.6	m^2
$a_{sv1,l}(x_{sv1})$	Orifice at pilot 1, to 0	see figure 6.6	m^2
$a_{sv2,h}(x_{sv2})$	Orifice at pilot 2, to p_f	see figure 6.6	m^2
$a_{sv2,l}(x_{sv2})$	Orifice at pilot 2, to 0	see figure 6.6	m^2
$w_{sv1,h}(x_{sv1})$	Orifice gradient at pilot 1, to p_h	from figure 6.6	m^2
$w_{sv1,l}(x_{sv1})$	Orifice gradient at pilot 1, to 0	from figure 6.6	m^2
$w_{sv2,h}(x_{sv2})$	Orifice gradient at pilot 2, to p_f	from figure 6.6	m^2
$w_{sv2,l}(x_{sv2})$	Orifice gradient at pilot 2, to 0	from figure 6.6	m^2
a_{lk}	Leakage orifice	7.8e-7	m^2
L_{svf1}	Length on which friction works, pilot 1	0.025	m
L_{svf2}	Length on which friction works, pilot 2	0.020	m
dD_{sv1}	Radial clearance at pilot 1	15e-6	m
dD_{sv2}	Radial clearance at pilot 2	15e-6	m

Table 6.4 *Double stage flow valve parameters obtained from technical drawings and material characteristics of a VT1-E valve body.*

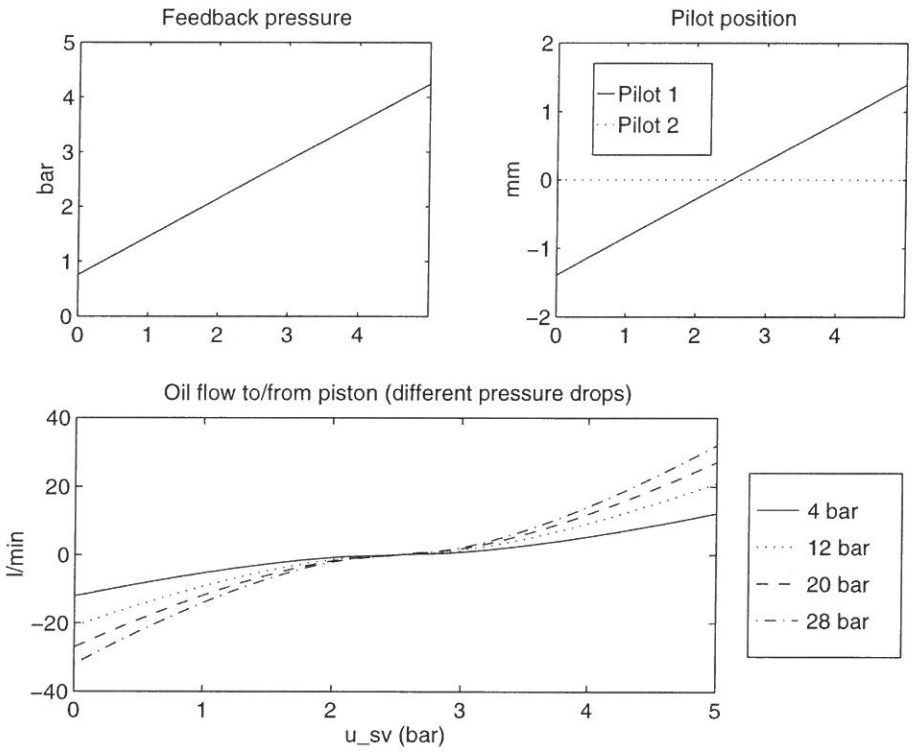

Figure 6.7 *Static characteristics of a double stage flow valve. At $u_{sv} = 2.5$ bar, the valve is closed ($x_{sv,1} = 0$) and the piston flow is zero. The position $x_{sv,1}$ of pilot 1 is proportional to the servo pressure u_{sv}, while pilot 2 hardly moves ($x_{sv,2} \approx 0$) due to the feedback circuit (spring $k_{sv,1}$ and feedback line with volume V_{fl}). The piston flow depends on the valve displacement and on the pressure drop over the valve orifice ($p_h - p_{sp}$ or p_{sp}).*

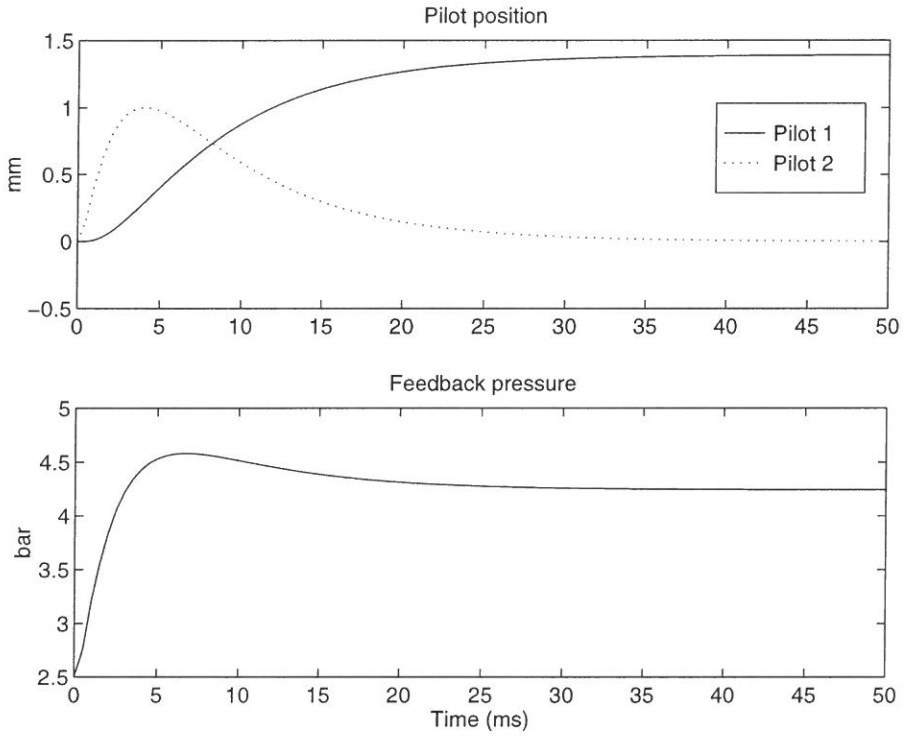

Figure 6.8 *Dynamic characteristics of a double stage flow valve. When the servo pressure u_{sv} changes step-wise with 2.5 bar, both pilots move. As predicted from the statics, pilot 2 goes back to its original position, whilepilot 1 displaces over 1.4 mm. Due to the high feedback gain, the settling time is very short (35 ms) and the end position is stabilized, which makes this valve excellent for flow steering. The feedback pressure p_{fl} is also proportional to the applied servo pressure and stabilizes fast.*

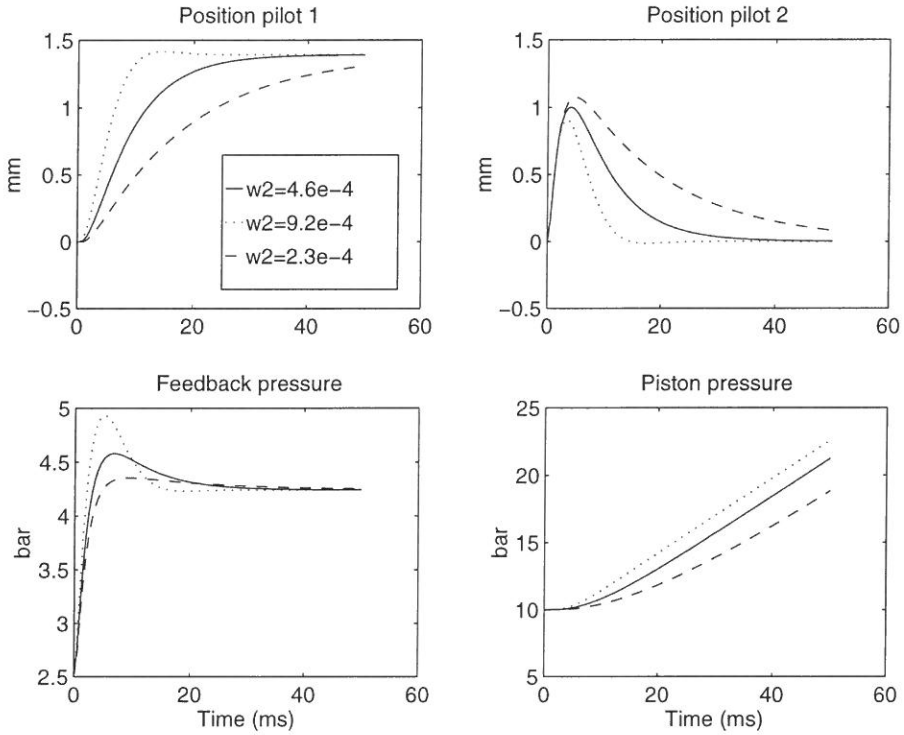

Figure 6.9 *Influence of the feedback gain $w_{sv,2}$ on the dynamic characteristics of the double stage flow valve. Increasing the orifice gradient at pilot 2 leads to faster dynamics (reduced settling time, increased overshoot). In practice, the orifice gradients at pilot 2 are designed in combination with the feedback volume V_{fl}.*

6.3.2 A flow valve with pressure feedback for piston control

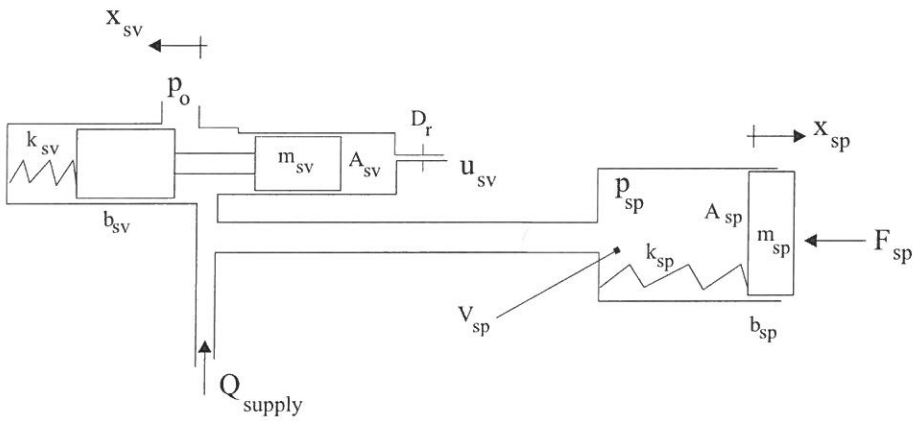

Figure 6.10 *A flow valve with pressure feedback for piston control. A pressure feedback circuit realizes a piston pressure that is proportional to the applied servo pressure* u_{sv}.

A functional model of a flow valve with pressure feedback is shown in figure 6.10. Except for the feedback surface A_{svd}, this type of valve looks like a single stage flow valve. It can be used as follows:

- The actuating signal u_{sv} might be a servo pressure or servo force. By adding a plunger-spring system, velocity actuation is also possible.
- This valve is only used in NO-configurations.

Here, a model for a pressure actuated valve is derived. In this case, the input signal u_{sv} represents the servo pressure p_{sv}. Before deriving the physical equations, the important valve parameters and typical values are indicated in table 6.5.

The mechanical equations are obtained from the force balances of the valve and the piston. The hydraulic equation is obtained from the flow balance of the piston volume:

$$\begin{aligned} m_{sv}\ddot{x}_{sv} &= u_{sv}A_{sv} + p_{sp}A_{svd} - F_{sv,0} - k_{sv}x_{sv} - b_{sv}\dot{x}_{sv} \\ &\quad -2C_dC_v|p_{sp} - p_o|a_{sv}\cos\theta_{sv} \\ &\quad -L_{sv}C_dw_{sv}\overset{\pm}{\sqrt{2\rho_{oil}|p_{sp} - p_o|}}\dot{x}_{sv} \qquad (6.15) \\ m_{sp}\ddot{x}_{sp} &= p_{sp}A_{sp} - b_{sp}\dot{x}_{sp} - k_{sp}x_{sp} - F_{sp} \qquad (6.16) \end{aligned}$$

Parameter	Meaning	Value	Units
m_{sv}	Mass of pilot	0.020	kg
b_{sv}	Total damping on pilot	30.6	Ns/m
k_{sv}	Spring constant	7000	N/m
$F_{sv,0}$	Spring pre-load	55	N
A_{sv}	Pilot section at servo side	13.9e-5	m^2
A_{svd}	Resulting feedback section	1.5e-5	m^2
C_d	Discharge coefficient	0.61	-
C_v	Velocity coefficient	0.98	-
$\theta_{sv}(x_{sv})$	Flow angle	69	^{o}
D_{sv}	Diameter of pilot	0.014	m
$w_{sv}(x_{sv})$	Valve orifice position derivative	from figure 6.11	m
$a_{sv}(x_{sv})$	Valve orifice	see figure 6.11	m^2
a_{lk}	Leakage orifice	2e-6	m^2
L_{sv}	Free flow length within the valve	0.020	m
V_{sp}	Piston volume	3e-4	m^3

Table 6.5 *Pressure feedback flow valve parameters obtained from technical drawings, material characteristics and dedicated experiments on a VT1-E valve body.*

$$\begin{aligned}\frac{V_{sp}}{B_{oil}}\dot{p}_{sp} &= Q_{supply} - A_{sp}\dot{x}_{sp} - C_d a_{lk}\sqrt[\pm]{\frac{2}{\rho_{oil}}|p_{sp}|} \\ &\quad -C_d a_{sv}\sqrt[\pm]{\frac{2}{\rho_{oil}}|p_{sp}-p_o|} \end{aligned} \tag{6.17}$$

By applying analytical linearization, the linearized equations are derived. After taking Laplace transforms, the following equations are obtained:

$$\begin{aligned}(m_{sv}s^2 + (b_{sv}+K_{fv})s + k_{sv} + K_{ff})\triangle X_{sv}(s) &= A_{sv}\triangle U_{sv}(s) + (A_{svd} - K_{fp})\triangle P_{sp}(s) \\ &\quad +K_{fp}\triangle P_o(s) \\ (m_{sp}s^2 + b_{sp}s + k_{sp})\triangle X_{sp}(s) &= A_{sp}\triangle P_{sp}(s) - \triangle F_{sp}(s) \\ (\frac{V_{sp}}{B_{oil}}s + K_{qp} + K_{lk})\triangle P_{sp}(s) &= \triangle Q_{supply}(s) - A_{sp}s\triangle X_{sp}(s) \\ &\quad -K_x\triangle X_v(s) + K_{qp}\triangle P_o(s)\end{aligned}$$

with the valve coefficients given by:

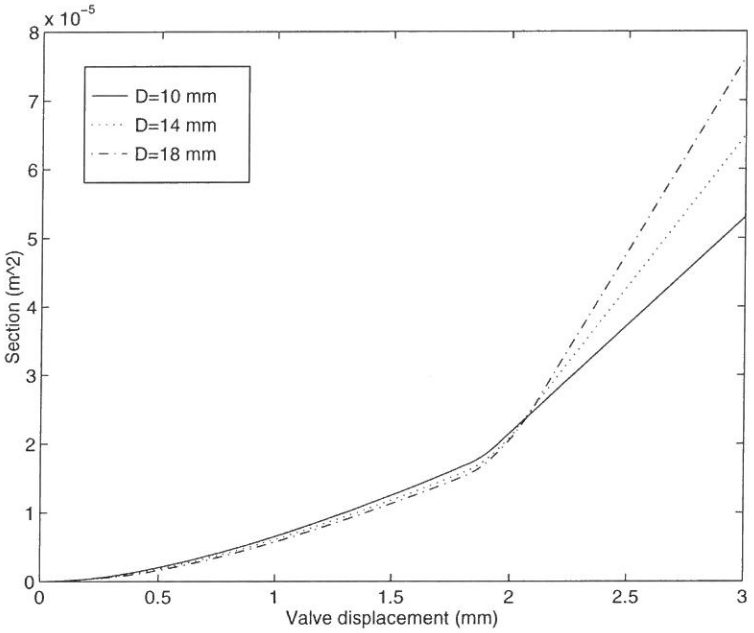

Figure 6.11 *Orifice as a function of the pilot position x_{sv}, for a flow valve with pressure feedback (computed from technical drawings, for different pilot diameters).*

$$
\begin{aligned}
K_{ff} &= 2C_d C_v w_{sv} |p_{sp} - p_o| \cos\theta_{sv} \\
K_{fv} &= L_{sv} C_d w_{sv} \sqrt[\pm]{2\rho_{oil}|p_{sp} - p_o|} \\
K_{fp} &= 2C_d C_v a_{sv} \cos\theta_{sv} \\
K_{qp} &= \frac{C_d a_{sv}}{\sqrt[\pm]{2\rho_{oil}|p_{sp} - p_o|}} \\
K_x &= C_d w_{sv} \sqrt[\pm]{\frac{2}{\rho_{oil}}|p_{sp} - p_o|} \\
K_{lk} &= \frac{C_d a_{lk}}{\sqrt[\pm]{2\rho_{oil}|p_{sp}|}}
\end{aligned}
$$

Define the state vector X_{pf} and the input vector U_{pf} as:

$$\mathrm{X}_{pf} = \begin{pmatrix} \triangle x_{sv} & \triangle \dot{x}_{sv} & \triangle x_{sp} & \triangle \dot{x}_{sp} & \triangle p_{sp} \end{pmatrix}'$$

$$\mathrm{U}_{pf} = \begin{pmatrix} \triangle u_{sv} & \triangle p_o & \triangle Q_{supply} & \triangle \dot{F}_{sp} \end{pmatrix}'$$

The linearized system is described by:

$$\dot{\mathrm{X}}_{pf} = \mathrm{A}_{pf}\mathrm{X}_{pf} + \mathrm{B}_{pf}\mathrm{U}_{pf} \tag{6.18}$$
$$\mathrm{Y}_{pf} = \mathrm{X}_{pf} \tag{6.19}$$

with:

$$\mathrm{A}_{pf} = \begin{pmatrix} 0 & 1 & 0 & 0 & 0 \\ -\frac{k_{sv}+K_{ff}}{m_{sv}} & -\frac{b_{sv}+K_{fv}}{m_{sv}} & 0 & 0 & \frac{A_{svd}-K_{fp}}{m_{sv}} \\ 0 & 0 & 0 & 1 & 0 \\ 0 & 0 & -\frac{k_{sp}}{m_{sp}} & -\frac{b_{sp}}{m_{sp}} & \frac{A_{sp}}{m_{sp}} \\ -\frac{K_x B_{oil}}{V_{sp}} & 0 & 0 & -\frac{A_{sp}B_{oil}}{V_{sp}} & -\frac{(K_{qp}+K_{lk})B_{oil}}{V_{sp}} \end{pmatrix}$$

$$\mathrm{B}_{pf} = \begin{pmatrix} 0 & 0 & 0 & 0 \\ \frac{A_{sv}}{m_{sv}} & \frac{K_{fp}}{m_{sv}} & 0 & 0 \\ 0 & 0 & 0 & 0 \\ 0 & 0 & 0 & -\frac{1}{m_{sp}} \\ 0 & \frac{K_{qp}B_{oil}}{V_{sp}} & \frac{B_{oil}}{V_{sp}} & 0 \end{pmatrix}$$

In practice, this valve is mainly used for piston pressure control (pressure steering). The characteristics of the valve are shown in figures 6.12, 6.13 and 6.14.

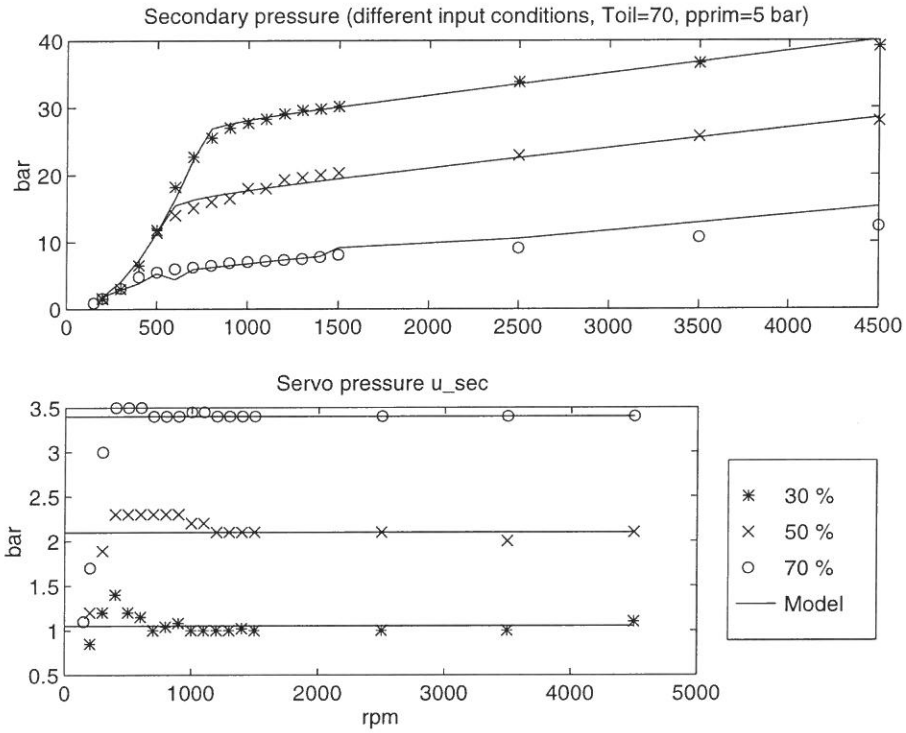

Figure 6.12 *Static characteristics of a flow valve with pressure feedback. The piston pressure is proportional to the applied servo pressure (or duty cycle). At low pump speeds, Q_{supply} is mainly used for leakage and the valve is closed, which results in low pressures. At higher pump speeds, the valve opens and pressure regulation starts. Due to flow forces, the piston pressure slightly depends on the pump speed. The leakage restriction and the spring preload were used as fit parameters. All other parameters that affect the statics are computed from technical data and material characteristics. The physical model fits the experiments very well, over a wide range of operation points, without addition of unrealistic parameter values.*

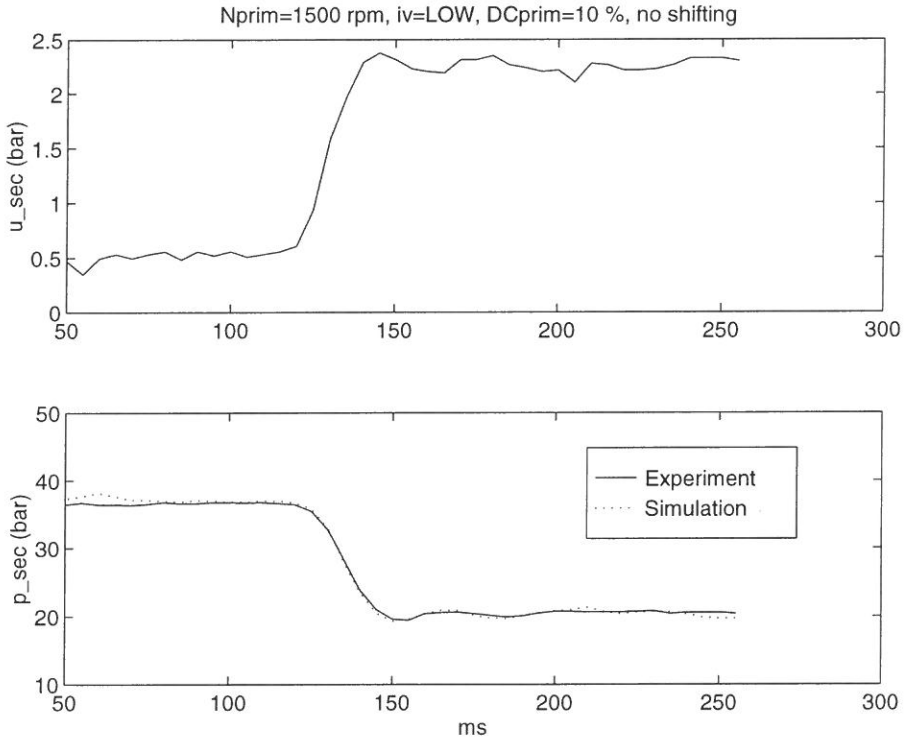

Figure 6.13 *Dynamic characteristics of a flow valve with pressure feedback (experiment versus simulation). At an increase in servo pressure u_{sv}, the piston pressure decreases proportionally (approximate gain of $-\frac{A_{svd}}{A_{sv}}$). Only the oil compressibility B_{oil} is used as a fit parameter, all other parameters that affect the dynamics are computed from technical data. With $B_{oil} = 1.6e8$ (and thus assuming an included air fraction $X_{air} = 1.1\%$, under a pressure of 30 bar), the model fits the experiment very well. In this experiment, the piston position was fixed, by blocking the piston.*

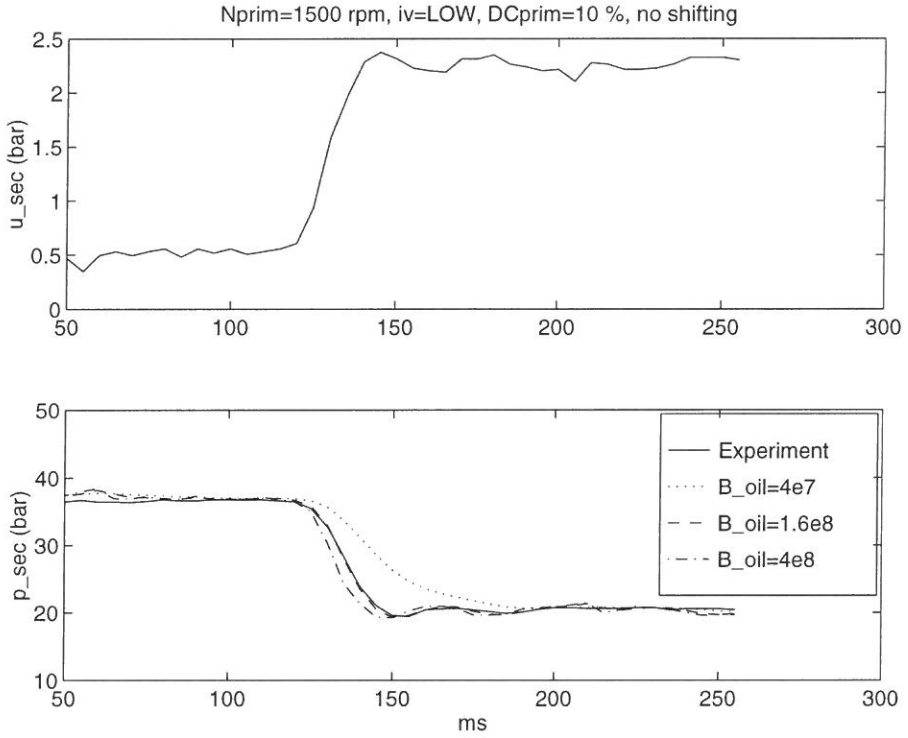

Figure 6.14 *Influence of included air on the dynamic characteristics of a flow valve with pressure feedback (experiment versus simulation). At an increase in servo pressure u_{sv}, the piston pressure decreases proportionally (approximate gain of $-\frac{A_{svd}}{A_{sv}}$). By increasing the included air fraction to 6.5 %, B_{oil} reduces with a factor 10 and the valve becomes rather slow. In practice, the oil is injected on the pulleys for lubrication and air will be included. In this simulation, the piston position was fixed, by blocking the piston.*

6.4 Control systems

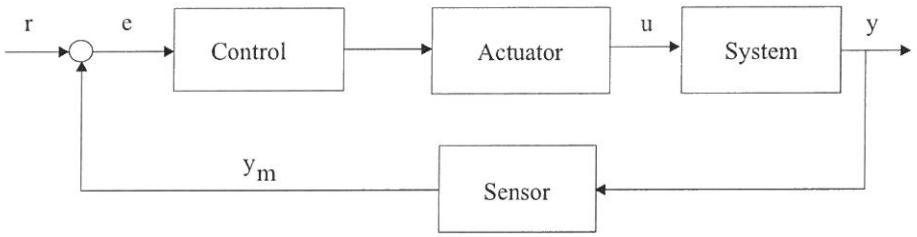

Figure 6.15 *Every control system contains elements for sensing, control and actuation. In hydro-mechanical control, two or more of these functions might be integrated in one component. In electro-hydraulical control, these functions are distributed over various dedicated components.*

In a control context, a control system is considered as a collection of components required to implement three functions (see figure 6.15):

- Sensing: observe the 'state' of the system and transform it into a signal suitable for the controller.
- Control: translate the difference between the desired 'state' and the 'observed' state into a corrective signal.
- Actuation: transform the corrective signal to an input for the controlled system.

For variator control, two different control systems are used:

- Hydro-mechanical control systems use pitot-assemblies, sensing shoes, bars and cams for sensing and for spool valve actuation. These control systems implement control in an analog way.
- Electro-hydraulic control systems use solenoid valves (pressure actuation) and linear electro-mechanical actuators (speed or force actuation) for spool valve actuation and electronic sensors for sensing. An ECU implements digital control.

6.4.1 Hydro-mechanical control

For an hydraulic controlled CVT (e.g. VT1-H), these functions are typically implemented as follows (see figure 6.1):

- Sensing

  Rotational speed sensing is realized by pitot assemblies. Each assembly consists of a revolving pitot chamber filled with oil and a stationary pitot pipe. As the chamber rotates, the pitot pipe detects an oil pressure relative to the chamber speed. By mounting assemblies on the engine shaft and on the primary shaft, pressures relative to the engine speed and the primary speed can be obtained. From experiments (see [VV 96c]), it follows that the generated pitot pressure p_{pit} (bar) and the rotational speed of the chamber $\dot{\theta}_{pit}$ (rpm) are related as (see figure 6.16):

  $$p_{pit} = 2.42\ 10^{-7}\ \dot{\theta}_{pit}^2 + 6.68\ 10^{-5}\ \dot{\theta}_{pit}$$

  The position of the primary pulley is monitored using a sensing shoe. The sensing shoe displacement provides information on the actual variator ratio.

  The kick-down or throttle cable is connected to a rotating cam. The cam rotation angle provides information of the actual throttle position.

- Control and actuation

  In the case of hydro-mechanical control, control and actuation are integrated functions.

  The pitot pressures are used for pressure actuation, while the displacements of the sensing shoe and the kick-down cam are used for velocity actuation.

  Control is realized by a suitable design of cams, plungers, springs, pilot sections and restrictions, taking into account the characteristics of the car, the drive train components, the variator and the spool valves.

For variator control, this type of control mechanism has advantages and disadvantages:

- The absence of vulnerable sensors, fail-safety and the implementation of analog control are the major advantages.
- The limited controller intelligence (no compensation for variations in pump flow, oil temperature and transmitted torque), the hardware implementation of the controller (inflexible intelligence, implemented controller depends on tolerances, intelligence is proportional to the number of used components) and the lack of modularity (a single controller simultaneously performs all tasks ranging from variogram control to piston pressure and speed control) are the major disadvantages.

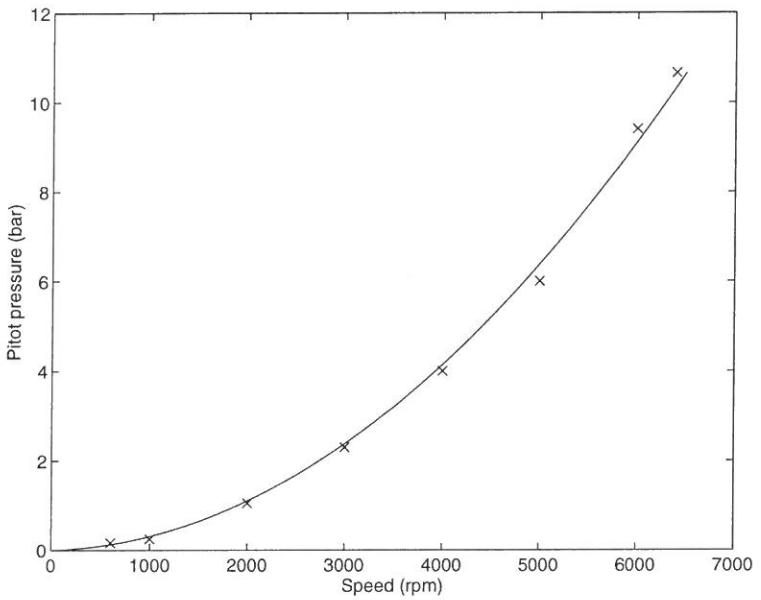

Figure 6.16 *Experimentally obtained pitot pressure parabola, for a VT1-H variator.*

6.4.2 Electro-hydraulic control

In this case, the three functions are implemented as follows:

- Sensing

  Pressure sensing, rotational speed sensing and temperature sensing is done by sensors with well-known static and dynamic characteristics. It is possible to obtain analog signals that are proportional to the actual pressure, speed or temperature, over a wide frequency band. Data-acquisition circuitry converts the analog signals into digital numbers for the ECU-processor.

- Control

  Control is implemented in software that runs on the ECU. A multi-level controller (drive train controller, outer controller, and inner controllers) is used to control the car.

- Actuation

  The digital control values from the ECU are translated into analog signals by the data-acquisition unit. These analog signals are send to the actuation units.

  Pulse width modulated solenoid valves are used for pressure actuation. In this case, a constant supply pressure is PWM-modulated to realize a PWM-modulated servo pressure, with a nominal value proportional to the applied duty-cycle (see figure 6.17) and a ripple inverse proportional to the basic frequency. This basic frequency is limited to 120 Hz, due to the inertance of the oil and the spools in the solenoid valves.

  Electro-mechanical actuators (linear displacement motors or rotational stepper motors) are used for velocity actuation (or for force actuation if carefully designed). In this case, electro-mechanical actuators with half-stepping or micro-stepping facilities and analog closed-loop position control are used to generate the required displacement or rotation. Half-stepping or micro-stepping facilities are required to increase positioning resolution, to reduce the force or torque ripple and to minimize the natural resonance problem of these actuators (see [Wat 89]). Digital control of the absolute position can be used to increase the positioning accuracy and to solve alignment problems.

For variator control, this type of control mechanism has advantages and disadvantages.

- The implementation of the controller in software (flexible intelligence, easy to adapt, almost unlimited complexity of the controller, reduction of the required number of hardware components) and the modularity of the control mechanism (separate functions in separate components) are the major advantages.
- From a fail-safe point of view, adding electronic components is disadvantageous.
- Other advantages and disadvantages are strongly related to the properties of the used components: PWM valves generate a rippled servo pressure and have a limited bandwidth, but are cheap and fail safe compared to analog pressure valves; electro-mechanical actuators have a high bandwidth and a high accuracy, but are expensive compared to solenoid valves.

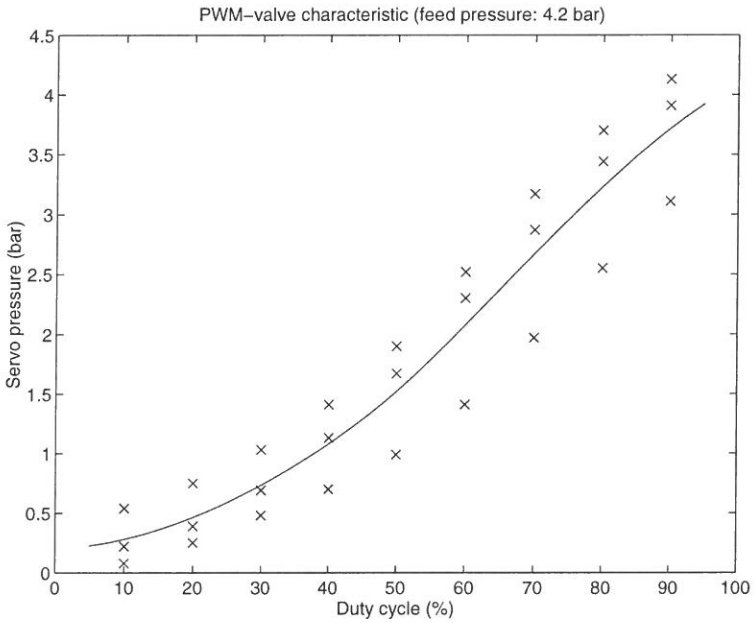

Figure 6.17 *Experimentally obatined servo pressure as a function of applied duty cycle, for a Bosch 3/2 PWM valve, under multiple operational conditions. Only in the 30-80 percent range, linearity may be assumed.*

Chapter 7

VIRTUES: VIRTUal Engineering Software

In this Chapter, we describe VIRTUES, a tailor-made Matlab/Simulink toolbox, that integrates the developed models, controllers and tools of Chapters 2, 3 ,4, 5 and 6, and the Matlab/Simulink tools for simulation, signal processing and optimization. Section 7.1 states the objectives of the toolbox and motivates the choices that were made. In Section 7.2, we treat the implementation of the models and we describe the developped database and interface.

7.1 Objectives

The number of technical CVT-related problems that were solved using a model-based approach increased as the research project evolved. Initially, computations at VCST were mainly restricted to static analysis. At this moment, most engineers at VCST use static and dynamic models for a wide variety of feasibility studies concerning CVT design and control. The implementation of our models in a flexible, user-friendly way was and is driven by their technical questions. Actually, the following objectives are already realized:

- Interactive time-domain and frequency-domain simulation

  The non-linear and linearized models of user-specified applications can easily be supplied with user-defined inputs, disturbances and/or parameters, to do numerical simulations in the time and frequency domain.

- Automatic evaluation of user-defined performance indices
  - Simulation of the CVT-benchmark test, to evaluate performance and fuel economy.
  - Comfort evaluation for specific deterministic inputs (tip-in, tip-out, kick-down).
- Automatic computation of static and dynamic valve body characteristics
- Automatic computation of parameter and input sensitivities
- Flexible interchange of components

  Components are easily interchanged[1]. This allows fast and flexible comparison of alternative components and control strategies. Regularly conducted comparisons are:
  - The usage of wet multi-plate clutch versus a torque converter.
  - The usage of a pp-configuration versus a pQ-configuration for variator control.
  - The usage of flow valves versus pressure valves, in an NO-configuration or an NC-configuration.
  - The usage of different types of control mechanisms and inner controllers.
- Interactive or automatic calibration of model parameters towards experiments

  To do so, linear total least squares (see [VHV 91]) and the nonlinear optimization toolbox from Matlab (see [MG 92]) are used.

7.2 VIRTUES: Virtual Engineering Software

The developped framework has been implemented in Matlab/Simulink, in a tailor-made tool box called VIRTUES (VIRTUal Engineering Software). In this tool box, the models and the proposed controllers are integrated with Matlab's dedicated tools for simulation, signal processing and optimization.
A graphical user interface and a CAD-database are added also. The software is able to run on both PCs and UNIX-workstations. Descriptions and demos of existing analysis and design packages were very helpful when deciding on the required features of our toolbox (see [FWKT 89], [Grace 89], [Lea 91], [LC 90], [Orl 94], [PSWN 85] and [Sim 96]).

[1] Causality problems are indicated and eliminated at an early stage, thanks to the bondgraph philosophy.

7.2.1 The model descriptions of VIRTUES

The developed models are organized in two separate tools:

- VIRTUES-CAR contains generic models of the car, the road, the load conditions, the drive train components, the variator and of the reduced models of the different valve-bodies and control mechanisms.
- VIRTUES-VALVES contains generic models of the various spool valves, valve-bodies, control mechanisms and the variator.

Each physical system is described by three strongly related models:

- The non-linear physical model (model 1)

  These models are obtained from 'first principles' and describe the static and dynamic behaviour of the components very accurately.

  These models are implemented as hierarchical block schemes in Simulink (see figure 7.1 for an example of the drive train model). A library of building blocks of physically parameterized components and a wide variety of controllers is constructed and allows fast interactive creation of new system models in a graphical way. (see [Van 97]).

- The static model and the model of the linearized dynamics (models 2, 3)

  The static equilibria are computed by numerically solving the static non-linear physical equations, using Matlab's optimization tool box (function fsolve.m).

  The linearization coefficients are obtained by applying singular perturbation on the non-linear physical equations. The linearized dynamics are described in a state-space form.

  The computation of the static equilibria and the computation of the linearization coefficients and the state-space matrices are implemented in Matlab code. A library of physically parameterized static codes and linearization codes for various components is available and allows fast computation of static characteristics, linearized dynamics and input and parameter sensitivities (see [Van 97]).

7.2.2 The VIRTUES database

This database contains the parameters of the physically parameterized generic models. The most important features of this database are:

- Component-oriented organization

  Each component is described by a generic model and by a specific component file containing all important component parameters and characteristics. For every new application of an existing structure, only the specific component file needs to be re-filled.

- Application-oriented library

  For each component, a number of existing applications and the corresponding component files are already filled and can easily be selected from a graphical menu.

  The following components can easily be combined and/or interchanged, and are tuned for a wide variety of existing applications (see [Van 96a]):

  - At car level: car speed profiles (ECE, Urban, Highway, constant speed), driver actions (kickdown, tip-in, tip-out, car speed control, brake operation), cars (Rover Metro, Rover 216, Rover 416, MGF, Renault Clio, Volvo 440, Volvo 850), road profiles (stochastic, sine) and various load conditions (wind, hill climbing).
  - At drive train level: combustion engines (B18U, N2-P20, 1.4K8TBI, 1.4K8MPI, 1.4K16MPI, 1.6K16MPI, 1.8K16MPI, 1.8K16MPI-VVC, and 2.0M16LTI,), couplings (wet multi-plate clutch P811, torque converter Daikin YT220), variators (VT1, VT2, VT3), pinion gear and drive train controllers (variogram (economy, sport, H-variogram), clutch mode and variator mode controllers, gain scheduled PI control, PI control with feedback linearization).
  - At variator level: variator characteristics ($\frac{K_p}{K_s}$, $\frac{di_v}{dt}$, η_v), variator pistons (primary and secondary piston), spool valves (clutch valve, primary valve, secondary valve, constant pressure valve), gear pumps (12 m, 14 mm) and variator controllers (outer controllers (pp or pQ), inner controllers for pressure and speed).
  - At valve-body level: actuators (cams, PWM-valves, electrical motors), spool valve configurations (and interactions: serial, parallel, hybrid), sensors (pressure sensors, position encoders, cams and linkages).

Examples of specific component files are given in figures 7.2 and 7.3.

7.2.3 The graphical user interface of VIRTUES

Instead of giving a full description of all available user interface facilities, a typical user's cycle is described. When analyzing an application, the following sequence of actions is undertaken:

1. Component selection

   Components can be selected from pop-up menus. Once a specific component is selected, the parameter file and the characteristics are shown on the screen, to allow a quick check by the user.

   In VIRTUES-CAR, this implies selection of the engine, the coupling, the variator, the pinion gear, the desired car speed profile, the variogram, the drive train and variator controllers and the reduced valve-body.

   In VIRTUES-VALVES, this implies selection of the secondary valve, the primary valve, the clutch valve, the control mechanisms, the piston controllers and the reduced variator.

2. Application definition

   Once all specific components are selected, the configuration can be saved as a new application, with a new user-defined name. This allows easy re-selection and documentation of an analyzed application.

3. Model selection

   Model selection is done via a pop-up menu. It is used to select the Simulink block-scheme (non-linear model) or the Matlab-code (static model and/or linearized dynamics) of a component.

4. Selection of simulation parameters

   Tuning of the major simulation parameters (start time, stop time, time step, start frequency, stop frequency, frequency step, integration algorithm, operating point for linearization) is done via sliders and pushbuttons.

5. Configuration of the simulation

   The applied input and disturbance signals, and the required outputs are selected interactively via the menu bar, or automatically via selection of the performance indices that need to be computed.

   For VIRTUES-CAR, the CVT-benchmark test for performance and fuel economy or specific comfort measures (tip-in, tip-out, kick-down) may be selected.

   For VIRTUES-VALVES, automatic computation of statical and dynamical spool valve characteristics or automatic computation of valve body characteristics may be selected.

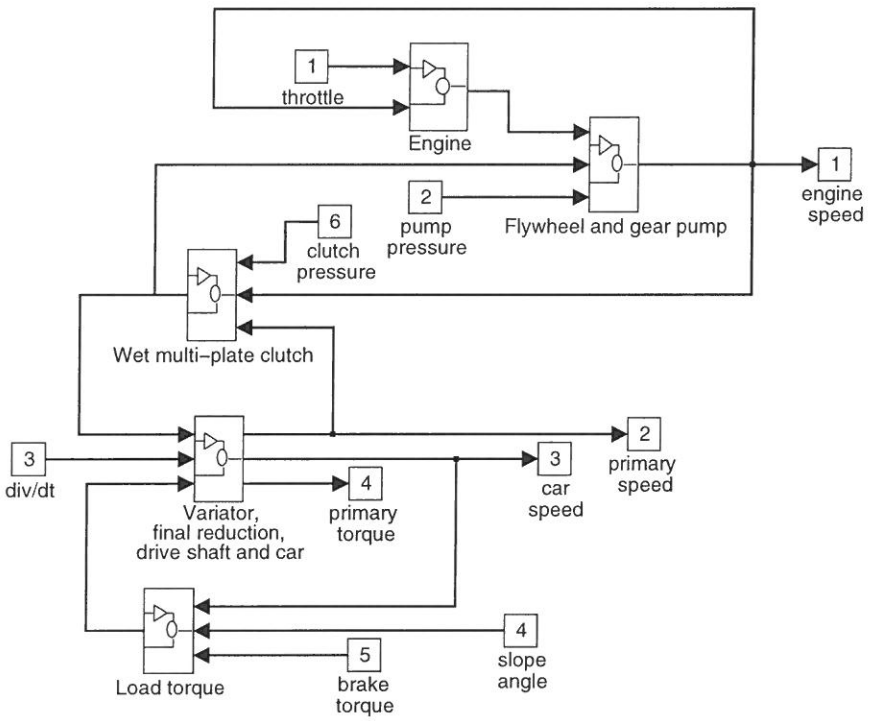

Figure 7.1 *Hierarchical Simulink block scheme of the drive train. To simulate drive cycles, this block is combined with a drive-train controller block and a driver model, and this block is used as a sub-block. Oppositely, this block contains multiple sub-blocks (engine, pump, clutch, ...) that are composed by combining multiple lower level blocks. By organizing component models in an hierarchical way, new models can easily be constructed with existing lower level blocks and embedded in existing higher level blocks.*

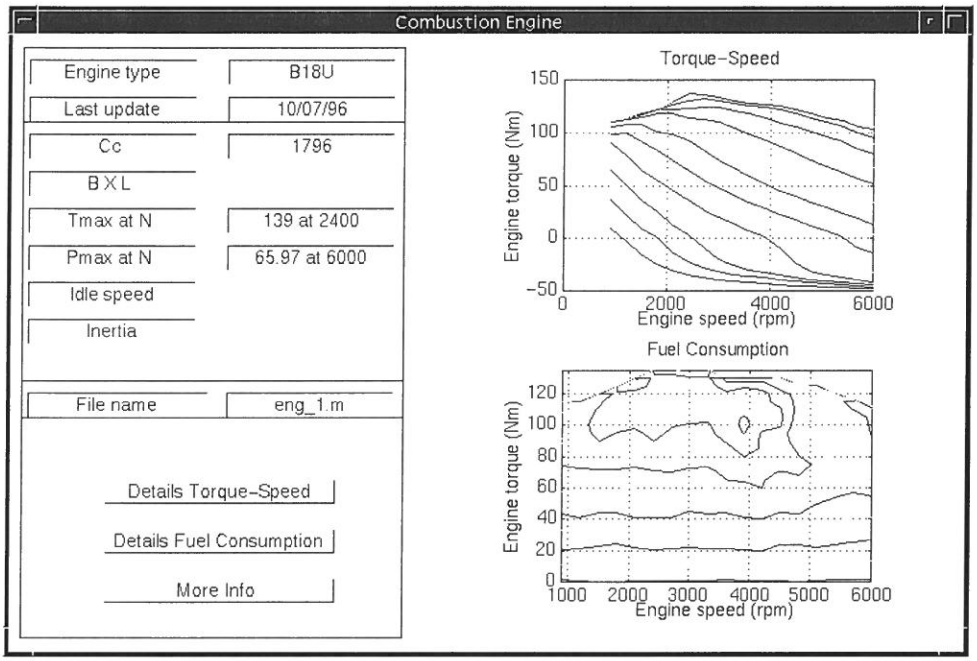

Figure 7.2 *Specific component file of a B18U combustion engine: all available engine data are shown, either in a numerical form or in a graphical form. This allows the user to do a quick check before running simulations. Push buttons allow to ask for additional information.*

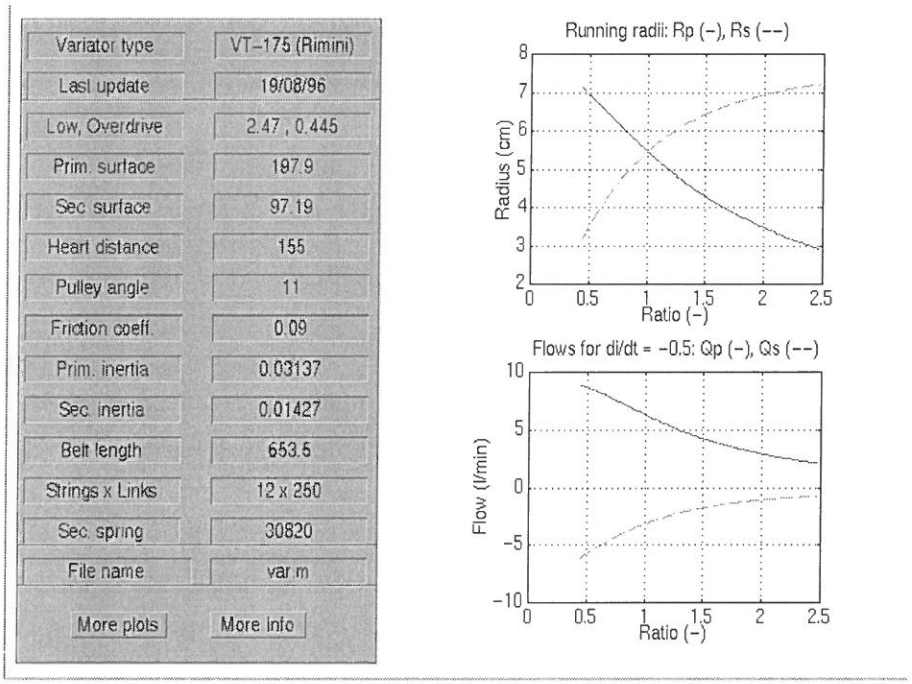

Figure 7.3 *Specific component file of a VT-175 variator: all available data are shown, either in a numerical form or in a graphical form. Graph computation and plotting is callback-driven, i.e. they are (re)computed when the component is selected or when parameters in the edit-boxes are changed. Push buttons allow to ask for additional information.*

6. Conduction of simulation

   By pressing the start button, all required information is computed and stored in pre-specified variables.

7. Plot selection

   Different plots in standardized formats are selected via a menu bar, to visualize the simulation results in a clear and attractive way.

7.3 Conclusions

The developed virtual engineering framework is implemented in Matlab-Simulink, in a dedicated tool box called VIRTUES (**VIRTU**al **E**ngineering **S**oftware). VIRTUES-CAR deals with analysis, design and control of the drive train. VIRTUES-VALVES deals with analysis and design of the valve-body and with control of the variator. A graphical interface and database facilities are added recently. Since this software actually serves as a design and analysis tool at VCST, it is a dynamic package, that is adapted, extended and improved permanently. It is only intended for internal use within VCST.

Chapter 8

A Test-Rig for Valve Body Analysis and Control

In this Chapter, we describe the test-rig that has been designed and constructed at SISTA, for experimental valve body analysis and inner control validation for VT2-E transmissions (VT2 transmission with an electro-hydraulic control unit). Section 8.2 shows the objectives of the test-rig and motivates the design choices that were made. Section 8.3 treats all steered input signals and measured output signals in detail. Section 8.4 describes the test-rig lay-out, its operation and the different components that have been used. In Section 8.5, we describe the software to obtain model calibration data (for the valve models in Chapter 6) and to validate the inner control loops proposed in Chapter 5.

8.1 Introduction

The test-rig consists of an electro-mechanical part (engine, VT2-variator), an electro-hydraulic actuation unit (valve-body and PWM valves), an electronic control and data acquisition system (sensors, PC, acquisition facilities, power amplifiers) and auxiliaries (cooling unit). Load conditions can not be emulated on this test rig, since no load (brake or flywheel) is present.

8.2 Objectives

The test rig has been constructed for two purposes:

- Model validation

  The static and dynamic characteristics of PWM valves, spool valves and pistons under different operational conditions are required to validate or calibrate the corresponding physical models that were derived in Chapters 5 and 6.

  Three spool valves (secondary valve, primary valve and clutch valve) and two pistons (secondary and primary piston) need to be analyzed under different operational conditions (pump flow Q_{gp}, oil temperature T_{oil} and shifting facilities (fixed pistons, interacting pistons)). This implies that a huge amount of experiments are required. Design of experiments, based on orthogonal arrays, is used to select experiments, in order to guarantee maximal information from a fixed number of experiments (see [Pha 89]).

- Validation of inner control algorithms

  The inner controllers for electro-hydraulic control of the secondary piston (pressure control) and the primary piston (pressure or speed control) need to be validated under specific operational conditions (pump flow Q_{gp}, oil temperature T_{oil} and shifting facilities (fixed pistons, interacting pistons)).

For these purposes, emulation of load conditions is not required.

8.3 Steered inputs and measured outputs

Two types of signals can be distinguished:

- Signals required for CVT control
  - Three PWM modulated current signals are used to steer the electro-hydraulic PWM valves.
  - Three servo pressures, three piston pressures and the primary and secondary rotation speed (to compute the axial piston speeds) are used for piston control. The inner controllers use these signals to compute the duty cycles of the PWM signals. The oil temperature is also measured and taken into account.

- Signals required for control of the environment
  - The desired engine rotation speed (constant or profile) is sent to the engine controller. The desired oil temperature is sent to the controller of the cooling unit.
  - The engine rotation speed, the primary rotation speed and the secondary rotation speed are monitored. The oil temperature is monitored also.

All signals are measured using specific sensors. The primary and secondary rotation speed are measured using wide-frequencyband inductance-based sensors, which are triggered by toothed discs mounted on the primary and secondary shaft. Strain gauges with a large bandwidth are used for pressure measurements. Thermocouple devices (type k) are used to measure the oil temperature.

The measurement range, the accuracy and the bandwidth (including signal conditioners and pre-filters) are listed in table 8.1

Signal	Range	Abs. accuracy	Bandwidth
Rotation speed	100 - 20000 rpm	3 rpm	25 Hz
Piston pressure	0.5 - 50 bar	0.2 bar	30 - 250 Hz
Servo pressure	0 - 10 bar	0.02 bar	30 - 250 Hz
Oil temperature	0 - 120°	0.1^o	1 Hz

Table 8.1 *Measurement range, accuracy and bandwidth of the test-rig sensing equipment. The overall bandwidth of the measured pressures can be adjusted by pre-filter adjustment. A high bandwidth is used when gathering data for model validation, while a lower bandwidth is used when doing control validation.*

8.4 Test-rig lay-out

The test rig (see figures 8.1 and 8.2) consists of an induction motor with a vector controller, a VT2-E variator with electro-hydraulic control facilities, an oil cooling unit and electronic control and data acquisition equipment (PC, acquisition facilities, sensors, filters and amplifiers) (see [VMD 94]).

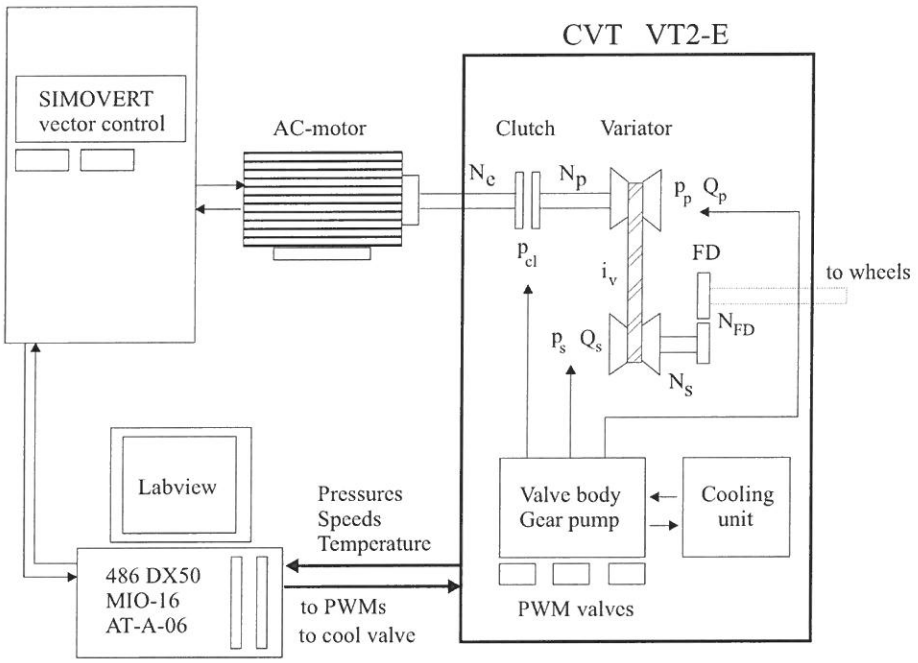

Figure 8.1 *Functional description of the test rig. The test rig consists of an induction motor with a vector controller, a VT2-E variator with electro-hydraulic control facilities, an oil cooling unit and electronic control and data acquisition equipment (PC, acquisition facilities, sensors, filters and amplifiers).*

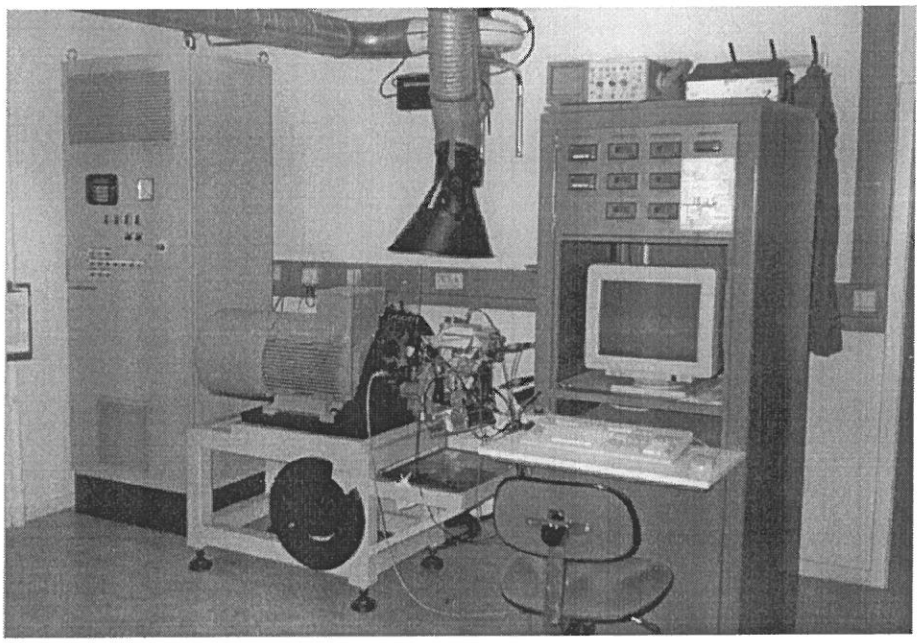

Figure 8.2 *Photograph of the test-rig (ESAT-SISTA, K.U.Leuven).*

8.4.1 The induction motor

The test rig is powered by an induction motor (22 kW, max. speed of 6000 rpm) with the aid of a Siemens Simovert 3560 inverter. The inverter is based on the vector control principle. This allows very accurate control of the speed and the delivered torque of the motor, and can be used to emulate a combustion engine.

8.4.2 The variator

An industrial CVT (VT2-E, from VCST in Sint-Truiden) is used. The transmission is equipped with three electro-hydraulic servo valves (Bosch 3/2 solenoid PWM valves). An enlarged oil reservoir allows placement of miniature sensors to measure the servo pressures. Different types of industrial valve-bodies can be installed (pp-configuration or pQ-configuration). Using industrial valve bodies (end products or design prototypes) has a lot of drawbacks from a purely scientific point of view, but is required for model validation and control validation under realistic circumstances, since internal interactions between spool

valves and pistons definitely influence the performance of the valve body and the variator.

8.4.3 The cooling unit

Basically, the cooling unit is a heat exchanger with opposite flow directions. Cold water (15°) is used for cooling of the hot transmission oil (20-100°). An electro-hydraulic servo valve controls the water flow, to realize controlled cooling. A temperature controller (PI) uses the reference temperature and the measured temperature to steer the electro-hydraulic servo valve.

8.4.4 The data acquisition and control system

Hardware

The control unit is a 486/DX50 PC with two acquisition cards and a 16 channel simultaneous sample-and-hold extension module. All signals are captured using a simultaneous sample-and-hold block of National Instruments in combination with a MIO-16 multi-purpose I/O PC-card:

- All signals are measured with specific sensors.
- All measured signals are sent to panel displays, that serve also as power supplies for the sensors. They generate analog signals ($\pm 10V$) which are proportional to the measured quantities. The motor speed signal is sent from the inverter to the I/O card as an analogue signal ($\pm 10V$).
- Anti-aliasing filters (switched capacitor sixth order Butterworth filters (MF6-50), with a tunable bandwidth) are applied before sampling takes place.

The outputs of the control unit (the inputs of the test-rig) are generated with a National Instruments AT-A-06 card:

- The reference duty cycles for the PWM valves are sent as analog signals to a PWM module, that generates appropriate PWM current signals. The basic frequency of the PWM signals may vary between 0 and 150 Hz. At higher frequencies, the inertance of the oil and the inertia of the servo spool become important and will result in incorrect operation of the PWM-valves.

- The reference motor speed is sent to the analog input card of the vector controller.
- The signal for the electro-hydraulic servo valve of the cooling system is also an analog voltage signal.

Software

The software for data-acquisition and real-time control is a combination of Labview and C. Graphical interfaces (push-buttons, dialog boxes, on-line monitoring) and build-in safety procedures (soft-start, alarms, emergency button, soft-stop) are used to increase safety and transparancy. Two programs are developed:

- CVT-Log

  CVT-Log is used to generate the static and dynamic characteristics of the valve body (see figure 8.3). The input signals for the test rig (CVT, engine and cooling) are generated with build-in function generators or via external, user-supplied sequences from Matlab. The collected signals are visualized in Labview (monitoring) and stored in ASCII-format (for model calibration and/or validation)

  DOE-techniques (orthogonal arrays) are used to design experiments that generate a maximum of information with a minimal number of experiments. Matlab is used to compute the list of candidate experiments. Data-Log is able to execute all listed experiments automatically.

- CVT-control

  CVT-Control is used to validate the inner controllers for variator control. To increase the computational speed and to allow flexible programming of complex control strategies, the control blocks are implemented in C.

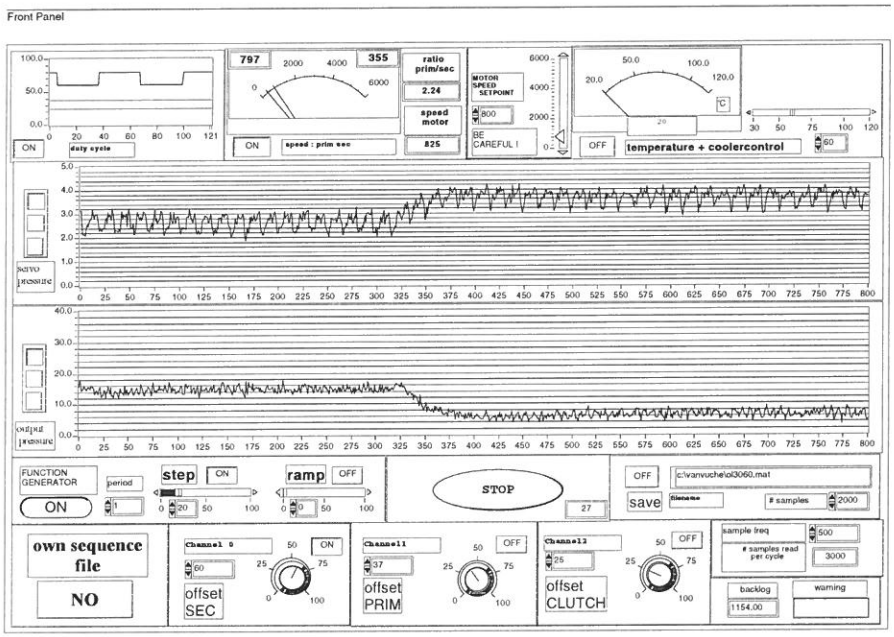

Figure 8.3 *CVT-Log is a Labview program to do static and dynamic open-loop experiments in a flexible and effective way.*

Chapter 9

Conclusions and open problems

9.1 Conclusions

In this book, we focused on the *development and application of virtual engineering techniques for design and control of Continuously Variable Transmissions*:

1. Physical modeling techniques are used to obtain generic models of the environment, the car, the drive train, the engine, the various types of couplings, the push-belt variator and the wide variety of valve-bodies.

   The characteristic behavior of each component as well as the interactions between components are described in detail. This leads to highly non-linear, multi-variable system equations, that are useful for both simulation-based analysis and design.
   Based on singular perturbation techniques, linearized equations are derived from the physical descriptions. These equations are physically parameterized and are useful for analytical analysis and design.

2. Specific experiments have been defined and conducted, to generate model calibration data. Design-of-experiments-techniques are used to increase the reliability of the experiments and to reduce the number of experiments.

   The generic models are tuned for a wide range of applications. The applications that have been considered are:

- **Cars**: Rover Metro, Rover 216, Rover 416, MGF, Renault Clio, Volvo 440 and Volvo 850. Preliminary work has been done for Daewoo, Daihatsu and Hyundai.
- **Combustion engines**: Volvo engines (B18U-1800 cc, N2-P20-2000 cc) and Rover engines (1.4K8TBI, 1.4K8MPI and 1.4K16MPI, all 1400 cc, 1.6K16MPI-1600 cc, 1.8K16MPI and 1.8K16MPI-VVC, both 1800 cc, and 2.0M16LTI-2000 cc).
- **Coupling elements**: a wet multi-plate clutch (P811) and a torque convertor (Daikin YT220).
- **Push-belt variators**: all important VCST variators (VT-175, VT-200, VT-3) and their application-specific variants.
- **Valve-bodies**: VCSTs hydro-mechanical controlled valve-body (VT1-H) and some of their electro-hydraulical controlled valve-bodies (VT1-E, EVT2, VTF). Valve-body models include the gear pump, the regulator and servo valves, the pulley and clutch pistons and the control system (actuators, sensors and intelligence).

3. The derived models have been used for design and optimization of the valves, the variator and the control system, for a wide variety of car-engine-coupling combinations.

   In this context, effective performance indices, based on customer's specifications and on experimental results are defined. Specific attention is paid to fuel consumption, dynamic car performance (accelerations, speed, hill-climbing), and vertical and longitudinal drive comfort.

4. Model-based controllers were designed, implemented and validated (if possible).

   Model-based optimization of the actual digital control algorithms (PID and (non-linear) static feedforward) has been done extensively. To analyse and validate these controllers, a computer-controlled test-rig has been constructed.

   Advanced model-based digital control algorithms are developped also. At this moment, these algorithms are being implemented and validated on the 'upgraded' power test-rig at VCST. Implementation in cars will only be possible when the electronic control unit (ECU) is no longer a cost constraint for series production.

   All derived controllers fully exploit the derived physical models. Feedback linearization theory and linear control theory are combined to design the controllers.

5. The virtual engineering framework has been implemented in Matlab and Simulink, in the tailor-made tool box VIRTUES (VIRTUal Engineering Software). In this tool box, the models and the proposed controllers are implemented. Dedicated techniques for model calibration, system analysis and optimization-based parameter design are implemented also.
   Currently, a graphical user interface and a CAD-database are being added.

9.2 Open problems

The increased potentials and the decreasing costs of electronic control for automotive applications, together with the stronger specifications from customers and government with respect to car performance, fuel economy and comfort created a need for research on CVTs in general, and for model-based design and control strategies of CVTs in special. The current set of models is quite accurate, and able to deal with a wide variety of design and control problems. The derived controllers are nearly optimal from a theoretical point of view; their performance is mainly limited by uncertainty on the physical parameters (e.g. oil compressibility, leakage orifice, discharge coefficient) and by inaccurate estimation of variables (e.g. engine torque, load torque, valve position). To increase the model accuracy, the performance of the controllers and the acceptance of the proposed approach, several options are available.

- The reliability and the acceptance of comfort simulations can be increased:
  - To increase the acceptance, it is important that the computed comfort quotations match with the comfort quotations given by so-called 'comfort-groups' (see [VCST 95]).
  - To increase reliability, more detailed car models and human sensitivity models might be required. Sensitivity models for harmonic disturbances are well known, but little is published about comfort under deterministic disturbances.
- The accuracy of the variator model can be improved:
  - By augmenting the theoretical variator efficiency models, such that they match with the experimental neural network model.
  - By augmenting the theoretical $\frac{K_p}{K_s}$ and $\frac{di_v}{dt}$ models, such that they match with the experimental models.
- Instead of using two decoupled inner controllers for variator control (one piston is controlled for shifting and one is controlled to avoid slip), a multiple input multiple output approach for variator control design can be used,

especially in the pressure steered case (pp). However, this is not trivial because:

  - An accurate static and dynamic belt-model is required to describe the mechanical interactions. A finite element approach holds promises, if valid assumptions on the friction phenomena are made.
  - An accurate model of the valve-body, that takes into account the hydraulic interactions between the different servo valves, must be added also. This can easily be done by combining the different valve models derived in Chapter 6.
  - A very complex non-linear finite element model will be the final result. Research on new control design techniques for this type of models will be required.

- Integrated design of the global actuation and control unit (control mechanisms, spool valves, pistons and oil pump) is required to further reduce the undesired hydraulic interactions that occur in actual industrial CVTs and to increase performance of the variator controllers.

- The use of adaptive techniques to estimate the uncertain parameters in the proposed controllers might help to further increase controller performance. Direct measurement of variables (e.g. variator ratio, engine torque) or more accurate estimation methods will also increase controller performance.

Appendix A

Parameter tuning using numerical optimization

In this Appendix, we describe a practical approach that has been used to tackle non linear parameter tuning problems during this research project. In Section A.1, we describe the various parameter tuning problems that were encountered. In Section A.2, we formulate the problem as a constrained optimization problem. Section A.3 explains a practical approach to state and solve the problem, and considers some practical issues. In Section A.4, we give an illustrative example.

A.1 Practical parameter tuning problems

The problem of tuning the free parameters of a given set of equations arises in many engineering applications:

- System modeling

  In system modeling, a set of physically parameterized non-linear (differential) equations must be matched with a set of static and/or dynamic experiments from a practical test-case. The physical parameters of the test-case must be computed, taking into account that these parameters can only vary over a specific range.

- System identification

  In system identification, a set of (non) linear differential equations must be matched with a set of dynamic experiments from a practical test-case. The parameters that lead to a minimal prediction error must be computed.

- Physical design

  In physical design, a set of physically parameterized non-linear (differential) equations must be matched with a set of static and/or dynamic performance specifications. The physical parameters of the system must be computed, to realize 'optimal' open-loop performance, taking into account that these parameters can only vary over a prescribed range.

- Control design

  In controller tuning, a set of (non) linear (differential) equations must be matched with a set of static and/or dynamic performance specifications. The parameters of the controllers must be computed, to realize 'optimal' closed-loop performance.

To solve these problems, two approaches can be used:

- Analytical approaches solve the problem analytically, allow fast and efficient computation of the solution, but are only applicable under very specific conditions.

- Numerical optimization methods solve the problem in an iterative way and are applicable under very mild conditions. The quality of the obtained solution (global optimum versus local optimum) and the computation speed are strongly related to the complexity (number of unknowns, number and type of nonlinearities) and the nature of the problem (convex or not).

Throughout this thesis, numerical optimization methods were used to solve most parameter tuning problems.

A.2 Mathematical formulation

Let $\vec{X}$ be the vector of n free parameters

$$\vec{X} = (x_1, \ldots, x_n)$$

The general mathematical formulation of a constrained optimization problem is given by:

$$\begin{aligned} \min_{\vec{X}} \quad & \vec{F}(\vec{X}) \\ s.t. \quad & \vec{G}(\vec{X}) \leq 0 \\ & \vec{H}(\vec{X}) = 0 \end{aligned} \tag{A.1}$$

$\vec{F}$ represents the set of k non-negative quality measures that must be optimized simultaneously. $\vec{G}$ represents the set of l inequality constraints that must be satisfied, while $\vec{H}$ represents the set of m equality constraints that must be taken into account. From these definitions, it follows that the set of feasible parameters $\mathcal{X}$ is given by:

$$\mathcal{X} = \{\vec{X} | \vec{G}(\vec{X}) \leq 0, \vec{H}(\vec{X}) = 0\}$$

and that the set of attainable performances $\mathcal{F}$ is given by:

$$\mathcal{F} = \{\vec{F}(\vec{X}) | \vec{X} \in \mathcal{X}\}$$

The general constrained optimization problem can now be reformulated as:

$$\min_{\vec{X} \in \mathcal{X}} \vec{F}(\vec{X})$$

To understand and solve this vector optimization problem, the concept of non-inferiority is introduced (see [Par 96]).

> Definition 1. *A design $\vec{X}^*$ is said to be non-inferior, if there are no other $\vec{X} \in \mathcal{X}$ such that:*
>
> $$\forall i : F_i(\vec{X}) \leq F_i(\vec{X}^*) and \exists j : F_j(\vec{X}) < F_j(\vec{X}^*)$$
>
> *A design $\vec{X}^*$ for which there exist designs $\vec{X} \in \mathcal{X}$ that satisfy the previous conditions, is said to be inferior, because some F_j can be decreased without increasing the remaining F_i.*

From this definition, it follows that a non-inferior design corresponds to a design that realizes an exact trade-off between the quality measures. Since there are many designs that satisfy these conditions, it is evident to think about a 'set of optimal solutions', instead of looking for a single solution.

> Definition 2. *If the set of all non-inferior designs is denoted by $\mathcal{X}_p$, then the set of non-inferior performances is given by*
>
> $$\mathcal{F}_p = \{\vec{F}(\vec{X}) | \vec{X} \in \mathcal{X}_p\}$$
>
> *The ultimate challenge is to find all non-inferior designs $\mathcal{X}_p$.*

In practice, it is the goal to find a non-inferior design $\vec{X} \in \mathcal{X}_p$ that corresponds to an 'acceptable' non-inferior performance $\vec{F} \in \mathcal{F}_p$. To solve this vector minimization problem, various methods are described in the literature. Although the method of inequalities (see [ZA 73]), hierarchical optimization (see [Toiv 84]) and interval elimination methods (see [PP 80]) perform quite well, we use methods based on function scalarization. To transform the vector minimization problem into a function minimization problem, different methods are used (depending on the problem that must be solved):

- Vector norm optimization

  In this approach, any norm of the weighted objectives vector $\vec{F}_{\vec{\lambda}}$

  $$\vec{F}_{\vec{\lambda}}(\vec{X}) = (\lambda_1 F_1(\vec{X}), \ldots, \lambda_n F_n(\vec{X}))$$

  can be minimized (with $\sum_{i=1}^{k} \lambda_i = 1$). The problem is stated as:

  $$\min_{\vec{X} \in \mathcal{X}} \| \vec{F}_{\vec{\lambda}}(\vec{X}) \|_p$$

  with p a strictly positive integer and the p-norm of a vector defined as:

  $$\| \vec{Y} \|_p = \left(\sum_{i=1}^{k} |Y_i|^p \right)^{\frac{1}{p}}$$

  For $p = 1$, the method reduces to the weighted-sum method (see [BS]), while for $p = \infty$, it reduces to the minimax method found in (see [FP 85]). By varying the weight vector $\vec{\lambda}$, different non-inferior designs can be obtained.

- The ϵ constrained method

  In this approach, the designer chooses one objective to be minimized, while the other objectives are required to be smaller than a value ϵ_j. The obtained non-inferior design is determined by the values ϵ_j. The problem is stated as:

  $$\min_{\vec{X} \in \mathcal{X}} F_i(\vec{X}) s.t. F_j(\vec{X}) \leq \epsilon_j, \forall j \neq i$$

- The goal attainment method

  Let $F^* = (F_1^*, \ldots, F_k^*)'$ be the designers preferred performance (the goal) and let $\vec{\lambda}$ be a desired search direction in the performance space, then this problem can be stated as:

$$\min_{\gamma} s.t. \vec{X} \in \mathcal{X}, F_i(\vec{X}) - \lambda_i \gamma \leq F_i^*, \forall i$$

If $\gamma \leq 0$, the designers goal is (over)attained, if $\gamma > 0$, the designers goal is under-attained and F^* turns out to be an unattainable performance.

Once the problem is transformed into a function minimization problem, the resulting non-linear programming problem must be solved. This problem can in general be stated as:

$$\min_{\vec{X}} f(\vec{X}) s.t. \vec{g}(\vec{X}) \leq 0, \vec{h}(\vec{X}) = 0$$

To solve it, the standard constrained nonlinear optimization method provided by Matlab is used (constr.m).

A.3 A practical approach

In practice, the following steps must be taken, to transform a practical parameter tuning problem into a constrained nonlinear optimization problem and to solve the resulting problem:

1. Determination of an effective parameterization, which implies specification of the free parameter vector $\vec{X}$.
2. Determination of effective performance indices, which implies selection and specification of the different quality measures of interest. In this step, the functions to evaluate all components of the vectors $\vec{F}$, $\vec{G}$ and $\vec{H}$ must be written down explicitly.
3. Determination of scaling vectors

   First, the free parameter vector $\vec{X}$ is scaled, in such a way that all components of the scaled parameter vector $\vec{X}_{sc}$ have the same order of magnitude.

   Next, the vectors $\vec{F}$, $\vec{G}$ and $\vec{H}$ are scaled, in such a way that all components of the scaled vectors $\vec{F}_{sc}$, $\vec{G}_{sc}$ and $\vec{H}_{sc}$ have the same order of magnitude.
4. Determination of an initial solution (if possible, a feasible initial solution).
5. Determination of the weight vector $\vec{\lambda}$
6. Optimization

   This last step can be repeated, to generate multiple non-inferior designs (the trade-off surface), or until an acceptable non-inferior design is found.

A.4 An illustrative example

Consider the problem described in [PM 76] of designing a dynamical control law $K(s)$ for the following one-degree-of-freedom (1DOF) configuration (see figure A.1).

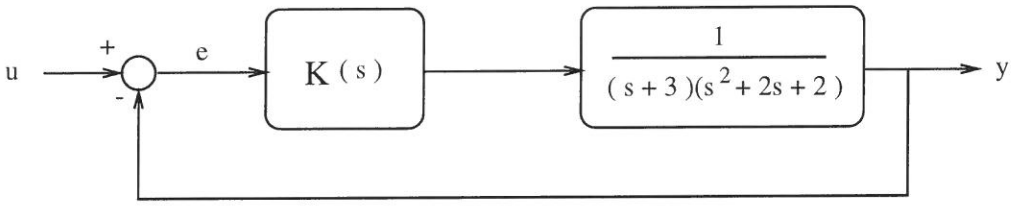

Figure A.1 *A 1DOF configuration with a control law $K(s)$ to be designed*

The first parametrization to investigate is a classical PI-control law. The controller is parametrized as:

$$K(s) = P + \frac{I}{s}$$

and the vector of unknowns $\vec{X}$ is given by $(x_1, x_2) = (P, I)$.

The design specifications of interest are:

- Realizability

  For the case of PI-control, no explicit condition on the parameters needs to be added.

- Stability

  From the Routh-Hurwitz stability test, it follows that the following conditions need to be satisfied:,

$$\begin{aligned} g_1 &= x_2 \geq 0 \\ g_2 &= 33 - x_1 \geq 0 \\ g_3 &= (33 - x_1)(7 + x_1) - 25x_2 \geq 0 \end{aligned}$$

- Bounds on the design variables

$$\begin{aligned} g_4 &= 100 - x_1 \geq 0 \\ g_5 &= 100 - x_2 \geq 0 \\ g_6 &= 100 + x_1 \geq 0 \\ g_7 &= 100 + x_2 \geq 0 \end{aligned}$$

- Zero steady state error for a step input

  No additional condition on the parameters is required, since the integral term in $K(s)$ guarantees a zero steady state error for step inputs.

- Realize a trade-off between overshoot and root of the squared error, for a step response.

  The overshoot of the unit step response $y(t)$ is computed as:

$$f_1 = \max\{\max(y(t) - 1), 0\}$$

  The root of the squared error or l_2-norm of the error signal $e(t)$ for a unit step input $u(t)$ is a measure for the tracking behaviour and is computed as:

$$f_2 = \left(\int_0^\infty e^2(t)dt\right)^{\frac{1}{2}}$$

The multi-objective optimization problem can be stated as

$$\min_{(x_1,x_2)} (f_1, f_2) \;\; s.t. \;\; (g_1, \ldots, g_7) \geq 0$$

This problem is transformed into a scalar minimization problem using the method of vector norm minimization. With $p = 1$, the problem becomes

$$\min_{\vec{X}} \;\; \lambda_1 f_1(\vec{X}) + \lambda_2 f_2(\vec{X}) \;\; \text{s.t.} \;\; (g_1, \ldots, g_7) \geq 0$$

with f_1 measuring the overshoot and f_2 a measure for the tracking error. By varying the weights, different non-inferior solutions on the trade-off curve $\mathcal{F}_p$ are found. As initial design, $(x_1, x_2) = (5, 10)$ is used.

The results for various weights are shown in table A.1. Figure A.2 shows the corresponding step responses, while figure A.3 shows the trade-off curve for a PI-controller[1].

[1] Notice that the obtained trade-off curve is in fact an upper approximation of the exact one. However, an evaluation of grid points over the considered parameter box showed that the obtained curve was a very good approximation of the exact curve.

(λ_1, λ_2)	(x_1, x_2)	(f_1, f_2)
$(0.95, 0.05)$	$(9.49, 2.26)$	$(0.0, 1.00)$
$(0.5, 0.5)$	$(8.40, 3.19)$	$(2.3, 0.94)$
$(0, 1)$	$(11.23, 4.69)$	$(20.8, 0.84)$

Table A.1 *PI-designs on the trade-off boundary. The overshoot is expressed in %. High values of λ_1 result in a small overshoot, high values of λ_2 result in small tracking errors.*

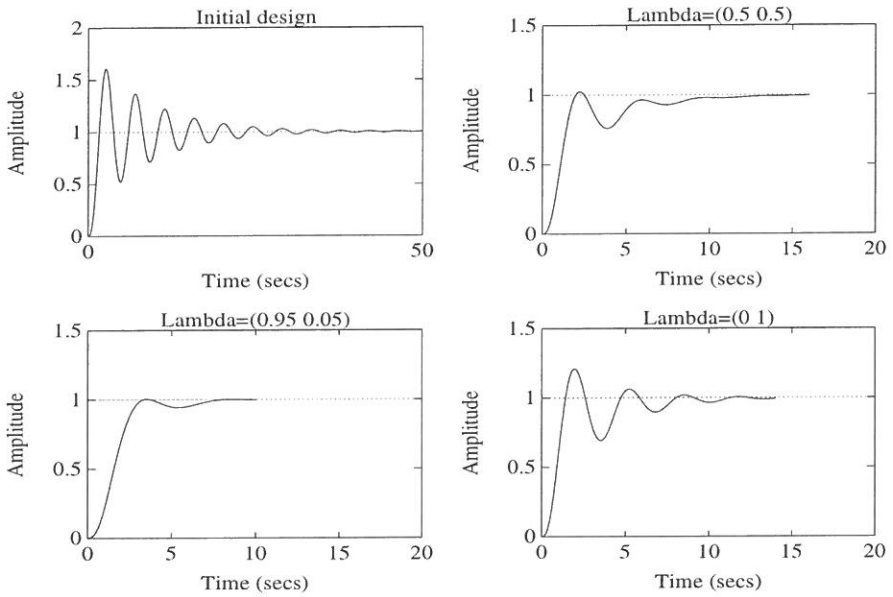

Figure A.2 *Step responses with a PI-controller: the initial design and non-inferior designs for various weights.*

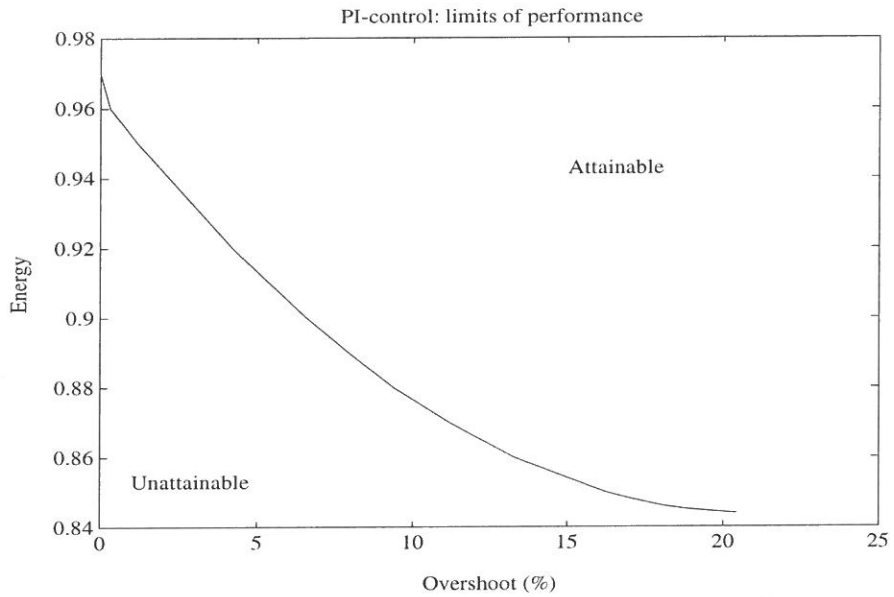

Figure A.3 *The trade-off curve for the classical PI-parametrization.*

The same problem is also solved for some other parametrizations:

- Two other classical parametrizations of the control law $K(s)$.
  - A compensator network
  - A PID-controller
- A Youla-parametrization of the control law $K(s)$.
  Instead of designing the control law $K(s)$ directly, the Youla parameter $Q(s)$ is designed first. Once $Q(s)$ is given, the control law $K(s)$ can readily be computed [Fra 88].

Table A.2 shows the different controllers, the parametrizations, the unknowns and the initial designs. To be able to compare the different types of control, the PI-parametrization is included also.
The resulting objective values (f_1, f_2) are shown in table A.3, for different weight values. Figure A.4 shows the trade-off curves for the different parametrizations. Since the trade-off curves can be computed for different control laws, these curves might be used to select both the parameters and the control law.
In this example, a PID-law turns out to be the best classical controller. Depending on the weight values, the modern controller performs better or worse than the best classical controller (see figure A.4).

Controller	Parametrization	Unknowns	Initial design
PI-controller	$K(s) = P + \frac{I}{s}$	$\vec{X} = (P, I)$	$(5, 10)$
Compensator network	$K(s) = K\frac{s-\alpha}{s(s+\alpha)}$	$\vec{X} = (K, \alpha)$	$(-5, 5)$
PID-controller	$K(s) = P + \frac{I}{s} + Ds$	$\vec{X} = (P, I, D)$	$(5, 10, 10)$
Modern controller	$Q(s) = \frac{\sum_{i=0}^{5} x_i s^i}{(s+2)(s+3)(s+4)(s+5)^2}$	$\vec{X} = (x_0, \ldots, x_5)$	$(6, 1, 1, 1, 1, 1)$

Table A.2 *Four different control laws to realize closed-loop performance.*

Name	$\vec{\lambda} = (0.95, 0.05)$	$\vec{\lambda} = (0.5, 0.5)$	$\vec{\lambda} = (0, 1)$
PI-controller	$(0.0, 1.00)$	$(2.3, 0.94)$	$(20.8, 0.84)$
Compensator network	$(0.0, 2.54)$	$(19.5, 2.02)$	$(29.3, 1.98)$
PID-controller	$(0.0, 0.39)$	$(3.0, 0.23)$	$(40.1, 0.13)$
Modern controller	$(0.1, 0.93)$	$(0.7, 0.22)$	$(18.9, 0.19)$

Table A.3 *Designs on the trade-off boundary, for four different control laws.*

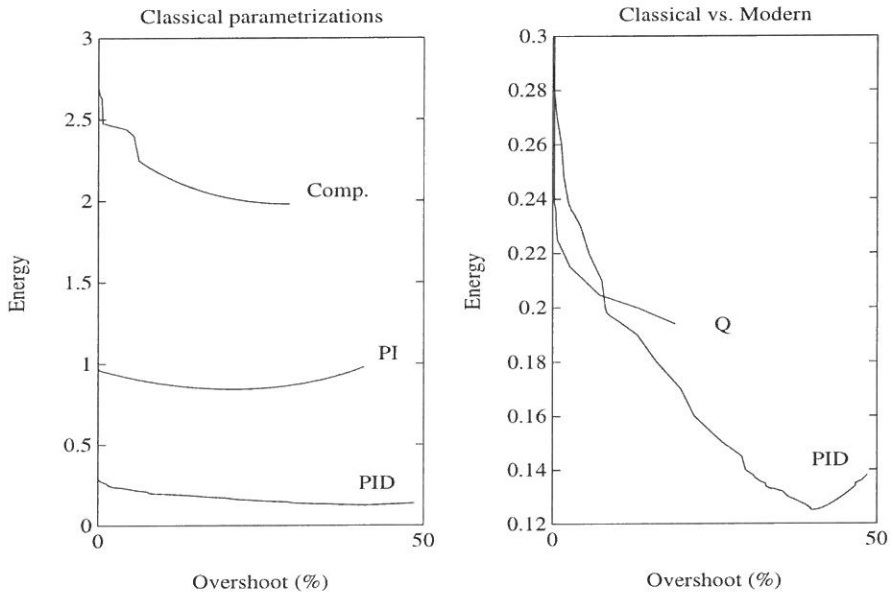

Figure A.4 *Trade-off curves for the classical parametrizations (l). For a certain type of controller, only the performances above the trade-off curve are attainable. Classical versus modern parametrization (r). Because a Q-parameter with a finite order is designed, the classical PID controller performs better than the modern controller for some weight values.*

Bibliography

[Ack 93] Ackermann J., *Robuste regelung: analyse und entwurf von linearen regelungssystemen mit unsicheren physikalischen parametern.* Springer-Verlag, Berlin, 1993.

[AW 84] Åström K. and Wittenmark B., *Computer controlled systems: theory and design.* Prentice Hall, 1984.

[Bac 93] Backé W., *The present and future of fluid power.* 80th Thomas Hawksley Memorial Lecture, Proc. IMechE, Part I, Vol. 207, pp. 193-212, 1993.

[Bak 92] Baker A.K., *Industrial brake and clutch design: a FERODO design manual.* Pentech Press, London, 1992.

[BSW 95] Beck H.P., Sourkounis C. and Wenske J., *Torsionsschwingungen in antriebssträngen mit hydrodynamischer kupplung.* Antriebstechnik 34-5, pp. 62-67, 1995.

[BW 91] Borg-Warner, *Borg-Warner automotive friction products.* Borg-Warner Automotive, 1991.

[BB 91] Boyd S. and Barrat C., *Linear controller design: limits of performance.* Prentice Hall, Information and System Sciences Series, New Jersey, 1991.

[BS] Brayton R.K. and Spence R., *CAD of electrical circuits. Part 2, sensitivity and optimization.* Elsevier Scientfic Publishing Company, 1990

[BE 91] Burrows C.R. and Edge K.A., *Fluid power systems modelling and control.* 4th Bath International Fluid Power Workshop, 1991.

[Buu 92] Buur J., *Does mechatronics need a special attitude?* Mechatronic Systems Engineering, Vol. 1, pp. 293-300, 1992.

[COYVBJF 84] Chan C., Omitsu T., Yang D., Volz T., Breitweiser D., Jamzadeh F.S. and Frank A., *System design and control considerations of automotive Continuously Variable Transmissions.* SAE paper 840048, 1984.

[CA 94] Crouse W.H. and Anglin D.L., *Automotive Engines.* Glencoe, Macmillan/McGraw-Hill, 1994.

[DDVDB 91] David J., De Moor B., Vandewalle J., De Moor M. and Berckmans D., *Trade-offs in linear control system design: a practical example.* ESAT, Dept. of Electrical Engineering, Katholieke Universiteit Leuven, Leuven, ESAT-SISTA Report 1991-04.

[Dev 93] De Vries T.J., *Theoretisch en praktisch onderzoek naar het rendement van de metalen V-band. (Theoretical and practical research of the metal V-belt's efficiency).* M.Sc. thesis, Eindhoven University of Technology, 1993, in Dutch.

[DH 95] Dorisen H.T. and Höver N., *Antriebsschlupfregelung (ASR) - Ein beitrag zur aktiven fahrsicherheit.* Automobiltechnische Zeitschrift (ATZ) 95-4, pp. 194-201, 1995.

[Dra 81] Dransfield P., *Hydraulic control systems. Design and analysis of their dynamics.* Springer-Verlag, New York, 1981.

[Dub 90] Dubbel, *Taschenbuch für den maschinenbau.* Springer-Verlag, Berlin, edited by Beitz W. and Küttner K.H., 1990.

[EVV 95] Espinosa J., Vanvuchelen P. and Vandewalle J., *Fuzzy scheduling to control a hydraulic servo system.* Journal A, Vol. 36, No. 3, pp. 51-55, 1995.

[Eur 91] *Publicatie-blad van de Europese Gemeenschappen.* No. L242, pp. 33-42, August 1991, in Dutch.

[FWKT 89] Fan M.K.H., Wang L.S., Koninckx J. and Tits A.L., *Software package for optimization-based design with user-supplied simulators.* IEEE Control Systems Magazine, pp. 66-71, January 1989.

[FMc 68] Fiaco A.V. and Mc Cormick G.P., *Non-linear programming: sequential unconstrained minimization techniques.* John Wiley and Sons, 1967.

[FP 85] Fleming P.J. and Pashkevich A.P., *Computer-aided control system design using a multi-objective optimization approach.* Proc. of the Control '85 Conference, Cambridge, UK, pp. 174-179, 1985.

[Fra 88] Francis B.A., *A Course in H_∞ Control.* Springer-Verlag, 1988.

[FPW 90] Franklin G.F., Powell J.D. and Workman M.L., *Digital control of dynamic systems.* Second edition, Addison-Wesley Publishing Company, New York, 1990.

[FM 92] Fukuba H. and Morita S., *Optimization control of the fuel consumption ratio for an engine-CVT-load system using decoupling control theory.* JSME International Journal, Series II, Vol. 35, No. 3, pp. 442-447, 1992.

[Fun 95] Funk W., *Zugmittelgetriebe: grundlagen, aufbau, funktion.* Springer-Verlag, Berlin, 1995.

[Gie 89] Gieles W.T.M., *Electronic control of continuously variable transmissions and its extension to engine-transmission management.* IMechE-papers, No. C382/048, pp. 133-138, 1989.

[Got 91] Gott P.G., *Changing gears: the development of the automotive transmission.* Society of Automotive Engineers Inc., SAE Historical Series, 1991

[GM 89] Götzmann W.H. and Meyer H., *Zur digitalen simulation von übergängen zwischen gleit- und haftreibung.* R. Oldenbourg Verlag, Automatisierungstechnik 37-10, pp. 399-400, 1989.

[Grace 89] Grace A.C.W., *Computer-aided control system design using optimization techniques.* PhD. thesis, University of Wales, Bangor, Gwynedd, UK, 1989.

[MG 92] Grace A.C.W., *Optimization toolbox, for use with Matlab.* The Mathworks Inc., Cochituate Place, 24 Prime Park Way, South Natick, MA 01760, 1992.

[Granda 90] Granda J.J., *Computer-aided design of dynamic systems.* California State University, Dept. of Mechanical Engineering, CA, USA, 1990.

[Granda 91] Granda J.J., *Modelling and simulation of electro-mechanical systems using computer graphics.* California State University, Dept. of Mechanical Engineering, CA, USA, 1991.

[GS 95] Guzzella L. and Schmid A.M., *Feedback linearization of spark-ignition engines with Continuously Variable Transmissions.* IEEE Transactions on Control Systems Technology, Vol. 3, No. 1, pp. 54-60, March 1995.

[HW 94] Heintze J. and Van der Weiden A.J.J., *Inner loop design and analysis for hydraulic actuators, with application to impedance control.* Delft University of Technology, Mechanical Engineering Systems and Control Group, 1994.

[Hel 94] Helsen S., *Gedrag en gewenst gedrag van een koppelomvormer.* VCST N.V., Rellestraat 2, Sint-Truiden, Belgium, R&D department, Report No. 1115/94, October 1994, in Dutch.

[Hey 88] Heywood J.B., *Internal combustion engine fundamentals.*, Mc Graw-Hill Book Company, Automotive Technology Series, 1988.

[Hur 94] Hurst K., *Rotary Power Transmission Design.* McGraw-Hill Book Company, 1994.

[HLJ 93] Hwang C.L., Lan C.H. and Jieng W.J., *The trajectory tracking of an electro-hydraulic servo-mechanism via a sliding mode controller.* Proc. IMechE, Part I, Vol. 207, pp. 135-142, 1993.

[IUK 95] Ide T., Udagawa A. and Kataoka R., *Simulation approach to the effect of the ratio changing speed of a metal V-belt CVT on the vehicle response.* Vehicle System Dynamics, No. 24, pp. 377-388, Swets & Zeitlinger, 1995.

[ISO 86] *Guide to the evaluation of human exposure to whole-body mechanical vibration.* Revision of ISO2631, Draft No. 7, 1986.

[JZY 94] Jinghong Y., Zhaoneng C. and Yuanzhang L., *The variation of oil effective bulk modulus with pressure in hydraulic systems.* Transactions of the ASME, Vol. 116, pp. 146-150, March 1994.

[JE 91a] Johnston D.N. and Edge K.A., *The impedance characteristics of fluid power components: restrictor and flow control valves.* Proc. ImechE, Part I, Vol. 205, pp. 3-22, 1991.

[JE 91b] Johnston D.N. and Edge K.A., *In-situ measurement of the wave speed and bulk modulus in hydraulic lines.* Proc. ImechE, Part I, Vol. 205, pp. 191-197, 1991.

[Jus 92] Jussila T., *Computational issues of PID controllers.* PhD. thesis, Tampere University of Technology, Finland, 1992 .

[KR 75] Karnopp D.C. and Rosenberg R.C., *System dynamics: a unified approach.* Wiley & Sons, New York, 1975.

[Ket 91] Ketelaars J.A.A., *Het langscomfort in een personenvoertuig, een literatuuronderzoek.* Eindhoven University of Technology, Laboratory for Automotive Engineering, Faculty of Mechanical Engineering, Report No. WOC/VT/R91.42, 1991, in Dutch.

[KL 93] Kortüm W. and Lugner P., *Systemdynamik und regelung von fahrzeugen: einführung und beispiele.* Springer-Verlag, Berlin, 1993.

[Lea 91] Leaney P.G., *Component oriented modelling of a valve controlled asymmetric cylinder drive using a generalized formulation for model linking.* Proc. ImechE, Part I, Vol. 205, pp. 285-298, 1991.

[LC 90] Lin C.A. and Chen S.H., *Optimization-based control system design.* Proc. of the 29th Conference on Decision and Control, Honolulu, Hawai, pp. 2462-2468, December 1990.

[LRWK 93] Liubakka M.K., Rhode D.S., Winkelman J.R. and Kokotović P.V., *Adaptive automotive speed control.* IEEE Transactions on Automatic Control, Vol. 38, No. 7, pp. 1011-1020, July 1993.

[Lju 87] Ljung L., *System identification - Theory for the user.* Prentice Hall, New Jersey, 1987.

[Luy 88] Luyckx J., *Berekening van Kp/Ks. (Computation of Kp/Ks).* VCST-VT N.V., Rellestraat 2, Sint-Truiden, Belgium, R&D department, Report No. 079/INCC/88, 1988, in Dutch.

[MD 93] Maclay D. and Dorey R., *Applying genetic search techniques to drive train modelling.* IEEE Control Systems, pp. 50-55, June 1993.

[Mlab] *Matlab for Unix computers, user's guide.* The Mathworks Inc., Cochituate Place, 24 Prime Park Way, South Natick, MA 01760.

[Mer 67] Merritt H.E., *Hydraulic control systems.* John Wiley and Sons, 1967.

[MLB 94] Micklem J.D., Longmore D.K. and Burrows C.R., *Belt torque loss in a steel V-belt continuously variable transmission.* Proc. IMechE, Part D., Vol. 208, pp. 91-97, 1994.

[MFMV 91] Milanese M., Fiorio G., Malan S. and Vicino A., *Robust performance design of nonlinearly perturbed control systems. Appeared in: Control of Uncertain Dynamic Systems.* International Workshop on Robust Control, Texas, CRC Press, pp. 113-124, March 1991.

[Mit 84] Mitschke M., *Dynamik der Kraftfahrzeuge, band A-B-C.* Springer-Verlag, Berlin, 1984.

[MVD 93] Minten W., Vanvuchelen P. and De Moor B., *Modeling of an electronically controlled continuously variable transmission.* Proc. of the International Conference on Bond Graph modeling, pp. 223-228, La Jolla, California, 1993.

[MMVD 95] Minten W., Moons C., Vanvuchelen P., and De Moor B., *Modeling of the CVT in a virtual engineering environment.* Proc. of the ROVA '95 International Conference, Bolton, United Kingdom, September 11-13, 1995.

[MS 92] Mom G. and Scheffers H., *De nieuwe Steinbuch, de complexe aandrijflijn, deel 3B*, Kluwer Technische Boeken BV, Antwerpen, 1993, in Dutch.

[MVMD 95] Moons C., Vanvuchelen P., Minten W. and De Moor B., *A computer-controlled test set-up for CVTs.* Proc. of the ROVA '95 International Conference, Bolton, United Kingdom, September 11-13, 1995.

[MV 96] Moons C. and Vanvuchelen P., *Modellen van de variator.* VCST N.V., Rellestraat 2, Sint-Truiden, Belgium, R&D department, IWT-Report No. 1, 1996, in Dutch.

[NSS 90] Narumi N., Suzuki H. and Sakakiyama R., *Trends of powertrain control.* SAE paper 901154.

[Ng 93] Ng W.Y., *Perspectives on search-based computer-aided control system design.* IEEE Control Systems, pp. 65-72, April 1993.

[Orl 94] Orlowski P.F., *Praktische regeltechnik.* Springer-Verlag, Berlin, 1994.

[Pac 76] Pacejka H.B., *Principles of plane motion of automobiles.* Proc. of the IUTAM Symposium on Dynamics of Vehicles on Roads and Tracks, Swets & Zeitlinger, 1976.

[Par 96] Pareto V., *Cours d' economie politique.* Lausanne, Rouge, 1896.

[PP 80] Payne A.N. and Polak E., *An interactive rectangle elimination method for bi-objective decision making.* IEEE Trans. on Automatic Control, AC-25, pp. 421-432, 1980.

[Per 92] Persson P., *Towards autonomous PID control.* PhD. thesis, Lund Institute of Technology, Sweden, 1992.

[Pha 89] Phadke M.S., *Quality engineering using robust design.* Prentice Hall, New Jersey, 1989.

[PM 76] Polak E. and Mayne D.Q., *An algorithm for optimization problems with functional inequality constraints.* IEEE Transactions on Automatic Control, Vol. AC-21, No. 2, pp. 184-193, April 1976.

[PMS 84] Polak E., Mayne D.Q. and Stimler D.M., *Control system design via semi-infinite optimization: a review.* Proc. of the IEEE, Vol. 72, No. 12, pp. 59-76, December 1984.

[PSWN 85] Polak E., Siegel P., Wuu T. and Nye W.T., *DELIGHT MIMO: an interactive optimization-based multi-variable control system design package.* Computer-Aided Control Systems Engineering, Elsevier Science Publishers B.V., North Holland, pp. 139-147, 1985.

[Rau 92] Rault A., *Mechatronics and bond graphs in the automotive industry.* PSA Peugeot Citroën, Velizy, France, 1992.

[Rek 90] Rekkers E.M., *Theoretisch en praktisch onderzoek naar het rendement van de Continu Variabele Transmissie. (Theoretical and practical research of the CVT's efficiency).* M.Sc. thesis, Eindhoven University of Technology, 1990, in Dutch.

[Roel 91] Roelofs H.B., *Tolerance optimization of servomechanisms.* PhD. thesis, University of Twente, 1991.

[Roo 91] Roovers G., *The CVT push-belt: developments in efficiency and application range.* Van Doorne's Transmissie B.V., Nederland, EAEC No. 91031, 1991.

[Rop 87] Röper H., *Anforderungen an die druckölversorgungseinheit hydraulisch gesteuerter CVT-getriebe.* Antriebstechnik 26-8, pp. 41-52, 1987.

[Rov 92] Rover Group Ltd., *VT-1 automatic transmission.* Rover Cars Service Publications, Oxford, 1992.

[Run 90] Runge W., *Simulationsverfahren für die Kfz-hydraulik - Schwerpunkt automatisch getriebe.* Olhydraulik und Pneumatik 34-6, pp. 420-428, 1990.

[SVR 92] Schaerlaeckens W. and Van Rooij J., *De metalen V-band, een theoretische benadering: algemene krachtenbeschouwing - het krachtenspel - de energetische verliezen in duwband en CVT.* Mechanische Technologie, pp. 14-19, pp. 21-26, pp. 22-27, February, March, April 1992, in Dutch.

[SM 93] Schmidt T. and Müller P.C., *A parameter estimation method for multibody systems with constraints.* University of Wuppertal, Dept. of Safety Control Engineering, 1993.

[SH 93] Shih M.C. and Ho S.N., *Hydraulic variable piston motor position control by using model reference adaptive control methods.* Mechatronics, Vol. 3, No. 6, pp. 689-704, 1993.

[Sim 96] *Simulink automotive examples.* The Mathworks Inc., Cochituate Place, 24 Prime Park Way, South Natick, MA 01760, 1996.

[Sno 80] Snoeys R. and Gobin R., *Riem- en kettingtransmissies. (Belt and chain transmissions).* Course Notes, Dept. of mechanical engineering, Katholieke Universiteit Leuven, VTK, Leuven, 1980, in Dutch.

[Spijk 94] Spijker E., *Steering and control of a CVT-based hybrid transmission for a passenger car.* PhD. thesis, Eindhoven University of Technology, 1994.

[SL 91] Slotine J.-J. and Li W.P., *Applied nonlinear control.* Prentice-Hall, 1991.

[ST 90] Styblinski M.A. and Tang T.S., *Experiments in non-convex optimization: stochastic approximation with function smoothing and simulated annealing.* Neural Networks, Vol. 3, pp. 467-483, 1990.

[Styb 91] Styblinski M.A., *Formulation of the drift reliability optimization problem.* Micro-electronics Reliability, Vol. 31, No. 1, pp. 159-171, 1991.

[Sun 88] Sun D.C., *Performance analysis of a variable speed-ratio metal V-belt drive.* Transactions of the ASME, Journal of Mechanisms, Transmissions and Automation in Design, Vol. 110, pp. 472-481, December 1988.

[SL 95] Sundermann C. and Langenbeck K., *Neuartiger hydraulischer schwingungsdämpfer.* Antriebstechnik 34-5, pp. 57-61, 1995.

[Toiv 84] Toivonen H.T., *A multi-objective linear quadratic Gaussian control problem.* IEEE Transactions on Automatic Control, AC-29, pp. 279-280, 1984.

[VHV 91] Van Huffel S. and Vandewalle J., *The total least squares problem: computational aspects and analysis.* Frontiers in Applied Mathematics Series, Vol. 9, SIAM, Philadelphia, Pennsylvania, 1991.

[VDM 96] Van Overschee P. and De Moor B., *Continuous-time frequency domain identification.* Proc. of the 13th IFAC World Congress, pp. 157-162, San Francisco, USA, July 1996.

[VD *et al* 96] Vanvuchelen P., De Moor B. *et al*, *Modeling, analysis, design and control of an electronically controlled continuously variable transmission (1-12).* Collected master's theses, ESAT, Dept. of Electrical Engineering, Katholieke Universiteit Leuven, Leuven, 1990-1996, in Dutch.

1. Vanvuchelen P. and Minten W., *Modelvorming en simulatie van een elektronisch gestuurde CVT.* K.U.Leuven, ESAT, juli 1991.
2. Verplancke J. and Verstraeten W., *Modelvorming, simulatie en optimalisatie van een elektronisch gestuurde CVT.* K.U.Leuven, ESAT, juli 1992.
3. Nijhout G., *Modelvorming en toerentalregeling van een elektronisch gestuurde CVT.* T.U.Delft (Erasmus), augustus 1992.
4. Boonen P. and Briers J., *Modelvorming, identificatie en controle van een elektronisch gestuurde hydraulische actuator.* K.U.Leuven, ESAT, juli 1993.
5. Christiaensen K. and Vercammen J., *Modelvorming en hoog-niveau regeling van elektronisch gestuurde CVT: een regelstrategie voor de koppeling.* K.U.Leuven, ESAT, juli 1993.

6. Jacobs F. and Janssen G., *Modelvorming en hoog-niveau regeling van een elektronisch gestuurde CVT: een regelstrategie voor de variator.* K.U.Leuven, ESAT, juli 1993.
7. Jacobs P., *Modelvorming van het secundaire circuit in een CVT.* K.I.H. De Nayer, juli 1993.
8. Anthonis J. and Van Vlierberghe A., *Regeling van actuatoren voor een CVT.* K.U.Leuven, PMA, juli 1994.
9. Deroo R., *Ontwerp van actuatoren voor een CVT.* K.U.Leuven, ESAT, juli 1994.
10. Schuermans R., *Regelen van een CVT.* K.U.Leuven, PMA, juli 1994.
11. De Vocht D. en De Leersnijder P., *Gebruik van een grafische programmeeromgeving voor de sturing van een testbank.* K.U.Leuven, ESAT, juli 1994.
12. Leenaerts K., *Virtual engineering: de kortste weg tussen specificatie en mechatronisch product.* K.U.Leuven, juli 1995.

[VDM 93] Vanvuchelen P. and De Moor B., *A multi-objective optimization approach for parameter setting in system and control design.* Proc. of the 16th IFIP Conference on system modeling and optimization, pp. 63-66, Compiegne, France, July 5-9, 1993.

[VDRV 93] Vanvuchelen P., De Moor B., Reniers D. and Vandemoortele P. *A mechatronics approach to design and control of an electronically controlled CVT.* Proc. of the 26th ISATA conference on Mechatronics, pp. 289-296, Aachen, Germany, September 13-17, 1993.

[VMD 94] Vanvuchelen P., Moons C. and De Moor B., *A computer controlled test setup for CVTs.* Proc. of the 1st Labview in Education Conference, Antwerpen, Belgium, June 30, 1994.

[VMMD 95] Vanvuchelen P., Moons C., Minten W. and De Moor B., *Electronic control of CVTs.* Proc. of the ROVA '95 International Conference, Bolton, United Kingdom, September 11-13, 1995.

[VVo 96a] Vanvuchelen P. and Vogelaar G.J., *VT1F: berekeningen koppelingsregeling.* VCST N.V., Rellestraat 2, Sint-Truiden, Belgium, R&D department, Report No. 468/96, 1996, in Dutch.

[VVo 96b] Vanvuchelen P. and Vogelaar G.J., *Analyse constante-drukventiel VT1F-K.* VCST N.V., Rellestraat 2, Sint-Truiden, Belgium, R&D department, Report No. 1027/96, 1996, in Dutch.

[VVo 96c] Vanvuchelen P. and Vogelaar G.J., *Analyse voedingsdrukventiel VT1F-K.* VCST N.V., Rellestraat 2, Sint-Truiden, Belgium, R&D department, Report No. 1148/96, 1996, in Dutch.

[VVo 96d] Vanvuchelen P. and Vogelaar G.J., *Analyse koppelingsventiel VT1F-K.* VCST N.V., Rellestraat 2, Sint-Truiden, Belgium, R&D department, Report No. 1401/96, 1996, in Dutch.

[Van 96a] Vanvuchelen P., *De VIRTUES database.* VCST N.V., Rellestraat 2, Sint-Truiden, Belgium, R&D department, Report No. 1358/96, 1996, in Dutch.

[Van 96b] Vanvuchelen P., *VTX: berekeningen CVT challenge.* VCST N.V., Rellestraat 2, Sint-Truiden, Belgium, R&D department, Report No. 467/96, 1996, in Dutch.

[Van 96c] Vanvuchelen P., *Metingen en berekeningen aan de slip van de P811-koppeling.* VCST N.V., Rellestraat 2, Sint-Truiden, Belgium, R&D department, VIRTUES documentation system, clutches and torque converters, section D, pp. 1-7, 1996, in Dutch.

[Van 96d] Vanvuchelen P., *Metingen en berekeningen aan de stijfheid van het VT1 koppelingspakket.* VCST N.V., Rellestraat 2, Sint-Truiden, Belgium, R&D department, VIRTUES documentation system, clutches and torque converters, section F, 1996, in Dutch.

[Van 96e] Vanvuchelen P., *Metingen en berekeningen aan de 12 mm oliepomp van VT1H.* VCST N.V., Rellestraat 2, Sint-Truiden, Belgium, R&D department, VIRTUES documentation system, actuation and control unit, section C, 1996, in Dutch.

[Van 97] Vanvuchelen P., *A user's manual for VIRTUES.* VCST N.V., Rellestraat 2, Sint-Truiden, Belgium, R&D department, Draft version, 1997.

[VV 96a] Vandemoortele P. and Vanvuchelen P., *Berekeningen en experimenten mbt centrifugaalwerking.* VCST N.V., Rellestraat 2, Sint-Truiden, Belgium, R&D department, VIRTUES documentation system, actuation and control unit, section D, 1996, in Dutch.

[VV 96b] Vandemoortele P. and Vanvuchelen P., *Berekeningen en experimenten mbt het rendement van de VT1-variator.* VCST N.V., Rellestraat 2, Sint-Truiden, Belgium, R&D department, VIRTUES documentation system, variators, section B, 1996, in Dutch.

[VV 96c] Vandemoortele P. and Vanvuchelen P., *Berekeningen en experimenten mbt pitot-druk opbouw bij de VT1-variator.* VCST N.V., Rellestraat 2, Sint-Truiden, Belgium, R&D department, VIRTUES documentation system, variators, section C, 1996, in Dutch.

[VV 96d] Vandemoortele P. and Vanvuchelen P., *Berekeningen en experimenten mbt olie-karakteristieken.* VCST N.V., Rellestraat 2, Sint-Truiden, Belgium, R&D department, VIRTUES documentation system, actuation and control unit, section F, 1996, in Dutch.

[VVM 96] Vandemoortele P., Vanvuchelen P. and Moons C., *Berekeningen en experimenten mbt Kp/Ks.* VCST N.V., Rellestraat 2, Sint-Truiden, Belgium, R&D department, VIRTUES documentation system, variators, section A, 1996, in Dutch.

[VCST 92] *Experimentele bepaling motor delay B18U.* VCST N.V., Rellestraat 2, Sint-Truiden, Belgium, R&D department, Reports Coördinatiecentrum, May 1992, in Dutch.

[VCST 95] *Dynamische product audit Variable Transmissie CPL.* VCST N.V., Rellestraat 2, Sint-Truiden, Belgium, Quality Assurance department, Werkinstructie W.58600/15.01/04, pp. 1-10, May 1995, in Dutch.

[VDI 87] *Einwirkung mechanischer schwingungen auf den menschen.* VDI Richtlinien 2057, VDI, 1987.

[Vie 80] Viersma T.J., *Analysis, synthesis and design of hydraulic servo systems and pipelines.* Elsevier Scientific Publishing Company, 1980.

[Vog 89] Vogelaar G.J., *Modelvorming van de hydraulische drukregeling in de valve-body van de elektronische CVT. (Modelling of the hydraulic control unit in the valve body of the electronic CVT.)* VCT B.V., Helmond, 1989, in Dutch.

[Wat 89] Watton J., *Fluid power systems: modelling, simulation, analog and micro-computer control.* Prentice Hall, 1989.

[WAB 91] Watton J. and Al-Baldawi R.A.H., *Performance optimization of an electro-hydraulic position control system with load-dependent supply pressure.* Proc. IMechE, Part I, Vol. 205, pp. 175-189, 1991.

[WN 93] Watton J. and Nelson R.J., *Mechatronic aspects of fluid power control.* Mechatronics, Vol. 3, No. 1, pp. 1-18, 1993.

[Xmath 96] Xmath, *Xmath Optimization Module.* Integrated Systems Inc., Santa Clara, CA, USA, 1996.

[YA 90] Yan W. and Anderson B.D.O., *The simultaneous optimization problem for sensitivity and gain margin.* IEEE Transactions on Automatic Control, Vol. 35, No. 5, pp. 558-563, May 1990.

[ZA 73] Zakian V. and Al-Naib U., *Design of dynamical and control systems by the method of inequalities.* Proc. of the IEE, Vol. 120, No. 11, pp. 1421-1427, November 1973.

[ZA 93] Zhuang M. and Atherton D.P., *Automatic tuning of optimum PID controllers.* IEE Proc., Part D, Vol. 140, No. 3, pp. 216-224, May 1993.

[ZN 42] Ziegler J. and Nichols N., *Optimum settings for automatic controllers.* Transactions on the A.S.M.E., no. 64, pp. 759-768, 1942.

Nederlandse Samenvatting

Mechatronica is op korte tijd een trefwoord geworden. De snelle opmars is te verklaren door het toenemende besef van de mogelijkheden van mechatronica. Hoewel een algemene definitie van mechatronica en mechatronische producten niet bestaat, herkennen we een mechatronisch product zodra we er mee in contact komen: een video-opnemer, een CD-speler, een printer, een elektronisch gestuurde wagen, een robot. Jacob Buur geeft in [Buu 92] de volgende definitie voor mechatronica:

> *Mechatronica is een technologie die mechanica, elektronica en informatie technologie combineert, om functionele interactie en ruimtelijke integratie tussen componenten,modules, producten en systemen te bekomen.*

Om mechatronica effectief te realiseren binnen een bedrijf, dient aan verschillende voorwaarden voldaan te worden:

- Het bedrijf moet in staat zijn innovatieve producten te ontwikkelen in relatieve korte tijdsspannes. Deze voorwaarde is noodzakelijk om competitiewaardig te blijven binnen de snel evoluerende markt.
- Het bedrijf moet beschikken over voldoende interdisciplinaire kennis. Dit laat toe om een gamma van alternatieve concepten te bedenken en te evalueren binnen een globale context.
- Het bedrijf moet beschikken over een ontwerpmethodologie, die ondersteund wordt door bruikbaar ontwerpgereedschap.

Voor het ontwikkelen van nieuwe producten in het algemeen, en mechatronische producten in het bijzonder, zijn er op dit ogenblik twee werkwijzen gangbaar:

- De klassieke prototype-gebaseerde aanpak steunt op het experimenteren met fysische prototypes. Op basis van metingen en met behulp van eerder opgedane kennis en ervaringen wordt een bestaand systeem geoptimaliseerd of aangepast.

- In de model-gebaseerde aanpak staat het wiskundig model van een product centraal. Op basis van simulaties en met behulp van wiskundige analyse- en ontwerptechnieken wordt het systeem geoptimaliseerd of aangepast.

In de in dit doctoraat voorgestelde 'virtual engineering' aanpak trachten we de voordelen van beide werkwijzen te combineren:

> *Gebaseerd op fysische wetmatigheden en specifieke experimenten wordt een nauwkeurig wiskundig model met fysische parameters opgesteld. Vervolgens wordt het werkelijke systeem (het prototype) vervangen door een virtueel systeem (het wiskundig model). Dit virtuele systeem wordt daarna geanalyseerd en geoptimaliseerd met behulp van krachtige simulatie- en optimalisatie-technieken. Uiteindelijk wordt het geoptimaliseerde virtuele systeem gerealiseerd en door de ontwerpers grondig gevalideerd.*

Hoewel deze aanpak vanzelfsprekend lijkt, is het effectief realiseren ervan allerminst vanzelfsprekend vanwege de grote toepassingsafhankelijkheid. Concreet betekent dit dat de globale aanpak op maat van de toepassing gerealiseerd moet worden.

Algemeen overzicht

In dit doctoraat wordt een 'virtual engineering' aanpak voor het ontwerpen en regelen van Continu Variabele Transmissies (CVT) voorgesteld en gerealiseerd.

- Fysische modelvorming wordt gebruikt om generische modellen te bepalen van de omgeving, de wagen, de aandrijflijn, de verbrandingsmotor, de natte platenkoppeling, de koppelomvormer, de duwbandvariator en de verschillende actuatoren.

  Zowel het karakteristieke gedrag van elke component, als de interactie tussen de verschillende componenten wordt gedetailleerd beschreven. Dit leidt tot fysisch geparametrizeerde, niet-lineaire systeembeschrijvingen. Singuliere perturbatie-technieken worden toegepast om deze beschrijvingen te

lineariseren. Dit leidt tot fysisch geparametrizeerde, lineaire systeembeschrijvingen. Beide beschrijvingen zijn bruikbaar voor analyse, fysisch ontwerp en regelaarontwerp.

- Deze generische modellen zijn vervolgens gecalibreerd voor een brede waaier van toepassingen. Specifieke experimenten werden gedefinieerd en uitgevoerd om calibratie-gegevens te genereren. Om de betrouwbaarheid van de experimenten te verhogen en om het aantal experimenten te beperken, worden DOE-technieken (DOE: design of experiments) toegepast.

  De volgende toepassingen werden beschouwd:

  - **Wagens**: Rover Metro, Rover 216, Rover 416, X, Y, Volvo 440 en Volvo 850. Vooronderzoek werd verricht voor verschillende Koreaanse autoconstructeurs.
  - **Verbrandingsmotoren**: Volvo motoren (B18U-1800 cc, N2-P20-2000 cc) en Rover motoren (7 types).
  - **Koppelingen**: een natte-platenkoppeling (P811) en een koppel omvormer (Daikin YT220).
  - **Duwbandvariatoren**: alle belangrijke variatoren van VCST (VT1, VT2, VT3) en hun toegepaste varianten.
  - **Kleppenhuizen**: het hydro-mechanische kleppenhuis van VCST (VT1-H) en verschillende elektro-hydraulische kleppenhuizen (VT1-E, VT2-E, VT1-F). Kleppenhuis-modellen omvatten de oliepomp, de regel- en servokleppen, de poelies en de koppelingszuiger en het regelsysteem (actuatoren, sensoren en regel-intelligentie).

- De afgeleide modellen werden gebruikt voor ontwerp en optimalisatie van kleppen, variatoren en regelsystemen, voor een brede waaier van wagen-motor-koppeling combinaties.

  Binnen deze context werden specifieke performantie-indices bepaald op basis van klantenspecificaties en ervaringsgegevens. Speciale aandacht werd besteed aan brandstofverbruik, dynamisch wagengedrag (acceleraties, snelheden, gedrag op een helling) en aan transversaal en longitudinaal comfort.

- Met behulp van de theorie van terugkoppelings-linearisatie en lineaire regelaars werden modelgebaseerde regel-algoritmen voor de aandrijflijn en de variator bepaald. Simulaties en experimenten werden gebruikt om deze regelaars te valideren.

  Een computer-gestuurde testbank is ontworpen en wordt gebruikt voor het analyseren van de ontworpen actuatoren en voor het valideren van een aantal voorgestelde regelaars.

- De ontwikkelde aanpak is in Matlab-Simulink geïmplementeerd. VIRTUES (VIRTUal Engineering Software) is een op maat gemaakt ontwerpgereedschap, dat alle ontwikkelde modellen en regelaars bevat. Specifieke methodes voor parameter-bepaling (o.a. voor modelcalibratie, fysisch ontwerp en regelaarinstelling) en voor systeem-analyse zijn eveneens beschikbaar. Een grafische gebruikersinterface en een open databank zijn aanwezig.

Op de volgende bladzijden worden de belangrijkste resultaten van elk hoofdstuk samengevat.

Hoofdstuk 1: Inleiding en Motivatie

Hoofdstuk 1 is inleidend en behandelt verschillende onderwerpen. Eerst worden de verschillende aspecten van mechatronica besproken en wordt aangetoond dat 'virtual engineering' in feite een logisch gevolg is van de mechatronica-idee. Bovendien wordt een typische 'virtual engineering' cyclus beschreven. Vervolgens wordt de lezer vertrouwd gemaakt met de bestudeerde toepassing. Na een algemeen overzicht van de ontwikkelingen op het gebied van automatische versnellingsbakken, worden specifieke aspecten van de Continu Variabele Transmissie behandeld. Tenslotte wordt een motivatie gegeven voor het opzetten en ontwikkelen van een 'virtual engineering' aanpak voor CVTs.

Een van de voornaamste factoren om mechatronica effectief te realiseren binnen een bedrijf is de beschikbaarheid van een efficiënte ontwerpaanpak en bijhorend ontwerpgereedschap. De voorgestelde 'virtual engineering' aanpak combineert de voordelen van verschillende werkwijzen; wiskundige modellen, opgesteld op basis van fysische wetmatigheden en gecalibreerd met behulp van metingen op een prototype, worden gecombineerd met krachtige simulatie- en optimalisatietechnieken, om een product te ontwerpen dat zo goed mogelijk voldoet aan alle ontwerpspecificaties. Een typische 'virtual engineering' cyclus dient als volgt te verlopen:

1. Functionele analyse van het product en decompositie in modules en componenten.

2. Analyse van de fysische werking van elke module en inventarisatie van alle nodige en beschikbare gegevens.

3. Wiskundige beschrijving op basis van fysische wetmatigheden. Dit leidt uiteindelijk tot een fysisch geparametrizeerd wiskundig model.

4. Calibratie van het model op basis van de technische tekeningen materiaaleigenschappen en experimentele gegevens.

5. Model-gebaseerde analyse van het systeem, via analytische technieken en numerieke simulatie.

6. Model-gebaseerde optimalisatie van het systeem, via analytische technieken en numerieke optimalisatie.

7. Realisatie van het geoptimaliseerde systeem en experimentele validatie.

Om de voorgestelde cyclus te vertalen op maat van de bestudeerde toepassing (het ontwerpen en regelen van Continu Variabele Transmissies), is een korte beschrijving van de CVT en de bijhorende problematiek noodzakelijk.

Een CVT is een speciaal type automatische versnellingsbak, die continu en traploos kan schakelen tussen een hoogste en een laagste overbrengingsverhouding. De DAF-Variomatic is de oudste en wellicht bekendste CVT. De steeds strenger wordende eisen inzake prestaties, verbruik en comfort van wagens enerzijds, en de enorme mogelijkheden van de CVT anderzijds, hebben gezorgd voor een hernieuwde belangstelling bij onderzoekers en wagenfabricanten voor de CVT, en in het bijzonder voor de elektronisch gestuurde CVT.

De voornaamste componenten van de in dit doctoraat beschouwde CVT zijn de duwbandvariator, de automatische koppeling (natte-platenkoppeling of koppelomvormer), de actuator en het regelsysteem. Om al deze componenten te ontwerpen en te combineren tot een verbeterde CVT is een 'Virtual engineering' aanpak noodzakelijk.

Dit doctoraat beschrijft stapsgewijs de modellen, technieken en middelen, die ontwikkeld zijn om 'virtual engineering' effectief te kunnen toepassen voor het ontwerpen en regelen van Continu Variabele Transmissies. Dit doctoraat is opgebouwd rond een toepassing (CVTs); in elk hoofdstuk worden bijkomende aspecten van de toepassing belicht en in de totale aanpak opgenomen. Voor specifieke details omtrent de veronderstelde fysische wetmatigheden of de gebruikte wiskundige technieken wordt uitgebreid verwezen naar de literatuur.

Hoofdstuk 2: Een systeem-theoretische benadering van voertuigen

Om een voertuig, uitgerust met een Continu Variabele Transmissie, te analyseren en optimaliseren op basis van simulaties, is een fysisch, wiskundig model van de

wagen en van de interacties met de omgeving noodzakelijk. Afhankelijk van de gedragingen die bestudeerd dienen te worden, kan men de complexiteit van het model wijzigen, m.a.w reductie en/of linearizatie doorvoeren.

In dit hoofdstuk worden achtereenvolgens de volgende modellen afgeleid:

- Nauwkeurige modellen van de omgevingskrachten, in dit geval rolweerstand en luchtweerstand, zijn noodzakelijk om betrouwbare prestatie- en verbruikssimulaties te bekomen. Experimentele gegevens van verschillende wagentypes zijn in rekening gebracht.

- Modellen van de stochastische verstoringen die aangrijpen op de wagen (wind dynamica en wegprofiel) zijn nuttig bij comfort-simulaties. Op basis van experimentele wind- en wegspectra worden eenvoudige lineaire toestandsruimte-beschrijvingen afgeleid.

- Rekening houdend met de karakteristieken van de wagen, de wielen en de ophanging, wordt een wagenmodel afgeleid dat toelaat de invloeden van het aandrijfkoppel, de wind en het wegprofiel op de transversale en longitudinale beweging van de wagen te bepalen. Dit resulteert in een stelsel van negen niet-lineaire tweede-orde differentiaalvergelijkingen met fysische parameters. Experimentele gegevens van verschillende wagentypes zijn in rekening gebracht. Dit model zal in Hoofdstuk 3 gebruikt worden om de invloed van de aandrijflijn op het wagencomfort te bepalen.

- Een gelineariseerd wagenmodel wordt bekomen met behulp van singuliere perturbatie-technieken. Dit gelineariseerd model zal in Hoofdstuk 3 gebruikt worden voor comfort-simulaties.

- Een gereduceerd wagenmodel dat enkel de longitudinale beweging beschrijft, wordt bekomen door middel van fysische modelreductie. Dit gereduceerde model zal in Hoofdstuk 3 gebruikt worden om de invloed van de aandrijflijn op de prestaties, het verbruik en het comfort van de wagen te bepalen. In Hoofdstuk 4 wordt dit gereduceerd model gebruikt bij het bepalen van een model-gebaseerde regelaar voor de aandrijflijn.

Hoofdstuk 3: Prestaties, verbruik en comfort van voertuigen

Om een systeem te kunnen optimaliseren met behulp van simulaties, dienen twee voorwaarden voldaan te zijn:

- De 'kwaliteit' van een systeem moet uitgedrukt kunnen worden met behulp van een beperkt aantal, objectieve performantie-indices.

- Deze performantie-indices moeten gerelateerd zijn aan meetbare grootheden en moeten op een eenvoudige manier uit de simulatie-resultaten berekend kunnen worden.

Bij het evalueren van de kwaliteit van een CVT in een bepaald voertuig, zijn de acceleratie-prestaties, het brandstofverbruik en het comfort van belang. In dit hoofdstuk worden op basis van klantenspecificaties en ervaringsgegevens een aantal bruikbare performantie-indices voor CVT-evaluatie gedefinieerd.

- Voor acceleratie-prestaties worden elf verschillende tests gedefinieerd, waaruit elf performantie-indices kunnen bepaald worden. Hiermee worden volgas prestaties, hellingsprestaties en gas-los prestaties (remmen op de motor) geëvalueerd. Het model van de aandrijflijn, ontwikkeld in Hoofdstuk 4, wordt gebruikt voor het uitvoeren van deze testen.

- Voor de beoordeling van het brandstofverbruik worden acht verschillende tests gedefinieerd, waaruit acht performantie-indices kunnen bepaald worden. Hiermee wordt het stationair verbruik bij deel-gas en het niet-stationair verbruik onder verschillende rij-condities geëvalueerd. Het model van de aandrijflijn, ontwikkeld in Hoofdstuk 4, wordt gebruikt voor het uitvoeren van deze testen.

- Hoewel comfort een subjectief gegeven is, wordt er in dit hoofdstuk een methode voorgesteld die comfort 'berekenbaar' maakt. Deze methode relateert comfort aan wagen-acceleraties en gebruikt eenvoudige acceleratie-gevoeligheidsmodellen van de mens om comfort te evalueren. Voor het uitvoeren van deze testen worden de wagenmodellen van Hoofdstuk 2 en het model van de aandrijflijn, ontwikkeld in Hoofdstuk 4, gecombineerd met de acceleratie-gevoeligheidsmodellen van de mens.

Hoofdstuk 4: Modelvorming en regeling van de aandrijflijn

Om de verschillende componenten van een CVT te optimaliseren en om een modelgebaseerde regeling van de aandrijflijn te bepalen, is een fysisch model van de aandrijflijn noodzakelijk.

In dit hoofdstuk worden modellen van de belangrijkste componenten van de aandrijflijn en van de interacties tussen deze componenten bepaald. De volgende aandrijflijn-componenten worden gemodelleerd:

- De verbrandingsmotor wordt beschreven door twee statische karakteristieken (koppel-toerental en verbruik). De vertraging tussen gasklepstand en brandstofinjectie en een vereenvoudigd model van de dynamische koppelopbouw is eveneens in rekening gebracht.
- De natte-platenkoppeling wordt beschreven door een moduleerbare wrijvingskarakteristiek. De langsdynamica van het mechanisch gedeelte van de koppeling wordt in rekening gebracht om de invloed van de koppelingsregeling bij wegrij-acties te beoordelen.
- De koppelomvormer wordt beschreven door twee statische karakteristieken (koppelvergroting en capaciteitsfactor).
- De tandwielpomp wordt beschreven als een variabele last voor de motor.
- De duwbandvariator wordt beschreven als een moduleerbare mechanische transformator, met een instelbare overbrengingsverhouding en een gekend koppelrendement.
- De eindreductie wordt beschreven als een ideale tandwielkast, met een vaste overbrengingsverhouding.
- De aandrijfas wordt beschreven als een lineaire torsie-veer.
- De wagen en de omgeving worden beschreven door het gereduceerd wagenmodel uit Hoofdstuk 2

De beschouwde aandrijflijn wordt beschreven met behulp van vier rotatie-inerties, die gekoppeld worden door deze geïdealiseerde componenten. Dit leidt uiteindelijk tot een stelsel van drie niet-lineaire tweede-orde differentiaalvergelijkingen met fysische parameters. Dit model wordt in Hoofdstuk 3 gebruikt voor simulaties van prestaties, verbruik en comfort.

Tenslotte wordt de regeling van de aandrijflijn besproken. Het variogram-concept wordt geïntroduceerd, om aan te geven hoe de wens van de bestuurder vertaald kan worden naar een gewenst motor-toerental. Vervolgens worden twee gereduceerde aandrijflijn-modellen afgeleid, die bruikbaar zijn voor het ontwerpen van een modelgebaseerde regeling. Deze regelingen worden als volgt ontworpen:

- Met behulp van terugkoppelings-linearizatie worden linearizerende regelaars bepaald.

- Voor de gelineariseerde systemen worden vervolgens eenvoudige lineaire regelaars bepaald.

Deze regelingen worden gebruikt bij het uitvoeren van de simulaties in Hoofdstuk 3.

Hoofdstuk 5: Modelvorming en regeling van de duwbandvariator

In tegenstelling tot de veronderstellingen, gemaakt in hoofdstuk 4, is de duwbandvariator niet ideaal, en is het instellen van de gewenste overbrengingsverhouding en het vermijden van bandslip niet vanzelfsprekend. In dit hoofdstuk worden de voornaamste modellen afgeleid die nodig zijn om de variator-regeling te begrijpen en te bepalen:

- De geometrische en kinematische relaties van de CVT worden bepaald, om een verband te leggen tussen de positie (snelheid) van de poelies en de overbrengingsverhouding (wijzigingssnelheid van de overbrengingsverhouding).

- Uit hydraulische overwegingen wordt een relatie bepaald tussen de gevraagde opregel-snelheid en het benodigde olie-debiet, terwijl een vereenvoudigd wrijvingsmodel van het band-poelie contact wordt gebruikt om de eis van over te brengen koppel te vertalen in minimaal nodige knijpdrukken. Uit experimentele gegevens wordt bovendien een statische relatie bepaald tussen de knijpkrachtverhouding en de gerealiseerde overbrenging.

- Een erg vereenvoudigd dynamisch model van de variator wordt gebruikt om de problematiek van de variator-regeling te beschrijven. Dit model beschrijft de mechanische interacties tussen de band en de poelies en houdt rekening met de hydraulische eigenschappen van de aandrijving. Een experimenteel model van het opschakelgedrag, zoals beschreven in [IUK 95], wordt eveneens voorgesteld. Dit model wordt gebruikt om het dynamisch gedrag van de variator te simuleren over het ganse werkingsgebied.

- Het rendement van de variator wordt eveneens geanalyseerd op basis van meetgegevens. Hieruit blijkt dat het rendement niet constant is, maar sterk afhangt van de knijpkrachten, de overbrengingsverhouding en de rotatiesnelheid. Hiermee is rekening gehouden bij de implementatie van het aandrijflijnmodel.

Vervolgens worden op basis van deze modellen twee regel-alternatieven voor de variator voorgesteld:

- Een drukgestuurde regeling, waarbij een 'outer' regelaar twee referentiedrukken berekent, die door de 'inner' druk-regelkringen worden gerealiseerd.
- Een druk-debietgestuurde regeling, waarbij een 'outer' regelaar een referentiedruk en een referentie-snelheid berekent, die door de 'inner' druk-regelkring en snelheid-regelkring worden gerealiseerd.

De 'outer' regelaars zijn een rechtstreeks gevolg van de afgeleide relaties voor de variator. De 'inner' regelaars houden enkel rekening met de hydraulische en mechanische eigenschappen van de aandrijving (regelklep en zuiger), niet met de interacties tussen de band en de poelies.

Hoofdstuk 6: Modelvorming en ontwerp van actuatoren

Om de componenten en de regelingen van de actuatoren voor de aandrijving van de variator en de koppeling te kunnen analyseren en optimaliseren met behulp van simulaties, zijn fysische modellen noodzakelijk. In dit hoofdstuk worden de belangrijkste componenten besproken en gemodelleerd. Eerst worden de karakteristieken van de olie-pomp, de zuiger en de transmissie-olie beschreven. Vervolgens worden drie belangrijke regelkleppen (één-trapsdebietklep, twee-trapsdebietklep en debietklep met druk-terugkoppeling) fysisch gemodelleerd:

- Op basis van fysische evenwichten wordt voor elke klep-zuigercombinatie een niet-lineair model opgesteld. Dit model wordt gebruikt voor het bepalen van de statische karakteristiek en bij het bepalen van de 'inner' regelaars in Hoofdstuk 5.
- Een gelineariseerd fysisch model wordt bekomen met behulp van singuliere perturbatie. Dit model wordt gebruikt voor het bepalen van de dynamische karakteristieken van de klep-zuigercombinatie.

Tenslotte worden de verschillende technologieën voor actuator-regeling besproken:

- Bij een hydro-mechanische actuator worden de meet-, regel- en aanstuurfuncties gerealiseerd met behulp van pitot-drukken (maat voor snelheid), mechanische aftasters (overbrengingsverhouding) en nokken (gaspedaalstand). In dit geval zijn alle regelingen (regeling van de aandrijflijn, outer regeling en inner regelingen van de variator) gerealiseerd in hardware.

- Bij een elektro-hydraulische en een elektro-mechanische actuator wordt de meetfunctie vervuld door specifieke sensoren, wordt een computer (ECU) gebruikt om te regelen en zorgen pulsbreedtegestuurde elektro-ventielen en elektro-motoren (translatie of rotatie) voor de aansturing van de regelkleppen. Alle eerder afgeleide modelgebaseerde regelstrategieën zijn enkel realiseerbaar met dze types actuatoren.

Hoofdstuk 7: Implementatie

In dit hoofdstuk wordt de software-implementatie van al de eerder afgeleide modellen en regelaars besproken.

Het ontwikkelingspakket VIRTUES (VIRTUal Engineering Software) is geschreven in Matlab, en integreert alle eerder afgeleide modellen en regelaars. Een aantal specifieke instrumenten voor simulatie, modelcalibratie, systeem-analyse en parameter-optimalisatie zijn eveneens beschikbaar. Dit pakket is ontwikkeld als ondersteunend pakket voor de CVT-ontwerpafdeling van VCST in Sint-Truiden, en is derhalve op maat en vraag van de 'klant' ontwikkeld. Het is bovendien een dynamisch en open pakket, d.w.z. het pakket wordt voortdurend uitgebreid (nieuwe toepassingen, nieuwe problemen), aangepast en verbeterd. Een grafische gebruikersinterface en een uitgebreide databank zijn recent toegevoegd.

Hoofdstuk 8: Een test-opstelling voor actuator-analyse en regelaar-validatie

Om op snelle en doeltreffende wijze te kunnen experimenteren met elektrisch gestuurde actuatoren is er aan de K.U.Leuven een computer-gestuurde teststand gebouwd.

Deze teststand werd gebruikt voor het uitvoeren van statische en dynamische metingen voor analyse van de actuatoren en calibratie van de bijhorende actuatormodellen. Bovendien werden de ontworpen 'inner' druk-regelingen op deze teststand gevalideerd.

Algemeen besluit

In dit doctoraat werd een 'virtual engineering' aanpak voor het ontwerpen en regelen van Continu Variabele Transmissies voorgesteld.

Het ontwikkelen van nauwkeurige fysische modellen was hierin van cruciaal belang. Stapsgewijs werden alle benodigde modellen afgeleid en, indien nodig, gelineariseerd of gereduceerd. Voor model-calibratie werden technische detailtekeningen, materiaalkarakteristieken en indien mogelijk (en nodig), calibratiemetingen gebruikt. Een aantal van deze calibratie-experimenten werd uitgevoerd op de computer-gestuurde test-opstelling die tijdens dit doctoraat gerealiseerd werd. Op basis van de modellen werden bovendien modelgebaseerde regelaars afgeleid en gevalideerd.

De modellen, de regelaars en de gebruikte instrumenten voor model-calibratie, systeem-analyse en parameter-optimalisatie werden tenslotte geïmplementeerd in Matlab-Simulink. VIRTUES is een dynamisch pakket, dat voortdurend uitgebreid en aangepast wordt. Het pakket beschikt over een grafische gebruikersinterface en heeft een uitgebreide databank die het merendeel van de gegevens van de recente toepassingen binnen VCST bevat. Tijdens dit doctoraat werden de modellen gebruikt voor analyse, dimensionering en regeling van diverse toepassingen. Op dit ogenblik wordt VIRTUES binnen VCST en door de auteur gebruikt als een ondersteunend pakket voor ontwerp en regeling van CVTs.